



NATO Science for Peace and Security Series - B:
Physics and Biophysics

Complexity in Chemistry and Beyond: Interplay Theory and Experiment

New and Old Aspects of Complexity
in Modern Research

Edited by
Craig Hill
Djamaladdin G. Musaev

 Springer



*This publication
is supported by:*

The NATO Science for Peace
and Security Programme

Complexity in Chemistry and Beyond: Interplay Theory and Experiment

NATO Science for Peace and Security Series

This Series presents the results of scientific meetings supported under the NATO Programme: Science for Peace and Security (SPS).

The NATO SPS Programme supports meetings in the following Key Priority areas: (1) Defence Against Terrorism; (2) Countering other Threats to Security and (3) NATO, Partner and Mediterranean Dialogue Country Priorities. The types of meeting supported are generally “Advanced Study Institutes” and “Advanced Research Workshops”. The NATO SPS Series collects together the results of these meetings. The meetings are co-organized by scientists from NATO countries and scientists from NATO’s “Partner” or “Mediterranean Dialogue” countries. The observations and recommendations made at the meetings, as well as the contents of the volumes in the Series, reflect those of participants and contributors only; they should not necessarily be regarded as reflecting NATO views or policy.

Advanced Study Institutes (ASI) are high-level tutorial courses intended to convey the latest developments in a subject to an advanced-level audience

Advanced Research Workshops (ARW) are expert meetings where an intense but informal exchange of views at the frontiers of a subject aims at identifying directions for future action

Following a transformation of the programme in 2006 the Series has been re-named and re-organised. Recent volumes on topics not related to security, which result from meetings supported under the programme earlier, may be found in the NATO Science Series.

The Series is published by IOS Press, Amsterdam, and Springer, Dordrecht, in conjunction with the NATO Emerging Security Challenges Division.

Sub-Series

- | | |
|---|-----------|
| A. Chemistry and Biology | Springer |
| B. Physics and Biophysics | Springer |
| C. Environmental Security | Springer |
| D. Information and Communication Security | IOS Press |
| E. Human and Societal Dynamics | IOS Press |

<http://www.nato.int/science>

<http://www.springer.com>

<http://www.iospress.nl>



Series B: Physics and Biophysics

Complexity in Chemistry and Beyond: Interplay Theory and Experiment

New and Old Aspects of Complexity
in Modern Research

edited by

Craig Hill

Department of Chemistry, Emory University, Atlanta, Georgia, USA

and

Djamaladdin G. Musaev

Department of Chemistry, Emory University, Atlanta, Georgia, USA

 Springer

Published in Cooperation with NATO Emerging Security Challenges Division

Proceedings of the NATO Advanced Research Workshop on
From Simplicity to Complexity in Chemistry and Beyond:
Interplay Theory and Experiment
Baku, Azerbaijan
28–30 May 2008

Library of Congress Control Number: 2012955938

ISBN 978-94-007-5550-5 (PB)
ISBN 978-94-007-5547-5 (HB)
ISBN 978-94-007-5548-2 (e-book)
DOI 10.1007/978-94-007-5548-2

Published by Springer,
P.O. Box 17, 3300 AA Dordrecht, The Netherlands.

www.springer.com

Printed on acid-free paper

All Rights Reserved

© Springer Science+Business Media Dordrecht 2012

This work is subject to copyright. All rights are reserved by the Publisher, whether the whole or part of the material is concerned, specifically the rights of translation, reprinting, reuse of illustrations, recitation, broadcasting, reproduction on microfilms or in any other physical way, and transmission or information storage and retrieval, electronic adaptation, computer software, or by similar or dissimilar methodology now known or hereafter developed. Exempted from this legal reservation are brief excerpts in connection with reviews or scholarly analysis or material supplied specifically for the purpose of being entered and executed on a computer system, for exclusive use by the purchaser of the work. Duplication of this publication or parts thereof is permitted only under the provisions of the Copyright Law of the Publisher's location, in its current version, and permission for use must always be obtained from Springer. Permissions for use may be obtained through RightsLink at the Copyright Clearance Center. Violations are liable to prosecution under the respective Copyright Law.

The use of general descriptive names, registered names, trademarks, service marks, etc. in this publication does not imply, even in the absence of a specific statement, that such names are exempt from the relevant protective laws and regulations and therefore free for general use.

While the advice and information in this book are believed to be true and accurate at the date of publication, neither the authors nor the editors nor the publisher can accept any legal responsibility for any errors or omissions that may be made. The publisher makes no warranty, express or implied, with respect to the material contained herein.

Preface

Complexity occurs in biological and synthetic systems alike. This general phenomenon has been addressed in recent publications by investigators in disciplines ranging from chemistry and biology to psychology and philosophy. Studies of complexity for molecular scientists have focused on breaking symmetry, dissipative processes, and emergence. Investigators in the social and medical sciences have focused on neurophenomenology, cognitive approaches and self-consciousness. Complexity in both structure and function is inherent in many scientific disciplines of current significance and also in technologies of current importance that are rapidly evolving to address global societal needs. The classical studies of complexity generally do not extend to the complicated molecular and nanoscale structures that are of considerable focus at present in context with these evolving technologies. This book reflects the presentations at a NATO-sponsored conference on Complexity in Baku, Azerbaijan. It also includes some topics that were not addressed at this conference, and most chapters have expanded coverage relative to what was presented at the conference. The editors, participants and authors thank funding from NATO for making this opus possible.

This book is a series of chapters that each addresses one or more of these multifaceted scientific disciplines associated with the investigation of complex systems. In addition, there is a general focus on large multicomponent molecular or nanoscale species, including but not limited to polyoxometalates. The latter are a class of compounds whose complicated and tunable properties have made them some of the most studied species in the last 5 years (polyoxometalate publications are increasing dramatically each year and are approaching 1,000 per year). This book also seeks to bring together experimental and computational science to tackle the investigation of complex systems for the simple reason that for such systems, experimental and theoretical findings are now highly helpful guiding one other, and in many instances, synergistic.

Chapters 1 and 2 by Mainzer and Dei, respectively, address “Complexity” from the general and philosophical perspective and set up the subsequent chapters to some extent. Chapter 3 by Gatteschi gives an overview of complexity in molecular magnetism and Chap. 4 by Glaser provides limiting issues and design concepts for

single molecule magnets. Chapter 5 by Cronin discusses the prospect of developing emergent, complex and quasi-life-like systems with inorganic building blocks based upon polyoxometalates, work that relates indirectly to research areas targeted in the following two chapters. Chapter 6 by Diemann and Müller describes giant polyoxometalates and the engaging history of the molybdenum blue solutions, one of the most complex self assembling naturally occurring inorganic systems known. Chapter 7 by Bo and co-workers discusses the computational investigation of encapsulated water molecules in giant polyoxometalates via molecular dynamics, studies that have implications for many other similar complex hydrated structures in the natural and synthetic worlds. Chapter 8 by Astruc affords a view of another huge field of complex structures, namely dendrimers, and in particular organometallic ones and how to control their redox and catalytic properties. Chapter 9 by Farzaliyev addresses an important, representative complicated solution chemistry with direct societal implications: control and minimization of the free-radical chain chemistry associated with the breakdown of lubricants, and by extension many other consumer materials. Chapters 10 and 11 address computational challenges and case studies on complicated molecular systems: Chap. 10 by Poblet and co-workers examines both geometrical and electronic structures of polyoxometalates, and Chap. 11 by Maseras and co-workers delves into the catalytic cross-coupling and other carbon-carbon bond forming processes of central importance in organic synthesis. Chapter 12 by Weinstock studies a classic case of a simple reaction (electron transfer) but in highly complex molecular systems and Chap. 13 by Hill, Musaeu and their co-workers describes two types of complicated multi-functional material, those which detect and decontaminate odorous or dangerous molecules in human environments and catalysts for the oxidation of water, an essential and critical part of solar fuel generation.

Craig L. Hill and Djamaladdin G. Musaeu
Department of Chemistry, Emory University
Atlanta, Georgia, USA

Contents

1	Challenges of Complexity in Chemistry and Beyond	1
	Klaus Mainzer	
2	Emergence, Breaking Symmetry and Neurophenomenology as Pillars of Chemical Tenets	29
	Andrea Dei	
3	Complexity in Molecular Magnetism	49
	Dante Gatteschi and Lapo Bogani	
4	Rational Design of Single-Molecule Magnets	73
	Thorsten Glaser	
5	Emergence in Inorganic Polyoxometalate Cluster Systems: From Dissipative Dynamics to Artificial Life	91
	Leroy Cronin	
6	The Amazingly Complex Behaviour of Molybdenum Blue Solutions	103
	Ekkehard Diemann and Achim Müller	
7	Encapsulated Water Molecules in Polyoxometalates: Insights from Molecular Dynamics	119
	Pere Miró and Carles Bo	
8	Organometallic Dendrimers: Design, Redox Properties and Catalytic Functions	133
	Didier Astruc, Catiá Ornelas, and Jaime Ruiz	
9	Antioxidants of Hydrocarbons: From Simplicity to Complexity	151
	Vagif Farzaliyev	
10	Structural and Electronic Features of Wells-Dawson Polyoxometalates	171
	Laia Vilà-Nadal, Susanna Romo, Xavier López, and Josep M. Poble	

11 Homogeneous Computational Catalysis: The Mechanism for Cross-Coupling and Other C-C Bond Formation Processes	185
Christophe Gourlaouen, Ataulpa A.C. Braga, Gregori Ujaque, and Feliu Maseras	
12 Electron Transfer to Dioxygen by Keggin Heteropolytungstate Cluster Anions	207
Ophir Snir and Ira A. Weinstock	
13 Multi-electron Transfer Catalysts for Air-Based Organic Oxidations and Water Oxidation	229
Weiwei Guo, Zhen Luo, Jie Song, Guibo Zhu, Chongchao Zhao, Hongjin Lv, James W. Vickers, Yurii V. Geletii, Djamaladdin G. Musaev, and Craig L. Hill	

Contributors

Didier Astruc Institut des Sciences Moléculaires, UMR CNRS N°5255, Université Bordeaux I, Talence Cedex, France

Carles Bo Institute of Chemical Research of Catalonia (ICIQ), Tarragona, Spain
Departament de Química Física i Química Inorgànica, Universitat Rovira i Virgili, Tarragona, Spain

Lapo Bogani Physikalisches Institut, Universität Stuttgart, Stuttgart, Germany

Ataulpa A.C. Braga Institute of Chemical Research of Catalonia (ICIQ), Tarragona, Catalonia, Spain

Leroy Cronin Department of Chemistry, University of Glasgow, Glasgow, UK

Andrea Dei LAMM Laboratory, Dipartimento di Chimica, Università di Firenze, UdR INSTM, Sesto Fiorentino (Firenze), Italy

Ekkehard Diemann Faculty of Chemistry, University of Bielefeld, Bielefeld, Germany

Vagif Farzaliyev Institute of Chemistry of Additives, Azerbaijan National Academy of Sciences, Baku, Azerbaijan

Dante Gatteschi Department of Chemistry, University of Florence, INSTM, Polo Scientifico Universitario, Sesto Fiorentino, Italy

Yurii V. Geletii Department of Chemistry, Emory University, Atlanta, GA, USA

Thorsten Glaser Lehrstuhl für Anorganische Chemie I, Fakultät für Chemie, Universität Bielefeld, Bielefeld, Germany

Christophe Goulaouen Institute of Chemical Research of Catalonia (ICIQ), Tarragona, Catalonia, Spain

Weiwei Guo Department of Chemistry, Emory University, Atlanta, GA, USA

Craig L. Hill Department of Chemistry, Emory University, Atlanta, GA, USA

Xavier López Departament de Química Física i Inorgànica, Universitat Rovira i Virgili, Tarragona, Spain

Zhen Luo Department of Chemistry, Emory University, Atlanta, GA, USA

Hongjin Lv Department of Chemistry, Emory University, Atlanta, GA, USA

Klaus Mainzer Lehrstuhl für Philosophie und Wissenschaftstheorie, Munich Center for Technology in Society (MCTS), Technische Universität München, Munich, Germany

Feliu Maseras Institute of Chemical Research of Catalonia (ICIQ), Tarragona, Catalonia, Spain

Unitat de Química Física, Edifici Cn, Universitat Autònoma de Barcelona, Bellaterra, Catalonia, Spain

Pere Miró Institute of Chemical Research of Catalonia (ICIQ), Tarragona, Spain

Achim Müller Faculty of Chemistry, University of Bielefeld, Bielefeld, Germany

Djamaladdin G. Musaev Department of Chemistry, Cherry L. Emerson Center for Scientific Computation, Emory University, Atlanta, GA, USA

Catiá Ornelas Institut des Sciences Moléculaires, UMR CNRS N°5255, Université Bordeaux I, Talence Cedex, France

Josep M. Poblet Departament de Química Física i Inorgànica, Universitat Rovira i Virgili, Tarragona, Spain

Susanna Romo Departament de Química Física i Inorgànica, Universitat Rovira i Virgili, Tarragona, Spain

Jaime Ruiz Institut des Sciences Moléculaires, UMR CNRS N°5255, Université Bordeaux I, Talence Cedex, France

Ophir Snir Department of Chemistry, Ben Gurion University of the Negev, Beer Sheva, Israel

Jie Song Department of Chemistry, Emory University, Atlanta, GA, USA

Gregori Ujaque Unitat de Química Física, Edifici Cn, Universitat Autònoma de Barcelona, Bellaterra, Catalonia, Spain

James W. Vickers Department of Chemistry, Emory University, Atlanta, GA, USA

Laia Vilà-Nadal Departament de Química Física i Inorgànica, Universitat Rovira i Virgili, Tarragona, Spain

Ira A. Weinstock Department of Chemistry, Ben Gurion University of the Negev, Beer Sheva, Israel

Chongchao Zhao Department of Chemistry, Emory University, Atlanta, GA, USA

Guibo Zhu Department of Chemistry, Emory University, Atlanta, GA, USA

Chapter 1

Challenges of Complexity in Chemistry and Beyond

Klaus Mainzer

*I can hardly doubt
that when we have some control of the arrangement of things on
a small scale
we will get an enormously greater range of possible properties
that substances can have.*

R.P. Feynman¹

Abstract The theory of complex dynamical systems is an interdisciplinary methodology to model nonlinear processes in nature and society. In the age of globalization, it is the answer to increasing complexity and sensitivity of human life and civilization (e.g., life science, environment and climate, globalization, information flood). Complex systems consist of many microscopic elements (molecules, cells, organisms, agents, citizens) interacting in nonlinear manner and generating macroscopic order. Self-organization means the emergence of macroscopic states by the nonlinear interactions of microscopic elements. Chemistry at the boundary between physics and biology analyzes the fascinating world of molecular self-organization. Supramolecular chemistry describes the emergence of extremely complex molecules during chemical evolution on Earth. Chaos and randomness,

¹Interesting in this context is that nonlinear *chemical*, dissipative mechanisms (distinguished from those of a *physical* origin) have been proposed as providing a possible underlying process for some aspects of biological self-organization and morphogenesis. Nonlinearities during the formation of microtubular solutions are reported to result in a chemical instability and bifurcation between pathways leading to macroscopically self-organized states of different morphology (Tabony, *J. Science*, **1994**, 264, 245).

K. Mainzer (✉)

Lehrstuhl für Philosophie und Wissenschaftstheorie, Munich Center for Technology in Society (MCTS), Technische Universität München, Arcisstrasse 21, D-80333 Munich, Germany
e-mail: mainzer@tum.de

growth and innovations are examples of macroscopic states modeled by phase transitions in critical states. The models aim at explaining and forecasting their dynamics. Information dynamics is an important topic to understand molecular self-organization. In the case of randomness and chaos, there are restrictions to compute the macrodynamics of complex systems, even if we know all laws and conditions of their local activities. Future cannot be forecast in the long run, but dynamical trends (e.g., order parameters) can be recognized and influenced (“bounded rationality”). Besides the methodology of mathematical and computer-assisted models, there are practical and ethical consequences: Be sensible to critical equilibria in nature and society (butterfly effect). Find the balance between self-organization, control, and governance of complex systems in order to support a sustainable future of mankind.

1.1 General Aspects

Complexity is a modern science subject, sometimes quite difficult to define exactly or to detail accurately its boundaries. Over the last few decades, astonishing progress has been made in this field and, finally, an at least relatively unified formulation concerning dissipative systems has gained acceptance. We recognize complex processes in the evolution of life and in human society. We accept physico-chemical and algorithmic complexity and the existence of archetypes in dissipative systems. But we have to realize that a deeper understanding of many processes—in particular those taking place in living organisms—demands also an insight into the field of “molecular complexity” and, hence, that of equilibrium or near-equilibrium systems, the precise definition of which has still to be given [1].

One of the most obvious and likewise most intriguing basic facts to be considered is the overwhelming variety of structures that—due to *combinatorial explosion*—can be formally built from only a (very) limited number of simple “building blocks” according to a restricted number of straight-forward “matching rules”. On the one hand, combinatorial theory is well-equipped and pleasant to live with. Correspondingly, it is possible to some extent to explore, handle, and use combinatorial explosion on the theoretical and practical experimental level. On the other hand, the reductionist approach in the natural sciences has for a long time focused rather on separating matter into its elementary building blocks than on studying systematically the phenomena resulting from the cooperative behaviour of these blocks when put together to form higher-order structures, a method chemists may have to get accustomed to in the future in order to understand complex structures [2].

Independent progress in many different fields—from algorithmic theory in mathematics and computer science via physics and chemistry to materials science and the biosciences—has made it possible and, hence, compels us to try to bridge the gap between the micro- and the macro-level from a structural (as opposed to a purely statistical, averaging) point of view and to address questions such as:

1. *What exactly is coded* in the ingredients of matter (elementary particles, atoms, simple molecular building blocks) with respect to the emergence of complex systems and complex behaviour? The question could, indeed, be based on the assumption that a “*creatio ex nihilo*” is not possible!
2. During the course of evolution, how and why did *Nature* form just those *complicated* and—in most cases—*optimally functioning, perfectionated molecular systems* we are familiar with? Are they (or at least some of them) appropriate models for the design of *molecular materials* exhibiting all sorts of properties and serving many specific needs?
3. While, on the one hand, a simple reductionist description of complex systems in terms of less complex ones is not always meaningful, how significant are, on the other hand, phenomena (properties) related to rather simple material systems within the context of *creating complex (e.g., biological) systems from simpler ones*?
4. In particular: Is it possible to find *relations which exist between supramolecular entities*, synthesized by chemists and formed by conservative self-organization or self-assembly processes, *and the most simple biological entities*? And how can we elucidate such relations and handle their consequences? In any case, a precondition for any attempt to answer these questions is a sufficient understanding of the “Molecular World”, including its propensities or potentialities [2, 3].
5. Self-organizing processes are not only interesting from an *epistemic* point of view, but for *applications* in materials, engineering, and life sciences. In an article entitled “There’s Plenty of Room at the Bottom”, Richard Feynman proclaimed his physical ideas of the *complex nanoworld* in the late 1950s [4]. How far can supramolecular systems in Nature be considered self-organizing “*nanomachines*”? *Molecular engineering* of nanotechnology is inspired by the self-organization of complex molecular systems. Is the engineering design of smart nanomaterials and biological entities a *technical co-evolution* and progression of natural evolution?
6. Supramolecular “transistors” are an example that may stimulate a revolutionary new step in the technology of *quantum computer*. On the other side, can *complex molecular systems* in nature be considered quantum computers with information processing of *qubits*? [5].

From a philosophical point of view, the development of chemistry is toward complex systems, from divided to condensed matter then to organized and adaptive systems, on to living systems and thinking systems, up the ladder of complexity.

Complexity results from multiplicity of components, interaction between them, coupling and (nonlinear) feedback. The properties defining a given level of complexity result from the level below and their multibody interaction. Supramolecular entities are explained in terms of molecules, cells in terms of supramolecular entities, tissues and organs in terms of cells, organisms in terms of tissues and organs, and so on up to social groups, societies, and ecosystems along a hierarchy of levels defining the taxonomy of complexity. At each level of increasing complexity novel features emerge that do not exist at lower levels, which are

explainable and deducible from but not reducible to those of lower levels. In this sense, supramolecular chemistry builds up a supramolecular science whose already remarkable achievements point to the even greater challenges of complexity in the human organism, brain, society, and technology.

1.2 Complexity in Systems Far from Equilibrium

The theory of nonlinear complex systems [6] has become a successful and widely used tool for studying problems in the natural sciences—from laser physics, quantum chaos, and meteorology to molecular modeling in chemistry and computer simulations of cell growth in biology. In recent years, these tools have been used also—at least in the form of “scientific metaphors”—to elucidate social, ecological, and political problems of mankind or aspects of the “working” of the human mind.

What is the secret behind the success of these sophisticated applications? The theory of *nonlinear complex systems* is not a special branch of physics, although some of its mathematical principles were discovered and first successfully applied within the context of problems posed by physics. Thus, it is not a kind of traditional “*physicalism*” which models the dynamics of lasers, ecological populations, or our social systems by means of similarly structured laws. Rather, nonlinear systems theory offers a useful and far-reaching justification for simple phenomenological models specifying only a few relevant parameters relating to the emergence of macroscopic phenomena via the nonlinear interactions of microscopic elements in complex systems.

The behaviour of single elements in large composite systems (atoms, molecules, etc.) with huge degrees of freedom can neither be forecast nor traced back. Therefore, in statistical mechanics, the deterministic description of single elements at the microscopic level is replaced by describing the evolution of probabilistic distributions. At critical threshold values, phase transitions are analyzed in terms of appropriate *macrovariables*—or “*order parameters*”—in combination with terms describing rapidly fluctuating random forces due to the influence of additional *microvariables*.

By now, it is generally accepted that this scenario, worked out originally for systems in thermal equilibrium, can also be used to describe the emergence of order in open dissipative systems far from thermal equilibrium (Landau, Prigogine, Thom, Haken, etc. [6]; for some details see Sect. 1.5). Dissipative self-organization means basically that the phase transition lies far from thermal equilibrium. Macroscopic patterns arise in that case according to, say, Haken’s “slaving principle” from the nonlinear interactions of microscopic elements when the interaction of the dissipative (“open”) system with its environment reaches some critical value, e.g., in the case of the Bénard convection. In a qualitative way, we may say that old structures become unstable and, finally, break down in response to a change of the control parameters, while new structures are achieved. In a more mathematical way,

the macroscopic view of a complex system is described by the evolution equation of a global state vector where each component depends on space and time and where the components may mean the velocity components of a fluid, its temperature field, etc. At critical threshold values, formerly stable modes become unstable, while newly established modes are winning the competition in a situation of high fluctuations and become stable. These modes correspond to the order parameters which describe the collective behaviour of macroscopic systems.

Yet, we have to distinguish between phase transitions of open systems with the emergence of order *far from* thermal equilibrium and phase transitions of closed systems with the emergence of structure *in* thermal equilibrium. Phase transitions in thermal equilibrium are sometimes called “conservative” self-organization or self-assembly (self-aggregation) processes creating ordered structures mostly, but not necessarily, with low energy. Most of the contributions to this book deal with such structures. In the case of a special type of self-assembly process, a kind of slaving principle can also be observed: A template forces chemical fragments (“slaves”), like those described in Sect. 1.3, to link in a manner determined by the conductor (template) [7], whereby a well defined order/structure is obtained. Of particular interest is the formation of a template from the fragments themselves [8].

1.3 Taking Complexity of Conservative Systems into Account and a Model System Demonstrating the Creation of Molecular Complexity by Stepwise Self-Assembly

A further reason for studying the emergence of structures in conservative systems can be given as follows: The theory of nonlinear complex systems offers a basic framework for gaining insight into the field of nonequilibrium complex systems but, in general, it does not adequately cover the requirements necessary for the adventurous challenge of understanding their specific architectures and, thus, must be supported by additional experimental and theoretical work. An examination of biological processes, for example those of a morphogenetic or, in particular, of an epigenetic nature, leads to the conclusion that here the complexity of molecular structures is deeply involved, and only through an incorporation of the instruments and devices of the relevant chemistry is it possible to uncover their secrets (footnote 1). Complex molecular structures exhibit multi-functionality and are characterized by a correspondingly complex behaviour which does not necessarily comply with the most simple principles of mono-causality nor with those of a simple straightforward cause-effect relationship. The field of genetics offers an appropriate example: One gene or gene product is often related not only to one, but to different characteristic phenotype patterns (as the corresponding gene product (protein) has often to fulfill several functions), a fact that is manifested even in (the genetics of) rather simple procaryotes.

Several nondissipative systems, which according to the definition of W. Ostwald are metastable, show complex behaviour. For example, due to their complex flexibility, *proteins* (or large biomolecules) are capable of adapting themselves not only to varying conditions but also to different functions demanded by their environment; the characteristics of *noncrystalline solids* (like glasses), as well as of *crystals grown under nonequilibrium conditions* (like snow crystals) are determined by their case history; *spin-glasses* exhibit complex magnetic behaviour [9]; *surfaces of solids* with their inhomogeneities or disorders² can, in principle, be used for storing information; *giant molecules (clusters)* may exhibit fluctuations of a structural type.³ Within the novel field of supramolecular magnetochemistry [10], we can also anticipate *complex behaviour*, a fact which will require attention in the future when a unified and interdisciplinarily accepted definition of complex behaviour of conservative systems is to be formed.

But is elucidating complexity *as a whole* an unsolvable, inextricable problem, leading to some type of a *circulus vitiosus*? Or is it possible to create a theory, unifying the theories from all fields that would explain different types of self-organization processes and complexity in general? The key to disentangle these problems lies in the elucidation of the relation between conservative and dissipative systems, which in turn is only possible through a clear identification of the relations between multi-functionality, deterministic dynamics, and stochastic dynamics.⁴

²Defects, in general—not only those related to the surface—affect the physical and chemical (e.g., catalytical) properties of a solid and play a role in its history. They form the basis of its possible complex behaviour.

³Fluctuation—static or nonstatic, equilibrium or nonequilibrium—usually means the deviation of some quantity from its mean or most probable value. (They played a key role in the evolution.) Most of the quantities that might be interesting for study exhibit fluctuations, at least on a microscopic level. Fluctuations of macroscopic quantities manifest themselves in several ways. They may limit the precision of measurements of the mean value of the quantity, or vice versa, the identification of the fluctuation may be limited by the precision of the measurement. They are the cause of some familiar features of our surroundings, or they may cause spectacular effects, such as the critical opalescence and they play a key role in the nucleation phase of crystal growth (see Sect. 1.8). Fluctuations or their basic principles which are relevant for chemistry have never been discussed on a general basis, though they are very common—for example in the form of some characteristic properties of the very large metal clusters and colloids.

⁴During cosmological, chemical, biological, as well as social and cultural evolution, *information* increased parallel to the generation of structures of higher complexity. The emergence of relevant information during the different stages of evolution is comparable with phase transitions during which structure forms from unordered systems (with concomitant entropy export). Although we can model certain collective features in natural and social sciences by the complex dynamics of phase transitions, we have to pay attention to important differences (see Sect. 1.6).

In principle, any piece of information can be encoded by a sequence of zeros and ones, a so-called {0,1}-sequence. Its (*Kolmogorov*) complexity can thus be defined as the length of the minimal {0,1}-sequence in which all that is needed for its reconstruction is included (though, according to well-known undecidability theorems, there is in general no algorithm to check whether a given sequence with such a property is of minimal length). According to the broader definition by C.F. von Weizsäcker, *information* is a concept intended to provide a scale for measuring the amount of form encountered in a system, a structural unit, or any other information-

For a real understanding of phase transitions, we have to deal not only with the structure and function of elementary building blocks, but also with the properties which emerge in consequence of the complex organization which such simple entities may collectively yield when interacting cooperatively. And we have to realize that such emergent *high-level* properties are properties which—even though they can be exhibited by complex systems only and cannot be directly observed in their component parts when taken individually—are still amenable to scientific investigation.

These facts are generally accepted and easily recognized with respect to crystallographic symmetry; here, the mathematics describing and classifying the emerging structures (e.g., the 230 space groups) is readily available [11]. But the situation becomes more difficult when complex biological systems are to be investigated where no simple mathematical formalism yet exists to classify all global types of interaction patterns and where molecular complexity plays a key role: The behaviour of sufficiently large molecules like enzymes *in complex systems* can, as yet, not be predicted computationally nor can it simply be deduced from that of their (simple chemical) components.

Consequently, one of the most aspiring fields of research at present, offering challenging and promising perspectives for the future [2] is to learn experimentally and interpret theoretically how relevant global interaction patterns and the resulting high-level properties of complex systems emerge by using ‘a’ stepwise procedure, to build ever more complex systems from simple constituents. This approach is used, in particular, in the field of *supramolecular chemistry* [12]—a basic topic of this book—where some intrinsic propensities of material systems are investigated. By focusing on phenomena like non-covalent interactions or multiple weak attractive forces (especially in the case of molecular recognition, host/guest complexation as well as antigene-antibody interactions), (template-directed) self-assembly, autocatalysis, artificial, and/or natural self-replication, nucleation, and control of crystal growth, supramolecular chemistry strives to elucidate strategies for making constructive use of specific large-scale molecular interactions, characteristic for *mesoscopic* molecular complexes and nanoscale architectures.

In order to understand more about related *potentialities* of material systems, we should systematically examine, in particular, self-assembly processes. *A system of genuine model character* [2,7,13], exhibiting a maximum of *potentiality* or *disposition* “within” the relevant solution, *contains very simple units with the shape of Platonic solids* [11]—or chemically speaking, simple mononuclear oxoanions [14]—*as building blocks* from which an extremely wide spectrum of complex

carrying entity (“*Information ist das Maß einer Menge von Form*”). There exists, of course, a great variety of other definitions of *information* which have been introduced within different theoretical contexts and which relate to different scientific disciplines. Philosophically speaking, a *qualitative* concept is needed which considers information to be a property neither of structure nor of function alone, but of that inseparable unit called *form*, which mediates between both.

polynuclear clusters can be formed according to a type of unit construction. In this context, self-assembly or condensation processes can lead us to the fascinating area of mesoscopic molecular systems.

A significant step forward in this field could be achieved by controlling or directing the type of linkage of the above-mentioned fragments (units), for instance by a template, in order to obtain larger systems and then proceeding accordingly to get even larger ones (with novel and perhaps unusual properties!) by linking the latter again, and so on. This is possible within the mentioned model system. Basically, we are dealing with a type of emergence due to the generation of ever more complex systems. The concept of emergence should be based on a pragmatically restricted reductionism. The dialectic unit of reduction and emergence can be considered as a “guideline” when confronted with the task of examining processes which lead to more and more complex systems, starting with the most simple (chemical) ones [2].

Fundamental questions we have to ask are whether complex near-equilibrium systems were a necessary basis for the formation of dissipative structures during evolution and whether it is possible to create molecular complexity stepwise by a conservative growth process corresponding to the following schematic description [13]:

$$\begin{array}{ccccccc} \text{I} & \text{III} & \text{V} & \text{VII} & (2N - 1) \\ 2 & 4 & 6 & & (2n) \end{array}$$

Here, the uneven Roman numerals, $2N - 1$, represent a series of maturation steps of a molecular system in growth or development and the even Arabic numerals $2n$ stand for ingredients of the solution which react only with the relevant “preliminary” or intermediate product, $2N - 1$. The species $2/n$ can themselves be products of self-assembly processes. The target molecule at the “end” of the growth process would be formed by some kind of (near equilibrium) symmetry breaking steps. The information it carries could, in principle, be transferred to other systems [13].

1.4 From Complex Molecular Systems to Quantum Computing

In human technology, information processing is based on computers. In the twentieth century, the invention of computers allowed complex information processing to be performed outside human brains. The history of computer technology has involved a sequence of changes from gears to relays to valves to transistors, integrated circuits and so on. Advanced lithographic techniques can etch logical gates and wires less than a micron across onto surfaces of silicon chips. Finally, we will reach the point where logic gates are so small that they consist of only a few atoms each. On the scale of human perception, classical (non-quantum) laws of nature are good approximations. But on the atomic and molecular level the laws

of quantum mechanics become dominant. If computers are to continue to become faster and therefore smaller, quantum technology must replace or supplement classical computational technology. *Quantum information processing* is connected with new challenges of *computational complexity* [15].

The basic unit of classical information is the bit. From a physical point of view a bit is a two-state system. It can be prepared in one of two distinguishable states representing two logical values 0 or 1. In digital computers, the voltage between the plates of a capacitor can represent a bit of information. A charge on the capacitor denotes 1 and the absence of charge denotes 0. One bit of information can also be encoded using, for example, two different polarizations of light (photons), or two different electronic states of an atom, or two different magnetic states of a molecular magnet. According to quantum mechanics, if a bit can exist in either of two distinguishable states it can also exist in *coherent superpositions* of them. They are further states in which an elementary particle, atom, or molecule represent both values, 0 and 1, simultaneously. That is the sense in which a quantum bit (*qubit*) can store both 0 and 1 simultaneously, in arbitrary proportions. But if the qubit is measured, only one of the two numbers it holds will be detected, at random. John Bell's famous theorem and EPR (Einstein-Podolsky-Rosen) experiments forbid that the bit is predetermined before measurement [16].

The idea of superposition of numbers leads to massive *parallel computation*. For example a classical 3-bit register can store exactly one of eight different numbers. In this case, the register can be in one of the eight possible configurations 000, 010, . . . , 111, representing the numbers 0–7 in binary coding. A quantum register composed of three qubits can simultaneously store up to eight numbers in a quantum superposition. If we add more qubits to the register its capacity for storing the complexity of quantum information increases exponentially. In general n qubits can store 2^n numbers at once. A 250-qubit register of a molecule made of 250 atoms would be capable of holding more numbers simultaneously than there are atoms in the known universe. Thus a quantum computer can in a single computational step perform the same mathematical operation on 2^n different input numbers. The result is a superposition of all the corresponding outputs. But if the register's contents are measured, only one of those numbers can be seen. In order to accomplish the same task a classical computer must repeat the computation 2^n times, or use 2^n different processors working in parallel.

At first, it seems to be a pity that the laws of quantum physics only allow us to see one of the outcomes of 2^n computations. From a logical point of view, quantum inference provides a final result that depends on all 2^n of the intermediate results. A remarkable *quantum algorithm* of Lov Grover uses this logical dependence to improve the chance of finding the desired result. Grover's quantum algorithm enables to search an unsorted list of n items in only \sqrt{n} steps [17]. Consider, for example, searching for a specific telephone number in a directory containing a million entries, stored in a computer's memory in alphabetical order of names. It is obvious that no classical algorithm can improve the brute-force method of simply scanning the entries one by one until the given number is found which will, on average, require 500,000 memory accesses. A quantum computer can examine all

the entries simultaneously, in the time of a single access. But if it can only print out the result at that point, there is no improvement over the classical algorithm. Only one of the million computational paths would have checked the entry we are looking for. Thus, there would be a probability of only one in a million that we obtain that information if we measured the computer's state. But if that quantum information is left unmeasured in the computer, a further quantum operation can cause that information to affect other paths. In this way the information about the desired entry is spread, through quantum inference, to more paths. It turns out that if the inference-generating operation is repeated about 1,000 times, (in general, \sqrt{n} times) the information about which entry contains the desired number will be accessible to measurement with probability 0.5. Therefore repeating the entire algorithm a few more times will find the desired entry with a probability close to 1.

An even more spectacular quantum algorithm was found by Peter Shor [18] for factorizing large integers efficiently. In order to factorize a number with n decimal digits, any classical computer is estimated to need a number of steps growing exponentially with n . The factorization of 1,000-digit numbers by classical means would take many times as long the estimated age of the universe. In contrast, quantum computers could factor 1,000-digit numbers in a fraction of a second. The execution time would grow only as the cube of the number of digits. Once a quantum factorization machine is built, all classical cryptographic systems will become insecure, especially the RSA (Rivest, Shamir and Adleman) algorithm which is today often used to protect electronic bank accounts [19].

Historically, the potential power of quantum computation was first proclaimed in a talk of Richard Feynman at the first Conference on the Physics of Computation at MIT in 1981 [15]. He observed that it appeared to be impossible in general to simulate the evolution of a quantum system on a classical computer in an efficient way. The computer simulation of quantum evolution involves an exponential slowdown in time, compared with the natural evolution. The amount of classical information required to describe the evolving quantum state is exponentially larger than that required to describe the corresponding classical system with a similar accuracy. But, instead of regarding this intractability as an obstacle, Feynman considered it an opportunity. He explained that if it requires that much computation to find what will happen in a multi-particle interference experiment, then the amount of such an experiment and measuring the outcome is equivalent to performing a complex computation.

A quantum computer is a more or less complex network of *quantum logical gates*. As the number of quantum gates in a network increases, we quickly run into serious practical problems. The more interacting qubits are involved, the harder it tends to handle the computational technology. One of the most important problems is that of preventing the surrounding environment from being affected by the interactions that generate quantum superpositions. The more components there are, the more likely it is that quantum information will spread outside the quantum computer and be lost into the environment. The process is called *decoherence*. Due to supramolecular chemistry, there has been some evidence that decoherence in complex molecules, such as molecular nano-magnets, might not be such a severe problem.

A molecular magnet containing vanadium and oxygen atoms has been described [5] which could act as a carrier of quantum information. It is more than one nanometer in diameter and has an electronic spin structure in which each of the vanadium atoms, with their net spin $\frac{1}{2}$, couple strongly into three groups of five. The magnet has a spin doublet ground and triplet spin excited state. ESR (Electronic Spin Resonance) spectroscopy was used to observe the degree of coherence possible. The prime source of decoherence is the ever-present nuclear spins associated with the 15 vanadium nuclei. The experimental results of [5] pinpoint the sources of decoherence in that molecular system, and so take the first steps toward eliminating them. The identification of nuclear spin as a serious decoherence issue hints at the possibility of using zero-spin isotopes in qubit materials. The control of complex coherent spin states of molecular magnets, in which interactions can be tuned by well defined chemical changes of the metal cluster ligand spheres, could finally lead to a way to avoid the roadblock of decoherence.

Independent of its realization with elementary particles, atoms, or molecules, quantum computing provides deep consequences for *computational universality* and *computational complexity of nature*. Quantum mechanics provides new modes of computation, including algorithms that perform tasks that no classical computer can perform at all. One of the most relevant questions within classical computing, and the central subject of computational complexity is whether a given problem is easy to solve or not. A basic issue is the time needed to perform the computation, depending on the size of the input data. According to Church's thesis, any (classical) computer is equivalent to and can be simulated by a universal Turing-machine. Computational time is measured by the number of elementary computational steps of a universal Turing-machine. Computational problems can be divided into complexity classes according to their computational time of solution. The most fundamental one is the class P which contains all problems which can be computed by (deterministic) universal Turing machine in polynomial time, i.e. the computational time is bounded from above by polynomial. The class NP contains all problems which can be solved by non-deterministic Turing-machine in polynomial time. Non-deterministic machines may guess a computational step by random. It is obvious by definition that P is a subset of NP. The other inclusion, however, is rather non-trivial. The conjecture is that $P \neq NP$ holds and great parts of complexity theory are based on it. Its proof or disproof represents one of the biggest open questions in theoretical informatics.

In quantum theory of computation the Turing principle demands the universal quantum computer can simulate the behavior of any finite physical system [20]. A stronger result that was conjectured but never proved in the classical case demands that such simulations can always be performed in a time that is at most a polynomial function of the time for the physical evolution. That is true in the quantum case. In the future, quantum computers will prove theorems by methods that neither a human brain nor any other arbiter will ever be able to check step-by-step, since if the sequence of propositions corresponding to such a proof were printed out, the paper would fill the observable universe many times over. In that case, computational problems would be shifted into lower complexity classes: intractable problems of classical computability would become practically solvable.

1.5 Information and Probabilistic Complexity

A dynamical system can be considered an information processing machine, computing a present or future state as output from an initial past state of input. Thus, the computational efforts to determine the states of a system characterize the computational complexity of a dynamical system. The transition from regular to chaotic systems corresponds to increasing computational problems, according to the computational degrees in the theory of computational complexity. In statistical mechanics, the information flow of a dynamical system describes the intrinsic evolution of statistical correlations between its past and future states. The *Kolmogorov-Sinai (KS) entropy* is an extremely useful concept in studying the loss of predictable information in dynamical systems, according to the complexity degrees of their attractors. Actually, the KS-entropy yields a measure of the prediction uncertainty of a future state provided the whole past is known (with finite precision) [21].

In the case of fixed points and limit cycles, oscillating or quasi-oscillating behavior, there is no uncertainty or loss of information, and the prediction of a future state can be computed from the past. In chaotic systems with sensitive dependence on the initial states, there is a finite loss of information for predictions of the future, according to the decay of correlations between the past states and the future state of prediction. The finite degree of uncertainty of a predicted state increases linearly to its number of steps in the future, given the entire past. But in the case of noise, the KS-entropy becomes infinite, which means a complete loss of predicting information corresponding to the decay of all correlations (i.e., statistical independence) between the past and the noisy state of the future. The degree of uncertainty becomes infinite.

The *complexity degree of noise* can also be classified by Fourier analysis of time series in signal theory. Early in the nineteenth century, the French mathematician Jean-Baptiste-Joseph Fourier (1768–1830) proved that any continuous signal (time series) of finite duration can be represented as a superposition of overlapping periodic oscillations of different frequencies and amplitudes. The frequency f is the reciprocal of the length of the period which means the duration $1/f$ of a complete cycle. It measures how many periodic cycles there are per unit time.

Each signal has a spectrum, which is a measure of how much variability the signal exhibits corresponding to each of its periodic components. The spectrum is usually expressed as the square of the magnitude of the oscillations at each frequency. It indicates the extent to which the magnitudes of separate periodic oscillations contribute to the total signal. If the signal is periodic with period $1/f$, then its spectrum is everywhere zero except at the isolated value f . In the case of a signal that is a finite sum of periodic oscillations the spectrum will exhibit a finite number of values at the frequencies of the given oscillations that make up the signal.

The opposite of periodicity is a signal whose values are statistically independent and uncorrelated. In signal theory, the distribution of independent and uncorrelated values is called white noise. It has contributions from oscillations whose amplitudes

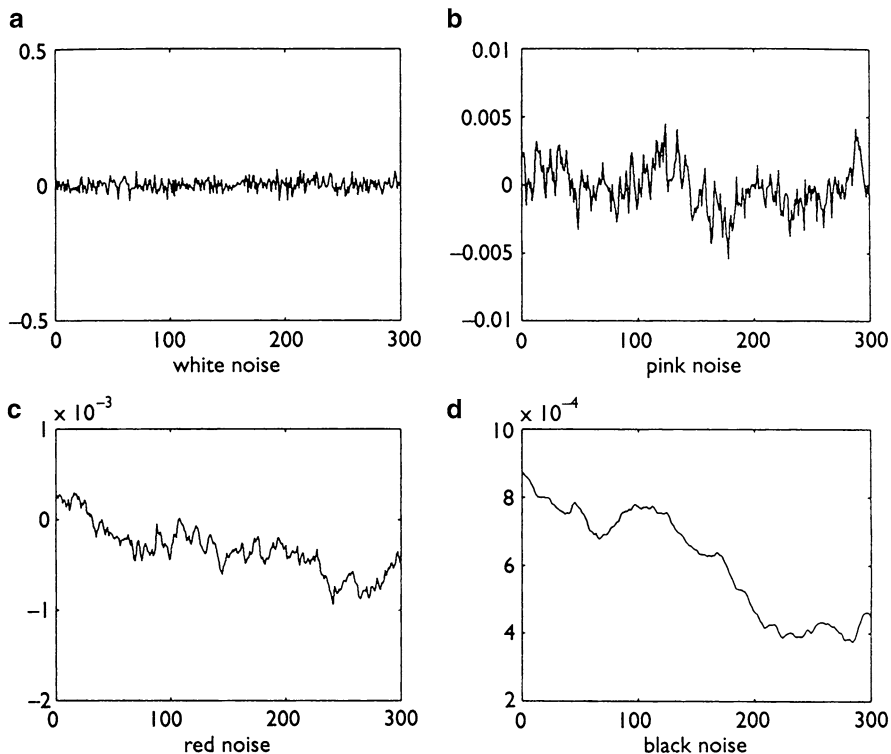


Fig. 1.1 Complexity degrees of $1/f^b$ - noise with *white noise* ($b = 0$), *pink noise* ($b = 1$), *red noise* ($b = 2$), and *black noise* ($b = 3$) [22] (Color figure online)

are uniform over a wide range of frequencies. In this case the spectrum has a constant value, flat throughout the frequency range. The contributions of periodic components cannot be distinguished.

But in nonlinear dynamics of complex systems we are mainly interested in complex series of data that conform to neither of these extremes. They consist of many superimposed oscillations at different frequencies and amplitudes, with a spectrum that is approximately proportional to $1/f^b$ for some b greater than zero. In that case, the spectrum varies inversely with the frequency. Their signals are called $1/f$ - noise. Figure 1.1 illustrates examples of signals with spectra of pink noise ($b = 1$), red noise ($b = 2$), and black noise ($b = 3$). White noise is designated by $b = 0$. The degree of irregularity in the signals decreases as b becomes larger.

For b greater than 2 the correlations are persistent, because upwards and downwards trends tend to maintain themselves. A large excursion in one time interval is likely to be followed by another large excursion in the next time interval of the same length. The time series seem to have a long-term memory. With b less than 2 the correlations are antipersistent in the sense that an upswing now is likely

to be followed shortly by a downturn, and vice versa. When b increases from the antipersistent to the persistent case, the curves Fig. 1.1 become increasingly less jagged.

The spectrum gets progressively smaller as frequency increases. Therefore, large-amplitude fluctuations are associated with long-wavelength (low-frequency) oscillations, and smaller fluctuations correspond to short-wavelength (high-frequency) cycles. For nonlinear dynamics pink noise with b roughly equal to 1 is particularly interesting, because it characterizes processes between regular order of black noise and complete disorder of white noise. For pink noise the fraction of total variability in the data between two frequencies $f_1 < f_2$ equals the percentage variability within the interval $cf_1 < cf_2$ for any positive constant c . Therefore, there must be fewer large-magnitude fluctuations at lower frequencies than there are small-magnitude oscillations at high frequencies. As the time series increases in length, more and more low-frequency but high-magnitude events are uncovered because cycles of longer periods are included. The longest cycles have periods comparable to the duration of the sampled data. Like all fractal patterns, small changes of signals are superimposed on larger ones with self-similarity at all scales.

In electronics, $1/f$ -spectra are known as flicker-noise, differing from the uniform sound of white noise with the distinction of individual signals [23]. The high-frequency occurrences are hardly noticed contrary to the large magnitude events. A remarkable application of $1/f$ -spectra delivers different kinds of music. The fluctuations of loudness as well as the intervals between successive notes in the music of Bach have a $1/f$ -spectrum. Contrary to Bach's pink-noise music, white-noise music has only uncorrelated successive values. The brain fails in finding any pattern in a structureless and irritating sound. On the other side, black-noise music seems too predictable and boring, because the persistent signals depend strongly on past values. Obviously, impressing music finds a balance between order and disorder, regularity and surprise.

$1/f$ -spectra are typical for processes that organize themselves to a critical state at which many small interactions can trigger the emergence of a new unpredicted phenomenon. Earthquakes, atmospheric turbulence, stock market fluctuations, and physiological processes of organisms are typical examples. *Self-organization*, *emergence*, *chaos*, *fractality*, and *self-similarity* are features of complex systems with nonlinear dynamics [24]. The fact that $1/f$ -spectra are measures of stochastic noise emphasizes a deep relationship of *information theory* and *systems theory*, again: all kinds of complex systems can be considered information processing systems. In the following, distributions of correlated and unrelated signals are analyzed in the theory of probability. White noise is characterized by the normal distribution of the Gaussian bell curve. Pink noise with a $1/f$ -spectrum is decisively non-Gaussian. Its patterns are footprints of complex self-organizing systems.

In complex systems, the behavior of single elements is often completely unknown and therefore considered a random process. In this case, it is not necessary to distinguish between chance that occurs because of some hidden order that may exist and chance that is the result of blind lawfulness. A stochastic process is assumed to be a succession of unpredictable events. Nevertheless, the whole process can be

characterized by laws and regularities, or with the words of A.N. Kolmogorov, the founder of modern theory of probability: “The epistemological value of probability theory is based on the fact that chance phenomena, considered collectively and on a grand scale, create non-random regularity.” [25] In tossing a coin, for example, head and tail are each assigned a probability of 1:2 whenever the coin seems to be balanced. This is because one expects that the event of a head or tail is equally likely in each flip. Therefore, the average number of heads or tails in a large number of tosses should be close to $1/2$, according to the law of large numbers. This is what Kolmogorov meant.

The outcomes of a stochastic process can be distributed with different probabilities. Binary outcomes are designated by probability p and $1 - p$. In the simplest case of $p = 1/2$, there is no propensity for one occurrence to take place over another, and the outcomes are said to be uniformly distributed. For instance, the six faces of a balanced die are all equally likely to occur in a toss, and so the probability of each face is $1/6$. In this case, a random process is thought of as a succession of independent and uniformly distributed outcomes. In order to turn this intuition into a more precise statement, we consider coin-tossing with two possible outcomes labeled zero or one. The number of ones in n trials is denoted by r_n , and the sample average r_n/n represents the fraction of ones in n trials. Then, according to the law of large numbers, the probability of the event that r_n/n is within some fixed distance to $1/2$ will tend to one as n increases without bound.

The distribution of values of samples clusters about $1/2$ with a dispersion that appears roughly bell-shaped. The bell-shaped Gaussian curve illustrates Kolmogorov’s statement that lawfulness emerges when large ensembles of random events are considered. The same general bell shape appears for several games with different average outcome like playing with coins, throwing dice, or dealing cards. Some bells may be squatter, and some narrower. But each has the same mathematical Gaussian formula to describe it, requiring just two numbers to differentiate it from any other: the mean or average error and the variance or standard deviation, expressing how widely the bell spreads.

For both independence and finite variance of the involved random variables, the *central limit theorem* holds: a probability distribution gradually converges to the Gaussian shape. If the conditions of independence and finite variance of the random variables are not satisfied, other limit theorems must be considered. The study of limit theorems uses the concept of the basin of attraction of a probability distribution. All the probability density functions define a functional space. The Gaussian probability function is a fixed point attractor of stochastic processes in that functional space. The set of probability density functions that fulfill the requirements of the central limit theorem with independence and finite variance of random variables constitutes the basin of attraction of the Gaussian distribution. The *Gaussian attractor* is the most important attractor in the functional space, but other attractors also exist.

Gaussian (and Cauchy) distributions are examples of stable distributions. A stable distribution has the property that it does not change its functional form. The French mathematician Paul Lévy (1886–1971) determined the entire class of stable

distributions [3]. Contrary to the Gaussian distribution, the non-Gaussian (“Lévy”) stable stochastic processes have infinite variance. Their asymptotic behaviour is characterized by distributions $P_L(x) \sim x^{-(1+\alpha)}$ with *power-law behaviour* for large values of x . Contrary to the smooth Gaussian bell-curve, their (“fat”) tails indicate fluctuations with a leptokurtic shape. Thus, they do not have a characteristic scale, but they can be rescaled with self-similarity. Besides the Gaussian distribution, non-Gaussian stable distributions can also be attractors in the functional space of probability density functions.

There is an infinite number of attractors, comprising the set of all the stable distributions. Attractors classify the functional space of probability density functions into regions with different complexity. The *complexity of stochastic processes* is different for the Gaussian attractor and the stable non-Gaussian attractors. In the Gaussian basin of attraction, finite variance random variables are present. But in the basins of attraction of stable non-Gaussian distributions, random variables with infinite variance can be found. Therefore, distributions with power-law tails are present in the stable non-Gaussian basins of attraction (compare reference 22, chapter 5.4).

Power-law distributions and infinite variance indicate high complexity of stochastic behaviour. Stochastic processes with infinite variance, although well defined mathematically, are extremely difficult to use and, moreover, raise fundamental questions when applied to real systems. In closed physical systems of equilibrium statistical mechanics variance is often related to the system temperature. In this case, infinite variance implies an infinite or undefined temperature. Nevertheless, power-law distributions are used in the description of open systems. They have increasing importance in describing, for example, complex economic and physiological systems. Actually, the first application of a power-law distribution was introduced in economics by Pareto’s law of incomes. Turbulence in complex financial markets is also characterized by power-law distributions with fat tails. In financial systems, an infinite variance would complicate the important task of risk estimation.

1.6 A System of High Complexity: Human Society and Economy

Obviously, the theory of complex systems and their phase transitions offers a successful formalism to model the emergence of order in Nature. The question arises how to select, interpret, and quantify the appropriate variables of complex models in the social sciences. In this case, the possibility to test the complex dynamics of the model is restricted: In general, we cannot experiment with human society. Yet, computer simulations with varying parameters may deliver useful scenarios to recognize global trends of a society under all sorts of conditions.

Evidently, human society is a complex multi-component system composed of diverse elements. It is an open system because there exist not only internal interactions through materials and information exchange (“ideas”) between the

individual members of a society, but also an interchange with the external environment, nature, and civilization. At the microscopic level (e.g., *micro-sociology* and *micro-economy*), the individual “local” states of human behaviour are characterized by different attitudes. Changes of society are related to changes in attitudes of its members. Global change of behaviour is modeled by introducing macrovariables in terms of attitudes of social groups (compare reference 22 chapter 8) [26].

In social sciences, one distinguishes strictly between biological evolution and the history of human society. The reason is that the development of nations, markets, and cultures is assumed to be guided by the intentional behaviour of humans, i.e., human decisions based on intentions, values, etc. From a microscopic viewpoint we may, of course, observe single individuals contributing with their activities to the collective macrostate of the society representing cultural, political, and economic order (and, hopefully, determined by the value of corresponding “order parameters”).

Yet, macrostates of a society do, of course, not simply average over its parts. Its order parameters strongly influence the individuals of the society by orientating (“enslaving”) their activities and by activating or deactivating their attitudes and capabilities. This kind of feedback is typical for complex dynamical systems. If the control parameters of the environmental conditions attain certain critical values due to internal or external interactions, the macrovariables may move into an unstable domain out of which highly divergent alternative paths are possible. Tiny unpredictable microfluctuations (e.g., actions of very few influential people, scientific discoveries, new technologies) may decide which of the diverging paths society will follow.

A particular *measurement problem* of sociology arises from the fact that sociologists observing and recording the collective behaviour of society are themselves members of the social system they observe. Sociologists strive to define and to record quantitatively measurable parameters of collective behaviour, using all sorts of “objective”, that is, empirical and quantitative methods. But, while the world of macroscopic physical phenomena will certainly not be changed in a scientifically relevant way by the fact that it is being explored and investigated, this does not necessarily hold true for social systems—a further justification for the obvious fact that scientific procedures used in classical physics are not simply transferable to the study of human social behaviour. This well-known sociological phenomenon of “self-observation in a society” confirms the complex dynamics of a society, i.e., the nonlinear feedback between individual activities at the microscopic level and its global macroscopic order states.

While systems in physics and chemistry are often taken for granted and are considered to be arbitrarily delimitable units of consideration, social systems cannot even be defined (and much less analyzed and studied) without simultaneously considering their environment and delineating their boundaries from their interval dynamics as well as from their interactions with all those features that do not pertain to the system. The problems which obviously arise in this context are carefully analyzed by N. Luhmann in his well-known system theory approach [27]. Problems of a similar nature arise when considering biological processes. In addition, it might

be worthwhile to take into account also the epistemological aspects discussed by N. Luhmann even in connection with the study of chemical and physical systems. A case in point is, for instance, the well-known fact that the dynamics of a protein cannot be understood without studying it in solution.

Social migration, economic crashes, and ecological catastrophes are very dramatic topics today, demonstrating the danger of global world-wide effects. It is not sufficient to have good intentions without considering the nonlinear effects of single decisions. Linear thinking and acting may provoke global chaos although we act locally with the best intentions. In this sense, even if we are not able to quantify all relevant parameters of complex social dynamics, the cognitive value of an appropriate model will consist in useful insights into the role and effect of certain trends relative to the global dynamics of our society. In other words, the operational value of such an approach depends upon the possibility of using the model in order to examine hypothetical courses of our society.

In economics as well as in financial theory uncertainty and information incompleteness prevent exact predictions. A widely accepted belief in financial theory is that time series of asset prices are unpredictable. Chaos theory has shown that unpredictable time series can arise from *deterministic nonlinear systems*. The results obtained in the study of physical, chemical, and biological systems raise the question whether the time evolution of asset prices in financial markets might be due to underlying nonlinear deterministic dynamics of a finite number of variables. If we analyze financial markets with the tools of nonlinear dynamics, we may be interested in the reconstruction of an attractor. In time series analysis, it is rather difficult to reconstruct an underlying attractor and its dimension d . For chaotic systems with $d > 3$, it is a challenge to distinguish between a chaotic time evolution and a random process, especially if the underlying deterministic dynamics are unknown. From an empirical point of view, the discrimination between *randomness* and *chaos* is often impossible. Time evolution of an asset price depends on all the information affecting the investigated asset. It seems unlikely that all this information can easily be described by a limited number of nonlinear deterministic equations.

Therefore, asserts price dynamics are assumed to be *stochastic processes*. An early key-concept to understand stochastic processes was the random walk. The first theoretical description of a random walk in the natural sciences was performed in 1905 by Einstein's analysis of molecular interactions. But the first mathematization of a *random walk* was not realized in physics, but in social sciences by the French mathematician, Louis Jean Bachelier (1870–1946). In 1900 he published his doctoral thesis with the title “Théorie de la Spéculation” [28]. During that time, most market analysis looked at stock and bond prices in a causal way: Something happens as cause and prices react as effect. In complex markets with thousands of actions and reactions, a causal analysis is even difficult to work out afterwards, but impossible to forecast beforehand. One can never know everything. Instead, Bachelier tried to estimate the odds that prices will move. He was inspired by an analogy between the diffusion of heat through a substance and how a bond price wanders up and down. In his view, both are processes that cannot be forecast precisely. At the level of particles in matter or of individuals in markets, the details are too complicated. One

can never analyze exactly how every relevant factor interrelate to spread energy or to energize spreads. But in both fields, the broad pattern of probability describing the whole system can be seen.

Bachelier introduced a stochastic model by looking at the bond market as a fair game. In tossing a coin, each time one tosses the coin the odds of heads or tails remain 1:2, regardless of what happened on the prior toss. In that sense, tossing coins is said to have no memory. Even during long runs of heads or tails, at each toss the run is as likely to end as to continue. In the thick of the trading, price changes can certainly look that way. Bachelier assumed that the market had already taken account of all relevant information, and that prices were in equilibrium with supply matched to demand, and seller paired with buyer. Unless some new information came along to change that balance, one would have no reason to expect any change in price. The next move would as likely be up as down.

In order to illustrate this smooth distribution, Bachelier plotted all of a bond's price-changes over a month or year onto a graph. In the case of independent and identically distributed price-changes, they spread out in the well-known bell-curve shape of a *normal* ("Gaussian") *distribution*: the many small changes clustered in the center of the bell, and the few big changes at the edges. Bachelier assumed that price changes behave like the random walk of molecules in a Brownian motion. Long before Bachelier and Einstein, the Scottish botanist Robert Brown had studied the erratic way that tiny pollen grains jiggled about in a sample of water. Einstein explained it by molecular interactions and developed equations very similar to Bachelier's equation of bond-price probability, although Einstein never knew that. It is a remarkable coincidence that the movement of security prices, the motion of molecules, and the diffusion of heat are described by mathematically analogous models. In short, Bachelier's model depends on the three hypotheses of (1) statistic independence ("Each change in price appears independently from the last"), (2) statistic stationarity of price changes, and (3) normal distribution ("Price changes follow the proportions of the Gaussian bell curve").

But the Dow charts demonstrate that the index changes of financial markets have no smooth distribution of a Gaussian bell curve (compare references 24 and 22, chapter 7.4). Price fluctuations of real markets are not mild, but wild. That means that stocks are riskier than assumed according to normal distribution. With the bell curve in mind, stock portfolios may be put together incorrectly, risk management fails, and trading strategies are misguided. Further on, the Dow chart shows that, with globalization increasing, we will see more crises. Therefore, our whole focus must be on the extremes now.

On a qualitative level, *financial markets* seem to be similar to *turbulence* in nature. Wind is an example of natural turbulence which can be studied in a wind tunnel. When the rotor at the tunnel's head spins slowly, the wind inside blows smoothly, and the currents glide in long, steady lines, planes, and curves. Then, as the rotor accelerates, the wind inside the tunnel picks up speed and energy. It suddenly breaks into sharp and intermittent gusts. Eddies form, and a cascade of whirlpools, scaled from great to small, spontaneously appears. The same emergence of patterns and attractors can be studied in the fluid dynamics of water.

The time series of a turbulent wind illustrates the changing wind speed as it bursts into and out of gusty, turbulent flow. Turbulence can be observed everywhere in nature. Turbulences emerge in the clouds, but also in the patterns of sunspots. All kinds of signals seem to be characterized by signatures of turbulence. Analogously, a financial chart can show the changing volatility of the stock market, as the magnitude of price changes varied wildly, from month to month. Peaks are during 1929–1934 and 1987. If one compares this pattern with a wind chart, one can observe the same abrupt discontinuities between wild motion and quiet activity, the same intermittent periods, and the same concentration of events in time. Obviously, the destructive turbulence of nature can also be observed in financial markets.

In modern physics and economics, phase transitions and nonlinear dynamics are related to *power laws*, *scaling* and *unpredictable stochastic* and *deterministic time series*. Historically, the first mathematical application of power-law distributions took place in the social sciences and not in physics. We remember that the concept of random walk was also mathematically described in economics by Bachelier before it was applied in physics by Einstein. The Italian social economist Vilfredo Pareto (1848–1923), one of the founder of the Lausanne school of economics, investigated the statistical character of the wealth of individuals in a stable economy by modeling them with the distribution $y \sim x^{-\nu}$, where y is the number of people with income x or greater than x and ν is an exponent that Pareto estimated to be 1.5 [29]. He noticed that his result could be generalized to different countries. Therefore, Pareto's law of income was sometimes interpreted as a universal social rule rooting to Darwin's natural law of selection.

But power-law distributions may lack any characteristic scale. This property prevented the use of power-law distributions in the natural sciences until mathematical introduction of Lévy's new probabilistic concepts and the physical introduction of new scaling concepts for thermodynamic functions and correlation functions (see ref. [40]). In financial markets, invariance of time scales means that even a stock expert cannot distinguish in a time series analysis if the charts are, for example, daily, weekly, or monthly. These charts are statistically self-similar or fractal.

Obviously, financial markets are more complex than the traditional academic theory believed. They are turbulent, not in the strict physical sense, but caused by their intrinsic complex stochastic dynamics with similar dangerous consequences like, for example, earthquakes, tsunamis, or hurricanes in nature. Therefore, financial systems are not linear, continuous, and computable machine in order to forecast individual economic events like planet's position in astronomy. They are very risky and complex, but, nevertheless, computational, because an appropriate stochastic mathematics allows to analyze and recognize typical patterns and attractors of the underlying dynamics. These methods support market timing. But there is no guarantee of success: Big gains and losses concentrate into small packages of time. The belief in a continuous economic development is refuted by often leaping prices, adding to the risk.

Markets are mathematically characterized by power, laws and invariance. A practical consequence is that markets in all places and ages work alike. If one can find market properties that remain constant over time or place, one can build useful

models to support financial decisions. But we must be cautious, because markets are deceptive. Their dynamics sometimes seem to provide patterns of correlations we unconsciously want to see without sufficient confirmation. During evolution, our brain was trained to recognize patterns of correlation in order to support our survival. Therefore, we sometimes see patterns where there are none (see ref. [41]). Systems theory and appropriate tools of complexity research should help to avoid illusions in markets.

1.7 A System with high Complexity: The Human Brain

Models of natural and social science are designed by the human brain. Obviously, it is the most remarkable complex system in the evolution of nature. The coordination of the complex cellular and organic interactions in an organism needs a new kind of self-organizing controlling [30]. That was made possible by the evolution of nervous systems that also enabled organisms to adapt to changing living conditions and to learn from experiences with its environment. The hierarchy of anatomical organizations varies over different scales of magnitude, from molecular dimensions to that of the entire central nervous system (CNS). The research perspectives on these hierarchical levels may concern questions, for example, of how signals are integrated in dendrites, how neurons interact in a network, how networks interact in a system like vision, how systems interact in the CNS, or how the CNS interact with its environment. Each stratum may be characterized by some *order parameters* determining its particular structure, which is caused by complex interactions of subelements with respect to the particular level of hierarchy.

On the micro-level of the brain, there are massively many-body-problems which need a reduction strategy to handle with the complexity. In the case of EEG-pictures, a complex system of electrodes measures local states (electric potentials) of the brain. The whole state of a patient's brain on the micro-level is represented by local time series. In the case of, e.g., petit mal epilepsy, they are characterized by typical cyclic peaks. The microscopic states determine macroscopic electric field patterns during a cyclic period. Mathematically, the macroscopic patterns can be determined by spatial modes and order parameters, i.e., the amplitude of the field waves. In the corresponding phase space, they determine a chaotic attractor characterizing petit mal epilepsy.

The neural self-organization on the cellular and subcellular level is determined by the information processing in and between neurons [42]. Chemical transmitters can effect neural information processing with direct and indirect mechanisms of great plasticity. Long time potential (LTP) of synaptic interaction is an extremely interesting topic of recent brain research. LTP seems to play an essential role for the neural self-organization of cognitive features such as, e.g., memory and learning. The information is assumed to be stored in the synaptic connections of neural cell assemblies with typical macroscopic patterns.

But while an individual neuron does not see or reason or remember, brains are able to do so. Vision, reasoning, and remembrance are understood as higher-level functions. Scientists who prefer a bottom-up strategy recommend that higher-level functions of the brain can be neither addressed nor understood until each particular property of each neuron and synapse is explored and explained. An important insight of the complex system approach discloses that emergent effects of the whole system are synergetic system effects which cannot be reduced to the single elements. They are results of *nonlinear interactions*. Therefore, the whole is more than the (linear) sum of its parts. Thus, from a methodological point of view, a purely bottom-up-strategy of exploring the brain functions must fail. On the other hand, the advocates of a purely top-down strategy proclaiming that cognition is completely independent of the nervous system are caught in the old Cartesian dilemma “How does the ghost drive the machine?”.

Today, we can distinguish several degrees of complexity in the CNS. The scales consider molecules, membranes, synapses, neurons, nuclei, circuits, networks, layers, maps, sensory systems, and the entire nervous system. The research perspectives on these hierarchical levels may concern questions, e.g., of how signals are integrated in dendrites, how neurons interact in a network, how networks interact in a system like vision, how systems interact in the CNS, or how the CNS interact with its environment. Each stratum may be characterized by some order parameters determining its particular structures, which is caused by complex interactions of subelements with respect to the particular level of hierarchy. Beginning at the bottom, we may distinguish the orders of ion movement, channel configurations, action potentials, potential waves, locomotion, perception, behavior, feeling and reasoning.

The different abilities of the brain need massively parallel information processing in a complex hierarchy of neural structures and areas. We know more or less complex models of the information processing in the visual and motoric systems. Even, the dynamics of the emotional system is interacting in a nonlinear feedback manner with several structures of the human brain. These complex systems produce neural maps of cell assemblies. The self-organization of somatosensory maps is well-known in the visual and motoric cortex. They can be enlarged and changed by learning procedures such as the training of an ape’s hand.

PET (Positron-Emission-Tomography) pictures show macroscopic patterns of neurochemical metabolic *cell assemblies* in different regions of the brain which are correlated with *cognitive abilities* and *conscious states* such as looking, hearing, speaking, or thinking. Pattern formation of neural cell assemblies are even correlated with complex processes of psychic states [31]. Perturbations of metabolic cellular interactions (e.g., cocaine) can lead to nonlinear effects initiating complex changing of behavior (e.g., addiction by drugs). These correlations of neural cell assemblies and order parameters (attractors) of cognitive and conscious states demonstrate the connection of neurobiology and cognitive psychology in recent research, depending on the standards of measuring instruments and procedures.

Many questions are still open. Thus, we can only observe that someone is thinking and feeling, but not, what he is thinking and feeling. Further on, we

observe no unique substance called consciousness, but complex macrostates of the brain with different degrees of sensoric, motoric, or other kinds of attention. Consciousness means that we are not only looking, listening, speaking, hearing, feeling, thinking etc., but we know and perceive ourselves during these cognitive processes. Our self is considered an order parameter of a state, emerging from a recursive process of multiple self-reflections, self-monitoring, and supervising our conscious actions. Self-reflection is made possible by the so-called mirror neurons (e.g., in the Broca area) which let primates (especially humans) imitate and simulate interesting processes of their companions. Therefore, they can learn to take the perspectives of themselves and their companions in order to understand their intentions and to feel with them. The emergence of subjectivity is neuropsychologically well understood.

The brain does not only observe, map, and monitor the external world, but also internal states of the organism, especially its emotional states. Feeling means self-awareness of one's emotional states which are mainly caused by the limbic system. In neuromedicine, the "*Theory of Mind*" (ToM) even analyzes the neural correlates of social feeling which are situated in special areas of the neocortex [30]. People, e.g., suffering from Alzheimer disease, lose their feeling of empathy and social responsibility because the correlated neural areas are destroyed. Therefore, our moral reasoning and deciding have a clear basis in brain dynamics.

From a neuropsychological point of view, the old philosophical problem of "*qualia*" is also solvable. Qualia mean properties which are consciously experienced by a person. In a thought experiment a neurobiologist is assumed to be caught in a black-white room. Theoretically, she knows everything about neural information processing of colors. But she never had a chance to experience colors. Therefore, exact knowledge says nothing about the quality of conscious experience. Qualia in that sense emerge by bodily interaction of self-conscious organisms with their environment which can be explained by the nonlinear dynamics of complex systems. Therefore, we can explain the dynamics of subjective feelings and experiences, but, of course, the actual feeling is an individual experience. In medicine, the dynamics of a certain pain can often be completely explained by a physician, although the actual feeling of pain is an individual experience of the patient [32].

In order to model the brain and its complex abilities, it is quite adequate to distinguish the following categories. In neuronal-level models, studies are concentrated on the dynamic and adaptive properties of each nerve cell or neuron, in order to describe the neuron as a unit. In network-level models, identical neurons are interconnected to exhibit emergent system functions. In nervous-system-level models, several networks are combined to demonstrate more complex functions of sensory perception, motor functions, stability control, etc. In mental-operation-level models, the basic processes of cognition, thinking, problem-solving, etc. are described.

In the complex systems approach, the microscopic level of interacting neurons should be modeled by coupled differential equations modeling the transmission of nerve impulses by each neuron. The *Hodgkin-Huxley equation* is an example of a *nonlinear diffusion reaction equation* with an exact solution of a traveling wave, giving a precise prediction of the speed and shape of the nerve impulse of electric

voltage. In general, nerve impulses emerge as new dynamical entities like ring waves in BZ-reactions or fluid patterns in *nonequilibrium dynamics*. In short: they are the “atoms” of the complex neural dynamics. On the macroscopic level, they generate a cell assembly whose macrodynamics is dominated by order parameters. For example, a synchronously firing cell-assembly represents some visual perception of a plant which is not only the sum of its perceived pixels, but characterized by some typical macroscopic features like form, background or foreground. On the next level, cell assemblies of several perceptions interact in a complex scenario. In this case, each cell-assembly is a firing unit, generating a cell assembly of cell assemblies whose macrodynamics is characterized by some order parameters. The order parameters may represent similar properties of the perceived objects.

In this way, we get a hierarchy of emerging levels of cognition, starting with the microdynamics of firing neurons. The dynamics of each level is assumed to be characterized by differential equations with order parameters. For example, on the first level of macrodynamics, order parameters characterize a visual perception. On the following level, the observer becomes conscious of the perception. Then the cell assembly of perception is connected with the neural area that is responsible for states of consciousness. In a next step, a conscious perception can be the goal of planning activities. In this case, cell assemblies of cell assemblies are connected with neural areas in the planning cortex, and so on. They are represented by coupled nonlinear equations with firing rates of corresponding cell assemblies. Even high-level concepts like self-consciousness can be explained by self-reflections of self-reflections, connected with a personal memory which is represented in corresponding cell assemblies of the brain. Brain states emerge, persist for a small fraction of time, then disappear and are replaced by other states. It is the flexibility and creativeness of this process that makes a brain so successful in animals for their adaption to rapidly changing and unpredictable environments.

1.8 Supplement

Several *basic* methods available for modeling self-organization processes can be applied, such as:

1. Phenomenological kinematic models;
2. Thermodynamical models (e.g., of irreversible thermodynamics);
3. Models of deterministic dynamics (differential equations for the order parameters);
4. Models of stochastic dynamics (*Chapman-Kolmogorov* equation for the probability distributions of order parameters);
5. Models of statistical physics (probability distributions of the microstates of a system).

While the thermodynamics of irreversible processes considers only time average values of physical quantities in nonequilibrium states, the modern theory of nonequilibrium fluctuations takes also deviations from these values into account. *Deterministic* and *stochastic elements* are included, for example, in Haken's concept of *synergetics* and *order parameters*. These two central planes (according to (3) and (4)) are framed by those of (2) and (5).

The modern stochastic theory is concerned with random processes that develop in time. If $x(t)$ is taken as such, a complete description of all statistical properties of $x(t)$ demands specification of an infinite number of *probability densities* $p_n(x_1, t_1; x_2, t_2; \dots; x_n, t_n)$ where $p_n(x, t) dx_1 dx_2 \dots dx_n$ is the joint probability that $x_1 < x(t_1) < x_1 + dx_1$, $x_2 < x(t_2) < x_2 + dx_2$, and so on [33, 34]. It is not possible to deal with generalized problems of this kind in practice and, thus, simplifying assumptions must be additionally introduced. It should be noted that for independent processes, knowledge of $x(t)$ at one time t does not imply knowledge about $x(t')$ at any other time t' . The simplest assumption that can be used for the correlation is that provided by *Markov*, whereby single-step *transition probabilities* form the important quantities in his model. A significant and widely used class of *Markov* models is that of *random walks*, in which case a particle makes random displacements $\mathbf{r}_1, \mathbf{r}_2, \dots$ at times t_1, t_2, \dots [35, 36] (The *excluded-volume random walk*, which is a non-Markovian type, *plays a role in the theory of polymer configurations*). Two main procedural possibilities are available to facilitate solving *Markovian* problems in continuous time, the first procedure leads to the *master* and the second to the *Fokker-Planck* equation. But, both techniques start out from an equation which is, basically, too general to tackle problems of a specific physical nature. The *master* equation which starts out from an observation of the *transition probabilities* in continuous one-dimensional state space can be reduced to a *Fokker-Planck* equation which would be valid for a particular kind of *conditional probability*. The related *Langevin* equation, which was successfully used for the understanding of the Brownian motion, integrates a stochastic element with respect to the dynamics of a system. *It provides a useful background for the understanding of complicated unknown crystallization processes in which extremely large cluster anions—like those mentioned above—formed in solution are involved* [13]. (A typical *Langevin* equation could be given as $mu + yu = F(t)$ where m is mass, u the velocity, yu a *damping force* and $F(t)$ a rapidly *fluctuating random force*). In general, crystal growth starts with a nucleation process, where random fluctuations play a key role—and which is rather complicated in cases where giant cluster species are involved. For the understanding of the whole crystal growth, microscopic and macroscopic theories have to be taken into account.

The important *Fokker-Planck* equation allows us, for instance, to draw some very close and important analogies between phase transitions occurring in *thermal equilibrium*, and certain order–disorder transitions in *nonequilibrium systems of physics, chemistry, biology, and other disciplines*. (Some relevant philosophical aspects are also considered in Chap. 15.) The equation for the *distribution function* of

the laser amplitude A , for instance, ($f(A) = N \exp(-l_1 A [2] - l_2 A [4]; l_{1/2}$ Lagrange parameter) is formally identical to that of the magnetization M as *order parameter* in the case of para/ferromagnets, whereby the corresponding *second order phase transition* can be treated by means of *Landau's theory* [37, 38].

In mathematical models of social dynamics, a socio-economic system is characterized on two levels, distinguishing the micro-aspect of individual decisions and the macro-aspect of collective dynamical processes in a society. The probabilistic macro-processes with stochastic fluctuations can be described by the *master equation of human socio-configurations*.

Each component of a socio-configuration refers to a subpopulation with a characteristic vector of behaviour. Concerning the migration of populations, the behaviour and the decisions to rest in or to leave a region can be identified with the spatial distribution of populations and their change. Thus, the dynamics of the model allows us to describe the phase transitions between global macrostates of the populations. In *numerical simulations* and *phase portraits of the migration dynamics*, the macro-phenomena can be identified with corresponding *attractors* such as, for instance, a stable point of equilibrium (“stable mixture”), two separated, but stable ghettos, or a limit cycle with unstable origin [33].

In economics, the Great Depression of the 1930s inspired economic models of *business cycles*. However, the first models were *linear* and, hence, required *exogenous shocks* to explain their irregularity. The standard econometric methodology has argued in this tradition, although an intrinsic analysis of cycles has been possible since the mathematical discovery of *strange attractors*. The traditional linear models of the 1930s can easily be reformulated in the framework of *nonlinear systems* [34].

According to several prominent authors, including Stephen Hawking, a main part of twenty-first century science will be on complexity research. The intuitive idea is that global patterns and structures emerge from locally interacting elements like atoms in laser beams, molecules in chemical reactions, proteins in cells, cells in organs, neurons in brains, agents in markets etc. by self-organization. But what is the cause of self-organization? Complexity phenomena have been reported from many disciplines (e.g. biology, chemistry, ecology, physics, sociology, economy etc.) and analyzed from various perspectives such as Schrödinger's order from disorder (Schrödinger 1948), Prigogine's dissipative structure [43], Haken's synergetics [44], Langton's edge of chaos [45] etc. But concepts of complexity are often based on examples or metaphors only. It is a challenge of future research to find the cause of self-organizing complexity which can be tested in an explicit and constructive manner. In a forthcoming book, we call it the local activity principle [39].

Boltzmann's struggle in understanding the physical principles distinguishing between living and non-living matter, Schrödinger's negative entropy in metabolisms, Turing's basis of morphogenesis [46], Prigogine's intuition of the instability of the homogeneous, and Haken's synergetics are in fact all direct manifestations of a fundamental principle of locality. It can be considered the complement of the second law of thermodynamics explaining the emergence of order from disorder instead of disorder from order, in a quantitative way, at least for reaction diffusion systems.

References

1. Siegel RW (1993) Exploring mesoscopia – the bold new-world of nanostructures. *Phys Today* 46:64
2. Müller A (1994) Supramolecular inorganic species: an expedition into a fascinating, rather unknown land mesoscopia with interdisciplinary expectations and discoveries. *J Mol Struct* 325:13
3. Ball P (1994) *Designing the molecular world*. Princeton University Press, Princeton
4. Feynman R (1961) There's plenty of room at the bottom. In: *Miniaturization*, vol 282., pp 295–296
5. Bertaina S, Gambarelli T, Mitra B, Müller A, Barbara B (2008) Quantum oscillations in a molecular magnet. *Nature* 453:203–206
6. (a) Mainzer K (2007) *Thinking in complexity: the complex dynamics of matter, mind, and mankind*, 5th edn. Springer, Berlin; (b) Nicolis G, Prigogine I (1989) *Exploring complexity: an introduction*. Freeman & Co. New York; (c) Nicolis G Prigogine I (1977) *Self-organization in nonequilibrium systems: from dissipative structures to order through fluctuations*. Wiley, New York; (d) Ebeling W, Feistel R (1994) *Chaos und Kosmos: Prinzipien der Evolution*. Spektrum, Heidelberg; (e) Haken H, Wunderlin A (1991) *Die Selbststrukturierung der Materie: Synergetik in der unbelebten Welt*. Vieweg, Braunschweig; (f) Cohen I, Stewart I (1994) *The Collapse of chaos: discovering simplicity in a complex world*. Penguin, New York
7. (a) Müller A (1991) *Nature* 352:115; (b) Müller A, Rohlfing R, Krickemeyer E, Bögge H (1993) *Angew Chem* 105:916; (c) (1993) *Angew Chem Int Ed Engl* 32:909; (d) Müller A, Reuter H, Dillinger S (1995) *Angew Chem* 107:2505; (e) (1995) *Angew Chem Int Ed Engl* 34:2328; (f) Baxter PNW (1996) In: Atwood JL, Davies JED, MacNicol DD, Vögtle F, Lehn J.-M (eds) *Comprehensive supramolecular chemistry*, vol 9, chap 5. Pergamon/Elsevier, New York, p 165
8. Müller A, Rohlfing R, Döring J, Penk M (1991) *Angew Chem* 103:575–577; (b) (1991) *Angew Chem Int Ed Engl* 30:588–590
9. Fischer KH, Hertz JA (1991) *Spin glasses*. Cambridge University Press, Cambridge
10. Gatteschi D, Sessoli R, Villain J (2006) *Molecular nanomagnets*. Oxford University Press, Oxford, p 299
11. (a) Vainshtein BK (1994) *Fundamentals of crystals: symmetry, and methods of structural crystallography*, 2nd edn. Springer, Berlin; (b) Zachariasen WH (1967) *Theory of X-Ray diffraction in crystals*. Dover Publications, New York
12. Lehn J.-M (1995) *Supramolecular chemistry: concepts and perspectives*. VCH, Weinheim
13. Müller A, Meyer J, Krickemeyer E, Beugholt C, Bögge H, Peters F, Schmidtman M, Kögerler P, Koop MJ (1998) *Chem Eur J* 4:1000–1006
14. Pope MT, Müller A (eds) (1994) *Polyoxometalates: from platonic solids to anti-retroviral activity*. Kluwer, Dordrecht
15. The idea of a quantum computer was initiated by R Feynman (1982) *Simulating physics with computers*. *Int J Theor Phys* 21:467–488
16. Bell JS (1964) On the Einstein-Podolsky-Rosen-Paradoxon. *Physics* 1:195–200
17. Ekert A, Gisin N, Huttner B, Inamori H, Weinfurter H (2000) Quantum cryptography. In: Bouwmeester D, Ekert A, Zeilinger A (eds) *The physics of quantum information. Quantum cryptography, quantum teleportation, quantum computation*. Springer, Berlin, chapter 2.4
18. Shor PW (1997) Polynomial-time algorithms for primitive factorization and discrete logarithms on a quantum computer. *SIAM J Comput* 26:1484–1509
19. Rivest RL, Shamir A, Adleman L (1978) A method for obtaining digital signatures and public-key cryptosystems. *Comm ACM* 21:120–126
20. Deutsch D (1985) Quantum theory, the Church-Turing principle and the universal quantum computer. *Proc R Soc Lond A* 400:97–117
21. Deco G, Schürmann B (2001) *Information dynamics: foundations and applications*. Springer, New York

22. Mainzer K (2007) *Thinking in complexity: the complex dynamics of matter, mind, and mankind*, 5th edn. Springer, Berlin, 199 pages
23. Press WH (1978) Flicker noise in astronomy and elsewhere. *Comment Astrophys* 7:103–119
24. Mandelbrot BB (1997) *Multifractals and 1/f noise*. Springer, Berlin
25. Gnedenko BV, Kolmogorov AN (1954) Limit distributions for sums of independent random variables. Addison-Wesley, Cambridge
26. Weidlich W (1989) Stability and cyclicity in social systems. In: Cambel AB, Fritsch B, Keller JU (eds) *Dissipative strukturen in integrierten systemen*. Nomos Verlagsgesellschaft, Baden-Baden, pp 193–222
27. Luhmann N (1997) *Die Gesellschaft der Gesellschaft*. Suhrkamp, Frankfurt a.M
28. Bachelier L (1900) *Théorie de la spéculation*, Dissertation, Annales Scientifiques de L'Ecole Normale Supérieure 17:21–86
29. Pareto V (1909) *Manuel d'Economie politique*. V. Giard and E. Brière, Paris
30. Förstl H (ed) (2007) *Theory of mind*. Neurobiologie und Psychologie sozialen Verhaltens. Springer, Berlin
31. Freeman WJ (2004) How and why brains create sensory information. *Int J Bifurc Chaos* 14:515–530
32. Dreyfus HL (1982) *Husserl, intentionality, and cognitive science*. MIT Press, Cambridge
33. (a) Mainzer K (2007) *Thinking in complexity: the complex dynamics of matter, mind, and mankind*, 5th edn, chap 8.2. Springer, Berlin; (b) Weidlich W (1994) Das Modellierungskonzept der Synergetik für dynamisch sozio-ökonomische Prozesse. In: Mainzer K, Schirmacher W (eds) *Quanten, Chaos und Dämonen*. B1 Wissenschaftsverlag, Mannheim, p 255
34. (a) Goodwin RM (1990) *Chaotic economic dynamics*. Clarendon Press, Oxford; (b) Lorenz H.-W (1989) *Nonlinear dynamical economics and chaotic motion*. Springer, Berlin; (c) Mainzer K (2007) *Thinking in complexity: the complex dynamics of matter, mind, and mankind*, 5th edn, chap 7. Springer, Berlin
35. Oppenheim I, Shuler KE, Weiss GH (1991) Stochastic Processes. In: Lerner RG, Trigg GL (eds) *Encyclopedia of physics*, vol 2. Wiley VCH, New York, p 1177
36. Feynman RP, Leighton RB, Sands M (1966) *The Feynman lectures on physics*. Vol. I. (chapter 6: probability). Addison-Wesley, Reading
37. Landau LD, Lifschitz EM (1987) *Lehrbuch der theoretischen physik*, Bd. 5: statistische physik. Teil 1, 8. Aufl. Akademie-Verlag, Berlin
38. See also book by Haken et al. in ref. 6
39. Mainzer K, Chua LO (2012) Local activity principle. The cause of complexity and symmetry breaking. Imperial College Press, London, chap. 1
40. Lévy P (1925) *Calcul des probabilités*. Gauthier-Villars, Paris
41. Mainzer K (2007) *Der kreative Zufall. Wie das Neue in die Welt kommt*. C. H. Beck, München, Chapter VII
42. Mainzer K (2008) The emergence of mind and brain: an evolutionary, computational, and philosophical approach. In: Banerjee R, Chakrabarti BK (eds) *Models of brain and mind*. Physical, computational and psychological approaches. Progress in brain research, vol 168. Elsevier, Amsterdam, pp 115–132
43. Prigogine I (1980). *From being to becoming*. Freeman
44. Haken H (1983) *Advanced synergetics: instability hierarchies of self-organizing systems and devices*. Springer, New York
45. Langton CR (1990) Computation at the edge of chaos: phase transitions and emergent computation. *Physica D* 42:12–37
46. Turing AM (1952) The chemical basis of morphogenesis. *Philos Trans R Soc Lond B* 14 237(641):37–72

Chapter 2

Emergence, Breaking Symmetry and Neurophenomenology as Pillars of Chemical Tenets

Andrea Dei

Abstract Since Heraclitus and Parmenides human thought was based on the research of the first principles governing the world. This necessity requires the adoption of an invariance concept which in turn is described by laws and theories defined by symmetry properties. Chemistry does not follow this paradigm, because of its intrinsic interest in inducing a break in the order towards the emergence of a new order through a symmetry breaking process. Indeed chemistry is basically the study of matter and its transformations. The manipulation of the matter always requires the adoption of a realistic approach, which is strongly contrasting with the definition of an absolute truth. The minds of chemists are continuously addressing the verification of the potentialities of Nature and these potentialities are always referred to a reference context defined by other chemical compounds. When these properties are considered from another point of view, they lose a part of their significance. Therefore chemists adopt a divergent pragmatism, which is rather clear from the neurophenomenological approach they use in the interaction with quantum world. In fact the approach discards the study of the essence of the real things, since only the knowledge of the relationships between the things is necessary. In this sense the answer the chemists obtain from their investigation of the microscopic properties of matter must be always considered as the resultant of the interactions of the microscopic object with its environment. A few examples concerning the decay behavior of magnetic systems in metastable states are discussed.

A. Dei (✉)

LAMM Laboratory, Dipartimento di Chimica, Università di Firenze, UdR INSTM,
Via della Lastruccia 3, 50019 Sesto Fiorentino (Firenze), Italy
e-mail: andrea.dei@unifi.it

2.1 Introduction

Scientists believe in the simplicity of nature. For this reason science development was mainly addressed to detect the regularities of the experimental phenomenology. This regularity has the strong advantage of the possible translation in a mathematical logic then allowing the possibility of communicating and teaching the observed experimental findings by using a so called objective tool. I wish to stress that this approach ritualizes the optimism of the scientist and that there are three main aspects involved in this statement. The first is the concept of symmetry: the simplicity of nature can be interpreted by means of geometric models or linear equations defining theories. We shall examine this point later. The second is the concept of objectivity, based on the presumption of the identification of the physical reality with the phenomenology. This is misleading, if the attributed objective is not clearly used as synonymous of verifiable. The third and final aspect is that the presumed regularity of the natural events may be associated with the religious beliefs, and is often interpreted as expression of divine laws. It is obvious that, if the mystic component dominates, the multiplicity of natural events is not important, as it occurred in the eastern approaches. But it is also true that even if this does not occur, some insidious philosophical perspectives can be introduced, as Avicenna made in his *The Book of Healing*. The philosophical principles and the natural laws – he argued – are eternal and unchangeable and cannot be contradicted by some experiences because of the lack of perfection of the world. This view was adopted by many cultures including Scholastics and I am surprised of finding it today too in the arguments of many academicians.

Chemistry is a weird science where the canon rules of simplicity and complexity are viewed as intrinsic coexisting denominators. If this proposition is shared, the prerequisites mentioned above do not fulfil the chemical world. The development of chemical research in its own different fields requires that the usual philosophical approaches must be modified and improved. This as an example is the case of the characterization of molecular systems in mesoscopic scale. A limited number of findings, which has been obtained in the Florence Laboratory for the study of magnetic materials (LAMM), will be discussed here with the aim of supporting this statement.

2.2 The Character of the Cognitive Approach

The basic approach to the knowledge requires the self-consciousness which determines the comprehension of the empirical data. Since pre-Socratics the phenomenon is interpreted as the entanglement of the perception of data and the self-consciousness of the observer, according to his own specific ordering rational principles. *Science exists because this process is undefined*. Thus theories can be formulated as resulting from the interpretation of phenomenology through an

overlap of the external inputs with the internal self-consciousness of the observer. This view reminds the Plato thought of the cognitive process. It should be mentioned that subjective comprehension of the external input may often provide the subjective output in the sense of decision or action. In summary, the observer selects the inputs from the environment, neglecting other potential inputs and this choice is highly individual. These inputs are interpreted in an individual fashion since they depend on the previous inputs (i.e. on the history of the observer) and this interpretation is irreversible, thus making life a continuous learning process. Finally they provide the basis for the causal action of the observer. It should be stressed out that the observer does not know the external reality world. He registers by senses the inputs and decides the necessary appropriate outputs. This is the neurophenomenological approach to the knowledge as formulated by Bateson, Maturana and Varela [1, 2]. In this sense this collection of inputs-outputs provides the network of the knowledge according to view of complexity (i.e. *self-organization of critically interacting components*), the output towards the environment giving rise to a new input which influences the environment. However it should be mentioned that complexity science [3–7] adopts another concept of subjectivity of the knowledge with respect to that, generally speaking, by Plato, since it is considered a tool used by an intelligent agent to help himself to achieve his personal goals. This consideration is particularly important for what concerns the role of the chemist.

If the knowledge is subjective, which is the meaning of an objective explanation of the phenomenology? An explanation can be defined objective when there exists the possibility of teaching it to other people in such a way that these people, according to their own culture, might understand it and then operate following it. The subjective character of the human knowledge can be considered also the fundament of Galileo's scientific revolution whose thought followed the neoplatonism which characterised the culture in Florence in the Renaissance. It is rather surprising to realise that this feeling disappeared in the culture of modernity. It may be considered obvious that the anthropocentric view of Francis Bacon which played a determining role. In a similar way the concept of science as associated to a synthetic *a priori* claim was formulated by Kant. Following this definition it supports the idea of absolute truths. Unfortunately for him nobody has firmly stressed that the absolute truth concept always requires the existence of a postulate and that the *a priori* conceptions of space and time depend on the nature of the living species and then it should be defined *a posteriori* claim, as shown by Lorenz two centuries later. The concepts of the utility and absolute truth may provide some explanations of the triumph of the quest of objectivity and determinism in the development of science. Therefore the success achieved by the mechanistic tools justifies the reasons of its epistemological stability.

The theory of complexity concerns a new approach of analysing the phenomenological world [3–6]. However, it is receiving less consideration by the scientists than it deserves. The reason of this difficulty probably resides in its own intrinsic generality which is often is believed too unfocused, vague and elusive to be considered a true basis to be adopted by in a scientific perspective. This is in particular true in physics and chemistry, whereas the complexity paradigm

looks particularly appealing in other disciplines like biochemistry, cell biology, psychology or sociology. The reasons of the different feelings experienced by researchers are rather easy to be explained.

Until the half of twentieth century the axioms of scientific methodology were dictated by the mechanism of the Newtonian thought which followed the Descartes proposal of reductionistic analysis. The success of this view lies in its own simplicity: the complexity of the world is only apparent and can be considered as resulting from the overlap of many different simple events. Therefore to understand the physical world means to analyse it in its basic constituents and to establish the laws which control their mutual relationships. Personally I stress that Feynman still in 1960 used the example of the world as a huge chessboard where the reciprocal position of the chess changes by obeying simple rules. Apparently the comparison he used is more or less the clockwork conception of Descartes. This view deeply influenced the development of the epistemology of the scientific thinking because of its simplicity, coherence and intuitive rationality. The discovery of quantum world reinforced this philosophy. The matter was found to be constituted by the same elementary particles and the different character of substances is due to the different reciprocal interaction and space arrangement of the constituent particles. Therefore changes, transformation and phenomena arise from the change of the interactions and positions of the same particles. In other words the physical phenomenology is determined by particular arrangements in the space and in the time and these arrangements are simply governed by a logic of cause-effect. The inherent simplicity of the approach therefore consists in designing experiments in which it is possible to understand the causal elements underlying the behaviours of the physical world. Therefore for sake of simplicity it is necessary to consider isolated systems. This deterministic view, which constitutes the basis of Newtonian thinking, did not change when the linear laws describing the simple motion of one particle were used for the statistical description of a system of particles, the space-time concept was redefined and normalized by relativity and the quantum mechanics substituted the classical one. In every case any phenomenology is regular and predictable because it's ontologically materialistic and its evolution, as determined in the absolute space time dimensions, obeys to linear laws. Whether the linearity of these laws would be just the representation of the human cognitive approach and the scientific activity should not concern any self-consciousness, purpose, aim, creativity, free will or decision of the researcher, since his task is devoted only to the detection of the pre-existing hidden properties of the matter, these arguments do not deserve any consideration.

2.3 Why Chemistry Is different?

There exists a basic misconception about the role of Chemistry in the development of Science [8]. This is a personal feeling but the following arguments well support this suggestion. The outstanding contribution of chemistry to scientific thought

found its own roots in demonstrating the dependence of the properties of matter on the nature of the constituents and their reciprocal interactions, rather than on macroscopic parameters like mass, length or temperature used in classical physics. This specificity, like that exhibited by emission or absorbance spectra, lead to the introduction of the operator concept, to the development of quantum mechanics and therefore to the method for understanding the different atomic interactions. However the largest part of modern philosophy of science has been written by the followers of logical positivism, *i.e.* the disciples of the philosophically minded physicists Schlik, Carnap, Hempel, Reichenbach, etc., past members of the Vienna and Berlin Circles. For this reason these disciples, and after them their disciples, have perpetuated the thought that the basis for the philosophy of science is theoretical physics. This misconception is a common belief in the academic world. In that sense the scientific world is conceived as a pyramid, the humanistic and social sciences constituting the basis and physics the apex. Following this view, chemistry is only a branch of physics and molecular chemistry is only an exercise in quantum mechanics. The whole concept can be summarised in the famous Dirac statement: [9]

The underlying physical laws necessary for the mathematical theory of a large part of physics and the whole of chemistry are thus completely known, and the difficulty is only that the exact application of these laws lead to equations much too complicated to be soluble.

The properties of macroscopic matter are related to the properties of its microscopic units. This is in agreement with the statement that the whole is nothing but the sum of its parts. The problem is what “the sum of its parts” means. Following Dirac, molecular properties are defined by the laws of quantum mechanics, although the application of these laws is much too complicated. But this is relatively unimportant since in principle a Laplace demon could easily solve them. For this reason the philosophers claim that Chemistry is a minor and unripe science, since the whole chemistry can be derived from the more comprehensive first principles of quantum mechanics. Therefore they are used to describe chemistry in terms of ontological or epistemological reductionism, the difference between the two approaches being unimportant in this context [10–12].

Somebody argues that this is an oversimplification taking into account the fact that the properties of a molecule are rather different from those of constituent atoms. Therefore the concept of emergent properties, *i.e.* the whole is something more than the sum of its parts, is introduced. However it is weird that many people define “emergentism” as opposite to reductionism. In fact if one assumes that the properties of molecules arise from interactions between the constituent atoms, it is obvious that emergentism is nothing but epistemological reductionism. I think that this conclusion is true also if the hypothesis of the existence of an asymmetric relationship between the molecular properties and the constituents properties is made. I think, however, that the basic mistake is that of considering physics and chemistry in the framework of the same context.

Chemistry basically is the study of matter and its transformations. Chemists are used to interpret their world in terms of representations but they are aware of this limit. Therefore even if they use different methods for representing matter, they do

not care about the difference between an absolute law and an operational model [13,14]. This occurs because in the manipulation of matter it is always necessary to adopt a realistic approach, which is in strong contrast with the classic critical path involved in the hypothesis-falsification processes. Indeed the planning and description of a new synthesis do not concern the definition of an absolute truth or the formulation of a law. The work of chemists involves only the determination of the microscopic constituents of the matter they prepare and they want to use this knowledge for synthesising new compounds, by obeying to a paradigm of purposes, decisions and creations. Their minds are continuously addressing the verification of the potentialities of Nature. In that sense the constituent units are considered only a tool or an instrument for creation purposes. Michael Faraday neglected the atomistic hypothesis of Dalton because of this feeling against matter being manipulated. Therefore for a chemist it is rather unimportant if the properties of a compound should be interpreted following classical physics or quantum mechanical models. In the same way it is rather unimportant if the transformations involve open or closed systems. These properties must be always referred to a context defined by other chemical compounds and this context cannot be shared with physics or biology. Indeed if this such an attempt at sharing is made, these properties become less significant. Watching Botticelli's Primavera paint, one might consider important to know whether the crystal lattice of the silver in the pencil, used by the artist for designing the draft, was cubic or hexagonal. But the aesthetic message involving the artist and the observer is basically different. The big difference between chemistry and theoretical physics lies in the different realistic purpose of the scientific research. In this sense the need of a well definite philosophical approach is lacking for a chemist. In the framework of logic positivism the basic event must be referred several times to the context of the discovery, without any need of context of justification.

2.4 Chemistry in the Context of the Science of Complexity

In both chemistry and physics there are therefore considerable biases towards simplification, thus ignoring the multidimensional character of the physical world. The usual statement that "chemistry finds its fundamentals in the laws of many-body physics" is false if it means that chemistry is nothing else that applied physics. In a similar way biology is not applied chemistry and sociology is not applied psychology. All the disciplines operate in a well-defined context.

The claimed pyramid of the supporters of the science of the complexity is a not necessary forcing prerequisite, but rather a search of methodological generalization. There are two mean reasons supporting this thought. The first is the awareness of the researchers about the limits of the whole scientific perspective as developed until the half of the past century. The scientific perspective until this period was mainly addressed to the idealization of the symmetry of the physical system under investigation or to the reversibility of the process. In agreement

with other commentators, I want to assign the kick-off of the new perspective to the 1948 article of Warren Weaver [15]. In this contribution Weaver summarized the development of the Science in three steps: (i) the search of an explanation of the phenomenology through linear equations relating two observables ($y = kx$), (ii) the use of statistical methods for describing systems constituted by a large number of non interacting particles (e.g. gas) (iii) the development of methods for describing systems constituted by mutually interacting particles. He defined these systems as characterized by an organized complexity and predicted that their characterization would be the main aim of the future scientists. It is obvious that many real situations concerning different disciplines share the same problem and the merit of the Warren proposition probably was that of unifying the perspectives of scientists operating in different fields. It is worth mentioning that other basic contributions like the systemic approach that Bogdanov, biologist and economist, formulated at the beginning of twentieth century in *Tektology*, and later Von Bertalanffy collected in *General Systems Theory* without mentioning him [16], the feed-back concept introduced by Wiener [17] and that concerning the autopoiesis of living systems by the Santiago school (Maturana and Varela) [2] are to be considered determining bricks in the development of the new scientific philosophy.

The second reason is of consequence to this omen and, in practice, it was given by the possibility of modern computer technology treating and solving with reasonable approximation complex nonlinear problems. Of course these mathematical methods can be in turn applied to solve the same problems required in the different fields.

Concepts like spontaneous emergence, which is familiar to chemists, is used to observe the irreversible transformation of matter at will. Emergence means the death of an old order and the birth of a new one. If this irreversible process can be described by means of mathematical methods by introducing a terminology using the expressions “order parameters” or “bifurcation schemes”, in my opinion there is no significant enrichment to the depth of the scientific observation, but it is also true that these expressions are not thoughtless slogans. In this sense, whenever believed that these concepts allow the possibility of sharing a common mathematical approach for analysing the observed results, there is no *caveat* to their use.

In a similar way the concept of broken symmetry deserves consideration. Symmetry means the invariance of a chemical structure with respect to spatial or time coordinates. More in general symmetry means the invariance of a theory with respect to its coordinates by a mathematical transformation group. It should be remembered that the exciting development of the natural sciences in the last two centuries has been preceded by the extraordinary development of mathematics in the same periods. Mathematics with Galois and Abel, Klein and Poincaré, Noether and Kolmogorov provided the concepts for getting out from the newtonian science. In particular the concept of symmetry and transformation groups triggered an amazing evolution in the scientific thought. The fact that many natural laws can be obtained by exploiting the property of symmetry is also, today, a matter of surprise and meditation. This awareness induced Einstein and many physicists to invest the logic process used in formulating theories. The usual deductive process of formulating a law by analysing the experimental data was substituted by an inductive process

based on the formulation of a theory built on some symmetry property with *a posteriori* justification of experimental data. This approach can be considered the obvious sublimation of the conservative and deterministic conception of natural world the scientists adopted in the first centuries of scientific revolution. In practice, the concept of symmetry well fitted and justified the harmony of any linear causality principle. However it is often found in chemistry that molecules and their collection in condensed phase adopt a lower symmetry than predicted by the theoretical expectations.

In the previous workshops of this series concerning complexity in chemistry [18, 19], in addition to the amazing symmetry and emergent properties characterizing the Platonic structures of some polyoxometallates, attention has been focused on the spontaneous symmetry breaking processes justifying the origin of chiral molecules and its biological consequences since biological information is inherently antisymmetric. But from a chemical point of view I think that the two main topics concern the origin of the entropy, with its inherent consequence of the arrow of time, and the inability of quantum theory to provide an exhaustive framework chemists may use for interpreting their experimental findings. I am arguing with this statement that the pillars of chemical thought lying in the possibility of transformation of matter and the interpretation of its properties can be drastically improved.

These two topics cannot be interpreted on the basis of classical or quantum physics, but it is possible to provide views appropriate for the chemist prejudice once adopted the philosophy of science of complexity. Classic and quantum physics are defined as symmetric with respect to time inversion. However the chemical reactions are irreversible. They approach their chemical equilibrium state by proceeding in only one direction and their reversion does not pertain to the observed phenomenology. Following Prigogine [20] time has the status of mathematical operator, which delivers two subsystems representing the future and the past. The time operator allows only physically asymmetric states and the second law of thermodynamics involves this symmetry breaking process with the evolution of the universe in the sense of an increase of entropy. Therefore the arrow of time is an example of downward causality imposed by the expansion of the universe. No upward causality is operative according to reductionist view, since it is not possible to predict the future of a system taking into account the properties of the constituent particles. The entropy growth can be conceived as the result of a symmetry breaking process.

2.5 Quantum Properties: Towards a New Self-Consciousness

The second topic concerns the description of quantum mechanics we adopt for interpretation of our experiments. Quantum mechanics provides a satisfactory explanation of all the phenomenology we are dealing with. A quantum system is described in its evolution by the deterministic linear Schroedinger equation

$$i\hbar(2\pi)^{-1}\delta|\psi\rangle/\delta t = \mathbf{H}|\psi\rangle \quad (2.1)$$

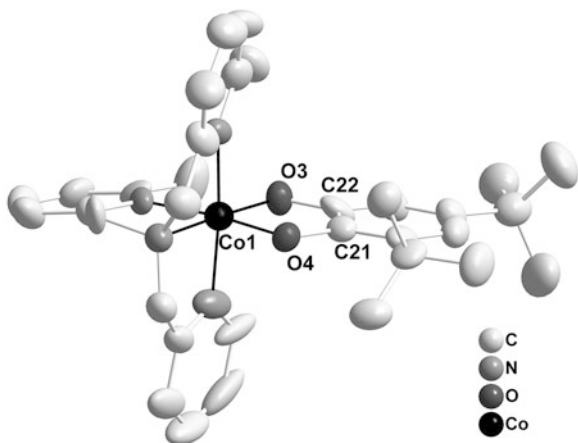
which provides via its Hamiltonian, \mathbf{H} , once the initial state of a quantum system is known, the possibility of determining the system state at an arbitrary time. The equation is basically similar to those holding in classical mechanics, but it does not provide any hint about the border occurring between the classical and quantum worlds. In addition, the equation defines the evolution of the system into a state containing many alternatives according to the principle of superposition, which is a fundamental aspect of the Schroedinger equation. However these alternatives do not exist in our measurements, since in practice we perceive only one of the possible alternatives and we obtain always the same result in our measurement. This led some physicists to doubt the significance of the theory especially with respect to its completeness. The key point is the jump of the description of the quantum system, usually indicated as the reduction or collapse of the vector space or of the wave packet, from a multiplicity of answers to the one we detect in our measurement. The matter therefore is whether quantum mechanics is a subjective projection of our self-consciousness or not. There has been a big debate about, starting from the Copenhagen interpretation [21] to the “Many Worlds (or Universes) Interpretation” [22] of Hugh Everett III. Personally I think that the original answer of the Copenhagen school is a good starting point for the discussion. In this interpretation there exists a division between the quantum world and the classical world. However a classical apparatus is always necessary for performing a measurement and this may justify why all the measurements yield the same results. The limit of this view lies in the necessity of the division. It is rather difficult to accept that the laws which are operative for the micro systems cannot hold in the macroscopic world. However following Zeh and Zürek [23–25] it should be emphasized that macroscopic systems are never isolated by their environments and therefore the Schrödinger’s equation, which is defined for a closed system, does not hold. Therefore for an open system the quantum coherence intrinsic in the superposition principle is lost and our measurements concern only the answers allowed by the quantum decoherence processes.

There are a lot of examples that can support this proposition. I find the results we obtained in our laboratory constitute a compelling example of this point of view. The discovery that some metal complexes may undergo redox isomeric interconversion upon irradiation at cryogenic temperatures opened a challenging topic in materials science because of the potential application of the phenomenon for designing memory devices [26–31]. In particular, we are investigating some cobalt-catecholato derivatives that exhibit a photoinduced interconversion



where L is an ancillary ligand, involving an intramolecular electron transfer between the coordinated catecholato and the metal acceptor. The structure of a simple 1:1 cobalt-catecholato complex undergoing this redox isomeric interconversion is sketched in Fig. 2.1.

Fig. 2.1 Molecular structure of the cationic moiety of $[\text{Co}(\text{Me}_2\text{tpa})(\text{DBCat})]\text{PF}_6$ (Me_2tpa = bis(6-methyl-(2-pyridylmethyl)) (2-pyridylmethyl)amine, DBCat = 3,5-di-*tert*-butylcatecholato). Hydrogen atoms have been omitted for clarity (See ref. [31])



The process is characterised by a large variation of the magnetic properties since the Co^{III} -Cat is diamagnetic and the Co^{II} ion is in a high-spin (*hs*) configuration and the semiquinonato (SQ) ligand is a radical species. The phototriggered electron transfer process occurs with a well defined mechanism, which couples the electronic ground state of the chromophore with its electronic excited states. The relaxation of the photoinduced metastable Co^{II} -(SQ) excited state to the ground state may involve several mechanisms, like internal conversion, intersystem crossing, vibrational relaxation and so on. Quantum mechanically, if the decay process occurs through intersystem crossing, as in the present case, we expect to have an activated radiationless transition between different electronic states of the chromophore. If the wave functions Ψ_i and Ψ_j describing the initial and the final electronic states, the rate constant k of the process is given by the following relationship

$$k = (4\pi^2/h)|V|^2G \quad (2.3)$$

where V is the electronic coupling matrix element $\langle \Psi_i | H | \Psi_j \rangle$ (H being the total electronic hamiltonian), which depends on the overlap between the wave functions Ψ_i and Ψ_j , and G is the thermally averaged nuclear Franck-Condon vibrational overlap factor. At high temperatures G is proportional to $\exp(-\Delta E/kT)$ and then the relaxation rate follows the Arrhenius law with the same dependence. At low temperature where only the ground state of Co^{II} -SQ species is populated, a temperature independent relaxation rate should be observed. In both cases, a tunnelling mechanism controls the nonadiabatic radiationless relaxation decay.

In principle the relaxation decay should follow a first order kinetics. However it is found that the relaxation rate cannot be fitted with the relationship,

$$\gamma(t) = \gamma(0)e^{-k(T)t}$$

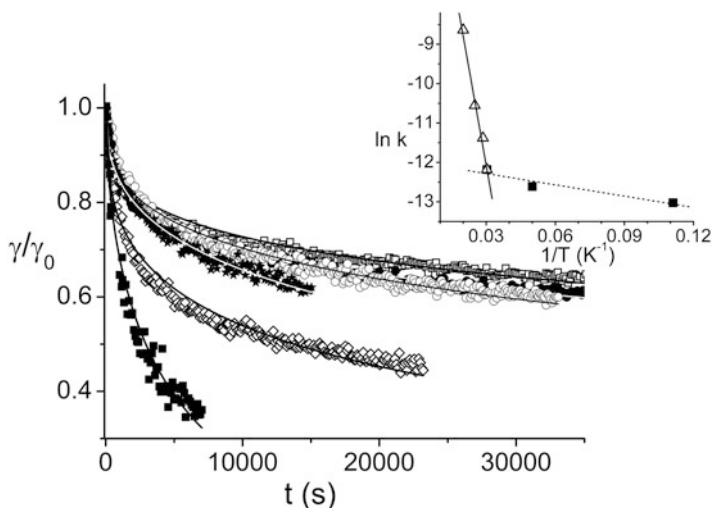


Fig. 2.2 Time evolution of the metastable photoinduced fraction of $\text{Co}(\text{Me}_2\text{tpa})(\text{DBCat})\text{PF}_6$ at 9 K (*empty squares*), 20 K (*full circles*), 33 K (*empty circles*), 35 K (*stars*), 40 K (*rhombs*) and 50 K (*full squares*) and the corresponding best fit parameters. The inset gives the corresponding Arrhenius plot, with two different regimes clearly distinguishable. See text for best fit parameters. (From ref. [30])

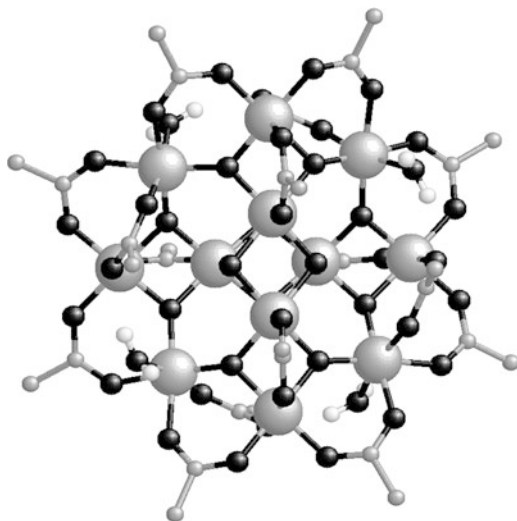
where $\gamma(0)$ and $\gamma(t)$ are molar fraction of the metastable species, when the irradiation is switched off and after a time t , respectively. This relationship holds if the decaying molecules interact in the same ways with the surrounding molecules and then the ΔE characterising the G factor and the rate constant are the same for all the molecules of the metastable species. Since the surroundings change continuously during the decay, the system is described by a set of ΔE values and a set of rate constants changing with time. From a mathematical point of view a reasonably approximate fitting of the observed decay experimental data is made by introducing a β exponential, thus obtaining a stretched exponential relationship

$$\gamma(t) = \gamma(0)e^{-k(T)t^\beta}$$

However in a complexity perspective we can describe the process through an evolution of the system towards an attractor with an increasing adaptation to the environment with a contemporary co-evolution of the surroundings. The overall process should be more properly described in terms of quantum coherence between the vibrational states and quantum decoherence with the environment.

A support to this view is obtained by plotting the experimental $\ln K(T)$ vs $1/T$. A plot of $\ln k = \ln(\tau^{-1})$ vs $1/T$ (τ being the relaxation time) indicates that the relaxation rate does not follow a simple Arrhenius law as expected for a single thermally activated process (Fig. 2.2).

Fig. 2.3 Molecular structure of the SMM archetype $\text{Mn}_{12}\text{O}_{12}(\text{O}_2\text{CR})_{16}(\text{H}_2\text{O})_4$

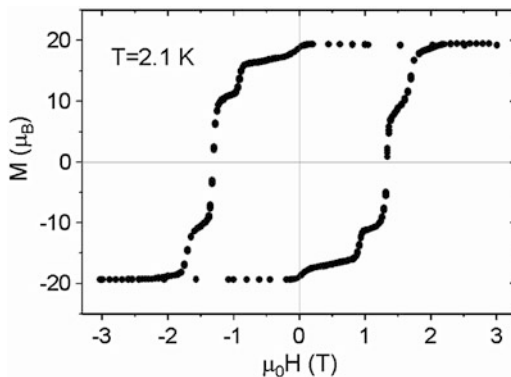


As a first approximation we might however find two thermally activated relaxation regimes characterised by very different parameters, one between 5 and 20 K and another one at higher temperatures (35–50 K). A tentative fit to the Arrhenius law ($\tau = \tau_0 \exp(-E_a/k_B T)$, where τ_0 is the relaxation time at infinite temperature and E_a is the activation barrier for the relaxation) gives in the low temperature region $\tau_0 = 5 \times 10^5$ s and $E_a = 9 \text{ cm}^{-1}$ and in the high temperature region $\tau_0 = 4.5$ s and $E_a = 242 \text{ cm}^{-1}$. It can be therefore suggested in the low temperature region a tunnelling mechanism is operative *but it is emphasized that a lattice-phonon assisted mechanism can be active as supported by the low E_a value*. This term can be attributed to quantum decoherence and once again supports the idea of a description of the decaying complex and its environment as involving *two closely coupled coevolving systems*. In the high temperature region the observed E_a value well agrees with the energy associated to the total-symmetric Co-O vibrational breathing mode, which is expected to be of the order of 300 cm^{-1} .

A most significant example is provided by the so called Single Molecule Magnets, the $[\text{Mn}_{12}\text{O}_{12}(\text{O}_2\text{CR})_{16}(\text{H}_2\text{O})_4]$ being the archetype (Fig. 2.3). As it is well known, this compound displays a slow magnetization relaxation below its blocking temperature without any perturbing magnetic field [32–37].

This means that the cluster may function as a single domain nanoscale magnetic particle. This behaviour results from the fact that the compound is characterised by a large ground-state spin combined with a huge Ising-type magnetic anisotropy, i.e. negative zero-field splitting. Under these conditions, the cluster mimics bulk behaviour because the magnetization has to undergo a large energy barrier to invert its direction. For this reason at cryogenic temperatures the relaxation times are extremely long and, in practice, the molecular system behaves as a nano-particle below its superparamagnetic limit. It is also important to stress that this molecule shows the same properties either in the condensed phase or a diluted state.

Fig. 2.4 Magnetization hysteresis loop measured on single crystal of $\text{Mn}_{12}\text{O}_{12}(\text{O}_2\text{CR})_{16}(\text{H}_2\text{O})_4$ at 2.1 K between magnetic fields of ± 5 T (From ref. [32,33])



The above considerations clearly suggest that this molecule provides us with an example of molecular nanomagnetism obtained by a bottom-up assembly process. Indeed it can be synthesised directly in the labs using the appropriate metal ions and carboxylate ligands. However the mutual relationships existing within the cluster of spins promote a top-down induced physical behaviour. Indeed, this compound shows the classical properties of magnetization hysteresis and combined with quantum properties like quantum tunneling of the magnetization through the energy barrier induced by the huge anisotropy. The key point is that the observed slow relaxation behaviour is due to its peculiar molecular properties. In this sense the SMMs are fundamentally different from classic bulk magnets, whose properties are due to long-range cooperative effects between the paramagnetic centres in the condensed phase [33–35].

The most relevant property of these compounds arises from the fact that their magnetization cannot undergo thermally activated relaxation processes at cryogenic temperatures because of a huge free energy barrier induced by anisotropy. However, in these conditions a temperature-independent relaxation process is detected and, therefore, it is a reasonable assumption that fluctuations induce a tunnelling process [32]. Indeed low temperature experiments clearly demonstrate the existence of quantum mechanical tunnelling of magnetization. In an applied magnetic field the magnetization shows hysteresis loop with a distinct staircase structure: the steps occur at values of the applied field where the energies of different collective spin states of the manganese cluster coincide (Fig. 2.4).

At these special values of the field relaxation from one spin state to another is enhanced. However at intermediate values of the field relaxation occurs presumably by coupling with the environment through a quantum decoherence mechanism as observed above for redox isomers (Figs. 2.5 and 2.6).

The relaxation dynamics are those of a non-adiabatic mechanism but, more important, at this stage they can be clearly interpreted in terms of a quantum mechanical model, thus supporting the existence of a magnetic field-induced separation between the ground state $S = 10$ energy levels. The problem is that the energies of the transitions are relatively small, of the same order of magnitude as those of the

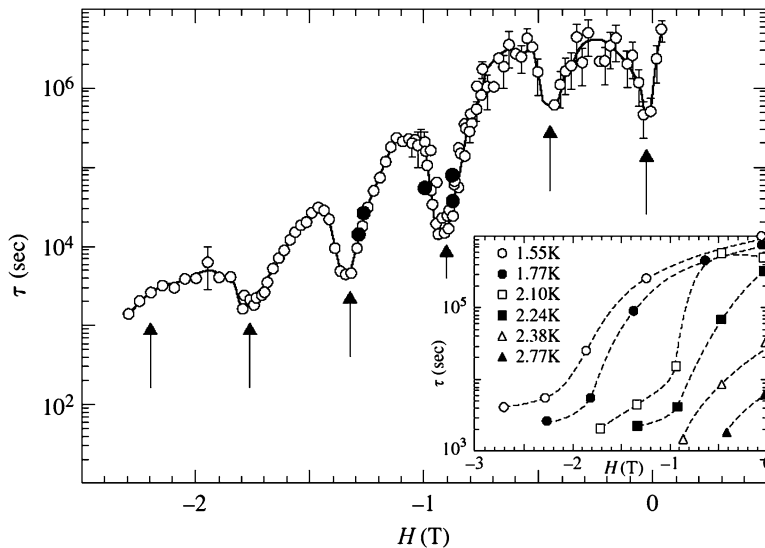
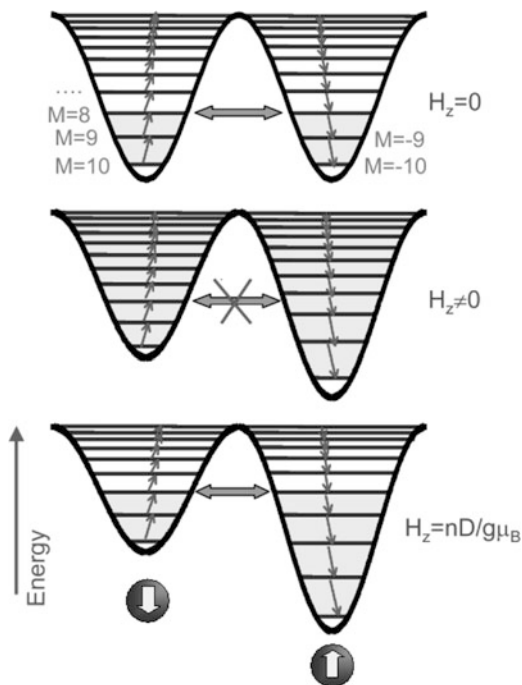


Fig. 2.5 Relaxation times at 2.1 K versus H for a single crystal of $Mn_{12}O_{12}(O_2CR)_{16}(H_2O)_4$. The inset shows that the relaxation time drops plotted against temperature in a $\log\text{-}\log$ scale for several applied fields (From ref. [32,33])

Fig. 2.6 Proposed H dependent relaxation mechanism of $Mn_{12}O_{12}(O_2CR)_{16}(H_2O)_4$



lattice phonons. In interpreting the experimental data, it is not possible, therefore, to neglect the thermal environment and hence quantum fluctuations are usually associated with a multi-phonon non-adiabatic relaxation mechanism involving a dissipative environment. Again we can describe this intrinsic thermodynamic irreversibility in terms of quantum de-coherence and *the cluster and its environment must be described again as coevolving systems*.

The observed phenomenology in my opinion emphasizes the nature of our knowledge about a quantum object. The above data show that this object cannot be properly described in its pure state, but even if quantum properties clearly show up from the observed relaxation behaviour, it cannot be separated from its environment. Therefore a proper description must involve the quantum object and its environment linked by their mutual relationships. The quantum system is not isolated, but belongs to a network and its properties are influenced by this membership. In this sense, the measurements concern the emergent properties of the system constituted by the quantum object and its environment and not those of the pure quantum subsystem (object) alone.

Therefore the problem concerns the correctness of the scientific definition of the system under investigation with the aim of formulating a correct representation of the system itself and exploiting some of its properties for technological purposes. This representation cannot concern its own reality, but as we emphasised at the beginning, the interpretation of the self-consciousness of an observer made directly or through an artefact, e.g. a measurement apparatus. If the point is the establishment of a boundary between a quantum object and a classical one, it should be emphasized that this measurement cannot be direct, but always the resultant of the interaction between the quantum object and its environment. In this sense since a quantum object is defined when it can be described by the Schrödinger equation, defining the evolution of the system and all its possible oncoming futures, this measurement is precluded. Indeed the Schroedinger description predicts that the system should be characterized by interference properties, and therefore the system cannot be described by such an equation when the interference properties run out. In quantum mechanics this occurs when the systems interacts with another system: the superposition principle (i.e. the coherence) underlying the quantum laws no longer holds, its violation being due to the coherence losses which are consequent to the interaction. This phenomenon is the quantum decoherence process and defines the transition between the quantum world and familiar classical reality.

This process can be either spontaneous, i.e. due to the interaction with the surrounding environment of the quantum object, or voluntary, i.e. induced by an external observer performing a measurement. In the classic Copenhagen School the interpretation made by Von Neumann [21] a measurement is claimed to be associated with the collapse (or reduction) of the wavefunction through a weird clouded mechanism. As a consequence of this collapse, observation of one of the possible values of the investigated system property is allowed. How and where this collapse would occur is a mystery, but in quantum physics the classical systems (the observers or their instruments) are postulated to be “collapsers”, thereby

justifying the possibility of the measurement action. It is rather unclear why the collapse should involve the quantum object and not the observer. The usual claimed justification lies in the consideration that observers and their instruments are huge respecters of the quantum object, and less influenced by the uncertainty defined by the Planck constant.

The bug is that the quantum mechanical description forces us to adopt the view of an observer-independent system, although the observer is the author of the description [25]. In other words quantum mechanics dictates the representation of the absolute essence of the system, like the weird entity constituted by the Leibniz monad. A measurement provides direct evidence for the type of information, which can be elicited from a physical system. If this is obvious when we are dealing with a classic object, it is less so with a quantum object. In the first case the measurement can be made without disturbing the classic object, but for a quantum object this cannot be made in principle. This is basic tenet of quantum mechanics. Now the reliability of the experimental measurements furnishes the basis for cognitive characterization of a physical system from an observer through his self-consciousness mechanisms. It is that which allows the possibility of obtaining coherent results from different independent observers. In principle for classical objects they may perform their observations without mutual disturbance. Thus reliability is a potential intrinsic property of the classical world but not for quantum objects. Traditional quantum mechanics condemns him to perennial frustration because of uncertainty in the systems themselves. The states of a quantum object do not have definite existence by themselves, but they are defined by the type of measurement affecting them. They can be thought as entanglements of both ontological and epistemic natures. As said above, it is absolutely meaningless to discuss a fully isolated quantum object. For this reason the interpretation of the concept of direct measurement by the Copenhagen School is hard to justify as well the boundary between the quantum and the classical objects.

If it is meaningless to conceive a direct measurement of a property of a quantum object, we must conclude that, as said above, we can only reach such information in an indirect way. The measurements we perform concern the way the quantum system communicates with the surrounding environment. Basically this means that our measurements retrieve the information conveyed by the quantum object to the environment. In this interaction much information about the perfectly coherent quantum system is destroyed by decoherence and we can measure only that associated with the so-called pointer states, which are those less affected by decoherence processes. In other words decoherence destroys the most part of superpositions. This is believed to occur through a super-selection mechanism induced by the environment itself. For this reason the reliability of the information and its inherent objectivity are defined by the degree of redundancy of the information conveyed by the quantum system. Only the states that survive this destruction process can be observed. Thus in contrast to the classical world, all the information about a physical system is objective; at the quantum level the objectivity concerns only a part, and in a certain sense becomes synonymous with “classical” which means predictable. However, it is important to stress that they are always related to a

quantum object. The environment provides noise in the observation and relaxation following its perturbing role. These considerations do not shed light about the problem of wavefunction reduction. They only point out which constitute evidence of the reduction process. The transition from the quantum object to the classic one is only matter of our consciousness. Following our perceptions, the outcome occurs when the entanglement of the two interacting systems (quantum object and environment as observer) is so large that the wavefunction is dispelled and the quantum observables are overwhelmed by the noise. At this step, the quantum object persists, but can no longer be quantified. Finally it is worth mentioning that the selection mechanism involves a structured correlation between the two systems. For this reason Zúrek defines this process “quantum Darwinism” [24,25], a term borrowed from its similarity with the evolutionary hypothesis. I want to mention here the close relation of this approach with the one believed to be operative in the evolution of our consciousness. Here it is rather clear that the correct approach predicts a well defined separation between the domain of the real objects and the information the living organism may detect. In the same way we may conclude that the scientific approach is determined by the world where the observer lives. For this reason science constitutes a cognitive domain determined by the ontology of the observation and by the operational coherence of the observers. Progress can be made if a network of relationships is operative and affects the self-consciousness of the observers. But it should be remembered that self-consciousness works again following the quantum principles: thus according to the science of complexity, any correlation is a registration, any quantum state is a record of some other quantum state.

2.6 Conclusions

In our life as researchers we are used to seek a reduction of the physical world to a one dimensional form looking for a situation where it is rather easy to draw a conclusion or to adopt a decision. However, there is no doubt that the adoption of more than one perspective may considerably improve our views about our activity. This is because, as we have mentioned above, it is not possible to define a phenomenology addressed to the isolation of the perceptions from the governing principles of the rationality. In the same way the Heraclitus statement “The way up and the way down are one and the same” to be interpreted as a conception of order of the physical world, could also be assumed to mean the adoption of an alternative view. The upward and downward causalities which are the central pillars of the science of complexity may improve the comprehension of a chemical emergent context and sometimes to privilege the relationships versus the quantitative properties may provide a different panorama. In my opinion, the basic starting point remains the subjectivity of the cognitive process following the intrinsic selection of the external inputs made by the observer according to his personal history and this determines the selection of the observer’s decisions and

actions. It is always worth reminding one that the eagle and the worm have different perspectives of the world and can give different answers in estimating the perimeter of the same island.

Acknowledgements I am strongly indebted with Professor Dante Gatteschi for discussions and the work he made in revising this manuscript. A significant acknowledgment is also due to Professor Roberta Sessoli for the elegant competence she used in simplifying the ideas contained in the first draft of the manuscript.

References

1. Bateson G (1972) Steps to an ecological mind. Ballantine, New York
2. Maturana H, Varela F (1980) Autopoiesis and cognition: the realization of the living. Reidel, Dordrechts
3. Waldrop MM (1992) Complexity: the emerging science at the edge of order and chaos. Viking, London
4. Mainzer K (1994) Thinking in complexity. The complex dynamics of matter, mind, and mankind. Springer, Berlin
5. Cilliers P (1998) Complexity and postmodernism. Understanding complex systems. Routledge, London
6. Heylighen F (1997) Classic publications on complex, evolving systems: a citation-based survey. Complexity 2:31
7. Ellis GFR (2006) Physics and the real world Found Phys 36:227
8. Dei A (2008) Molecular magnetism: a philosophical perspective from a biased point of view. Inorg Chim Acta 361:3344
9. Dirac PAM (1929) Quantum Mechanics of many-electron systems. Proc R Soc Lond A123:714
10. Schummer J (2003) The philosophy of chemistry. Endeavour 27:37
11. Bishop RC (2005) Patching physics and chemistry together. Phil Sci 72:710
12. McIntyre L (2007) The philosophy of chemistry: ten years later. Synthese 155:337
13. Whitesides GM (2004) Assumptions: taking chemistry in new directions. Angew Chem Int Ed 43:3632
14. Hoffmann R (2007) What might philosophy of science look like if chemists built it? Synthese 155:321
15. Weaver W (1948) Science and complexity. Am Sci 36:536
16. Von Bertalanffy L (1968) General system theory: foundations, development, applications. George Braziller, New York
17. Rosenblueth A, Wiener N, Bigelow J (1943) Behavior, purpose and teleology. Phil Sci 10:18
18. Müller A, Dress A, Vögtle F (eds) (1996) From simplicity to complexity in chemistry – and beyond, part I. F. Vieweg and sohn mbH, Braunschweig, Wiesbaden
19. Mainzer K, Müller A, Saltzer WG (eds) (1998) From simplicity to complexity part II. F. Vieweg and sohn mbH, Braunschweig, Wiesbaden
20. Nicolis G, Prigogine I (1989) Exploring complexity. Freeman, New York
21. von Neumann J (1955) Mathematical foundations of quantum mechanics. Princeton University Press, Princeton
22. Everett H (1957) Relative state formulation of quantum mechanics. Rev Mod Phys 29:454
23. Zeh HD (1970) On the interpretation of the measurements in quantum theory. Found Phys 1:69
24. Zurek WH (1991) Decoherence and the transition from quantum to classical. Phys Today 44:36
25. Zurek WH (2003) Decoherence, einselection, and the quantum origins of the classical. Rev Mod Phys 75:715

26. Sato O, Tao J, Zhang Y-Z (2007) Control of magnetic properties through external stimuli. *Angew Chem Int Ed* 46:2152
27. Sato O, Cui A, Matsuda R, Tao J, Hayami S (2007) Photoinduced valence tautomerism in Co complexes. *Acc Chem Res* 40:361
28. Dei A, Gatteschi D, Sangregorio C, Sorace L (2004) Quinonoid metal complexes: toward molecular switches. *Acc Chem Res* 37:827
29. Carbonera C, Dei A, Létard J-F, Sangregorio C, Sorace L (2004) Thermally and light-induced valence tautomeric transition in a dinuclear cobalt-tetraoxolene complex. *Angew Chem Int Ed* 43:3136
30. Beni A, Dei A, Rizzitano M, Sorace L (2007) Unprecedented optically induced long-lived intramolecular electron transfer in cobalt-dioxolene complexes. *Chem Commun* :2160
31. Beni A, Dei A, Laschi S, Rizzitano M, Sorace L (2008) Tuning the charge distribution and photoswitchable properties of cobalt-dioxolene complexes by using molecular techniques. *Chem Eur J* 14:1804
32. Thomas L, Lioni FR, Ballow R, Gatteschi D, Sessoli R, Barbara B (1996) Macroscopic quantum tunnelling of magnetization in a single crystal of nanomagnets. *Nature* 383:145
33. Gatteschi D, Sessoli R (2003) Quantum tunnelling of magnetization and related phenomena in molecular materials. *Angew Chem Int Ed* 42:268, and references therein
34. Sessoli R, Gatteschi D, Caneschi A, Novak MA (1993) Magnetic bistability in a metal-ion cluster. *Nature* 365:141
35. Christou G, Gatteschi D, Hendrickson DN, Sessoli R (2000) Single-molecule magnets. *MRS Bull* 25:66
36. Sessoli R (2008) Molecular nanomagnetism in Florence: advances and perspectives. *Inorg Chim Acta* 361:3356
37. Barbara B (2008) Quantum nanomagnets: from relaxation to coherence. *Inorg Chim Acta* 361:3371

Chapter 3

Complexity in Molecular Magnetism

Dante Gatteschi and Lapo Bogani

Abstract We present a perspective of the status of molecular magnetism and highlight its potentiality in the study of complex systems. The trend in MM during the last few years has been initially from simple to complex behaviour, followed by a change of direction, giving more attention to simpler systems: from 3D to 0D, 1D, 2D systems. However structural simplicity does not necessarily imply a simplification of the properties. Moreover this trend allowed better understanding the properties of isolated constituent units. Analysis indicates that this field of chemical and physical sciences will continue to develop.

3.1 Introduction

The theme of the workshop (and of this book) is certainly a very complex one. In fact the mother-of-all-knowledge, Wikipedia, allows at least 35 different definitions for complexity. Furthermore the definition of complexity is much more complex than just saying “something with many parts in intricate relation”. The operative definition we will adopt is: “complexity must be situated in between order and disorder: complex systems are neither regular and predictable (like the rigid frozen arrangement of molecules in a crystal) nor random and chaotic (like the

D. Gatteschi (✉)

Department of Chemistry, University of Florence, INSTM, Polo Scientifico Universitario,
Via della Lastruccia 3, 50019 Sesto Fiorentino, Italy
e-mail: dante.gatteschi@unifi.it

L. Bogani

Physikalisches Institut, Universität Stuttgart, Pfaffenwaldring 57, D-70550, Stuttgart, Germany
e-mail: lapo.bogani@pi1.physik.uni-stuttgart.de

ever-changing movement of molecules in a gas). They exhibit a mixture of both dimensions, being roughly predictable in some aspects, surprising and unpredictable in others" [1].

While mathematics and physics find their ancestry in the crystal-clear, "apollinean" bright logics of Greek geometry, Chemistry is the progeny of the dirty, dark, "dionisiac", mysteriously magical alchemy. It is born out of the struggle with mud, unresolved mixtures, impure reactants and inexplicable or unwanted products, not from carefully worded definitions and axioms, point-like objects or geometrical trajectories. This dark, lowly origin has much to do with complexity, and with the chemist's constant struggle to direct and understand the unruly behaviour of matter and substances. The product of this fight is a science in which empirical observation and laboratory trials are still the main approach to synthetic problems, with an overall little room left for theoretical predictions. In fact being able to model even basic reactions or the effect of simple drugs is still a major challenge in today's theoretical Chemistry. The chemist's (or alchemist's) constant struggle with complexity has left an indelible mark upon the discipline, as plainly shown even by a superficial lexical analysis of a chemist's vocabulary. Chemists talk of activated-complexes, of complexation reactions and of metal complexes, whose initial rationalization and characterization led to the first (and up to 1973 the only) Nobel Prize in Inorganic Chemistry. Werner's work made what was complex in 1892 no longer complex in 2000, but metal complexes do retain some features of what is understood as complexity. They are built up from constituent units that exist independently one from the other, but that afford new structures and new properties when something (what we call a complexation reaction, in fact) happens and they merge into a new identity. From this self-initiating union unique and sometimes radically different properties emerge.

Self-assembly and emergency are indeed two of the many faces of complexity. But complexity is something more, it does not lead to well-ordered systems, rather to something that is neither completely ordered nor completely disordered. In the language of Physics and Chemistry this means that we are somewhere in between the gas and the crystal, closer to the liquid, or perhaps even more similar to an aperiodic crystal, which is the expression used by Schrödinger when trying to understand the physics of hereditary transmission [2]. And these features emerge spontaneously through a process of self-organization: "the spontaneous emergence of global structure out of local interactions. Spontaneous means that no internal or external agent is in control of the process".

In all cases a complex system is something that does not allow us to make predictions (if we can make any at all) from rough models or an imprecise knowledge of the starting conditions. Once a complex process has begun, it will not lead to "roughly the same result" whatever the initial conditions. The forces in play will rather direct it towards one of innumerable, extremely different possible evolutions. To predict the final outcome is clearly difficult, and often requires an impossibly precise knowledge of the initial conditions, as well as an unrealistic control over the external environment. Sometimes, as we will show in the following, even infinitely small deviations from the assumed parameters can lead to dramatically different outcomes.

This fact leads us closer to the likely way of thinking of Babylonian mathematicians than to Euclidean geometry. To put it in Feynmann's words [3]: "There are two kinds of ways of looking at mathematics: the Babylonian tradition and the Greek tradition. Euclid discovered that there was a way in which all the theorems of geometry could be ordered from a set of axioms that were particularly simple. The Babylonian attitude is that you know all of the various theorems and many of the connections in between, but you have never fully realized that it could all come up from a bunch of axioms." In studying complexity we are left with a Babylonian method, and not the Euclidian or Greek method, for a minimum deviation from the ideal axiomatic conditions leads to catastrophically different outcomes.

Anyway, complexity is not just simple chaos, as the processes involved push towards some evidently important goal. This is usually obtained by the presence of some adaptability of the elements constituting the complex system, as in the typical complex system that is the free-market economy, in which each individual component tries to adapt himself to the changing conditions of his environment so as to obtain the maximum gain. Other examples of this point emerge clearly by considering other typical complex processes (all of which poorly understood). Species evolve, adapting to different environments and developing new organs and functionalities, like wings and eyes, in which each component has no meaning and utility without the other ones. Neurons in the brain, even now struggling to afford an idea of complexity, form complex, ever-changing patterns that, as far as we understand, materially allow us to formulate and develop thoughts. Societies develop niche specialized groups, social classes and highly complex moral and ethical systems, in perennial mutation to overcome the challenges they meet. In fact, by considering our society a complex system (hardly a bold assumption) it is easy to recognize how each of us, as a tiny element struggles and adapts himself, altering in the process his environment and the overall behaviour of the complex system. With this picture in mind it will possibly be easier to recognize the symptoms of complexity in physical and chemical systems, following these overall common traits that link economy, sociology, biology, physics, chemistry and a number of other disciplines.

These are the operative criteria, right or wrong as they may be, that we will use in this Chapter, trying to find interesting examples showing the role of Chemistry in complexity or of complexity in Chemistry. Perhaps we need also define what Chemistry is and this is certainly a minefield in an environment with a philosophical bent. Again we will make a bold assumption, namely that the research field that has been developed in the Florence School of Inorganic Chemistry in the last 40 years can provide interesting chemical examples of complex processes. The dominant theme will be about the magnetic properties of molecules, a research field with large overlap with those of classical solid state materials.

Indeed complex behaviour for instance is well documented in systems with highly correlated electrons [4], like those which give rise to colossal magneto-resistance, or high T_c superconductors, two phenomena where magnetic properties play a key role. In general transition metal oxides provide a large variability of properties. However the traditional approach to these systems is of the top-down

type, i.e. starting from a bulk, massive system, and cutting it in smaller and smaller pieces of the desired shape and size. This approach, which is the one currently used in the miniaturization of electronic components has, to our purposes, the intrinsic defect that we can usually design the properties of the resulting systems. A more natural approach to observe the emergence of new properties is the bottom-up one. A field where the bottom-up approach is that of Molecular Magnetism, MM [5–9], which will provide us with hopefully interesting examples in the following sections.

MM is a very interdisciplinary area indeed, where chemical ingenuity is used to design new classes of magnetic materials, which are then characterized with all sorts of sophisticated physical techniques. The observed properties, if deemed interesting enough, are eventually interpreted developing suitable theoretical tools that usually make use of both classical and quantum physics. The collaboration in the field of biomedicine is increasing and engineers are warming up their engines to start to design novel types of devices based on new types of complex systems.

The organization of the Chapter will be the following. In Sect. 3.2 we provide a short overview of the origin and development of MM. Section 3.3 is devoted to Molecular Nanomagnetism, a rapidly expanding area where the bottom up approach of MM is producing excellent results. In particular, we will mention molecules comprising a (large) number of interacting magnetic centers, which can be considered as the MM equivalent of quantum dots. Among the potential developments of these systems is that of molecular spintronics and quantum computing. Sections 3.4, 3.5 and 3.6 are devoted to one-dimensional magnets, the equivalent of quantum wires. We will start from the discussion of a strange form of self-organization in a partially ordered system. The interplay between superparamagnetic and spin glass behaviour will follow. The last section devoted to 1D materials will be dedicated to the experimental evidence of a sophisticated phase, called chiral phase. The problems associated with Self Assembled Monolayers, SAMs, of magnetic molecules will be the topic of Sect. 3.7. The last part will be dedicated to conclusions and perspectives.

3.2 Magnetism and Molecular Magnetism

Magnetism is a fundamental property of matter that attracted much interest from the time of its discovery. The use of magnetism in Chemistry can be associated with the development of Ligand Field theory, which provided key information for relating the structure of complexes with their paramagnetic properties, which in turn, are dictated by the number of unpaired electrons in the molecule. Researchers measured the magnetic properties of polycrystalline powders in the assumption of non-interacting centers: single molecule properties were measured by measuring Avogadro numbers of centers. A sketch showing some milestones in the development of molecular magnetism are shown in Fig. 3.1.

The first step is represented by $\text{Co}(\text{Me}_6\text{tren})\text{Br}_2$, a five-coordinate complex, which was an example of the possibility of successfully investigating low-symmetry

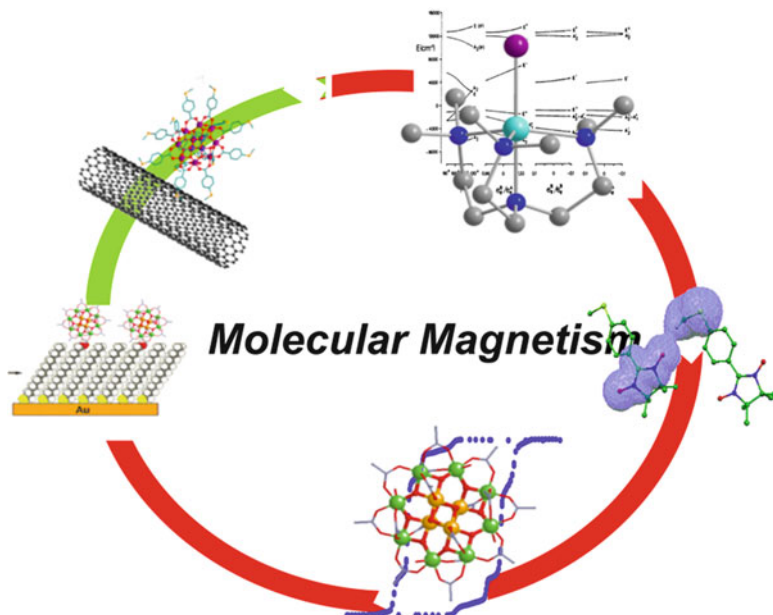


Fig. 3.1 Time evolution from magnetochemistry to molecular magnetism and molecular spintronics

compounds [10]. However, no great degree of complexity is to be found in simple paramagnets. We remind that the paramagnetic properties were measured on bulk samples with the assumption of non-interacting magnetic centers. Pure paramagnets are the magnetic equivalent of ideal gases, which, from the beginning of thermodynamics, constitute textbook examples of non-complex behaviour.

The birth of MM is associated to the discovery that organic compounds, which often are electric insulators, behave, under certain conditions, as conductors. Indeed it was an important result, and after a few years organic conductors are finally on the market. It was not long before somebody asked himself if it might be possible to synthesize organic magnets. The optimistic answer was “why not”, but it must be stated that, despite some important success, the dream of room-temperature organic magnets is far from becoming reality. In our opinion the problem is that, in order to have a ferromagnet, it is necessary to build a 3D network of interacting centers. Experience proved that this is very difficult to achieve using molecules. Better results towards room temperature molecular magnets, were achieved by taking advantage of transition metal ions, because they can easily provide the unpaired electrons needed for the magnetic behaviour. It must be stressed that $V(\text{TCNE})_2$, a room temperature ferrimagnet [11], is characterized by large structural disorder that has hampered, despite titanic efforts, the determination of its crystal structure. Structural disorder leads to magnetic disorder, and the molecular compounds provided

useful testing ground for various theoretical models. All these models consider some random disorder, which is somehow an ingredient for complex behaviour.

However on moving from paramagnets to magnets the point of view had completely changed and the interactions between centers, which were avoided in step 1 started to be actively looked for in step 2. Ferromagnetism is a cooperative property and the measurements are performed on bulk samples. Ordered states are searched; these are not examples of complexity. In fact ferro- (or ferri- or antiferro-) magnets are magnetic analogues of solids.

The weakness of molecules in giving 3D magnets becomes a strength in the synthesis of low dimensional magnets, zero-, one-, and two-dimensional [5–9]. In these systems complex behaviour can be observed, especially in zero- and one-dimensional materials, as discussed in the following paragraphs.

In the last few years the interest of MM has shifted to the investigation of individual molecules, possibly using self-assembled monolayers, SAMs and self-assembled structures, as shown in Fig. 3.1. In a sense we started from the investigation of individual molecules, but measuring bulk samples, and finished by investigating individual molecules addressing them directly. Indeed a long way, which is by no means concluded: the new field of molecular spintronics is opening [12].

3.3 Nanomagnets and SMMs

The most exciting results in MM have been associated with synthesis of molecules with a number of magnetic centers that can be considered as nanomagnets [8]. The first such molecule was originally reported [13] by Lis in 1980, but the first successful attempts to interpret the puzzling magnetic properties only came a few years later. The compound was a cluster comprising 12 manganese ions, usually referred to as Mn₁₂Ac, where Ac stands for acetate. The ground $S = 10$ state was correctly assigned [14] and the huge easy axis type magnetic anisotropy measured. Eventually it was discovered that the relaxation time of the magnetization becomes extremely long at low temperature [15]: single molecule magnets, SMMs, were thus born. Shortly after it was found that the magnetization relaxes through tunnelling at low temperature [16,17].

The success made with SMMs prompted many laboratories to synthesize all kinds of polynuclear compounds with a rush to increase the blocking temperature, i.e. the temperature at which the relaxation time of the magnetization is equal to the time scale of the measurement used. In a top down approach, as was used for magnetic nanoparticles, this behaviour is described as superparamagnetic and the relaxation time is expected to follow an Arrhenius law:

$$\tau = \tau_0 \exp(\Delta/kT) \quad (3.1)$$

where τ is the relaxation time, τ_0 is the pre-exponential factor (the high T limit of the relaxation), Δ is the barrier associated to the anisotropy of the nanoparticle, and k the Boltzmann constant.

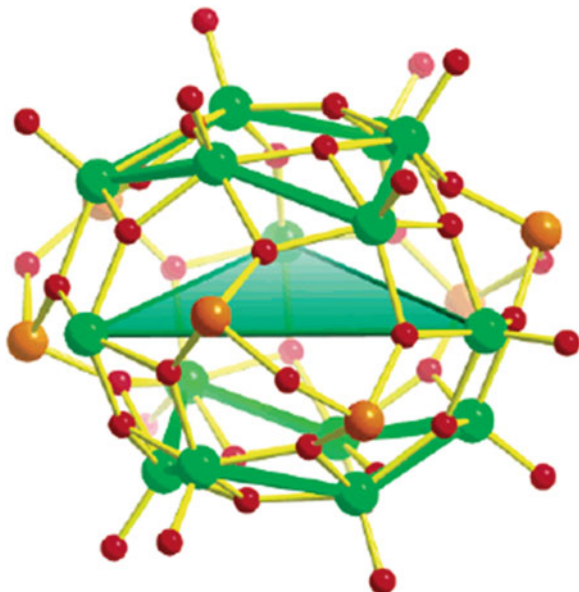
A similar law was obtained by using a bottom-up approach, i.e. extending [18] to the clusters the Orbach process employed for simple paramagnets. In this simplified model, the barrier is expected to depend on DS^2 , where S is the spin of the ground state and D its zero field splitting. However it is not probable that really high T_B will be achieved because the DS^2 rule is an oversimplification, and the pre-exponential factor τ_0 , which is poorly understood, yet has a paramount importance. We will come back to τ_0 in Sect. 3.6 but here we want only to notice that in order to have τ of 100 s at room temperature DS^2 must be ca. 5,000 K if τ_0 is 10^{-5} s. The longest τ_0 values so far reported have been around 10^{-6} s.

Beyond SMMs magnetic clusters of interest to the theme of the conference and this book are systems with antiferromagnetically coupled spins on odd member rings. Triangular clusters of metal ions have long been known and investigated for their interesting magnetic properties [19]. If the coupling between the spins is antiferromagnetic and the three coupling constants are equal to each other, there is no way to put the three spins according to an up–down scheme. For three $S = \frac{1}{2}$ spins the ground state is provided by a degenerate doublet of $S = \frac{1}{2}$, a quartet state being at higher energy. The spins are said to be frustrated, because they are under the influence of two competing equivalent interactions [20]. The main result is that degenerate states are created, which can be rapidly changed under the effect of external perturbation. Spin frustration is a necessary ingredient of complexity in magnets. As all degenerate states they are prone to degeneracy lifting either by spin-phonon or spin-orbit coupling [21]. Small variations in the coupling give rise to large variations in the properties. This has been observed in simple triangular clusters and in complex structures like Kagome lattices [22]. In all the above-mentioned systems spin frustration has its basis on AF triangular arrangements. Recently detailed studies have been performed on inorganic systems where the spins are located on a tetrahedron (which after all has four triangular faces) [23,24]. The system is akin to the structure of ice, an indeed it has been called spin-ice [25]. However this is not at all the only possibility and more examples will be given below.

An early example of complex structure based on frustrated triangles is shown in Fig. 3.2. It can be described [26] as a layered compound formed by oxovanadium(IV) ions, $S = \frac{1}{2}$, arranged in two hexagons sandwiching a triangle of oxovanadium(IV), V15. The AF coupling in the hexagons quenches the magnetization of the external layers. At low T the system can be described magnetically as a frustrated triangle, which in Heisenberg coupling gives two degenerate spin doublets. The introduction of additional perturbations associated to phonon or spin orbit coupling removes the degeneracy. Indeed it has been shown that antisymmetric exchange, determined by spin orbit coupling, removes the degeneracy, splitting the two lowest Kramers doublets by a few mK [27].

Two-level systems are currently under investigation as possible q-bits, i.e. bits that exploit quantum effects [28]. One of the main problems encountered in preparing a q-bit is decoherence, i.e. the interactions of the spin with all the

Fig. 3.2 Structure of V15 with the scheme of the exchange pathways involving the 15 oxovanadium (IV), $S = 1/2$ centers. *Green*, V, *red*, O, *brown*, As (Color figure online)



rest of the world, which tend to wash out quantum information. A possibility of measuring quantum coherence is that of measuring Rabi oscillations [29], as first suggested in 1937. Pulsed EPR experiments on diluted organic radicals have long known to observe Rabi oscillations [30]. Recently measurements on diluted samples of V15 have evidenced that, notwithstanding unfavourable features, like the presence of 15 vanadium nuclei, with $I = 7/2$, and numerous protons, quantum coherence is maintained for a relatively long time. However the nuclear spins, which are entangled with the electron spins, can be manipulated through suitable pulse techniques [31].

Several other classes of magnetic molecules, including other triangular systems, are currently being tested. It would be interesting to have larger odd member rings to check the possibilities of observing quantum coherence, but systems like that are exceedingly rare. Only recently some limited success has been achieved, by starting from an antiferromagnetic eight-membered ring of chromium(III), $S = 3/2$ [32]. Two different types of derivatives were obtained following two different strategies. In one case the ring was selectively substituted in such a way that a chromium(III) is substituted by a nickel(II), $S = 1$, Cr7Ni [33]. In the other nonanuclear rings with 8 Cr^{III} and one Ni^{II}, Cr8Ni, were obtained by cutting one bond and pasting in a nickel ion [34]. The presence of a hetero ion gives two possibilities of frustration effects in Cr8Ni, depending on the relative value of the Cr-Cr and of the Cr-M coupling constant. If the former dominates the frustrated spin is the M one, while in the opposite case the Cr-Cr spins will be frustrated. This behaviour is sketched in Fig. 3.3. The ring can be compared to a spin Moebius ring, with the kink in correspondence of the frustrated sites. In fact the position of the kink depends on

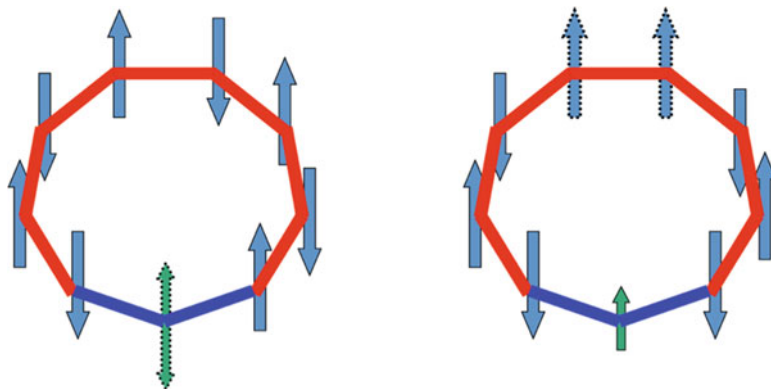


Fig. 3.3 Possible spin frustration effects in Cr₇Ni antiferromagnetic rings

the relative value of the Cr-Cr and the Cr-Ni exchange interactions. In the former case it is expected that the kink is on Ni. Magnetic measurements yielded evidence of a ground $S = 0$, the magnetic susceptibility undergoing two, rather than the usual single, maxima. The first excited levels have $S = 1$. EPR spectra showed that indeed the kink of the Moebius strip is on the Cr.

In Cr₇Ni, which has a ground $S = \frac{1}{2}$ state, measurements of the longitudinal, T_1 , and transverse T_2 relaxation times showed pretty long values which raised excitement about the possibility of using AF clusters for QC [35].

3.4 Self Organization Among Magnetic Chains

Nitronyl nitroxides are a class of particularly versatile stable organic radicals that can coordinate to transition metal ions with their oxygen atoms in many different ways. Originally reported by Ullman, they have subsequently been largely used as magnetic building blocks for many different types of magnetic materials [36,37]. A sketch of the NITR radicals is shown in Fig. 3.4. Quite often they bind to transition metal ions yielding one-dimensional materials according to the scheme shown in Fig. 3.5, where the oxygen donors bind to two different metal ions. The magnetic properties of the linear structures, Fig. 3.5a,b will be described in Sects. 3.5, 3.6, and 3.7.

At the time of the investigation on the use of NITR radicals in MM the focus was on the synthesis of bulk ferro- or ferri-magnets, therefore attempts were made [38] to increase the dimensionality of the magnetic interactions, i.e. passing from one-dimensional magnetic materials, which do not sustain long range order, to two- and ideally three dimensional materials. Instead of using as coligands hexafluoroacetylacetonates, which block 4 coordination sites in an octahedral environment carboxylates were used.

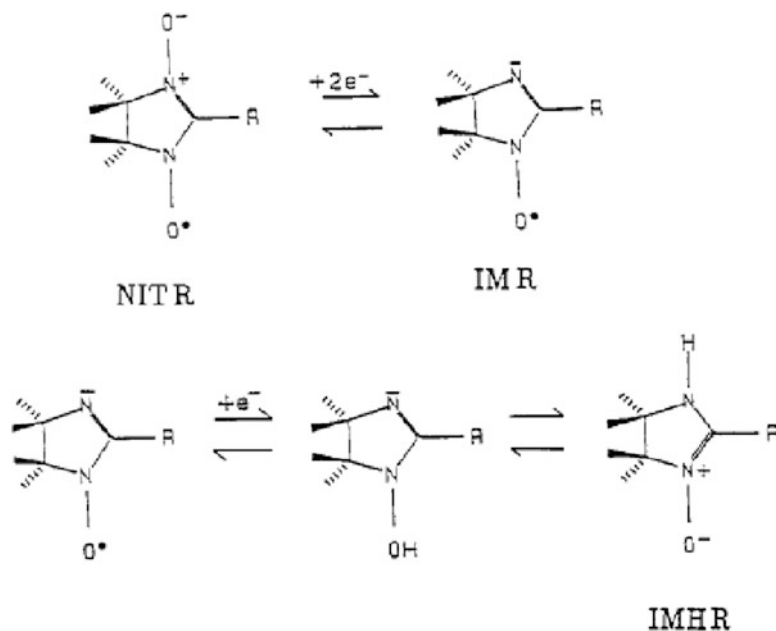
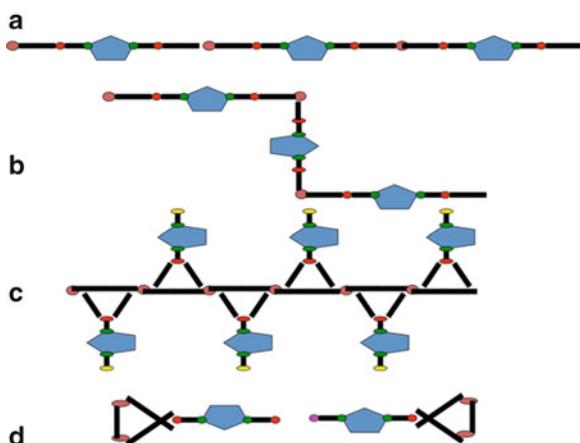


Fig. 3.4 Redox states of nitronyl nitroxides

Fig. 3.5 Possible coordination polymers comprising metal ions and nitronyl nitroxide radicals



These ligands in fact changed completely the coordination environment of the metal ions: the carboxylates bridge in a μ -1,3 fashion two different Mn ions, each Mn ion being coordinated to four different carboxylates. The coordination octahedra are completed by the oxygen atoms of two different NO groups. However the analytical, spectral and magnetic data show that half of the NITMe radicals have been reduced to IMHMe, as schematized in Fig. 3.4. The latter is stable in

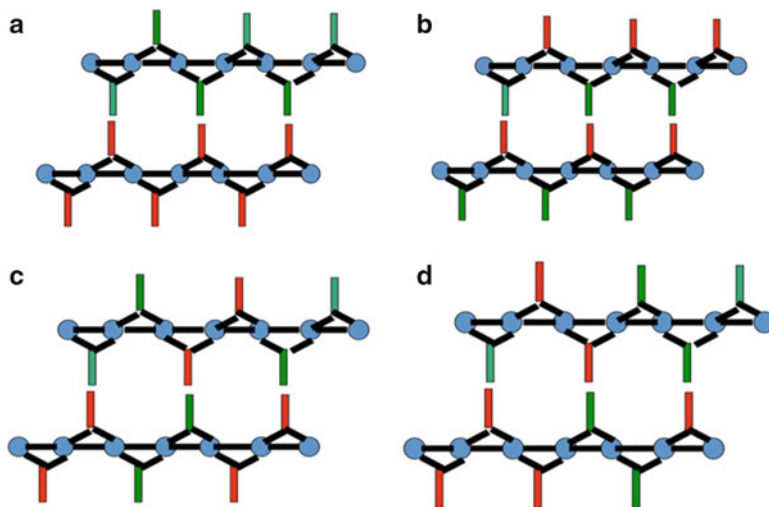


Fig. 3.6 Possible types of partially ordered structures of Mn carboxylates NITR-IMHR

two tautomeric forms, with the H attached to the nitrogen in one form and to the oxygen in the other case. The interpretation of the structure is that the NO groups coordinated to the Mn ions can belong to a NITMe or a IMHMe ligand, statistically (Fig. 3.5c). On the other side of the ligand there will be a NO group for the former and a N—H for the latter as sketched in Fig. 3.6. We indicate with a red arrow a NO and with a green one a NH group. X-ray diffraction experiments evidenced that structural disorder is present, particularly on the side of the ligand far from the metal ion. The manganese chains, formed through the carboxylate bridges are therefore connected in a two dimensional structure by a network of hydrogen bonds. The ligands stretch out of the chain, alternate ligands pointing in opposite directions.

The observed disorder does not explain how the molecules are actually organized. The most ordered, and consequently least probable, models are depicted in Fig. 3.6a–c. a corresponds to segregation of chains, i.e. one chain is M-NITMe, the neighbouring ones M-IMHMe, b to a regular alternation of NITMe and IMHMe on the same chain, c to double alternation. This does not correspond to disorder, unless different planes have different orientation. The most probable model is d, which features complete disorder for the ligands on one chain. However it is not complete disorder in the planes, because one chain forces the two neighbouring ones to be half correlated with itself: it is an intermediate situation between complete disorder and emerging correlations.

Some entropy considerations help in understanding the disorder/complexity of the system (Prof. A. Rettori: private communication). Let us start from the case of independent chains. Assuming that in each chain, comprising M sites, there are 50% red and 50% green arrows then the number of configurations per chain, n_1 , is given by:

$$n_1 = \frac{M!}{\left(\frac{M!}{2}\right)^2} \quad (3.2)$$

and the number of configurations per N chains, n_N , is simply $(n_1)^N$. If we introduce a strong interchain interaction, which requires that if on chain i there is a green arrow on the corresponding site on $i + 1$ there is a red arrow the number of configurations per N chains becomes as shown below:

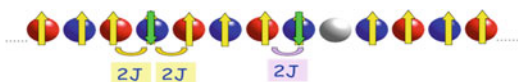
$$n_N = \frac{M!}{\left(\frac{M!}{2}\right)^2} \left[\frac{\frac{M!}{2}}{\frac{M!}{4}} \right]^{N-1} \approx \left[\frac{\frac{M!}{2}}{\frac{M!}{4}} \right]^N \quad (3.3)$$

The magnetic data show that indeed the correlations increase rapidly on decreasing temperature. Clearly there are too many unknowns to extract meaningful quantities from the data. However the model *d* allows for some considerations. The possible exchange interactions can be guessed as follows for the in-chain interactions: Mn-NITMe, J , should be antiferromagnetic of the order of 10^2 cm^{-1} ; Mn-Mn through a IMHMe, J' , should be weakly AF, order 10^0 cm^{-1} . For the interactions between chains they are mainly determined by radical-radical interactions, J'' of the order 10^0 – 10^1 cm^{-1} . If these assumptions are correct it is possible to estimate the magnetic properties by considering the statistical occupation of the NITMe and IMHMe molecules. In such a case the magnetic data should correspond to the sum of a Mn-radical chain plus that of a Mn-Mn chain. Attempts to use this model were unsuccessful.

3.5 Single Chain Magnets: Superparamagnetic vs Spin Glass

An obvious extension of SMMs, also in the perspective of increasing the blocking temperatures, is provided by one-dimensional materials. In fact it was discovered that a chain of alternating cobalt(II) and NITR radicals gives rise to slow relaxation of the magnetization and magnetic hysteresis of molecular origin [39]. These systems were called single chain magnets, SCMs, by analogy to SMMs [40]. The common features between the two classes of compounds are essentially the need of an easy axis type, Ising, anisotropy and of exceedingly small inter-molecular interactions [41,42]. The interpretation of their magnetic behaviour was based on a model originally developed by Glauber [43] in the 1960s for one dimensional Ising ferromagnets. The Ising anisotropy is brought about by cobalt(II) ions. The Glauber model starts from flipping one spin, as shown in Fig. 3.7, which can be performed only breaking two bonds, thus paying the corresponding energy cost of 4 J, the Ising coupling constant. The relaxation time of the magnetization τ follows the same equation (1) worked out for SMMs. The barrier Δ is equal to 4 J. The interesting result is that the relaxation of the magnetization follows an exponential

Fig. 3.7 One dimensional M-NiTR chain in the presence of defects



dependence on an energy barrier as observed in SMMs. In principle the barrier can be much higher in SCMs as compared to SMMs, providing opportunities for high T_B systems. In fact in SMMs the barrier is determined by the zero field splitting effect, and rarely exceeds 10 K for individual ions while coupling constants are on the order of 10^2 K.

The above considerations are very basic ones. In fact additional mechanisms have been taken into consideration, which have given more physical insight in the SCM mechanism. Beyond considering ideal systems it is necessary to take into account real systems with their defects and impurity sites. In fact one key feature of one-dimensional magnets is a strong dependence on the presence of impurities, which break the only available interaction path along the chain. The meaning of these words is easily grasped looking at Fig. 3.7. Each center is connected to two neighbouring centers; if a site is defective, for instance it hosts a diamagnetic impurity, the coupling between its left and right neighbours is destroyed. This would not be the case in a 2D or 3D system, where it would be possible to re-establish the interaction bypassing the defective site. Real SCMs, therefore cannot be schematized as infinite chains but, rather, should be viewed as a collection of independent segments of different lengths [41,42,44–46]. The segments are delimited by two defective sites. The presence of defects could be an essential point in quenching the divergence of the spin correlation length and, consequently, suppressing three-dimensional ordering thus facilitating the possibility of observing SCM behavior. In fact, in an ideal chain with Ising coupling, the spin correlation length increases exponentially with decreasing T , and even very weak inter-chain interactions, like the dipolar ones, should determine the crossover to 3D magnetic order and wipe out the SCM phase.

By taking into account the role of defects, two main dynamical regimes can then be individuated [45]. In the high temperature regime, in which the average length \bar{L} of the segments is much longer than the spin correlation length, ξ , the dynamics is governed by the formation of excitations inside the chains with the same energy cost $4J$ of the infinite system and the single relaxation time predicted is $\tau_\infty = \tau_0 \exp(-4J/k_B T)$. When \bar{L} is shorter than ξ , at lower temperature, the dynamics is dominated by spin flips at the end points, which have a halved energy cost $2J$. The excitation can then propagate along the chain at no energy cost and, following a random walk path, can then reach the other end of the segment with probability $1/L - 1$. It can be shown using statistical arguments [47–50] that the relaxation time τ_L of a segment of L spins now depends on the segment length:

$$\tau_L = L \tau_0 \exp(-2J/k_B T) \quad (3.4)$$

In many cases the relaxation of the magnetization is found to depend exponentially on the barrier but the pre-exponential factor τ_0 was orders of magnitude shorter than observed in SMM. This behaviour is generally attributed to a transition to a spin glass-like state, SGL.

SGL systems are undoubtedly good examples of complexity [51]. They appear when two fundamental ingredients are present in the magnetic system: disorder and frustration. The first ingredient is evidently common in all complex systems, and can arise here from either structural disorder (e.g. randomly defective atomic sites, randomly placed magnetic object in a diamagnetic matrix) or from other physical parameters (e.g. randomly oriented magnetic axes, magnetic nanoobjects of random size). The presence of several degenerate states leads to several possible configurations of the system. It is clear that, having many degrees of freedom the system, when subjected to a stimulus, can respond following a number of different paths, in a very complex way. Overall the final result will be roughly the same, but each time the process is repeated a very different path will be followed. Depending on how lucky we are, reaching this exit can take a relatively short or an enormously long time. At low temperatures SGL systems can take such long times to arrive at the final state (i.e. the exit) that we can sometimes follow their journey. Below a certain temperature, anyway, the system will invariably completely loose itself in the labyrinth of its possible configurations and will never reach the exit. In physical terms it undergoes a transition to a disordered, frozen state of the magnetization. It thus shows an hysteresis cycle without ordering in a three dimensional (3D) magnetic structure [51]. Above the frozen magnetization state, a distribution of relaxation times $G(\tau)$ is to be expected [52], in agreement with the two requirements of the simultaneous presence of randomness and frustration $G(\tau)$ is roughly gaussian and narrow just above the freezing temperature, and enormously broadens and often changes shape on lowering the temperature [52, 53]. This is connected to the fact that interparticle (or intercluster) competing interactions are also necessary to have a number of degenerate thermodynamic states with different microscopic configurations, one of the key features of SGs. Such interactions often vary with the degree of freezing of the system and thus give different contributions to the blocking of the magnetization. In particular, on lowering the temperature, an increasing number of spins of the system become blocked and different interactions (long-range ones in particular) become more efficient, thus broadening the spectrum of relaxation times. The presence of $G(\tau)$ is a necessary ingredient of this phenomenon, due to the simultaneous presence of both frustration and disorder, and it is thus said to have an *intrinsic* character.

The presence of impurities and defects that break the chains of a SCM system into *non-interacting* segments can give rise to a distribution of relaxation times $G(\tau)$, which is connected to the distribution of lengths (or polydispersity) of the segments, $D(L)$. Such a distribution affects the slow dynamics of the system but is not a necessary ingredient to it and, thus, is said to have an *extrinsic* character [52]. If the non-magnetic breaks are randomly distributed inside the magnetic chains, as can be assumed for crystalline defects or inserted diamagnetic impurities, the function $D(L)$ can be derived [54] and, normalized, takes the form:

$$D(L) = [\ln(1 - c)]^2(1 - c)^{L-1}L \quad (3.5)$$

where c is the concentration of defects inside the chain and L is the length of the segment.

In SCMs the shape of $G(\tau)$ depends only on the geometrical length of the chains and remains the same on decreasing the temperature, with only a peak shift to higher τ values due to the activated process. On the contrary the SG distributions become evidently broader at low temperatures and, if no assumptions are made, can possibly change shape [53]. As a consequence the Arrhenius law describes a physically meaningful mechanism for SCMs, as it reflects the shift of the median of $G(\tau)$, together with the whole distribution, to higher relaxation times [52,53]. The energy barrier is then directly linked to the exchange constant J and the intercept τ_0 must then typically be of the order of 10^{-13} – 10^{-10} s, a plausible value for the single spin flip time, or longer. In SGs, on the contrary, the Arrhenius law has no direct physical meaning, as already pointed out [50–54], for it follows the shift of the median value of a spreading distribution. As a consequence it often (but not always) affords unphysically fast τ_0 values [52]. Sometimes, depending on the spreading of the distribution in exam, one does not even obtain a straight line, but a curved one [52].

The link between SGL systems and SCMs can appear by creating systems whose chains weakly interact with a different sign than the intrachain interactions. In this case the competing interactions of the intra and interchain coupling, together with the naturally occurring disorder of the impurities of the chains, create the two fundamental conditions to observe SGL behaviour. It is interesting to note, anyway, that by using molecular materials it is possible to tune, to some extent, the ratio between the intra and interchain couplings, leading to different behaviours in structurally very similar compounds.

It is now interesting to note how some common traits defining a complex system lead to amazing similarities among very different systems, indicating a common way of treating them even when we are in presence of completely different disciplines. For examples Glauber dynamics, used to model the behaviour of SCMs [43], is also used to interpret social dynamics like those of a classroom, or the changing of opinions before elections [55]. In these cases the magnetic centers are individuals, the “up/down” spin states are transformed into “favourable/unfavourable” or “happy/unhappy” states and the magnetic interactions are considered as the persuasion capability of people within reach of each individual. These models can effectively predict with good approximation for situations where communication between the individuals is somewhat limited, like the spreading of an exact solution to a problem in a classroom during an examination, or the changing mood of a line of betters. By the way more sophisticated models, in which the true complexity of social networks is taken into account, are needed to model social groups. When these models are used a big step further can be made, and some comprehension can be gained on many systems. In this context SGL materials have astonishing similarities to neural and social networks and their physics is increasingly used to study these very different subjects. In fact it has been shown that a SGL system can be used to

store memories of previous events, and can evolve in its manifold energy landscape so as to accommodate more or change the existing ones. Analogously, societies seem to possess some form of intrinsic “memory” that renders them more prone or impermeable to occurring events. The main point of contact between these systems is that they all intrinsically possess some form of randomness in the connectivity network. And, by better looking, we can realize that, while random connections are made among their constituent units, there is a common feature that rules the overall behaviour: each of the constituent units are not spatially limited in their connections. They can connect to very different points, even far away, and do not possess a predetermined number of connections, like in usual crystalline systems. While one atom in a crystal will always interact with the same neighbouring atoms, in these networks, which are called “scale-free” networks, this is not true anymore. In this case the number of connections a single node has to other nodes can vary of orders of magnitude, and is provided by a power law. The fraction $P(k)$ of nodes in the network having k connections to other nodes goes (for large k values) as $P(k) \sim k^{-\gamma}$, where γ is a constant whose value is typically in the range $2 < \gamma < 3$. This leads to the fact that a few nodes, called “hubs”, have a very large number of connections, and thus dominate the functioning of the system. The power law distribution highly influences the network topology. It turns out that the major hubs are closely followed by smaller ones. These ones, in turn, are followed by other nodes with an even smaller degree and so on. This hierarchy allows for a fault tolerant behavior. Since failures occur at random and the vast majority of nodes are those with small degree, the likelihood that a hub would be affected is almost negligible. Even if such event occurs, the network will not lose its connectedness, which is guaranteed by the remaining hubs. Recent results seem to indicate that such networks are indeed present in social interactions and neuronal systems, establishing an interesting point of contact between sociology and biomedicine. This has in turn led to the theoretical study of SGL dynamics in scale-free networks of interconnections. While the obtained theoretical results are promising, it is clear that an experimental system could be even more interesting. Anyway standard magnetic materials are crystalline and cannot produce the kind of interconnections needed in a scale-free network. In this area it is clear that possible advances, if they can be made, will come from the domain of molecular magnetism, where molecular structures and organic ligands can afford a larger number of interconnections, once again showing their potentiality in the study of complex systems.

3.6 Chiral Transitions

Chirality, i.e. the handedness of properties has long been investigated both theoretically and with many different types of experimental approaches. In fact chirality is present in many different phenomena starting from elementary particles up to biological systems. A basic form of chirality is helicity: a simple example is represented by a spiral staircase, another by DNA. Helicity has long been observed

in magnets. Some rare earth metals in the ordered phase are characterized by helical structures which originates from competing interactions. A simpler class of helimagnets is provided by one dimensional materials, and MM has provided quite a few examples. An open problem in one-dimensional helimagnets is the mechanism of transition from the fully disordered paramagnetic phase to the ordered helices. The question is if there are only two phases possible, or if an intermediate phase, in which some symmetry breaking is possible. Before showing that indeed a chiral intermediate phase is possible let me make a short detour.

In the last few years there has been an increasing attention devoted to the investigation of the properties of magnetic systems containing ingredients which had long be neglected. One of these ingredients, rare earth ions, initially was not added to the recipes of magnetic materials on the assumption of giving rise to weak magnetic coupling. The issues were not wrong, and at the beginning of the MM saga people were not thinking so intensively as they are doing now in terms of magnetic anisotropy. When SMM showed how deeply the magnetic properties of a system can be influenced by the presence of anisotropic ions, rare earths were re-discovered to be tasty additives [56–58]. New types of SMM and SCM were reported in which 4f electrons were coupled to 2s and 2p orbitals of organic radicals or to d orbitals of transition metal ions. The approach was successful and some new types of SCM were obtained [41, 42]. However, rather unpredictably the most important results were obtained by using gadolinium(III) together with NITR radicals [59].

Gadolinium(III), with seven unpaired electrons has very low anisotropy, therefore it is not suitable to give rise to SCMs, especially when the other magnetic building block is as isotropic as a NITR radical. However in early experiments it was found that χT at room temperature is close to the value expected for weakly coupled gadolinium(III), $S = 7/2$ and radical, $S = 1/2$. Assuming not interacting spins, χT should be a constant, while switching on nearest neighbour, NN, interactions, χT should diverge at low temperature either in a ferro- or ferri-magnetic behaviour. It was assumed that beyond NN interactions also next nearest neighbour, NNN, interactions must be included. In fact the NNN interactions determine spin frustration, which is synonymous with complex behaviour. In fact the simple spin-up-spin-down description does not work any more, the low-lying levels are largely degenerate, and small perturbations dramatically affect the ground state. A simplified description of the spin orientations, using an Ising type approximation, are depicted in Fig. 3.8a which correspond to a compromise state with two spins up and two spin down. A more realistic view of the spins in the chain is shown in Fig. 3.8b.

The need to introduce NNN interactions is not limited to GdNITR chains, but has recently been observed in other systems, among which we can take into consideration LiCu_2O_2 [60]. One metal ion is copper(I) and the other is copper(II) with segregated valences. The copper(II) centers form two leg triangular ladders, similar to those shown in Fig. 3.8a. A magnetic phase transition is observed at 25 K below which neutron diffraction evidenced an incommensurate antiferromagnetic order. The NN interaction is ferromagnetic, while the NNN are antiferromagnetic and dominant.

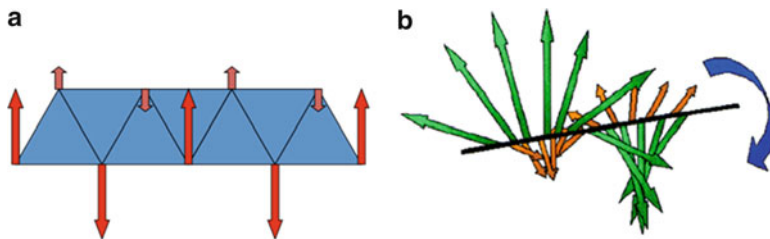
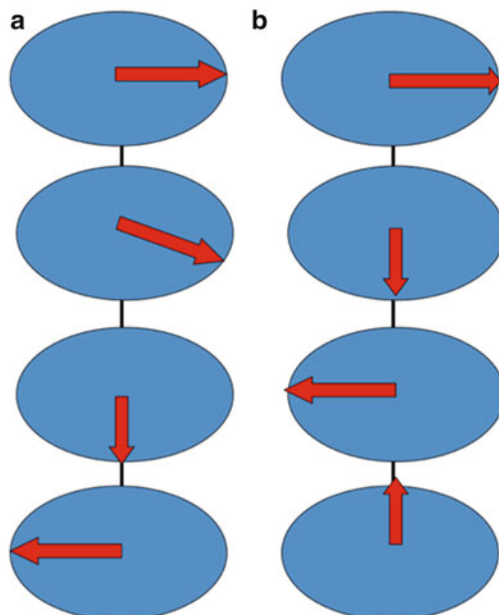


Fig. 3.8 Spin orientation in GdNITR chains with Next-Nearest-Neighbor interactions. **a** Ising limit. **b** XY limit

In GdNITR it was not possible to perform neutron experiments, but low temperature specific heat measurements showed the presence of two order–disorder transitions at 1.88 and 2.19 K, respectively [61]. Surprisingly the μ SR (muon spin resonance) and magnetization measurements provided evidence only of the lower temperature transition. The observed behaviour depends on the fact that the different techniques monitor different types of electron spin correlation functions. The correlation functions indicate the probability that if spin say k has $m_s = \frac{1}{2}$ at $t = 0$ spin j has spin $\frac{1}{2}$ at time t . They give information on how much the spins feel each other. The description of the spin dynamics requires the correlation between four spins. In the μ SR experiment the four-spin correlation function can be treated as the product of two two-spin correlation functions, one involving the muon and the other the electron spin. Two-spin correlation functions are also involved in magnetization experiments, while specific heat measurements are sensitive to both four- and two-spin correlation functions. Therefore the experimental results show that the lower T transition is a regular magnetic transition, while the upper T is of different type.

The lower transition corresponds to the long range helical order in which all the helices are either right handed or left handed, with constant pitch, as shown in Fig. 3.9b. The corresponding phase can be named a helical spin solid phase. Solid is here used only as an analogy to indicate a completely ordered state. The high temperature phase on the other hand, the paramagnetic phase, corresponds to a gas, with only local order. The third phase is the complex phase, where all the spins form either right or left helices, and in a domain only helices of one sign are present [62]. However the pitch is not regular as shown in Fig. 3.9a. The intermediate phase, the chiral phase, can be considered as a helical spin liquid. The chiral phase has rotational invariance, but not translational invariance. It is like if a drunk mason must build a spiral staircase and makes all different steps, although of course in going from one step to the other he has to bend in the same sense. This phase had long been suggested by Villain, but no real example had been found. As the temperature is lowered the correlation length between the spins increases, and eventually it diverges when all the spins point towards their equilibrium position. The growth of the correlation length is determined by the exchange interaction and scales with a

Fig. 3.9 Helical structure of the spins in GdNITR chains: “a” is for *chiral*, and “b” is for *helical*



power law. Anyway there is another correlation length to be taken into consideration though, that of chirality, which diverges exponentially at low temperature.

It is this difference in the temperature dependence of the behaviour that allows the existence of the intermediate chiral phase where translational symmetry is broken but rotational symmetry is conserved.

3.7 (Self) Organizing Magnetic Molecules

As shown in Fig. 3.1, the current trend in MM is that of addressing individual molecules. The new opportunities provided by techniques like SPM (Scanning Probe Microscopies) and TEM (Tunnelling Electron Microscopy), which have reached atomic resolution, afford the development of new concepts and devices. One of the buzzwords which is currently used to resume for the researchers and for the general public the potential future developments, ready to change our everyday life, is that of molecular spintronics [12]. Spintronics itself was officially born in 1989 when Fert [63] and Grunberg [64] discovered that a magnetic multilayer shows an extremely high field dependence of the electric resistance. Magnetoresistance was by no means new, having been discovered by W. Thomson, Lord Kelvin in 1857. To quote his words: “*I found that iron, when subjected to a magnetic force, acquires an increase of resistance to the conduction of electricity along, and a diminution of resistance to the conduction of electricity across, the lines of magnetization*”. It took

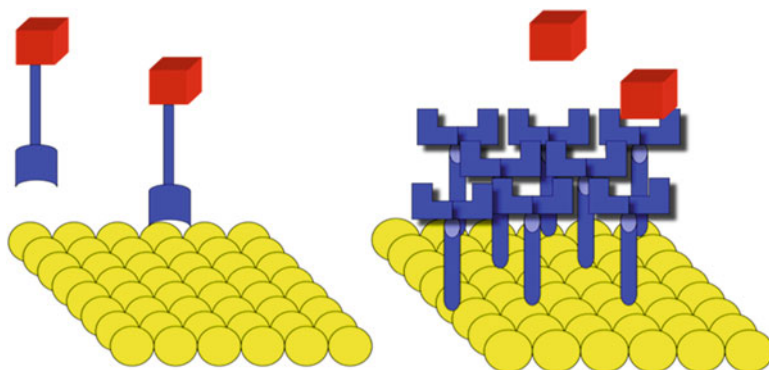


Fig. 3.10 Two schemes for organizing magnetic molecules on surfaces. *Left* prefunctionalized molecule; *right* prefunctionalized surface

some time to understand the physical origin of the phenomenon, *i.e.* the interaction of the electron spin with the magnetic moment of the layers. What had changed was the possibility to exploit the rapidly developing nanotechnologies to design and implement new types of devices. In fact after Giant Magnetic Resistance many other related research areas were explored, Chemical aspects of spintronics were recently reviewed [65]. Among the systems which are closer to be implemented are biosensors based on GMR which are full of promises, because they are sensitive, can be integrated on a large scale in lab-on-a-chip systems.

Again somebody asked: “why not to try to dream of revolutionary devices where transport is performed through one single molecule? We could then start using quantum phenomena to influence our current!” If spintronics is the ability of injecting, manipulating and detecting electron spins into solid-state systems molecular spintronics is about spin polarized currents carried through molecules. Among the possible molecules it is tempting to use SMMs or, more generally, magnetic molecules.

The organization of magnetic molecules is a prerequisite to molecular spintronics. There are several different techniques that can be used, based on physical, chemical and self-assembly methods. Early attempts used Langmuir Blodgett films [66], while recently the deposition on various substrates has been more diffusely employed [67–69]. Among the substrates conducting thin films of non-magnetic (gold, silicon, graphite), or magnetic (cobalt, nickel) [70] materials have been preferentially used. It will be difficult in any case then to be sure of what is the result, and if the target molecules are indeed conserved after the treatment made to organize them.

Not unexpectedly many efforts have been made to organize Mn₁₂ SMM. Two different strategies have been developed, depicted in Fig. 3.10.

In order to organize molecules on a gold surface it is possible to prepare a derivative of the molecule with a functional group containing sulphur, which should interact covalently with the surface anchoring the molecule. In terms of strength

of Au-S bond it would be preferable a thiol but this creates problems with the Mn1 core which comprises Mn^{III} and Mn^{IV} which are sensitive to redox agents. A thioether group is safer but the bond energy is much smaller than for a thiol (ca. 60 vs 120 kJ mol⁻¹). Several thioether containing carboxylates were tested, taking advantage of the lability of the acetate ligands in Mn12Ac, and self assembled submonolayers were obtained [67]. The first tests were performed using STM, which showed objects of the right size to be compatible with Mn12 clusters. Another approach which was used [68] on silicon followed a different strategy. The surface was preliminarily treated with docking molecules capable of reacting with the surface of Si. The self assembled monolayer so formed contains carboxylate groups which are then reacted with Mn12 clusters.

It is apparent that a topographic check of the structure of the Mn12 clusters is not sufficient to make sure that the molecules are intact. XPS and ToF-SIMS provided further evidence, but not yet enough. A serious check of the deposited molecules should come from direct measurement of the magnetic properties. Direct magnetometry measurements are ruled out by the small quantity of magnetic material which is present in the monolayers, but XMCD, using synchrotron radiation, provided the answer. XMCD measures the different absorption of right and left circularly polarized light, which is due to the magnetization of the sample. The measurements are made at wavelengths that discriminate the various atoms present, and they are further sensitive to the oxidation state. XMCD spectra, gave two types of findings, one good news, one not good. The good news is that the technique is strong enough to measure the magnetization of the sample, the bad news is that the sample contains sizeable quantities of Mn^{II} in addition to the expected Mn^{III} and Mn^{IV}.

The story does not end here. Many efforts were made to avoid partial reduction of Mn12, but it was impossible to reproduce the magnetization (and in particular the magnetic hysteresis) of the bulk. We concluded that Mn12 clusters are intrinsically labile also due to the interactions with the substrate. All the features that make Mn12 prone to sensitivity to the environment, like mixed valence and Jahn-Teller distortions, which give the exciting properties of the bulk, wipe out on surfaces.

3.8 Conclusions

This Chapter had two goals, showing the present status of MM and highlighting its potentiality in the study of complex systems, possibly providing some examples where some sort of complex behaviour is operative. The trend in MM during the last few years has been initially from simple to complex behaviour, as we tried to show in this work. Then there was a change of direction, giving more attention to simpler systems: from 3D to 0D, 1D, 2D. However structural simplicity does not necessarily imply a simplification of the properties. Moreover this trend allowed better understanding the properties of isolated constituent units. With this understanding it has then been possible to better comprehend their individual role

in more complex networks, where some form of interaction is present. Chemically this has also allowed introducing another typical ingredient of complexity, *i.e.* self-assembly. The last step on this road is now towards single molecule addressing. It may seem the final frontier of simplicity, but it is not the case. Even if we learn to address single molecules, they are never isolated from the environment, as shown by the attempts to develop quantum computing. Only from observation of single molecules can we then start tuning and rationalizing all the complex links of a single magnetic center with all that surrounds it.

The field will continue to develop because it has developed a critical mass of researchers, mainly chemists and physicists. Now that some seminal work has sparked interest in the subject, more work will be done, in an positive-feedback mechanism that is quite typical of complex phenomena. In this and several other aspects the researcher's community behaves in a complex way, switching to new fields and establishing new connections while trying to adapt to ever-changing challenges. In this sense, even the study of complexity is subject to a complex behaviour, and while MM has remained relatively isolated this far more has to come from the interaction with biologists, physicians, engineers, etc.. Maybe another story of complexity, to be studied by future generations.

References

1. Heylighen F (2008) Complexity and self-organization. In: Bates MJ, Maack MN (eds) Encyclopedia of library and information sciences. Taylor & Francis
2. Schrödinger E (1944) What is life? The physical aspect of the living cell. Cambridge University Press, Cambridge
3. Feynman RP (1967) The character of physical law. MIT, Cambridge
4. Dagotto E (2005) Science 309:257
5. Kahn O (1993) Molecular magnetism. VCH, Weinheim
6. Miller JS, Drillon M (eds) (2001–2004) Magnetism: molecules to materials I-V. Wiley VCH, Weinheim
7. Winpenny RJP (ed) (2006) Structure and bonding. Springer, Berlin, p 122
8. Gatteschi D, Sessoli R, Villain J (2006) Molecular nanomagnets. Oxford University Press, Oxford
9. Gatteschi D, Bogani L, Cornia A, Mannini M, Sorace L, Sessoli R (2008) Solid State Sci 10:1701–1709
10. Banci L, Bencini A, Benelli C, Gatteschi D, Zanchini C (1982) Struct Bonding (Berl) 52:37
11. Manriquez JM, Yee GT, McLean RS, Epstein AJ, Miller JS (1991) Science 252:1415
12. Bogani L, Wernsdorfer S (2008) Nat Mat 7:179
13. Lis T (1980) Acta Crystallog B36:2042
14. Caneschi A, Gatteschi D, Sessoli R, Barra A-L, Brunel L-C, Guillot M (1991) J Am Chem Soc 113:5873
15. Sessoli R, Gatteschi D, Caneschi A, Novak MA (1993) Nature 365:141
16. Friedman JR, Sarachik MP, Tejada J, Ziolo P (1996) Phys Rev Lett 76:3830
17. Thomas L, Lioni F, Ballou R, Gatteschi D, Sessoli R, Barbara B (1996) Nature 383:145
18. Villain J, Hartmann BF, Sessoli R, Rettori A (1994) Europhys Lett 27:159
19. Cannon DR, White RP (1988) Progr Inorg Chem 36:195
20. Ramirez AP (1994) Ann Rev Mater Sci 24:453

21. Tsukerblat BS, Belinski MI, Fainzil'berg VE (1987) *Sov Sci Rev B Chem (Engl Transl)* 9:339
22. Awaga K, Okuno T, Yamaguchi A, Hasegawa M, Inabe T, Maruyama Y, Wada N (1994) *Phys Rev B* 49:3975
23. Lau GC (2006) *Nat Phys* 2:249
24. Bramwell ST (2006) *Nat Phys* 2:218
25. Harris MJ, Bramwell ST, McMorro DF, Zeiske T, Godfrey KW (1996) *Phys Rev Lett* 79:2554
26. Gatteschi D, Pardi L, Barra A-L, Müller A, Döring J (1991) *Nature* 354:463
27. Tarantul A, Tsukerblat B, Muller A (2007) *Inorg Chem* 46:161
28. Leuenberger LN, Loss D (2001) *Nature* 410:789
29. Rabi II (1937) *Phys Rev* 51:637
30. Mehring M, Mende J, Scherer W (2003) *Phys Rev Lett* 90:153001
31. Bertaina S, Gambarelli S, Mitra T, Tsukerblat B, Muller A, Barbara B (2008) *Nature* 453:06962
32. van Slageren J, Sessoli R, Gatteschi D, Smith AA, Helliwell M, Winpenny REP, Cornia A, Barra AL, Jansen AGM, Rentschler E, Timco GA (2002) *Chem-Eur J* 8:277–285
33. Larsen F, McInnes E, Mkami HE, Overgaard J, Piligkos S, Rajaraman G, Rentschler E, Smith A, Smith G, Boote V (2003) *Angew Chem Int Ed* 42:101
34. Cador O, Gatteschi D, Sessoli R, Larsen FK, Overgaard J, Barra AL, Teat SJ, Timco GA, Winpenny REP (2004) *Angew Chem Int Ed* 43:5196–5200
35. Ardavan A, Rival O, Morton JLL, Blundell SJ, Tyryshkin AM, Timco GA, Winpenny REP (2007) *Phys Rev Lett* 98:057201
36. Luneau D, Rey P (2005) *Coord Chem Rev* 249:2591
37. Caneschi A, Gatteschi D, Sessoli R, Rey P (1989) *Acc Chem Res* 22:392
38. Caneschi A, Gatteschi D, Melandri MC, Rey P, Sessoli R (1990) *Inorg Chem* 29:4228
39. Caneschi A, Gatteschi D, Lalioi N, Sangregorio C, Sessoli R, Venturi G, Vindigni A, Rettori A, Pini MG, Novak MA (2001) *Angew Chem Int Ed* 40:1760–1763
40. Clerac R, Miyasaka H, Yamashita M, Coulon C (2002) *J Am Chem Soc* 124:12837
41. Coulon C, Miyasaka H, Clérac R (2006) *Struct Bonding Berl* 122:163–206
42. Bogani L, Vindigni A, Sessoli R, Gatteschi D (2008) *J Mater Chem* 18:4750
43. Glauber RJ (1963) *J Math Phys* 4:294
44. Bogani L, Sessoli R, Pini MG, Rettori A, Novak MA, Rosa P, Massi M, Fedi ME, Giuntini L, Caneschi A, Gatteschi D (2005) *Phys Rev B* 72:064406
45. Bogani L, Caneschi A, Fedi ME, Gatteschi D, Massi M, Novak MA, Pini MG, Rettori A, Sessoli R, Vindigni A (2004) *Phys Rev Lett* 92:207204
46. Vindigni A, Rettori A, Bogani L, Caneschi A, Gatteschi D, Sessoli R, Novak MA (2005) *Appl Phys Lett* 27:073102
47. Luscombe JH, Luban M, Reynolds JP (1996) *Phys Rev E* 53:5852–5860
48. Kamphors Leal da Silva J, Moreira AG, Sa Barreto FC (1995) *Phys Rev E* 52:4527–4528
49. Vindigni A (2008) *Inorg Chim Acta* 361:3731
50. Mydosh A (1993) *Spin glasses: an experimental introduction*. Taylor & Francis, London
51. Fisher KH, Hertz JA (1993) *Spin glasses*. Cambridge University Press, Cambridge
52. Binder K, Young AP (1986) *Rev Mod Phys* 58:801
53. Van Hemmen JL, Morgenstern I (eds) (1986) *Heidelberg colloquium on spin glasses, lecture notes in physics*. Springer, Berlin, p 192
54. Bogani L (2006) *Magnetic and optical study of molecular magnets*. Ph.D. Thesis
55. Zhou W-X, Sornette D (2007) *Eur Phys J B: Cond Mat Comp Sys* 55:175
56. Benelli C, Gatteschi D (2002) *Chem Rev* 102:2369
57. Costes JP, Clemente-Juan JM, Dahan F, Milon J (2004) *Inorg Chem* 43:8200
58. Ramirez AP, Hayashi A, Cava RJ, Siddharthan R, Shastry BS (1999) *Nature* 399:333
59. Benelli C, Caneschi A, Gatteschi D, Pardi L, Rey P (1990) *Inorg Chem* 29:4223
60. Masuda T, Zheludev A, Bush A, Markina M, Vasiliev A (2004) *Phys Rev Lett* 92:177201
61. Cinti F, Rettori A, Pini MG, Mariani M, Micotti E, Lascialfari A, Papinutto N, Amato A, Caneschi A, Gatteschi D, Affronte M (2008) *Phys Rev Lett* 100:057203
62. Villain J (1978) *Ann Isr Phys Soc* 2:565
63. Baibich MN, Broto JM, Fert A, Dan FNV, Petroff F (1988) *Phys Rev Lett* 61:2472

64. Binasch G, Grünberg P, Saurenbach F, Zinn W (1989) *Phys Rev B* 39:4828
65. Felser C, Fecher GH, Balke B (2007) *Angew Chem Int Ed* 46:668
66. Clemente-Leon M, Sover H, Coronado E, Mongotaud C, Gomez-Garcia CJ, Delhaes P (1998) *Angew Chem Int Ed* 37:2842
67. Cornia A, Fabretti AC, Pacchioni M, Zobbi L, Bonacchi D, Caneschi A, Gatteschi D, Biagi R, Del Pennino U, De Renzi V, Gurevich L, Van der Zant HJ (2003) *Angew Chem Int Ed* 42:1645
68. Condorelli GG, Motta A, Fragala IL, Giannazzo F, Raineri V, Caneschi A, Gatteschi D (2004) *Angew Chem Int Ed* 43:4081–4084
69. Voss S, Fonin M, Rudiger U, Burgert M, Groth U, Dedkov YS (2007) *Phys Rev B* 75:045102
70. Wende H, Bernien M, Luo J, Sorg C, Ponpandian N, Kurde J, Miguel J, Piantek M, Xu X, Eckhold P, Kuch W, Baberschke K, Panchmatia PM, Sanyal B, Oppeneer X, Eriksson O (2007) *Nat Mater* 6:516

Chapter 4

Rational Design of Single-Molecule Magnets

Thorsten Glaser

Abstract Single-molecule magnets possess a superior property in comparison to other polynuclear but only paramagnetic transition metal complexes: single-molecule magnets can be magnetized and they remain magnetized, even in the absence of an external magnetic field. They exhibit a hysteresis in the magnetization in analogy to the well-established solid-state magnets. Due to these promising properties, single-molecule magnets have attracted a great deal of research. However, the key property, the blocking temperature, has not been increased since the discovery of the first single-molecule magnet **Mn₁₂**. A reason for this failure may be found in the prevalence of serendipitous approaches to new single-molecule magnets: metal ions and small ligands are reacted in the hope to obtain a new single-molecule magnet. The massive characterization of **Mn₁₂** has shed light on necessary requirements for a polynuclear transition metal complex to behave as a single-molecule magnet. Besides the usually accepted two requirements (i.e. a high spin ground state and a magnetic anisotropy), a control of the molecular topology seems to be highly demanded. In order to reduce the tunneling through the anisotropy barrier, the rhombicity of the spin ground state should be close to zero. This requires at least a molecular C_3 symmetry. Additionally, the overall metal ion arrangement should be lower than a cubic. Otherwise, the local magnetic anisotropies cancel each other by projecting onto the spin ground state. We have performed a ligand design in accordance to the above given requirements, which will be presented here. The triplesalen ligand combines the phloroglucinol bridging unit for high spin ground state and a salen like coordination environment for local magnetic anisotropies. In addition, this ligand is C_3 symmetric and imposes a C_3 symmetry on its complexes. The first example of a rationally designed single-molecule magnet, **Mn₆Cr³⁺**, will be described in some detail.

T. Glaser (✉)

Lehrstuhl für Anorganische Chemie I, Fakultät für Chemie, Universität Bielefeld,
Universitätsstr. 25, D-33615 Bielefeld, Germany
e-mail: thorsten.glaser@uni-bielefeld.de

4.1 Introduction to Molecule-Based Magnetic Materials

The design and synthesis of molecule-based magnets has attracted considerable interest over the past two decades. The synthetic efforts have focused on the assembly of molecular building blocks to form supramolecular magnetic materials [1–5]. The discovery of $[\text{Cp}^*_2\text{Fe}]^+[\text{TCNE}]^-$, (**1**, $\text{Cp}^* = \text{pentamethylcyclopentadienyl}$, $\text{TCNE} = \text{tetracyanoethylene}$) in 1985, a compound comprised of molecular building blocks, which exhibits a spontaneous long-range ferromagnetic order at 4.8 K [6–8] started the field of molecule-based magnets. It is important to differentiate between the field of molecular magnetism in general and molecule-based magnets in specific. The quite mature field of molecular magnetism deals with the properties of mononuclear or polynuclear transition metal complexes [9]. In the latter, a strong focus is on the exchange interaction between the paramagnetic centers in the polynuclear complexes. Despite these intramolecular interactions there are only very weak intermolecular interactions between the molecules and therefore the bulk samples are only paramagnetic; they exhibit no magnetization without an applied magnetic field. Compounds that are synthesized from molecular building blocks under the typical mild reaction conditions of molecular chemistry but which exhibit a hysteresis in the magnetization and which remain a magnetization at zero external fields are magnets in analogy to solid-state magnets and are termed molecule-based magnets.

Since the discovery of the fascinating properties of **1**, a number of molecule-based magnets have been reported showing long-range ordering below a critical temperature (Curie temperature, T_c) [1–3,9–11]. Several compounds were reported with T_c 's exceeding room temperature: $\text{V}(\text{TCNE})_x \cdot y(\text{CH}_2\text{Cl}_2)$ (**2**) is a non-crystalline non-stoichiometric compound with an estimated $T_c \approx 400$ K [12,13] and $\text{V}_{0.42}^{\text{II}}\text{V}_{0.58}^{\text{III}}[\text{Cr}^{\text{III}}(\text{CN})_6]_{0.86}$ is a non-stoichiometric compound with $T_c = 315$ K [14].

The existing molecule-based magnets can be roughly divided into four main categories:

1. Compounds based on metallocenes and/or polycyanoradical anions

The structure of **1** consists of chains of alternating $[\text{Cp}^*_2\text{Fe}]^+$ and $[\text{TCNE}]^-$ units both having a $S = 1/2$ ground state. The intra-chain interaction is ferromagnetic with $J = 13 \text{ cm}^{-1}$ ($H = -2J\mathbf{S}_1\mathbf{S}_2$) [8]. Below 4.8 K, a weak coupling between the chains leads to the observed spontaneous magnetization. The origin of the intra-chain interaction is still a matter of controversy and a charge transfer and a spin-polarization mechanism are discussed [15–17]. A stronger exchange interaction ($J = 53 \text{ cm}^{-1}$) is determined for **2** leading to the much higher T_c [18]. Numerous variations of the cyclopentadienyl ligand, the metal ion, and the tetracyanoradical anion were reported in the literature [18–20].

2. Cyanide-bridged compounds based on Prussian blue

There exist a large number of 3-dimensional cyanide-bridged compounds of the general composition $\text{M}_x^{\text{A}}[\text{M}^{\text{B}}(\text{CN})_6]_y$ with close structural analogy to the archetype Prussian blue, $\text{Fe}_4^{\text{III}}[\text{Fe}^{\text{II}}(\text{CN})_6]_3$, with varying metal centers and

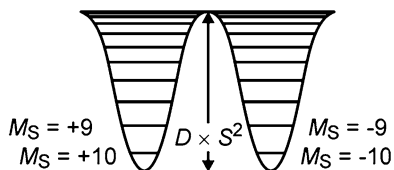


Fig. 4.1 Energy Level diagram for a $S = 10$ spin system with a negative zero-field splitting parameter D . Note that the drawing in form of potential wells is only to guide the eyes. The x -axis has no physical meaning

stoichiometries [21–26]. The strong interactions between the spin centers in three dimensions lead to high T_c 's. Most of these compounds are non-stoichiometric which yield mixed-valence systems. $\text{Cr}_{1.29}^{\text{II}}[\text{Cr}_{1.14}^{\text{III}}(\text{CN})_6]$ can be electrochemically switched between a paramagnetic and a ferrimagnetic phase [27] and $\text{K}_{0.2}\text{Co}_{1.4}[\text{Fe}(\text{CN})_6] \cdot 6.9\text{H}_2\text{O}$ is reported to be a photomagnetic switch in which light-induced electron transfer between Fe^{II} l.s./ Co^{III} l.s. and Fe^{III} l.s./ Co^{II} h.s. leads to a change in T_c and the saturation magnetization [28, 29].

3. 1-Dimensional systems and their 2- and 3-dimensional extensions

The archetypes of 1-dimensional chain compounds synthesized from molecular building blocks are $[\text{Mn}^{\text{II}}(\text{OH}_2)\text{Cu}^{\text{II}}(\text{pba})(\text{OH}_2)] \cdot 2\text{H}_2\text{O}$ (**3**, pba = 1,3-propylenbisoximato) and $[\text{Mn}^{\text{II}}\text{Cu}^{\text{II}}(\text{pbaOH})(\text{H}_2\text{O})_3] \cdot 3\text{H}_2\text{O}$ (**4**, pbaOH = 2-Hydroxo-1,3-propylenbisoximato). The ferrimagnetically coupled chains order due to weak antiferromagnetic inter-chain interactions in **3** and weak ferromagnetic inter-chain interactions in **4** at 2.4 and 4.6 K, respectively [9, 30–32]. Based on the success of the concept of ferrimagnetic chains, 1-, 2-, and 3-dimensional architectures using oxalate-, dithiooxalate, oxamide, oxamate, and azide were synthesized [33–42]. Most of these compounds possess only low T_c 's due to weak interactions between the metal centers and low local spin values of the metal centers chosen (Mn^{II} h.s. has a large spin $S = 5/2$ but undergoes only weak exchange couplings due to the low covalency of the Mn^{II} -ligand bonds). An interesting extension is the introduction of a bridging radical ligand like nitronylnitroxides [43–50] and tetracyanoradical anions [51–54].

4. Single-molecule magnets

Polynuclear complexes with a high spin ground state S_t and a magnetic anisotropy with an easy axis (phenomenologically parametrized in a spin-Hamiltonian approach, $H = D \times S_z^2$, by a negative zero-field splitting parameter D) can show hysteresis in the magnetization of pure molecular origin, *i.e.* no long-range order is needed. The relaxation from the $m_S = -S_t$ in the $m_S = +S_t$ state is hindered by an energy barrier $D \times S_t^2$ greater than kT (Fig. 4.1).

The two archetypes of SMMs are the family of dodecanuclear manganese carboxylate complexes $\text{Mn}_{12}\text{OCOR}$ [55–63] and an octanuclear iron complex Fe_8 [64–67]. Both possess an $S_t = 10$ spin ground state; the zero-field splittings of the ground states are $D \sim -0.5$ and $D \sim -0.19 \text{ cm}^{-1}$ for Mn_{12}OAc and Fe_8 ,

respectively. The special properties of single-molecule magnets (SMMs) makes them potential candidates for applications in quantum computing and in ultimate high-density memory storage devices in which each bit of digital information is stored on a single molecule [68–73].

4.1.1 High Spin Ground States

The high spin ground states in these systems usually arise from competing antiferromagnetic interactions of different magnitudes between the paramagnetic centers leading to complicated spin ladders. Our approach to develop new types of molecule-based magnets may be summarized by a quote of the late Olivier Kahn: ‘The normal trend for the molecular state is the pairing of electrons [...] with a cancellation of the electron spins. The design of a molecule-based magnet requires that this trend be successfully opposed’ [74].

From the study of exchange interactions between paramagnetic centers in the past 30 years, we have identified three general strategies for achieving ferromagnetic couplings, which we try to apply for the rational development of new molecule-based magnets:

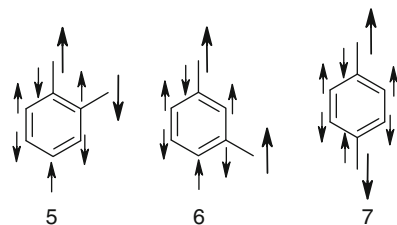
1. the use of orthogonal magnetic orbitals [75–77] (2nd Goodenough-Kanamori rule) [78–84],
2. the double exchange mechanism [85–87] in face-sharing octahedral [88–90], and
3. the spin-polarization mechanism [91–95] via *meta*-phenylene linkages [96–101].

In this contribution, the rational design of SMMs with the application of the spin-polarization mechanism is presented in some detail. Therefore, the principles of the spin-polarization mechanism are shortly introduced below. We discussed several theoretical approaches to spin-polarization in a recent account [102].

4.2 The Spin-Polarization Mechanism

It is well established in organic chemistry that the *meta*-phenylene linkage of organic radicals and carbenes leads to ferromagnetic interactions, while in the corresponding *ortho*- and *para*-phenylene linkages, the interaction is antiferromagnetic [92–95, 103–105]. This simple, heuristic phenomenon is usually attributed to a general mechanism termed spin-polarization. A simple explanation is the following: a localized, unpaired electron of say α -spin interacts differently with the two paired electrons in a bonding MO. While the unpaired electron experiences a Coulomb repulsion by both electrons in the bonding MO, some exchange stabilization occurs for the electrons of like spin, i.e. the α -spin electrons. This leads to different potentials felt by the two electrons in the bonding MO due to the presence of the unpaired electron. Thus, the two electrons in the bonding orbital are not equal

Scheme 4.1



anymore and therefore the spatial distribution and the energy of the MOs they occupy must differ; the two bonding electrons are spin-polarized by the unpaired electron. The consequence in a simple picture is a higher probability for the α -spin electron to be close to the unpaired electron and for the β -spin electron to be close to the neighbouring atom bonded to the atom with the unpaired electron. This leads to an induction of a spin-density of opposite sign at the neighbouring atom.

This treatment provides a simple picture for explaining the observed ferromagnetic $S_t = 1$ ground state in the *meta*-phenylene-bridged diradical **6** as compared to the antiferromagnetic ground state in the *ortho*- and *para*-isomers **5** and **7**, respectively: the sign of the spin-density of the atoms in the bridging benzene unit of the atoms alternates [106]. This is illustrated in Scheme 4.1 and provides the opportunity to develop high-spin organic radicals and carbenes on the back of an envelope.

This concept was applied to transition metal complexes by using various bridging units. Some complexes with pyrimidine used as a *meta*-phenylene bridging unit indeed exhibit ferromagnetic interactions [107–110]. While these reports seem to show that the spin-polarization mechanism, originally developed for organic radicals and carbenes, can be adapted in coordination chemistry, bridging pyrimidine units facilitate antiferromagnetic couplings in other transition metal complexes [111–120].

On the other hand, McCleverty, Ward, Gatteschi, and coworkers [121] have been able to correlate the exchange couplings in dinuclear Mo complexes of extended polypyridyl and polyphenol ligands with the bridging topology by the spin-polarization mechanism [122–127]. In the contents of this account, the first application of 1,3,5-trihydroxybenzene (phloroglucinol) should be highlighted, which they used as bridging ligand for three Mo^{V} complex fragments [124]. Parallel to our efforts to employ phloroglucinol as bridging unit in trinuclear complexes of first-row transition metal ions, Journaux and coworkers developed bridging units based on 1,3-diaminobenzene and 1,3,5-triaminobenzene [128–134].

The above given examples indicate that the concept of spin-polarization, which almost always works in organic chemistry to predict ferromagnetic interactions and to rationally develop new high-spin compounds, cannot be applied in a straightforward manner to transition metal complexes and more research on this aspect is necessary to understand the intrinsic differences of spin-polarization in organic molecules and in transitional metal complexes in more detail.

4.2.1 Design Principle

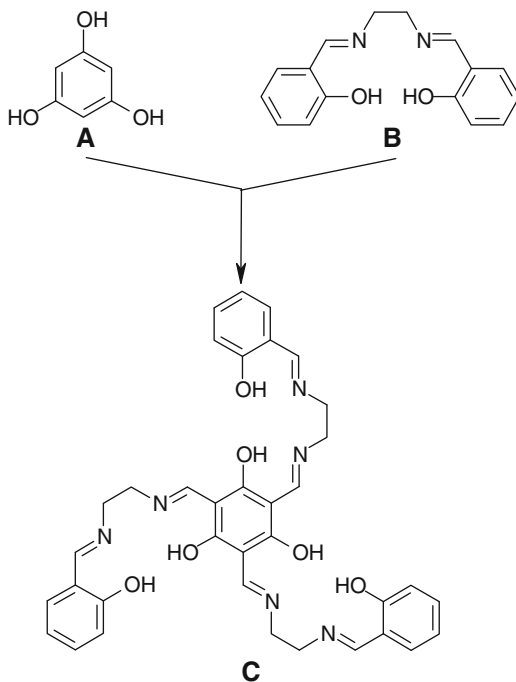
The fundamental requirement for a SMM is the occurrence of an energy barrier $D \times S_t^2$ (Fig. 4.1). Thus, the necessary prerequisites for SMMs are a high spin ground state S_t combined with a strong magnetic anisotropy D_{S_t} and a rational approach to develop new SMMs must take these prerequisites into account. In order to rationally design polynuclear complexes with high spin ground states S_t , predictable combinations of ferro- and ferrimagnetic couplings are key requirements (vide supra). The magnetic anisotropy of the ground state (D_{S_t}) is a complicated quantity, but has its main contribution usually from the projection of the single-site anisotropies (D_i) onto the spin ground state S_t , while dipolar and anisotropic interactions yield only minor contributions [135–138]. Since zero-field splittings are tensor quantities, the projection of the single-site zero-field splittings onto the spin ground state may vanish when the metal ion arrangement approaches a cubic symmetry. Thus, a rational design of SMMs additionally requires a control of the molecular topology which can usually not be achieved by simply increasing the nuclearity of complexes using small bridging ligands. Another prerequisite for a SMM to function as a data storage is the minimization of the quantum-mechanical magnetization tunneling which provides an alternative pathway for spin-reversal and thus the loss of information [139–141]. This tunneling mechanism is directly related to the rhombic component of the magnetic anisotropy expressed by E_{S_t} which is exactly zero for complexes with at least a threefold axis.

In summary, there are three requirements for a targeted synthesis of SMMs: (i) a high spin ground state S_t , (ii) a source of single-site anisotropies D_i , and (iii) a control of the molecular symmetry, which must be at least of C_3 symmetry, but which must be lower than a cubic symmetry. In order to have no necessity to rely on a serendipitous fulfillment of these requirements (as in **Mn₁₂OCOR**), these requirements must be the basis for the design of a proper polynucleating ligand of low flexibility.

In order to fulfill all these requirements for SMMs, we have designed the C_3 -symmetric triplesalen ligand **C** (Scheme 4.2) which combines the phloroglucinol bridging unit **A** for high spin ground states with the coordination environment of a salen ligand **B** for strong magnetic anisotropy. The phloroglucinol bridging unit **A** acts as a ferromagnetic coupler in trinuclear transition metal complexes by the spin-polarization mechanism (vide supra). In order to introduce magnetic anisotropy we have chosen a salen-like coordination environment **B** which is known to cause a pronounced magnetic anisotropy by its strong ligand field in the basal plane [142].

The magnetic anisotropy (anisotropy in the **g**-tensor and zero-field splitting) of transition metal ions without first-order orbital momentum arises from the combined effects of a symmetry reduction from O_h and mixing of excited states into the ground state by spin-orbit coupling. The greater the deviation from octahedral symmetry, the larger is the magnetic anisotropy for a given transition metal ion. For example, in the case of Mn^{III} complexes in a tetragonal elongated octahedral coordination

Scheme 4.2

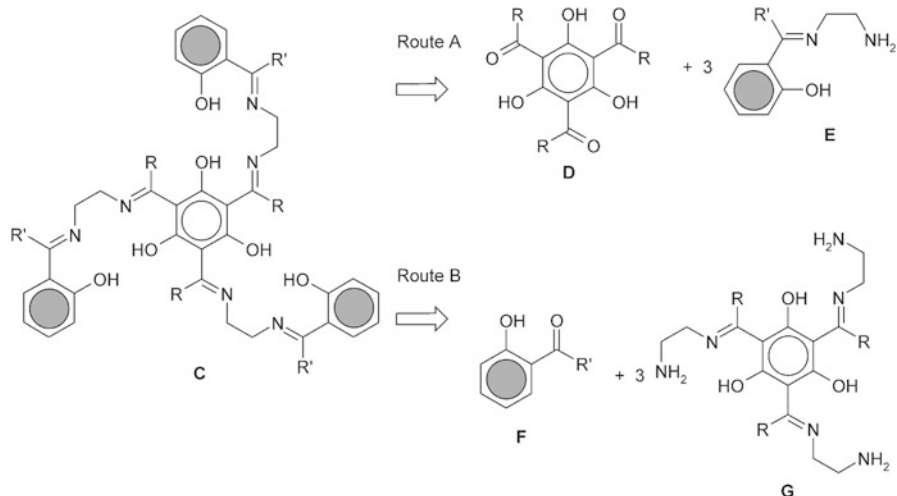


environment zero-field splittings D in the range of -1.17 to -4.52 cm^{-1} have been reported [135,143–149].

A ligand intensively studied for the last century with a very strong ligand field in the basal plane is the salen ligand ($\text{H}_2\text{salen} = N,N'$ -bis(salicylidene)ethylenediamine). The axial positions are mostly occupied by weak ligands, or one or both of the axial coordination sites are vacant. This tetragonally elongated ligand field gives rise to mononuclear complexes with a relative strong single-site magnetic anisotropy. A well studied example is the Jacobsen's catalyst (R,R)- N,N' -bis(3,5-di-*tert*-butylsalicylidene)-1,2-cyclohexanediamine [150–152]. Campbell et al. studied the catalyst upon addition of substrate by dual-mode EPR spectroscopy and determined a zero-field splitting of $D = -2.5$ cm^{-1} for the Mn^{III} ($S = 2$) species [153].

4.2.2 The Synthesis of Triplesalen Ligands

The targeted triplesalen ligand C contains three unsymmetrically substituted ethylenediamine units making the synthesis not trivial. The preparation of symmetrical salen ligands involves the Schiff-base condensation of ethylenediamine or another diamine with two equivalents of an aldehyde or keton. The synthesis of an unsymmetrically substituted salen derivative must involve in a first step the isolation

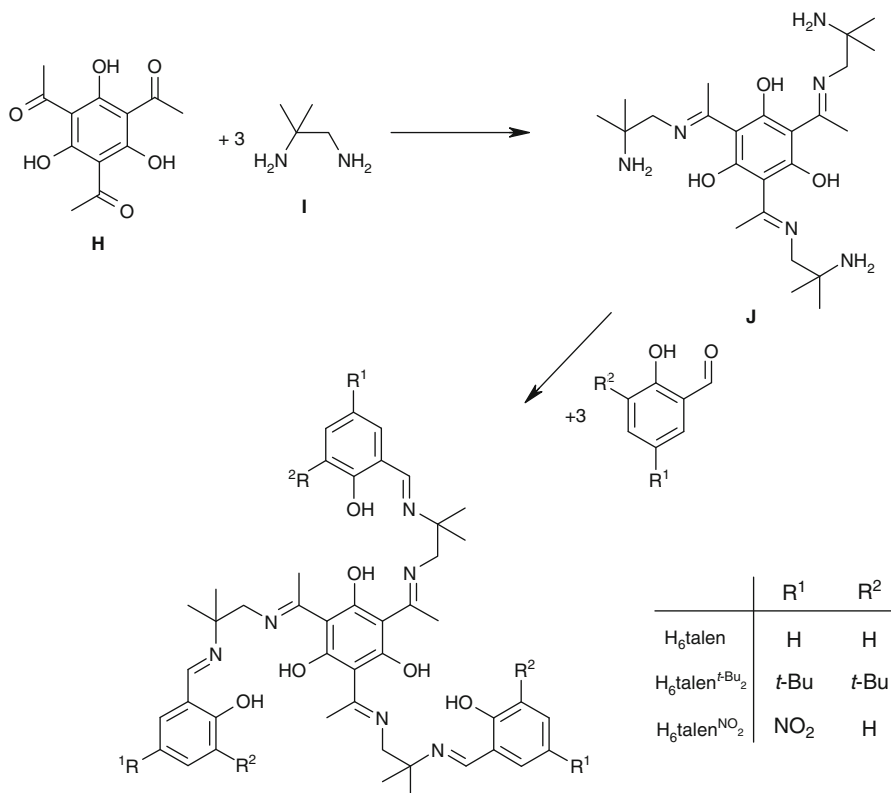


Scheme 4.3

of a mono-condensated ethylenediamine, a salen half-unit [154–156]. Two reaction routes are in principle feasible for the preparation of the targeted triplesalen ligand **C** (Scheme 4.3). Route A requires the synthesis of a salen half-unit **E** in the first step which reacts in the second step with a carbonyl derivative of phloroglucinol **D**. Route B requires the synthesis of a half-unit of the triplesalen ligand **G** which reacts in the second step with a *o*-carbonyl derivative of phenol **F**.

The half-unit **E** of salen is not accessible. Even the reaction of salicylaldehyde with a 20-fold excess of ethylenediamine at low temperatures yields only the symmetric salen. Thus, the key step in the synthesis of a triplesalen ligand **C** is the preparation of a half-unit, either **E** or **G**. Several methods for the preparation and isolation of derivatives of the parent salen half-unit **E** are described in the literature [155–159]. We applied several of these methods for the synthesis of a triplesalen ligand and obtained various new compounds [160]. However, the successful synthesis of a triplesalen ligand is based on an observation of Elias and coworkers [158]. They reported that the slightly modified diamine **I** (Scheme 4.4) reacts with its sterically more crowded amine function not with ketones to form ketimines, but only with aldehydes to form aldimines. On the other hand, the less crowded amine function does react with aldehydes as well with ketones to form imines. Thus, the reaction of the diamine **I** with the triketone **H** affords chemoselectively the triple ketimine **J**, which corresponds to the triplesalen half-unit **G**. In a second step, the triple ketimine **J** can be reacted with a simple salicylaldehyde (corresponding to **F**) to yield the desired triplesalen (Scheme 4.4).

We have synthesized several substituted triplesalen ligands [161, 162], but for this context we want to focus only on the *t*-butyl derivative $H_{6\text{talen}}^{t\text{-Bu}_2}$.

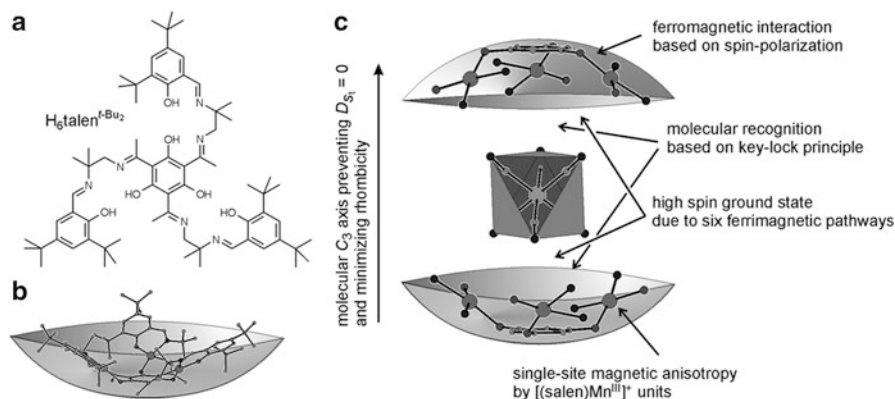


Scheme 4.4

4.2.3 Complex Synthesis

The axial positions of metal salen complexes are easily reacted with hexacyanometallates. The resulting compounds vary in nuclearity and dimensionality. A hexacyanometallate can coordinate 1–6 metal salen units and the metal salen unit can adopt 1 or 2 hexacyanometallate in its axial positions. Thus, the reaction of a hexacyanometallate and a metal salen unit can lead to discrete heteropolynuclear complexes (0D) of various nuclearity, but also 1D chains, 2D sheets, and 3D networks can result [163–172]. While these compounds exhibit interesting properties, the nuclearity and the dimensionality is difficult to control.

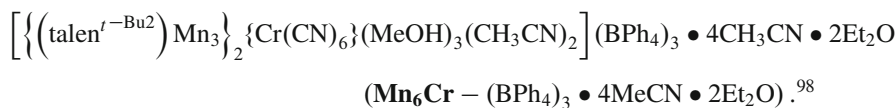
Trinuclear complexes of the *tert*-butyl derivative H₆talen^{*t*-Bu₂} (Scheme 4.5a) are not flat but bowl-shaped (Scheme 4.5b). This ligand folding preorganizes the three metal ions for a facial coordination by three N-donor atoms of a hexacyanometallate favoring the formation of heptanuclear complexes M₆^AM^B by molecular recognition in analogy to the key-lock principle (Scheme 4.5c).



Scheme 4.5

An anticipated heptanuclear $\text{Mn}_6\text{Cr}^{3+}$ assembly fulfills all the requirements for SMMs, namely: (i) the tripesalen bridge should favor a parallel spin alignment of the three Mn^{III} ions of a molecular $[(\text{talen}^{t\text{-Bu}2})\text{Mn}_3^{\text{III}}]^{3+}$ building block while the ferrimagnetic $\text{Mn}^{\text{III}}\text{-N}\equiv\text{C-Cr}^{\text{III}}$ pathways enforce a high spin ground state of $S_t = 21/2$ without any competing interactions, (ii) the $[(\text{salen})\text{Mn}^{\text{III}}]^+$ subunits provide a pronounced single-site D_i , (iii) the C_3 symmetry precludes that the single-site D_i s compensate completely by projecting onto S_t , and (iv) the molecular C_3 axis enforces $E_{S_t} = 0$ thus minimizing the disturbing tunneling probability.

The reaction of $\text{H}_6\text{talen}^{t\text{-Bu}2}$, $\text{Mn}(\text{OAc})_2 \cdot 4\text{H}_2\text{O}$, and $\text{K}_3[\text{Cr}(\text{CN})_6]$ in the molar ratio 2:6:1 in a $\text{MeOH}/\text{H}_2\text{O}$ mixture yields after addition of NaBPh_4 and recrystallization from $\text{MeCN}/\text{Et}_2\text{O}$ large brownish-black single-crystals of



The high yield of 78% indicates the success of the anticipated molecular recognition process of the three molecular building blocks.

The molecular structure of the trication $[\{(\text{talen}^{t\text{-Bu}2})\text{Mn}_3\}_2\{\text{Cr}(\text{CN})_6\}]^{3+}$ consists of two trinuclear manganese tripesalen complexes bridged by a central $[\text{Cr}(\text{CN})_6]^{3-}$ as a sixfold connector (Fig. 4.2). The manganese ions are coordinated in their basal planes by the N_2O_2 donor set of the salen-like coordination environment. The nitrogen atoms of the $[\text{Cr}(\text{CN})_6]^{3-}$ occupy apical positions. The remaining coordination sites to complete an octahedral coordination environment are either occupied by weakly coordinated solvent molecules or this position remains unoccupied. The Jahn-Teller axis of the Mn^{III} ions is along the $\text{Mn-N}^{\text{C}\equiv\text{N}}$ bonds. The different occupation of the sixth positions results in an only approximate C_3 symmetry.

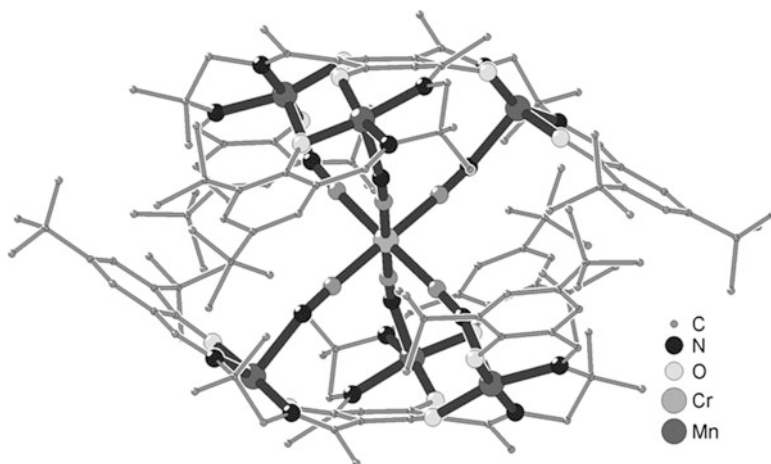


Fig. 4.2 Molecular structure of the trication $\text{Mn}_6\text{Cr}^{3+}$. For sake of clarity the loosely bound solvent molecules have been omitted

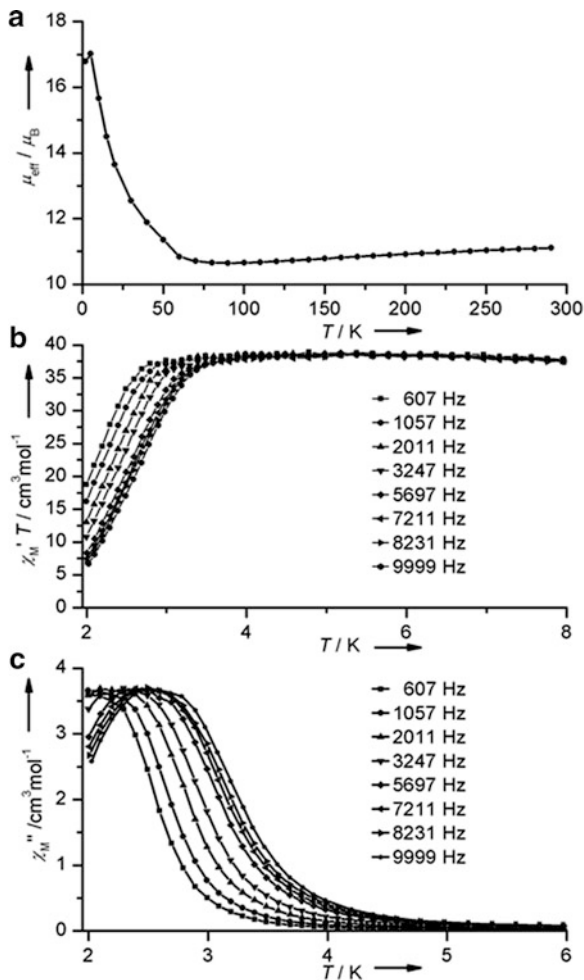
While as usual the $\text{Cr}-\text{C}\equiv\text{N}$ connection is almost linear ($175\text{--}177^\circ$), the $\text{C}\equiv\text{N}-\text{Mn}$ unit is bent with angles of $160\text{--}162^\circ$. This bending aligns the manganese ions towards the molecular C_3 axis. It is important to note that the crystal structure contains $\text{Mn}_6\text{Cr}^{3+}$ with two different orientations. The angle between their pseudo C_3 axes is 41.7° .

4.2.4 Magnetic Properties

Temperature-dependent magnetic susceptibility measurements (at 0.05 T) on powdered samples of $\text{Mn}_6\text{Cr}-(\text{BPh}_4)_3$ reveals $\mu_{\text{eff}} = 11.10 \mu_{\text{B}}$ at 290 K (Fig. 4.3a). This implies the occurrence of antiferromagnetic interactions, because the theoretical value for an uncoupled spin system of 6 Mn^{III} ($S_i = 2$) and 1 Cr^{III} ($S_i = 3/2$) with $g_i = 1.98$ is $12.48 \mu_{\text{B}}$. With decreasing temperature, μ_{eff} decreases slightly and exhibits a minimum of $10.65 \mu_{\text{B}}$ at 90 K. Further temperature decrease results in a steep increase of μ_{eff} to $17.02 \mu_{\text{B}}$ at 5 K and a small subsequent decrease down to 2 K. This temperature dependence is typical for a ferrimagnetically coupled complex which enforces an antiparallel orientation of the central Cr^{III} spin with the terminal Mn^{III} spins resulting in a $S_t = 21/2$ ground state. The low temperature μ_{eff} value does not reach the theoretical value of $21.76 \mu_{\text{B}}$ for $S_t = 21/2$ with $g = 1.98$ due to the combined influence of zero field splitting, saturation, and intermolecular interactions.

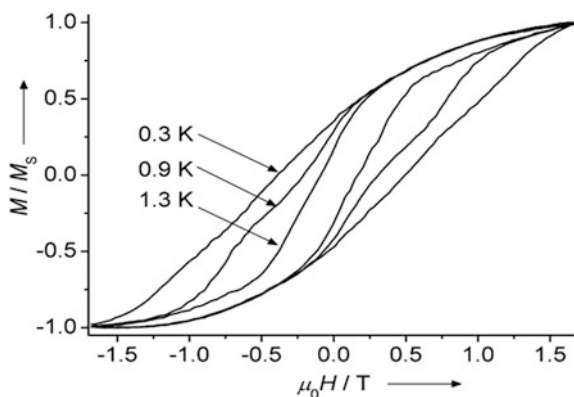
Alternating current (ac) magnetic susceptibility measurements in zero dc field allow to probe slow magnetization relaxation indicating SMMs behaviour. The applied oscillating field probes the dynamics of this reorientation, as the out-of-

Fig. 4.3 Temperature dependence of (a) μ_{eff} (dc), (b) $\chi_M' \cdot T$ (ac), and (c) χ_M'' (ac) for a microcrystalline sample of $\text{Mn}_6\text{Cr}(\text{BPh}_4)_3$. The ac data were measured at zero dc field with a 3 G ac field at the indicated frequencies. Lines are only to guide the eyes



phase signal (χ_M'') is at maximum when the frequency of the ac field equals the relaxation rate of the magnetization. In Fig. 4.3b, c, the temperature dependence of $\chi_M' \cdot T$ and χ_M'' at different ac frequencies is shown. The $\chi_M' \cdot T$ values are almost temperature-independent which means that only the ground state is populated at these temperatures. The sharp decrease of the $\chi_M' \cdot T$ signals is accompanied by the appearance of frequency-dependent χ_M'' values proving the slow relaxation of the magnetization. The energy barrier U_{eff} for the relaxation can be derived from an Arrhenius plot as 25.4 K with $\tau_0 = 8 \times 10^{-10}$ s. Although, the occurrence of frequency-dependent χ_M'' maxima is already considered as a key signature of a SMM, only hysteresis loops obtained from magnetization vs dc field provide finite evidence of a SMM. Single-crystal magnetization data on $\text{Mn}_6\text{Cr}(\text{BPh}_4)_3 \cdot 4\text{MeCN} \cdot 2\text{Et}_2\text{O}$ have been obtained using a 2DEG Hall probe magnetometer

Fig. 4.4 Hysteresis loops measured at a sweep rate of 50.3 mT s^{-1} on a single crystal of Mn_6Cr (BPh_4)₃·4MeCN·2Et₂O at different temperatures



(Fig. 4.4). Although two orientations of $\text{Mn}_6\text{Cr}^{3+}$ with an angle of 41.7° prevail in the single-crystal, hysteresis loops with significant coercive fields below 1.5 K are clearly apparent.

4.3 Conclusions

It is interesting to compare our results on $\text{Mn}_6\text{Cr}^{3+}$ using the rationally developed triplesalen ligand with a closely related $\text{Mn}_6\text{Cr}^{3+}$ complex, prepared using the standard salen ligand. The reaction of $[\text{Cr}(\text{CN})_6]^{3-}$ with $[(\text{salen})\text{Mn}(\text{OH}_2)]^+$ results in the formation of a heptanuclear complex $[\{(\text{salen})\text{Mn}^{\text{III}}\}_6\{\text{Cr}(\text{CN})_6\}]^{3+}$, which exhibits a high spin ground state of $S_t = 21/2$ by ferrimagnetic interactions [173]. Although, $[(\text{salen})\text{Mn}^{\text{III}}]^+$ units are incorporated as a source of single-ion magnetic anisotropy, this heptanuclear complex was shown not to behave as a SMM [174]. The difference in the two $\text{Mn}_6\text{Cr}^{3+}$ complexes is that the one using normal salen has a close to cubic arrangement of the 6 Mn^{III} ions around the central Cr^{III} ion, while the triplesalen ligands pull its three Mn^{III} ions closer together. This results in a symmetry reduction from O_h to C_3 and the non-cancelling of the local anisotropies in the triplesalen complex.

In summary we have developed a three component building block system by considering all necessary properties required for SMMs. The first member of this new class, $\text{Mn}_6\text{Cr}^{3+}$, has a $S_t = 21/2$ ground state accompanied by sufficient magnetic anisotropy to provide a relative high barrier for the reversal of the magnetization. The key features of this unprecedented class are a self-assembly process of the molecular building blocks by molecular recognition and the deviation from a cubic metal ion arrangement by the constraints of the triplesalen ligand backbone. The syntheses and study of other members of this new class of $\text{M}_6^{\text{A}}\text{M}^{\text{B}}$ compounds is currently performed in our laboratories.

Acknowledgements I gratefully acknowledge financial support from the Fonds der Chemischen Industrie, der Deutschen Forschungsgemeinschaft, dem Bundesministerium für Bildung und Forschung, der Dr. Otto Röhm Gedächtnisstiftung as well as the universities of Münster and Bielefeld. I deeply appreciate the fundamental work of one of my first co-workers, Dr. Maik Heidemeier, who started this project and who did all the syntheses described herein. Additionally, I am very thankful to my collaborators and friends to this project: Dr. Eckhard Bill, Dr. Thomas Weyhermüller (both MPI for Bioinorganic Chemistry), Prof. Paul Müller (University of Nürnberg/Erlangen), and Dr. Rolf-Dieter Hoffmann (University of Münster).

References

1. Gatteschi D, Kahn O, Miller JS, Palacio F (eds) (1991) *Magnetic molecular materials*, vol 198, NATO ASI Series, Series E: Appl. Sciences. Kluwer Acad. Publ, Dordrecht
2. Miller JS, Epstein AJ (1994) *Angew Chem Int Ed Engl* 33:385–415
3. Coronado E, Delhaès P, Gatteschi D, Miller JS (eds) (1996) *Molecular magnetism: from molecular assemblies to the devices*, vol 321, NATO ASI Series, Series E: Applied Sciences. Kluwer Academic Publishers, Dordrecht
4. Miller JS, Drillon M (2001–2005) *Magnetism: molecules to materials*, vol I-V. Wiley-VCH, Weinheim
5. Miller JS (2000) *Inorg Chem* 39:4392–4408
6. Miller JS, Krusic PJ, Epstein AJ, Reiff WM, Zhang JH (1985) *Mol Cryst Liq Cryst* 120:27–34
7. Miller JS, Calabrese JC, Epstein AJ, Bigelow RW, Zhang JH, Reiff WM (1986) *J Chem Soc, Chem Comm* 1026–1028
8. Miller JS, Calabrese JC, Rommelmann H, Chittipeddi S, Epstein AJ, Zhang JH, Reiff WM (1987) *J Am Chem Soc* 109:769–781
9. Kahn O (1993) *Molecular magnetism*. VCH Publisher, New York
10. Gatteschi D (1994) *Adv Mat* 6:635–645
11. Turnbull MM, Sugimoto T, Thompson LK (eds) (1996) *Molecule-based magnetic materials*, vol 644, ACS Symposium Series. ACS, Washington, D. C
12. Manriquez JM, Yee GT, McLean RS, Epstein AJ, Miller JS (1991) *Science* 252:1415–1417
13. Gordon DC, Deakin L, Arif AM, Miller JS (2000) *J Am Chem Soc* 122:290–299
14. Ferlay S, Mallah T, Ouahes R, Veillet P, Verdaguer M (1995) *Nature* 378:701–703
15. McConnel HM (1967) *Proc Robert A Welch Found Conf* 11:144
16. Kollmar C, Kahn O (1991) *J Am Chem Soc* 1991:7987–7994
17. Kollmar C, Couty M, Kahn O (1991) *J Am Chem Soc* 113:7994–8005
18. Miller JS, Epstein AJ (1998) *J Chem Soc Chem Comm* 1319–1325
19. Miller JS, Epstein AJ, Reiff WM (1988) *Chem Rev* 88:201–220
20. Zhang J, Ensling J, Ksenofontov V, Gutlich P, Epstein AJ, Miller JS (1998) *Angew Chem* 110:676–679
21. Verdaguer M, Bleuzen A, Marvaud V, Vaissermann J, Seuleiman M, Desplanches C, Scullier A, Train C, Garde R, Gelly G, Lomenech C, Rosenman I, Veillet P, Cartier C, Villain F (1999) *Coord Chem Rev* 190–192, 1023–1047
22. Mallah T, Thiebaut S, Verdaguer M, Veillet P (1993) *Science* 262:1554–1557
23. Entley WR, Girolami GS (1994) *Inorg Chem* 33:5165–5166
24. Entley WR, Treadway CR, Wilson SR, Girolami GS (1997) *J Am Chem Soc* 119:6251–6258
25. Dujardin E, Ferlay S, Phan X, Desplanches C, Moulin CCD, Sainctavit P, Baudelet F, Dartyge E, Veillet P, Verdaguer M (1998) *J Am Chem Soc* 120:11347–11352
26. Ferlay S, Mallah T, Ouahes R, Veillet P, Verdaguer M (1999) *Inorg Chem* 38:229–234
27. Sato O, Iyoda T, Fujishima A, Hashimoto K (1996) *Science* 271:49–51
28. Sato O, Iyoda T, Fujishima A, Hashimoto K (1996) *Science* 272:704–705
29. Verdaguer M (1996) *Science* 272:698–699

30. Kahn O (1987) *Struct Bonding* 68:89–167
31. Kahn O, Pei Y, Verdager M, Renard JP, Sletten J (1988) *J Am Chem Soc* 110:782–789
32. Nakatani K, Bergerat P, Codjovi E, Mathoniere C, Yu P, Kahn O (1991) *Inorg Chem* 30:3977–3978
33. Karasawa S, Sano Y, Akita T, Koga N, Itoh T, Iwamura H, Rabu P, Drillon M (1998) *J Am Chem Soc* 120:10080–10087
34. Decurtins S, Schmalle HW, Schneuwly P, Ensling J, Gutlich P (1994) *J Am Chem Soc* 116:9521–9528
35. Laget V, Hornick C, Rabu P, Drillon M, Ziessel R (1998) *Coord Chem Rev* 180:1533–1553
36. Yufit DS, Price DJ, Howard JAK, Gutschke SOH, Powell AK, Wood PT (1999) *Chem Comm* 1561–1562
37. Batten SR, Hoskins BF, Moubaraki B, Murray KS, Robson R (1999) *J Chem Soc, Dalton Trans* 2977–2986
38. Batten SR, Jensen P, Kepert CJ, Kurmoo M, Moubaraki B, Murray KS, Price DJ (1999) *J Chem Soc, Dalton Trans* 2987–2997
39. Escuer A, Vicente R, ElFallah MS, Kumar SB, Mautner FA, Gatteschi D (1998) *J Chem Soc, Dalton Trans* 3905–3909
40. Tamaki H, Zhong ZJ, Matsumoto N, Kida S, Koikawa M, Achiwa N, Hashimoto Y, Okawa H (1992) *J Am Chem Soc* 114:6974–6979
41. Ribas J, Escuer A, Monfort M, Vicente R, Cortes R, Lezama L, Rojo T (1999) *Coord Chem Rev* 195:1027–1068
42. Manson JL, Arif AM, Miller JS (1999) *Chem Comm* 1479–1480
43. Caneschi A, Gatteschi D, Sessoli R, Rey P (1989) *Acc Chem Res* 22:392–398
44. Caneschi A, Gatteschi D, Renard JP, Rey P, Sessoli R (1989) *J Am Chem Soc* 111:785–786
45. Caneschi A, Ferraro F, Gatteschi D, Rey P, Sessoli R (1991) *Inorg Chem* 30:3162–3166
46. Luneau D, Rey P, Laugier J, Fries P, Caneschi A, Gatteschi D, Sessoli R (1991) *J Am Chem Soc* 113:1245–1251
47. Caneschi A, Gatteschi D, Sessoli R, Rey P, Cabello CI (1992) *J Mat Chem* 2:1283–1287
48. Caneschi A, Chiesi P, David L, Ferraro F, Gatteschi D, Sessoli R (1993) *Inorg Chem* 32:1445–1453
49. Caneschi A, Gatteschi D, Sessoli R (1993) *Inorg Chem* 32:4612–4616
50. Halcrow MA, Brechin EK, McInnes EJJ, Mabbs FE, Davies JE (1998) *J Chem Soc, Dalton Trans* 2477–2482
51. Miller JS (1994) *Adv Mat* 6:322–324
52. Brandon EJ, Kollmar C, Miller JS (1998) *J Am Chem Soc* 120:1822–1826
53. Brandon EJ, Arif AM, Burkhart BM, Miller JS (1998) *Inorg Chem* 37:2792–2798
54. Rittenberg DK, Sugiura K, Sakata Y, Mikami S, Epstein AJ, Miller JS (2000) *Adv Mat* 12:126–130
55. Lis T (1980) *Acta Cryst* 36:2042–2046
56. Boyd PDW, Li QY, Vincent JB, Folting K, Chang HR, Streib WE, Huffman JC, Christou G, Hendrickson DN (1988) *J Am Chem Soc* 110:8537–8539
57. Sessoli R, Gatteschi D, Caneschi A, Novak MA (1993) *Nature* 365:141–143
58. Sessoli R, Tsai HL, Schake AR, Wang SY, Vincent JB, Folting K, Gatteschi D, Christou G, Hendrickson DN (1993) *J Am Chem Soc* 115:1804–1816
59. Thomas L, Lioni F, Ballou R, Gatteschi D, Sessoli R, Barbara B (1996) *Nature* 383:145–147
60. Tsai HL, Eppley HJ, Devries N, Folting K, Christou G, Hendrickson DN *J Chem Soc, Chem Comm* 1745–1746
61. Sun ZM, Ruiz D, Dille NR, Soler M, Ribas J, Folting K, Maple MB, Christou G, Hendrickson DN (1999) *Chem Comm* 1973–1974
62. Boskovic C, Pink M, Huffman JC, Hendrickson DN, Christou G (2001) *Am Chem Soc* 123:9914–9915
63. Boskovic C, Brechin EK, Streib WE, Folting K, Bollinger JC, Hendrickson DN, Christou G (2002) *J Am Chem Soc* 124:3725–3736
64. Wieghardt K, Pohl K, Jibril I, Huttner G (1984) *Angew Chem Int Ed Engl* 23:77–78

65. Delfs C, Gatteschi D, Pardi L, Sessoli R, Wieghardt K, Hanke D (1993) *Inorg Chem* 32: 3099–3103
66. Barra AL, Debrunner P, Gatteschi D, Schulz CE, Sessoli R (1996) *Europhys Lett* 35:133–138
67. Barra A-L, Bencini F, Caneschi A, Gatteschi D, Paulsen C, Sangregorio C, Sessoli R, Sorace L (2001) *Chem Phys Chem* 2:523–531
68. Tejada J, Chudnovsky EM, del Barca E, Hernandez JM, Spiller TP (2001) *Nanotechnology* 12:181–186
69. Tejada J (2001) *Polyhedron* 20:1751–1756
70. Awschalom DD, Di Vincenzo DP, Smyth JJ (1992) *Science* 258:414–421
71. Leuenberger MN, Loss D (2001) *Nature* 410:789–793
72. Cornia A, Fabretti AC, Pacchioni M, Zobbi L, Bonachi D, Caneschi A, Gatteschi D, Biagi R, Del Pennino U, De Renzi V, Gurevich L, Van der Zant HSJ (2003) *Angew Chem Int Ed* 42:1645–1648
73. Dahlberg ED (1995) *Phys Today* 48:34–40
74. Kahn O (2000) *Acc Chem Res* 33:647–657
75. Kahn O (1985) *Angew Chem Int Ed* 24:834–850
76. Verdager M (2001) *Polyhedron* 20:1115–1128
77. Glaser T, Theil H, Liratzis I, Weyhermüller T, Bill E (2006) *Inorg Chem* 45:4889–4891
78. Goodenough JB (1955) *Phys Rev* 79:564
79. Goodenough JB (1958) *J Phys Chem Solids* 6:287
80. Goodenough JB (1963) *Magnetism and the chemical bond*. Interscience, New York
81. Kanamori J (1959) *J Phys Chem Solids* 10:87–98
82. Anderson PW (1959) *Phys Rev* 115:2–13
83. Anderson PW (ed) (1963) *Magnetism*. Academic, New York
84. Weihe H, Güdel HU (1997) *Inorg Chem* 36:3632–3639
85. Anderson PW, Hasegawa H (1955) *Phys Rev* 100:675–681
86. Zener C (1951) *Phys Rev* 82:403–405
87. Blondin G, Girerd J-J (1990) *Chem Rev* 90:1359–1376
88. Glaser T, Beissel T, Bill E, Weyhermüller T, Schünemann V, Meyer-Klaucke W, Trautwein AX, Wieghardt K (1999) *J Am Chem Soc* 121:2193–2208
89. Glaser T, Kesting F, Beissel T, Bill E, Weyhermüller T, Meyer-Klaucke W, Wieghardt K (1999) *Inorg Chem* 38:722–732
90. Glaser T, Wieghardt K (1998) In: Hodgson KO, Solomon EI (eds) *Spectroscopic methods in bioinorganic chemistry*, ACS symposium series, ACS, Washington, DC, pp 314–331
91. Longuet-Higgins HC (1950) *J Chem Phys* 18:265–274
92. Iwamura H (1990) *Adv Phys Org Chem* 26:179–253
93. Dougherty DA (1991) *Acc Chem Res* 24:88–94
94. Ovchinnikov AA (1978) *Theoret Chim Acta* 47:297–304
95. Yoshizawa K, Hoffmann R (1995) *J Am Chem Soc* 117:6921–6926
96. Glaser T, Gerenkamp M, Fröhlich R (2002) *Angew Chem Int Ed* 41:3823–3825
97. Glaser T, Heidemeier M, Grimme S, Bill E (2004) *Inorg Chem* 43:5192–5194
98. Glaser T, Heidemeier M, Weyhermüller T, Hoffmann R-D, Rupp H, Müller P (2006) *Angew Chem Int Ed* 45:6033–6037
99. Glaser T, Heidemeier M, Fröhlich R (2007) *Compt Rend Chim* 10:71–78
100. Glaser T, Heidemeier M, Strautmann JBH, Bögge H, Stämmler A, Krickemeyer E, Huenerbein R, Grimme S, Bothe E, Bill E (2007) *Chem Eur J* 13:9191–9206
101. Theil H, Frhr v, Richthofen C-G, Krickemeyer E, Stämmler A, Bögge H, Glaser T (2008) *Inorg Chim Acta* 361:916–924
102. Glaser T, Theil H, Heidemeier M (2008) *C R Chimie* 11:1121–1136
103. Rajca A (2002) *Chem Eur J* 8:4834–4841
104. Iwamura H, Koga N (1993) *Acc Chem Res* 26:346–351
105. Oberhausen KJ, O'Brien RJ, Richardson JF, Buchanan RM, Costa R, Latour JM, Tsai HL, Hendrickson DN (1993) *Inorg Chem* 32:4561–4565
106. Okamoto M, Teki Y, Takui T, Kinoshita T, Itoh K (1990) *Chem Phys Lett* 173:265–270

107. Mitsubori S.-i, Ishida T, Nogami T, Iwamura H (1994) *Chem Lett* 285–288
108. Ishida T, Mitsubori S.-i, Nogami T, Takeda N, Ishikawa M, Iwamura H (2001) *Inorg Chem* 40:7059–7064
109. Ishida T, Nakayama K, Nakagawa M, Sato W, Ishikawa Y (1997) *Synth Met* 85:1655–1658
110. Lloret F, de Munno G, Julve M, Cano J, Ruiz R, Caneschi A (1998) *Angew Chemie* 110: 143–145
111. Ishida T, Mitsubori S.-i, Nogami T, Iwamura H (1993) *Mol Cryst Liq Cryst* 233:345–350
112. Yasui M, Ishikawa Y, Akiyama N, Ishida T, Nogami T, Iwasaki F (2001) *Acta Cryst B* 57: 288–295
113. Feyerhem R, Abens S, Günther D, Ishida T, Meißner M, Meschke M, Nogami T, Steiner M (2000) *J Phys Condens Matter* 12:8495–8509
114. Ezuhara T, Endo K, Matsuda K, Aoyama Y (2000) *New J Chem* 24:609–613
115. Omata J, Ishida T, Hashizume D, Iwasaki F, Nogami T (2001) *Inorg Chem* 40:3954–3958
116. Ishida T, Kawakami T, Mitsubori S.-i, Nogami T, Yamaguchi K, Iwamura H (2002) *J Chem Soc, Dalton Trans* 3177–3186
117. Kusaka T, Ishida T, Hashizume D, Iwasaki F, Nogami T (2000) *Chem Lett* 1146–1147
118. Zusai K, Katayama T, Ishida T, Nogami T (2000) *Mol Cryst Liq Cryst* 343:121–126
119. Nakayama K, Ishida T, Takayama R, Hashizume D, Yasui M, Iwasaki F, Nogami T (1998) *Chem Lett* 497–498
120. Corbin DR, Francesconi LC, Hendrickson DN, Stucky GD (1981) *Inorg Chem* 20:2084–2089
121. McCleverty JA, Ward MD (1998) *Acc Chem Res* 31:842–851
122. Cargill Thompson AMW, Gatteschi D, McCleverty JA, Navas JA, Rentschler E, Ward MD (1996) *Inorg Chem* 35:2701–2703
123. Bayly SR, Humphrey ER, de Chair H, Paredes CG, Bell ZR, Jeffery JC, McCleverty JA, Ward MD, Totti F, Gatteschi D, Courric S, Steele BR, Screttas CG (2001) *J Chem Soc, Dalton Trans* 1401–1414
124. Ung VA, Thompson A, Bardwell DA, Gatteschi D, Jeffery JC, McCleverty JA, Totti F, Ward MD (1997) *Inorg Chem* 36:3447–3454
125. Ung VA, Couchman SM, Jeffery JC, McCleverty JA, Ward MD, Totti F, Gatteschi D (1999) *Inorg Chem* 38:365–369
126. Bayly SR, McCleverty JA, Ward MD, Gatteschi D, Totti F (2000) *Inorg Chem* 39:1288–1293
127. Bencini A, Gatteschi D, Totti F, Sanz DN, McCleverty JA, Ward MD (1998) *J Phys Chem A* 102:10545–10551
128. Fernández I, Ruiz R, Faus J, Julve M, Lloret F, Cano J, Ottenwaelder X, Journaux Y, Munoz C (2001) *Angew Chem Int Ed* 40:3039–3042
129. Pereira CLM, Pedroso EF, Stumpf HO, Novak MA, Ricard L, Ruiz-Garcia R, Rivière E, Journaux Y (2004) *Angew Chem Int Ed* 43:956–958
130. Pardo E, Bernot K, Julve M, Lloret F, Cano J, Ruiz-Garcia R, Pasán J, Ruiz-Perez C, Ottenwaelder X, Journaux Y (2004) *Chem Comm* 920–921
131. Pardo E, Bernot K, Julve M, Lloret F, Cano J, Ruiz-Garcia R, Delgado FS, Ruiz-Perez C, Ottenwaelder X, Journaux Y (2004) *Inorg Chem* 43:2768–2770
132. Foxon SP, Torres GR, Walter O, Pedersen JZ, Toftlund H, Hüber M, Falk K, Haase W, Cano J, Lloret F, Julve M, Schindler S (2004) *Eur J Inorg Chem* 335–343
133. Paital AR, Mitra T, Ray D, Wong WT, Ribas-Ariño J, Novoa JJ, Ribas J, Aromi G (2005) *Chem Comm* 5172–5174
134. Ottenwaelder X, Cano J, Journaux Y, Riviere E, Brennan C, Nierlich M, Ruiz-Garcia R (2004) *Angew Chem Int Ed* 43:850–852
135. Bencini A, Ciofini I, Uytterhoeven MG (1998) *Inorg Chim Acta* 274:90–101
136. Bencini A, Gatteschi D (1990) *Electron paramagnetic resonance of exchanged coupled systems*. Springer, Berlin
137. Gatteschi D, Sorace L (2001) *J Solid State Chem* 159:253–261
138. Glaser T (2004) *Angew Chem* 115:5846–5848
139. Gatteschi D, Sessoli R (2003) *Angew Chem Int Ed* 42:268–297

140. Gatteschi D, Sessoli R, Villain J (2006) *Molecular nanomagnets*. Oxford University Press, Oxford
141. Wernsdorfer W (2001) *Adv Chem Phys* 118:1–93
142. Kennedy BJ, Brain G, Horn E, Murray KS, Snow MR (1985) *Inorg Chem* 24:1647–1653
143. Basler R, Tregenna-Piggot PLW, Dobe C, Güdel HU, Janssen S, McIntyre GJ (2001) *J Am Chem Soc* 123:3377–3378
144. Barra AL, Gatteschi D, Sessoli R, Abbati GL, Cornia A, Fabretti AC, Uytterhoeven MG (1997) *Angew Chem Int Ed Engl* 36:2329–2331
145. Krzystek J, Telser J, Hoffman BM, Brunel L-C, Licoccia S (2001) *J Am Chem Soc* 123:7890–7897
146. Bendix J, Gray HB, Golubkov G, Gross Z (2000) *J Chem Soc, Chem Commun* 1957–1958
147. Krzystek J, Telser J, Pardi LA, Goldberg DP, Hoffman BM, Brunel L-C (1999) *Inorg Chem* 38:6121–6129
148. Goldberg DP, Telser J, Krzystek J, Montalban AG, Brunel L-C, Barrett AGM, Hoffman BM (1997) *J Am Chem Soc* 119:8722–8723
149. Limburg J, Vrettos JS, Crabtree RH, Brudvig GW, de Paula JC, Hassan A, Barra A-L, Duboc-Toia C, Collomb M-N (2001) *Inorg Chem* 40:1698–1703
150. Larrow JF, Jacobsen EN, Gao Y, Hong Y, Nie X, Zepp CM (1994) *J Org Chem* 59:1939–1942
151. Larrow JF, Jacobsen EN (1997) *Org Synth* 75:1–10
152. Zhang W, Jacobsen EN (1991) *J Org Chem* 56:2296–2298
153. Campbell KA, Lashley MR, Wyatt JK, Nantz MH, Britt RD (2001) *J Am Chem Soc* 123:5710–5719
154. Hernández-Molina R, Mederos A (2004) In: McCleverty JA, Meyer TJ (eds) *Comprehensive coordination chemistry II*, vol 1. Elsevier, Ltd, Oxford, pp 411–446
155. Lopez J, Liang S, Bu XR (1998) *Tetrahedron Lett* 39:4199–4202
156. Janssen KBM, Laquieira I, Dehaen W, Parton RF, Vankelecom IFJ, Jacobs PA (1997) *Tetrahedron: Asymmetry* 8:3481–3487
157. Atkins R, Brewer G, Kokot E, Mockler GM, Sinn E (1985) *Inorg Chem* 24:127–134
158. Böttcher A, Elias H, Eisenmann B, Hilms E, Huer A, Kniep R, Röhr CZ (1994) *Naturforsch B* 49:1089–1100
159. Fernandez Garcia MI, Fondo M, Garcia Deibe AM, Fernandez Fernandez MB, Gonzalez AMZ (2000) *Anorg Allg Chem* 626:1985–1991
160. Glaser T, Heidemeier M, Hahn FE, Pape T, Lügger T (2003) *Z Naturforsch B* 58:505–510
161. Glaser T, Heidemeier M, Lügger T (2003) *Dalton Trans* 2381–2383
162. Glaser T, Heidemeier M, Fröhlich R, Hildebrandt P, Bothe E, Bill E (2005) *Inorg Chem* 44:5467–5482
163. Long JR (ed) (2003) *Molecular cluster magnets*. In: *Chemistry of nanostructured materials*. World Scientific, Hong Kong
164. Miyasaka H, Matsumoto N, Okawa H, Re N, Gallo E, Floriani C (1996) *J Am Chem Soc* 118:981–994
165. Re N, Gallo E, Floriani C, Miyasaka H, Matsumoto N (1996) *Inorg Chem* 35:6004–6008
166. Miyasaka H, Ieda H, Matsumoto N, Re N, Crescenzi R, Floriani C (1998) *Inorg Chem* 37:255–263
167. Re N, Crescenzi R, Floriani C, Miyasaka H, Matsumoto N (1998) *Inorg Chem* 37:2717–2722
168. Miyasaka H, Matsumoto N, Re N, Gallo E, Floriani C (1997) *Inorg Chem* 36:670–676
169. Verdagner M, Bleuzen A, Marvaud V, Vaissermann J, Seuleiman M, Desplanches C, Scullier A, Train C, Garde R, Gelly G, Lomenech C, Rosenman I, Veillet P, Cartier C, Villain F (1999) *Coord Chem Rev* 192:1023–1047
170. Ohba M, Okawa H (2000) *Coord Chem Rev* 198:313–328
171. Beltran LMC, Long JR (2005) *Acc Chem Res* 38:325–334
172. Rebillay J-N, Mallah T (2006) *Struct Bonding* 122:103–131
173. Shen XP, Li BL, Zou JZ, Xu Z, Yu YP, Liu SX (2002) *Trans Met Chem* 4:372
174. Choi HJ, Sokol JJ, Long JR (2004) *Inorg Chem* 43:1606–1608

Chapter 5

Emergence in Inorganic Polyoxometalate Cluster Systems: From Dissipative Dynamics to Artificial Life

Leroy Cronin

Abstract Polyoxometalates are a subset of metal oxides that represent a diverse range of molecular clusters with an almost unmatched range of physical properties and the ability to form dynamic structures that can bridge multiple length scales from the nanoscale to the micron scale. In this article the prospect of developing emergent, complex and possibly even life-like systems with inorganic building blocks based upon polyoxometalates is discussed.

5.1 Introduction

The organisation of matter across length scales [1], starting from well defined building blocks, is a key challenge in the design of advanced functional materials and devices perhaps mimicking, or even bettering, nature using well defined principles and processes [2]. Many approaches have been proposed for the development of materials that grow from the molecular to nano- and meso- scale; for example the transformation of crystalline materials [3], aggregation of nanoparticles [4], or interfacial self-assembly of polymers [5], and amphiphilic systems [6] or combinations of these, to name but a few. Further, the dynamic self-assembly [7] of such systems is incredibly important since this will allow the understanding of how matter can be organised under both equilibrium and far-from-equilibrium conditions [8]. As well as possibly giving some important insights regarding the emergence of life [9], understanding such systems may allow the design of functional devices which could take advantage of architectures accessible only under far-from-equilibrium conditions.

L. Cronin (✉)

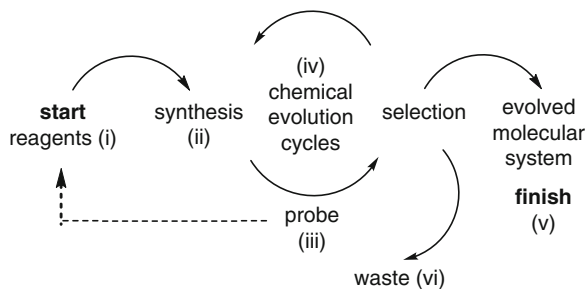
Department of Chemistry, University of Glasgow, Glasgow G12 8QQ, UK
e-mail: Lee.Cronin@glasgow.ac.uk

Patterned, or highly structured assemblies can be formed spontaneously in systems which are exposed to fluxes of matter and energy [8]. These assemblies can sustain themselves far from equilibrium whilst the fluxes are maintained, leading to the emergence of temporal and spatial structures. Key examples are the Belousov-Zhabotinsky (BZ) reaction [10] where an oscillating chemical reaction in a thin film can give rise to temporal pattern formation, and crystal gardens [11–13] which yield spatially defined structures formed by seeding a saturated solution of silicates with a crystal of a transition metal salt. Although these systems are incredibly rich, and a vast amount of research has been carried out, they are still poorly understood and it is very difficult to develop controllable examples in the laboratory to allow systematic studies [13].

5.2 Emergence and Chemical Complexity

Emergence is a very general, yet poorly articulated phenomenon [14]. Quite literally, an emergent property arises from a complex system containing a multiplicity of simple or well defined interactions. The concept can be applied not only to physical systems, a good example is pattern formation in the thin film BZ reaction [15], with many interacting components, but also to social, economic, and political systems [16]. In inorganic chemistry emergence can affect many processes from crystallisation [17] (for instance, it may be possible to understand polymorphism if it were treated like an emergence property), to self-assembly [18], and most importantly the self assembly of building blocks across many length scales [19]. The main question posed in this article is the idea that dynamic inorganic systems can be engineered to interact in a cooperative manner to build complex and functional systems, right from the molecular to the nano, and on to the macro scale. In this respect dynamic inorganic systems may be excellent models to probe chemical complexity.

For instance if a system can be engineered where a source of energy and reactive building blocks are co-located, ideally allowing both feedback of information (more complex architectures templating other architectures) and the development of autocatalytic reaction cycles, then it may be possible to observe a self-replicating, metabolising inorganic system that can undergo evolution. This could in turn allow us to design autonomous functional ‘inorganic’ systems, gain a greater understanding of the origin of life and even allow the synthesis of a new type of inorganic life based on non-biological, inorganic, building blocks, see Scheme 5.1. Such an achievement would surely be extraordinary and raise questions about how living systems are classified and recognised [20]. In this article we propose that the use of a particular class of inorganic clusters, polyoxometalates [21], may have the correct properties to fulfil such an ambition: the development of inorganic living systems or systems that can undergo evolutionary processes (Scheme 5.1).



Scheme 5.1 A representation of a process that could allow the ‘*evolution*’ of molecular building blocks. Although this would not itself represent a ‘*living*’ system [20], the use of evolutionary principles in the ‘*inorganic-world*’ would represent a major step forward

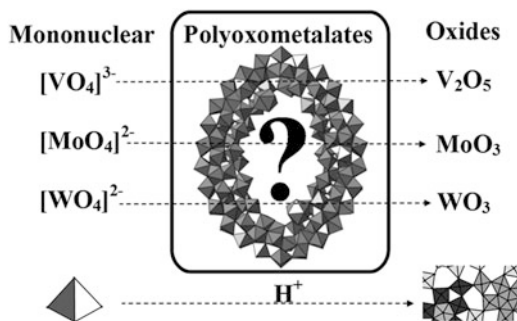
5.3 Polyoxometalates

Polyoxometalates (POMs), anionic oxide clusters of the early transition metals, represent a vast class of inorganic materials with a virtually unmatched range of properties applicable to biology, magnetism, material science, and catalysis [21]. POM clusters are based upon conserved building blocks and appear to have a great deal of desirable characteristics applicable for nanoscale assembly. This is because nanoscale polyoxometalate clusters provide an arguably unrivalled structural diversity of molecules displaying a wide range of important physical properties and nuclearities; these cover the range from 6 to 368 metal ions in a single molecule and are assembled under ‘one-pot’ reaction conditions [21]. At the extreme, these clusters are truly macromolecular, rivalling the size of proteins, and are formed by self-assembly processes [22].

The POM clusters tend to be anionic in nature, being based upon metal oxide building blocks with a general formula of MO_x , (where M is Mo, W, V and sometimes Nb and x can be 4, 5, 6 or 7). POM-based materials have a large range of interesting physical properties [23–27] which result from their many structures, the ability to delocalise electrons over the surface of the clusters, and the ability to incorporate heteroanions, electrophiles and ligands, and to encapsulate guest molecules within a the metal-oxo cage defined by the POM. Further, POM clusters have been shown to exhibit superacidity [23], catalytic activity [23], photochemical activity [24], ionic conductivity [25], reversible redox behaviour [26], bistability [27], cooperative electronic phenomena [24], the ability to stabilize highly reactive species [26], and extensive host guest chemistry [27]. In this context it is important to realise that the most stable product in the polymerisation of metal oxo-building blocks is the metal oxide itself, see Fig. 5.1.

The large number of structural types in polyoxometalate chemistry [29] can be broadly split into three classes. (i) Heteropolyanions: these are metal oxide clusters that include hetero anions such as SO_4^{2-} or PO_4^{3-} . These represent by far the most

Fig. 5.1 Polyoxometalates are formed in experimental conditions that allow linking of polyhedra. Discrete structures are formed as long as the system is not driven all the way to the oxide. One such example, in this case a part of a $\{\text{Mo}_{256}\text{Eu}_8\}$ cluster unit [28], is depicted in the square



explored subset of POM clusters with over 5,000 papers being reported on these compounds during the last 4 years alone. Much of this research has examined the catalytic properties of POMs with great emphasis on the Keggin $\{\text{XM}_{12}\text{O}_{40}\}$ and the Wells-Dawson $\{\text{X}_2\text{M}_{18}\text{O}_{62}\}$ (where $\text{M} = \text{W}$ or Mo and $\text{X} =$ a tetrahedral template) anions which represent the archetypal systems. In particular W-based POMs are robust and this has been exploited to develop W-based Keggin ions with vacancies that can be systematically linked using electrophiles to larger aggregates [29]. (ii) Isopolyanions: these are composed of a metal-oxide framework, but without the internal heteroatom / heteroanion. As a result, they are often much more unstable than their heteropolyanion counterparts [30]. However they also have interesting physical properties such as high charges and strongly basic oxygen surfaces which means they are attractive units for use as building blocks [19]. (iii) Mo-blue and Mo-brown reduced POM clusters: these are related to molybdenum blue type species, which was first reported by Scheele in 1783 [31].

Their composition was largely unknown until Müller *et al.* reported, in 1995, the synthesis and structural characterisation of a very high nuclearity cluster $\{\text{Mo}_{154}\}$ crystallised from a solution of Mo-blue, which has a ring topology [32]. Changing the pH and increasing the amount of reducing agent along with incorporation of a ligand like acetate facilitates the formation of a $\{\text{Mo}_{132}\}$ spherical ball-like cluster [33]. This class of highly reduced POM clusters represents one of the most exciting developments in POM chemistry and with many potential spin off applications in nanoscience and in the development of an inorganic systems chemistry.

5.4 The Origin of Life

When the earth formed some 4.6 billion years ago, it was a lifeless, barren place, but, one billion years later, it was literally covered with organisms [34]. The transition from the lifeless planet to the planet we see today is totally without explanation and has fascinated philosophers and scientists for hundreds of years. Since the

1600s, it was universally accepted that small creatures could arise by ‘spontaneous generation’ in mud or decaying matter (higher organisms such as humankind etc. did not present a problem as God was believed to be the creator). However, Louis Pasteur proved that spontaneous generation was not viable and he showed that micro-organisms arose from parents.

This discovery then begged the question – where do these micro-organisms come from? At the same time the theory of natural selection was proposed by Charles Darwin and this gave a route by which species of life could adapt to a given environment, through environmental pressure and random mutations and become fitter or better adapted to a given set of environmental circumstances [35]. Further improvements would mean better adapted species. Thus, it has been shown that natural selection, repeated generation after generation, leads inevitably to the evolution of complex organisms from simple ones. The revolution in our understanding of molecular biology, the genome and the role of DNA in information storage and replication and its susceptibility to mutation thereby provides a robust mechanism that allows evolution from the molecular level to the whole organism level [36].

The ultimate conclusion implies that all current life-forms could have evolved from a single simple progenitor – an organism now referred to as life’s last common ancestor, and advances in bio-informatics will almost certainly lead to further clarify this [37]. Therefore, one very significant question remains, where does the common ancestor come from? This question was addressed in the 1950s when the famous Miller-Urey [38] experiment was devised to simulate the conditions present on the pre-biotic earth, as suggested by Oparin and Haldane [39]. For the Miller-Urey experiment, a closed system, i.e. bell jar, was constructed that comprised an “atmosphere” of methane, ammonia, water and hydrogen above an “ocean” of water. Then the gases were subjected to “lightning” in the form of a continuous electrical discharge. After several days, analysis of the system revealed that up to 2% of the carbon present in the system was found converted into the simplest amino acids. However, this experiment did not yield any evidence for nucleic acids (mainly because the elemental components were not present) and little progress has been made experimentally that may provide a chemical link between the pre-biotic world and the last ancestor (Fig. 5.2).

In fact this line of investigation, *via* direct chemical experiments was almost completely abandoned, and in the late 60’s it was proposed that RNA could be a possible precursor and this was termed the ‘RNA-world’ [40]. RNA would be both the information carrier and the catalyst, and a fair amount of research, including the discovery of ribozymes and enzymes made of RNA provided a possible route to the last ancestor. Despite these advances, however, the fundamental question still remains: What were the chemical steps that allowed the emergence of chemical complexity that could eventually lead to the onset of life, with or without the RNA world? Implicit within this question are further questions such as – how was DNA, with four based pairs, selected as a information carrier, why are only 20 amino acids utilised by proteins and what mechanism lead to the chiral world? Was there chemical evolution before bio-chemical evolution? Was the origin of life inorganic?

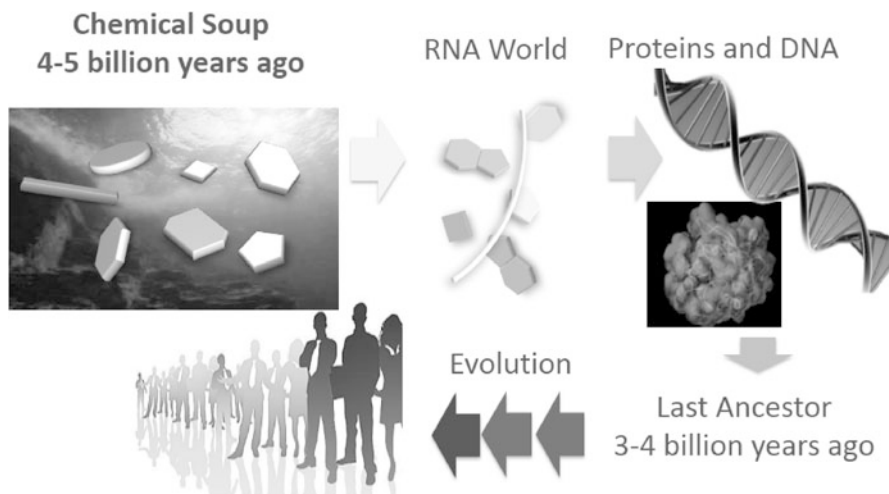


Fig. 5.2 A possible route from the pre-biotic earth to life and then to humans; however the ‘jump’ between the chemical soup and the RNA world, or its equivalent in other scenarios, is totally unknown

5.5 Polyoxometalate Super Structures – Potential DNA and Proteins for the Inorganic Living World?

Although perhaps rather speculative, during the rest of this article I will attempt to argue that inorganic systems based upon polyoxometalate clusters, and the associated building blocks, could provide a real experimental approach to develop artificial life. By utilising clusters built from inorganic building blocks, it will also be possible to engineer host-guest (lock-key) and templating interactions (based upon both strong and weak molecular interactions) that will allow the transfer of structural (genetic information) from one cluster to another. Also, the presence of many types of building blocks plus the proven tolerance of defects and imperfect matching allows a type of mutation to be built into the mating events. Finally, and most exciting, is that the use of inorganic systems allows the possibility of incorporating a REDOX based metabolism that is either based upon the clusters, or is coupled to them via the redox potentials of the individual building blocks. For instance, in preliminary work in our laboratory we have shown that polyoxometalate clusters (which normally grow under reduction) can undergo periodic growth in the presence of an oscillating chemical reaction. Polyoxometalate-based building blocks seem like perfect candidates as they are extremely easy to produce, from $[\text{MoO}_4]^{2-}$ as a precursor, and give rise to a large number of building blocks (cf. amino-acids and nucleic acids) which have been shown to undergo an extraordinary range of growth processes to polyoxomolybdate-based clusters [21] (cf. proteins and DNA / RNA), see Fig. 5.3.

The polymerization and cluster growth process is complex [21], yet the actual synthesis is more straightforward, occurring in a ‘one-pot’ reaction in a single step

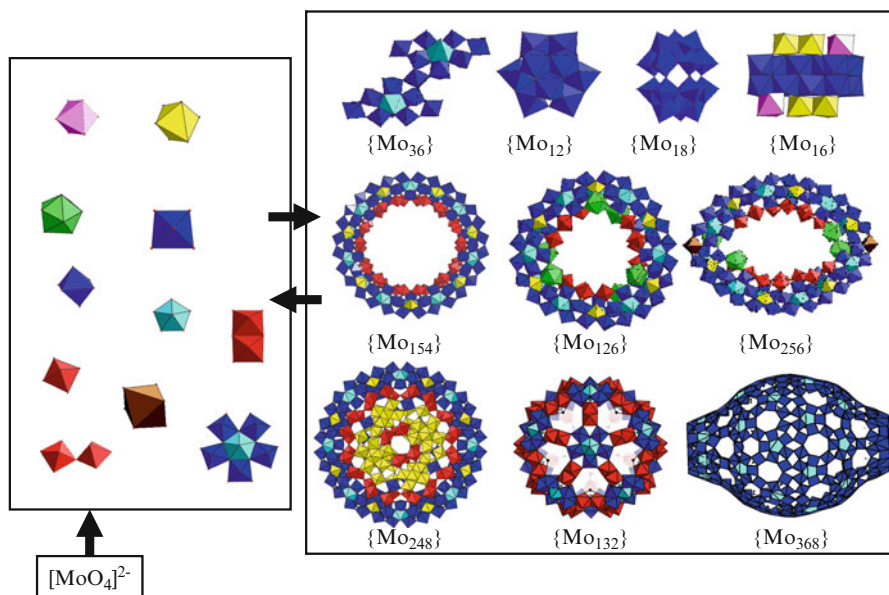


Fig. 5.3 A representation of the building blocks available from the simple $[\text{MoO}_4]^{2-}$ precursor and representations of the crystal structures of some of the POM clusters isolated to date. These clusters represent some of the largest molecules yet isolated. For instance the $\{\text{Mo}_{36}\}$ cluster is about the same size as the protein hemoglobin [34]

as a function of the following parameters; pH, ionic strength, temperature, cation type, concentration of $[\text{M}]$, type of reducing agent present and additional electrophiles and linking units. However, to be able to start generating complex cluster architectures that can interact and set up various assembly-disassembly cycles with autocatalysis and replication, we need to demonstrate that such interactions are possible.

In preliminary experiments Müller et al. [35] have shown that it is possible to encapsulate a $\{\text{Mo}_{36}\}$ cluster within a big wheel $\{\text{Mo}_{154}\}$ cluster. This means that it is possible to imagine that the cluster assembly-disassembly process can be used to template or amplify the selection of other clusters, forming a complex library of interconverting species that can adapt to a given fitness landscape, see Fig. 5.4 [36].

5.6 Discussion and Conclusions

The investigation of complex self assembling and organising systems that demonstrate emergent properties is sure to expand dramatically in the coming years. Researchers are fast realising that principles for supramolecular self-assembly, when applied to systems that can form dissipative structures, can lead to the emergence

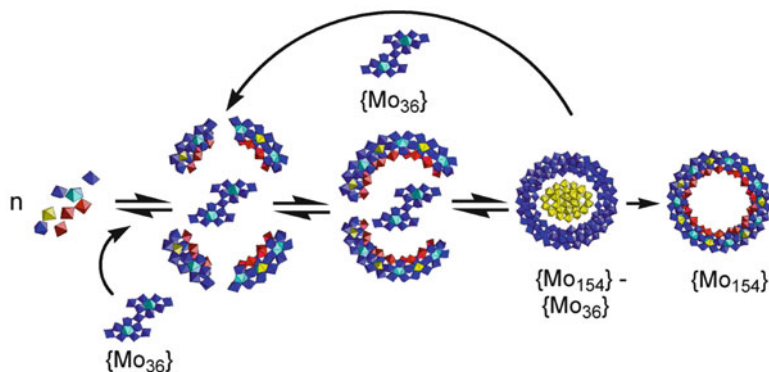


Fig. 5.4 Schematic showing a possible route to the templating of the $\{\text{Mo}_{154}\}$ cluster by the $\{\text{Mo}_{36}\}$ cluster. The $\{\text{Mo}_{36}\}$ cluster can then be viewed as the genetic material in this case, and this forms spontaneously under the reaction conditions that allow cluster growth

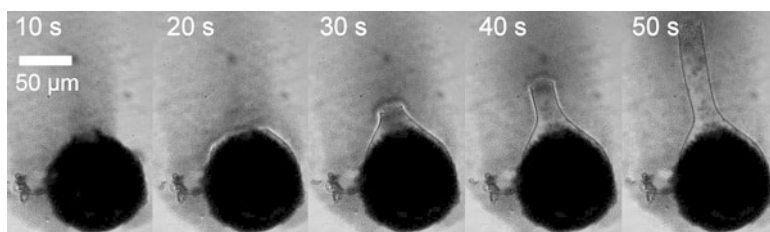


Fig. 5.5 Time lapse sequence showing the real time development of a membrane around a crystal of a polyoxometalate and the extension of the membrane away from the crystal

of adaptive chemistries. The study of these chemistries appears to be falling under the umbrella of ‘systems-chemistry’ and it is entirely feasible that such systems will display ‘life-like’ characteristics [20]. To develop feasible living entities it can be hypothesised that only systems that have cellular compartments, or artificial chemical cells (CHELLS) [20] formed by a membrane, can allow the formation of objects that are able to develop into living entities.

In this respect inorganic systems can also be manipulated to form functional compartments. Similar to the crystal gardens [11–13] we, in preliminary work, have demonstrated that it is possible to take crystals of a polyoxometalate material and transform the crystalline state into a functional semi-permeable membrane and osmotically pump material through a tubular structure formed by the metal-oxide membrane during crystal dissolution, see Fig. 5.5. Such processes could well be used to develop a POM-based CHELL.

In summary, the choice of polyoxometalates as a building block system to develop approaches to artificial inorganic life may seem outlandish, but I hope that I have demonstrated that the rich structural architectures and self assembly processes required to construct such architectures will inspire future work. Certainly

the choice of polyoxometalate building blocks to construct artificial living systems is justified by their rich physical properties, incredible diverse structures based upon conserved building blocks and finally, by the fact that any entity would not be able to survive outside the laboratory given the poor availability of the required building blocks in our environment.

Acknowledgements I would like to acknowledge and thank Achim Müller for many discussions about emergence and the prospects of cluster-based inorganic life. I would also like to thank Craig Hill and Jamal Musaev for organising the NATO conference on Complexity and NATO for funding.

References

1. Cölfen H, Mann S (2003) Higher-order organization by mesoscale self-assembly and transformation of hybrid nanostructures. *Angew Chem Int Ed* 42:2350–2365
2. Mann S (2008) Life as a nanoscale phenomenon. *Angew Chem Int Ed* 47:5306–5320
3. Banfield JF, Welch SA, Zhang H, Ebert TT, Penn RL (2000) Aggregation-based crystal growth and microstructure development in natural iron oxyhydroxide biomineralization products. *Science* 289:751–754
4. Liu TB, Diemann E, Li HL, Dress AWM, Müller A (2003) Self-assembly in aqueous solution of wheel-shaped Mo₁₅₄ oxide clusters into vesicles. *Nature* 426:59–62
5. Capito RM, Azeveo HS, Velichko YS, Mata A, Stupp SL (2008) Self-assembly of large and small molecules into hierarchically ordered sacs and membranes. *Science* 319:1812–1816
6. Zhang J, Song YS, Cronin L, Liu TB (2008) Self-assembly of organic-inorganic hybrid amphiphilic surfactants with large polyoxometalates as polar head groups. *J Am Chem Soc* 130:14408–14409
7. Pradeep CP, Long DL, Newton GN, Song YF, Cronin L (2008) Supramolecular metal oxides: programmed hierarchical assembly of a protein-sized 21 kDa [(C₁₆H₃₆N)₁₉{H₂NC(CH₂O)₃P₂V₃W₁₅O₅₉}₄]⁵⁻ polyoxometalate assembly. *Angew Chem Int Ed* 47: 4388–4391
8. Maselko J, Strizhak P (2004) Spontaneous formation of cellular chemical system that sustains itself far from thermodynamic equilibrium. *J Phys Chem B* 108:4937–4939
9. Cairns-Smith AG (2008) Chemistry and the missing era of evolution. *Chem Eur J* 14:3830–3839
10. Yang LF, Dolnik M, Zhabotinsky AM, Epstein IR (2000) Oscillatory clusters in a model of the photosensitive Belousov-Zhabotinsky reaction system with global feedback. *Phys Rev E* 62:6414–6420
11. Collins C, Zhou W, Mackay AK, Klinowski J (1998) The ‘silica garden’: a hierarchical nanostructure. *Chem Phys Lett* 286:88–92
12. Cartwright JHE, Garcí-Ruiz JM, Novella ML, Otálora F (2002) Formation of chemical gardens. *J Colloid Interface Sci* 256:351–359
13. Thouvenel-Romans S, Steinbock O (2003) Oscillatory growth of silica tubes in chemical gardens. *J Am Chem Soc* 125:4338–4341
14. Chen IA (2006) The emergence of cells during the origin of life. *Science* 314:1558–1559
15. Li N, Zhao JP, Wang JC (2008) Complex dynamics and enhanced photosensitivity in a modified Belousov-Zhabotinsky reaction. *J Chem Phys* 128:244509
16. Mainzer K (1997) Thinking in complexity, the complex dynamics of matter, mind, and mankind, 3rd edn. Springer, Berlin, New York/Heidelberg
17. Cashell C, Corcoran D, Hodnett BK (2005) Effect of amino acid additives on the crystallization of l-glutamic acid. *Cryst Growth Des* 5:593–597

18. Pileni MP (2008) Self-assembly of inorganic magnetic nanocrystals: a new physics emerges. *J Phys D-App Phys* 41:134002
19. Long D-L, Cronin L (2006) Towards polyoxometalate-integrated nanosystems. *Chem Eur J* 12:3698–3706
20. Cronin L, Krasnogor N, Davis BG, Alexander C, Robertson N, Steinke JHG, Schroeder SLM, Khlobystov AN, Cooper G, Gardner PM, Siepmann P, Whitaker BJ, Marsh D (2006) The imitation game—a computational chemical approach to recognizing life. *Nat Biotechnol* 24:1203–1206
21. Long D-L, Burkholder E, Cronin L (2007) Polyoxometalate clusters, nanostructures and materials: from self assembly to designer materials and devices. *Chem Soc Rev* 36:105–121
22. Cronin L (2002) The potential of pentagonal building blocks. In: Meyer G, Naumann D, Wesemann L (eds) *Inorganic chemistry highlights*. Wiley-VCH, Weinheim, pp 113–121
23. (a) Neumann R, Dahan M (1997) A ruthenium-substituted polyoxometalate as an inorganic dioxygenase for activation of molecular oxygen. *Nature* 388:353–355; (b) Mizuno N, Misono M (1998) Heterogeneous catalysis. *Chem Rev* 98:199–218
24. (a) Katsoulis DE (1998) A survey of applications of polyoxometalates. *Chem Rev* 98:359–387; (b) Yamase T (1998) Photo- and electrochromism of polyoxometalates and related materials. *Chem Rev* 98:307–325
25. Rütther T, Hultgren VM, Timko BP, Bond AM, Jackson WR, Wedd AG (2003) Electrochemical investigation of photooxidation processes promoted by sulfo-polyoxometalates: coupling of photochemical and electrochemical processes into an effective catalytic cycle. *J Am Chem Soc* 125:10133–10143
26. Sattari D, Hill CL (1993) Catalytic carbon-halogen bond-cleavage chemistry by redox-active polyoxometalates. *J Am Chem Soc* 115:4649–4657
27. Müller A, Das SK, Talismanov S, Roy S, Beckmann E, Bögge H, Schmidtman M, Merca A, Berkle A, Allouche L, Zhou Y, Zhang L (2003) Trapping cations in specific positions in tuneable “artificial cell” channels: new nanochemistry perspectives. *Angew Chem Int Ed* 42:5039–5044
28. Müller A, Krickemeyer E, Meyer J, Bögge H, Peters F, Plass W, Diemann E, Dillinger S, Nonnenbruch F, Randerath M, Menke C (1995) $[\text{Mo}_{154}(\text{NO})_{14}\text{O}_{420}(\text{OH})_{28}(\text{H}_2\text{O})_{70}]^{(25 \pm 5)-}$: a water-soluble big wheel with more than 700 atoms and a relative molecular mass of about 24000. *Angew Chem Int Ed* 34:2122–2124
29. Pope MT (1987) Isopolyanions and heteropolyanions. In: Wilkinson G, Gillard RD, McCleverty JA (eds) *Comprehensive coordination chemistry*, vol 3. Pergamon Press, Oxford/New York, pp 1023–1058
30. Cronin L (2004) High nuclearity polyoxometalate clusters. In: McCleverty JA, Meyer TJ (eds) *Comprehensive coordination chemistry II*, vol 7. Elsevier, Amsterdam, pp 1–57
31. Scheele W (1971) In: Hermbstädt DSF (ed) *Sämtliche Physische und Chemische Werke*, vol 1. M. Sändig oHG, Niederwalluf/ Wiesbaden, pp 185–200 (reprint: Original **1793**)
32. Cronin L, Beugholt C, Krickemeyer E, Schmidtman M, Bögge H, Kögerler P, Luong TKK, Müller A (2002) “Molecular symmetry breakers” generating metal-oxide-based nanoobject fragments as synthons for complex structures: $[\{\text{Mo}_{128}\text{Eu}_4\text{O}_{388}\text{H}_{10}(\text{H}_2\text{O})_{81}\}]^{20-}$, a giant-cluster dimer. *Angew Chem Int Ed* 41:2805–2808
33. Müller A, Krickemeyer E, Bögge H, Schmidtman M, Peters F (1998) Organizational forms of matter: an inorganic super fullerene and keplerate based on molybdenum oxide. *Angew Chem Int Ed* 37:3359–3363
34. Müller A, Beckmann E, Bögge H, Schmidtman M, Dress A (2002) Inorganic chemistry goes protein size: a Mo_{368} nano-hedgehog initiating nanochemistry by symmetry breaking. *Angew Chem Int Ed* 41:1162
35. Müller A, Kögerler P, Kuhlmann C (1999) A variety of combinatorially linkable units as disposition: from a giant icosahedral Keplerate to multi-functional metal-oxide based network structures. *Chem Commun* 1347–1358

36. Miras HN, Cooper GJT, Long DL, Bögge H, Müller A, Streb C, Cronin L (2010) Unveiling the transient template in the self-assembly of a molecular oxide nanowheel. *Science* 327:72–74
37. Theobald DL (2010) A formal test of the theory of universal common ancestry. *Nature* 465:219–222
38. (a) Miller SL (1953) A production of amino acids under possible primitive earth conditions. *Science* 117(3046):528–529; (b) Miller SL, Urey HC (1959) Organic compound synthesis on the primitive earth. *Science* 130(3370):245–251
39. Oparin AI (1952) *The origin of life*. Dover Publications, New York
40. (a) Gilbert W (1986) *The RNA World*. *Nature* 319:618; (b) Orgel LE (1968) Evolution of the genetic apparatus. *J Mol Biol* 38:381–393

Chapter 6

The Amazingly Complex Behaviour of Molybdenum Blue Solutions

Ekkehard Diemann and Achim Müller

Abstract We describe the history and provide a better understanding of the long-time puzzle of “molybdenum blue solutions”. Furthermore, with the discovery of various other structurally well-defined, giant, hydrophilic molybdenum-oxide based species, inorganic chemists have successfully pushed the size limit of inorganic ions into the nanometer scale. Consequently, this progress provides new challenges in different fields, for example, the physical chemistry of solutions. The giant anions show totally different solution behaviour when compared to regular inorganic ions, owing to their sizes and especially their surface properties.

6.1 Historical Survey

Our story starts when *phlogiston* (derived from the Greek “to burn”) was thought to be involved in every kind of combustion, i.e. in our modern view of redox processes. The underlying theory originated with Johann Joachim Becher in the late seventeenth century and was extended by Georg Ernst Stahl. It states that flammable materials contain *phlogiston*, a substance without colour, taste, or weight that is liberated on burning. Once burned, the dephlogisticated substance was then in its “true” form, the *kalx* (chalk). This way of thinking influenced the early chemists for almost a century (Figs. 6.1 and 6.2).

Two discoverers of oxygen, Carl Wilhelm Scheele (Sweden) and Joseph J. Priestley (England) (Fig. 6.3) were phlogistonists while the third discoverer Antoine de Lavoisier (France) was the first leading antiphlogistonist. In fact, it was Scheele [2] who described the first reproducible experiment related to the “molybdenum blue solutions” that were obtained by a redox process. It should be noted that

E. Diemann (✉) • A. Müller

Faculty of Chemistry, University of Bielefeld, Universitätsstr. 25, D-33615 Bielefeld, Germany
e-mail: e.diemann@uni-bielefeld.de; a.mueller@uni-bielefeld.de



Fig. 6.1 J. J. Becher (1635–1682) thought matter to be composed of *terra lapida* (stone; the principle of solids), *terra mercurialis* (mercury; the principle of weight and lustre), and *terra pinguis* (fat, oil; the principle of combustibility). When heated in air (calcination) metals lose *terra pinguis* and form *kalx* (chalk, from the Greek word for ash)

Scheele (Figs. 6.3 and 6.4) discussed this with the important Swedish chemist, Torbern Bergman (1735–1784) (“A Man Before His Time”) [3]. Interestingly, such blue solutions also exist naturally: centuries ago the Native Americans observed the “blue waters”—the solution of natural *soluble molybdenum blue* formed by partial oxidation of molybdenite, MoS_2 (forming the mineral *ilsemannite*, approximate formula $\text{Mo}_3\text{O}_8 \cdot n\text{H}_2\text{O}$) near today’s Idaho Springs and the Valley of the Ten Thousand Smokes [4].

In his *Chemische Untersuchung über das Molybdänum oder Wasserbley* (Chemical Studies on Molybdenum or Water Lead) [2], which refers to work done between 1778 and 1783, Scheele was already aware that molybdenum blue was a reduced molybdenum oxide (i.e., in his terms, containing *phlogiston*) (Fig. 6.4). However, it took almost 40 years before Jöns Jakob Berzelius (Fig. 6.3) reported the first formula for the blue powder isolated from such solutions [5]. Over time, this analysis has been repeated by several groups with slightly varying results ($\text{MoO}_x \cdot n\text{H}_2\text{O}$, $x = 2.5 - 2.96$, $n = 3 - 5$, cf. Table 6.1), owing to, as we now know, the formation of species with varying degrees of reduction and, therefore, slightly differing compositions. The later investigations are described in the following paragraph (information taken from ref. 4).

Although Wilhelm Biltz (Fig. 6.3) in 1903–1905 found negatively charged species of colloidal size in these solutions, the question of the respective cations was never raised [4]. Even Duclaux and Titeica (1929), who found that the solutions of molybdenum blue flocculated when positively charged colloids such as $\text{Al}(\text{OH})_3$ or electrolytes such as NaCl were added, did not refer to this point [4]. A possible reason might be that the molecular mass of the solutes from the molybdenum blue solutions obtained from freezing point depression experiments [4] by Marchetti (1899) and Dumanski (1910) was 440–481 g/mol, which is



Fig. 6.2 From J. J. Becher's ideas Georg Ernst Stahl (1660–1734) developed the *Theory of Phlogiston* which was extensively used until the end of the eighteenth century. Its use was not unsuccessful for the chemists of that time and led finally to the discovery of hydrogen (H. Cavendish, 1766), nitrogen and oxygen (C. W. Scheele, 1772–1777; J. J. Priestley, 1774). Later, for a long time this theory was thought to be useless, however, today we know that it contained some reasonable ideas. In this context the Swiss chemist Gerold Schwarzenbach [1] pointed out “that during the combustion process something is transferred from the metal to the oxygen, namely electrons. Burnable matter indeed does not contain phlogiston but is characterized by the fact that its atoms can release electrons”. Furthermore, the early chemists were already aware that the *kalxs* could contain varying amounts of phlogiston (i.e. electrons) thus anticipating oxidation numbers and oxidation states. As the great physicochemist Wilhelm Ostwald stated about a century ago, a theory kept successfully for almost one century cannot be entirely wrong



Fig. 6.3 (from left) Joseph J. Priestley (1733–1804), Carl Wilhelm Scheele (1742–1786), Jöns Jakob Berzelius (1779–1848) and Wilhelm Biltz (1877–1943)

194 XI. Chemische Untersuchung

§. 9.

1 Das die Erde nicht ungeneigt ist, das Brenn-
bare anzuziehen, zeigt sich aus der blauen Farbe,
welche der Sublimat von der Lichtflamme bekommt
(§. 4.). Das sie felbiges auf dem nassen Wege an-
nimmt, beweist ebenfalls die blaue Farbe (§. 7. b.).
a) Um nun hiervon gewisser zu werden, wurde die
Wasserbleyerde mittelst ein wenig Alkali (§. 7. e.) in ko-
chendem Wasser aufgelöst. Zu dieser Auflösung goss
ich einige Tropfen Salzsäure, und theilte sie in meh-
rere Theile. Zu jedem Theile that ich Feilspäne
unterschiedener Metalle, die Auflösung bekam bald
eine bläulichte Farbe, die immer mehr zunahm, und
nach Verlauf einer Stunde, wenn man die Flasche
dann und wann schüttelte, sehr schön und dunkel-
blau wurde. Das diese Farbe vom Brennaren her-
kömmt, läst sich aus Folgenden schliessen, wenn man 1)
2) mit der Metalle selbst, die Erdarten derselben nimmt,
entsteht keine Aenderung der Farbe. 2) Tröpfelt
man in eine solche Auflösung einige Tropfen Sal-
petersäure, und setzt sie in die Wärme, so verschwin-
det die Farbe *). Es ist also nicht zu bewundern,
dass das Silber und Quecksilber angegriffen wird,
weil hier eine doppelte Verwandtschaft wirkt, nem-

*) Ohnfreitig gründet sich die Entstehung dieser blauen Farbe,
auf eine vorgehende Reduktion der Wasserbleysäure.
Ohne sie aber vom Brennaren abzuleiten, kann sie auch
wohl eine Folge von dem Verluste des Oxygens seyn, wel-
ches die Wasserbleysäure an die Metalle absetzt. H.

3 lich die der Salzsäure auf die metallische Erde und der
Wasserbleyerde auf das Brennare der Metalle; Gold
wird nicht angegriffen. b) Schüttet man zu der vor-
erwähnten Auflösung zu viel Salzsäure, so ent-
steht keine blaue, sondern eine gelbe Farbe, die
endlich braun wird, wenn man die Mischung mit
Metallen in Digestion stellt. Hier scheint die Er-
de mehr Brennbares anzuziehen; denn wenn man
diese Auflösung in eine Auflösung von Wasserbley-
erde tröpfelt; so wird das Brennare mehr zertheilt,
und die Mischung wird blau. c) Blutlauge, worin
eine Säure prädominirt, präzipitirt diese im Wasser
aufgelöste Erde braun; und Galläpfelinfusion dun-
kelbraun.

(1) That the **earth** tends to attract the **burn-
able** is shown by the blue colour which the
sublimate gets from the lightening flame...
(2) That the colour stems from the **burnable**
follows from the fact that there is no change
of colour when we take instead of the metals
their earths (= oxides) [...] the colour
vanishes when nitric acid is added ...
Part (3) describes roughly the
synproportional reaction of a strongly
reduced (brownish) solution with an
unreduced (colourless) molybdate solution
yielding a blue mixture.

Fig. 6.4 Facsimile from Scheele's chapter *Chemische Untersuchung über das Molybdänum oder Wasserbley*, where he describes his experiments with molybdenum blue solutions [2]. For an understanding see also legend of Fig. 6.2

Table 6.1 The composition of "Molybdenum Blue" of the type $\text{MoO}_x \cdot n \text{H}_2\text{O}$, data taken from ref. 4

x	n	
2.8	n	Berzelius (1826) [5]
2.5	3	Rammelsberg (1866)
2.66	n	Muthmann (1887)
2.66	5	Marchetti (1899)
2.8	n	Guichard (1900), Lautie (1934)
2.96	3.5	Klason (1901)
2.85	3	Bailhache (1901)
2.86	n	Junius (1905)

similar to that of a single Mo_3O_8 entity (416 g/mol) plus some moles of water. Thus, most of the early researchers regarded those solutes as small single neutral molecular entities of this composition (neglecting the contribution from any cation). This interpretation remained *state-of-the-art* until almost the end of the twentieth

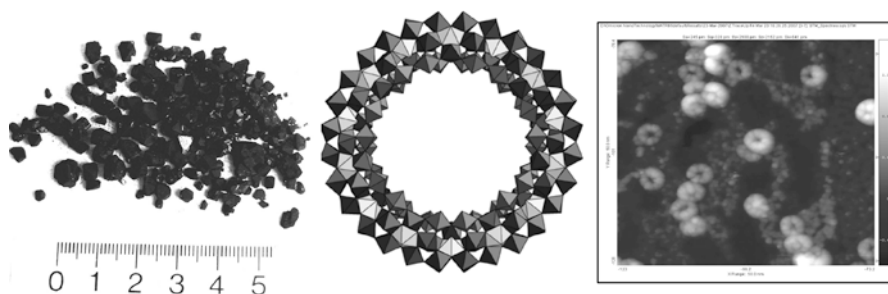


Fig. 6.5 (*left*) Crystals of “molybdenum blue” that today normally are synthesized by using reducing agents like hydrazine or dithionite. In that case the 14 MoNO_3^{3+} are replaced by 14 MoO_4^{4-} groups (for the corresponding formula $[\text{Mo}_{154}\text{O}_{462}\text{H}_{14}(\text{H}_2\text{O})_{70}]^{14-} = [(\text{MoO}_3)_{154}\text{H}_{14}(\text{H}_2\text{O})_{70}]^{14-}$ see refs. [7, 8, 12]), (*middle*) polyhedral presentation of the cluster anion (view parallel to the approx. C_7 axis) and (*right*) Scanning Tunneling Microscopy (STM) picture of the $\{\text{Mo}_{154}\}$ units sprayed on Au(111) kept at 77 K under UHV (courtesy H. Fuchs, L. Chi et al., Univ. of Münster)

century when chemists succeeded for the first time to get crystals from these solutions. However, it took more than 3 years from the first preliminary published data [6] to determine the exact formula of the first crystalline compound, that is, $(\text{NH}_4)_{28}[\text{Mo}_{154}(\text{NO})_{14}\text{O}_{448}\text{H}_{14}(\text{H}_2\text{O})_{70}] \cdot n\text{H}_2\text{O}$ containing the $\{\text{Mo}_{154}\}$ giant wheel cluster anions (Fig. 6.5) [7]. One reason was due to the problem of determining the number of protons and the small amount of cations disordered in the lattice. (A simple determination of the anion charge was also not possible as we refer to a mixed-valence species of Robin-Day type III, i.e. with delocalized electrons.) The above mentioned compound was obtained from the blue solutions when hydroxylamine was used as the reducing agent [6].

From the first crystal structure, it became evident why earlier trials failed to result in a crystalline material, namely, because it has a very high solubility in water owing to the hydrophilic surface of the cluster anion (caused mainly by a large number of coordinated H_2O ligands) but also due to its negative charge (presence of H^+ and cations), and the high electron density on the surface due to the 28 delocalized electrons (for this and other properties see refs. [7–10]). This information resulted in the development of a facile synthetic method referring to destroying the hydration shell and thus decreasing the solubility of the crystals formed. Since this breakthrough also pure crystalline materials were synthesized and structurally characterized in which the “wheels” were linked to chains and layers [11] and additionally compounds containing hollow, spherical- [8a–c,12] and “hedgehog”-shaped [8a–c,13] clusters, with diameters in the range of several nanometers. Such giant polyoxomolybdates (POMs) are formally formed by connecting MoO_6 or MoO_7 polyhedral units via corners or edges (for structural details, cf. refs. [7,8a–c,12]).

6.2 New Puzzle—Soluble But Still Aggregate

6.2.1 Light Scattering and TEM Studies

The discovery and structural characterization of the wheel-shaped giant polyoxomolybdates offered a first comment on the historical “blue waters” puzzle. However, it did not allow to understand a further puzzle, namely, the formation of larger, more complex structures from freshly prepared $\{\text{Mo}_{154}\}$ solutions containing initially the monomeric giant molecular wheels. Figure 6.6 displays the probability distribution as obtained from small angle X-ray scattering (SAXS) measurements for a solution freshly prepared (A) and aged for 48 h (B) which clearly shows the beginning growth leading to regular structural features.

Parallel to this finding we observe an increasing strength of a Tyndall effect from those solutions. As we know, the Tyndall effect is the result of scattered light from suspended particles of colloidal size and is not expected to appear in classical inorganic salt solutions containing homogeneously distributed soluble (small) inorganic ions. These giant wheel-shaped anions, which are highly soluble in water and other polar solvents such as alcohols and even acetone, do not, despite their size persist as discrete ions, obviously contradicting our common knowledge; instead, they further aggregate into large spherical assemblies [14] (Fig. 6.7). These do not look like the aggregates formed by less soluble species, which usually have broad size distributions and tend to continue to grow while finally precipitating

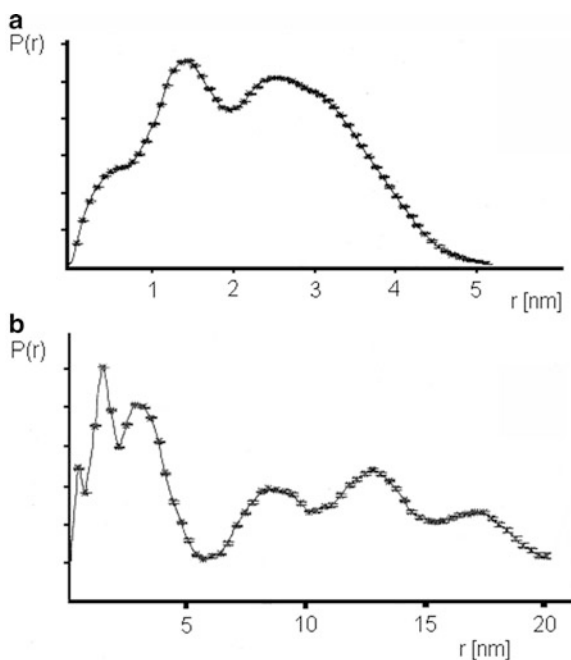


Fig. 6.6 Probability distribution $P(r)$ as obtained from SAXS data of (a) freshly prepared $\{\text{Mo}_{154}\}$ solutions and (b) from the same solution after 48 h [14]

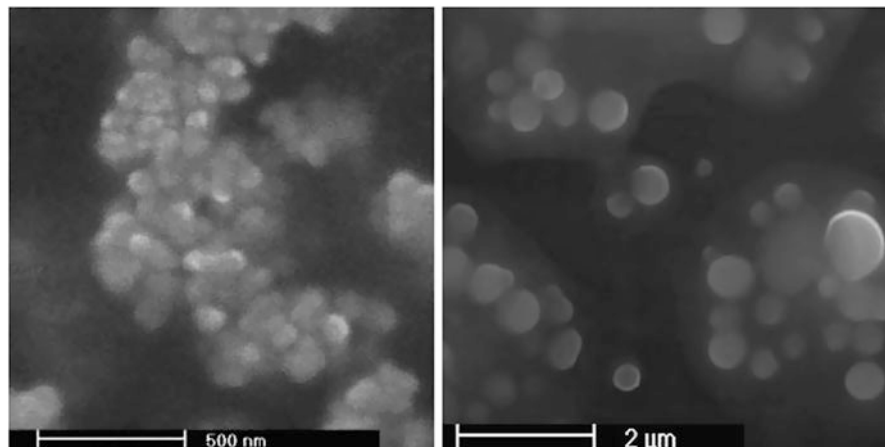


Fig. 6.7 Scanning Electron Micrographs under H_2O saturation pressure (ESEM): residues of (*left*) methanolic and (*right*) acetic solutions of Mo blue. The sizes of the vesicles in these solvents vary considerably compared to those in aqueous systems discussed in the present paper

from the solution. The supramolecular structures formed by the wheel-shaped macroions are hollow and are fairly stable in solution. An energy dispersive X-ray spectroscopy analysis (EDX) showed considerable quantities of solvent existing inside the aggregates, while the aggregates could suddenly burst when switching the scanning electron microscope from environmental mode (ESEM, $p = 15$ mbar) to the high vacuum mode (SEM, $p < 10^{-6}$ mbar) [14].

In addition, a surprisingly narrow size distribution of the aggregates formed by the blue wheels was also observed employing dynamic light scattering (DLS) [14]. These findings attracted us to further pursue this problem. We thought that both static as well as dynamic light scattering (SLS and DLS) measurements [15] would be useful for obtaining more information about those macroionic solutions. SLS measures the scattered intensity from sample solutions at different scattering angles and concentrations. This results in information about the particles in solution, such as weight-average mass (M_w) and radius of gyration (R_g), as well as the nature of interparticle interactions. SLS data are usually treated by the *Zimm* plot. On the other hand, DLS measurements are used to determine the hydrodynamic radius (R_h) and the size distribution of particles (e.g., polymers, colloids, or biomacromolecules) in solution, by using special software such as CONTIN [16].

The CONTIN analysis of the DLS measurement shows that the $\{\text{Mo}_{154}\}$ macroions aggregate in solution into larger, almost monodisperse structures with an average R_h of 44–45 nm (Fig. 6.8, inset). SLS data show that the average R_g of the aggregates is 45.2 ± 1.4 nm (Fig. 6.8), which means R_g is almost equal to R_h (for a solid spherical particle $R_g = 0.77R_h$). The ratio R_g/R_h increases if more mass in a sphere is distributed closer to the surface. We also know from the SEM pictures as shown in Fig. 6.7 that the aggregates are spherical. If a spherical object has all

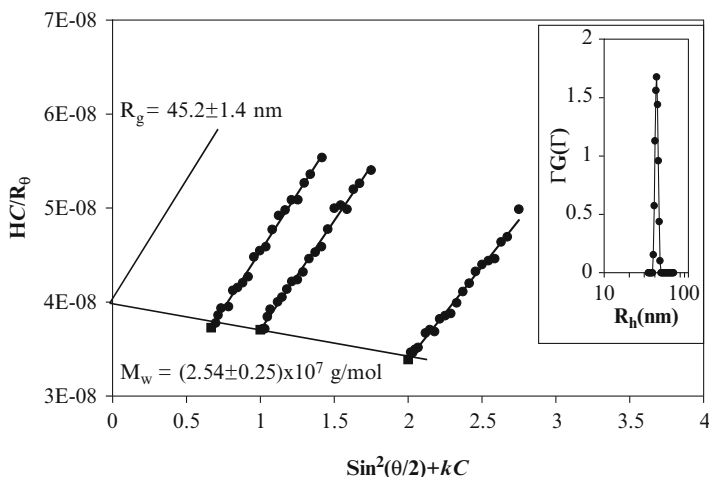


Fig. 6.8 Zimm plot based on SLS measurements on $\{\text{Mo}_{154}\}$ aqueous solutions (three different concentrations were measured), yielding an average R_g of 45.2 nm; (inset) CONTIN analysis of DLS data (scattering angle 60°) on the same solution, showing an average R_h value of 44–45 nm. For spherical particles, $R_h = R_g$ suggests that all the mass is distributed on the surface of the sphere, that is, a vesicle structure

its mass on its surface, the ratio R_g/R_h approaches 1, which corresponds to a typical model for a hollow sphere.

Consequently, our results indicate that the aggregates in solution are not “solid clusters”, but vesicle-like hollow spheres. More interestingly, the mass of the aggregates (M_w) as determined by SLS is $2.54 \times 10^7 \text{ g/mol}$ and corresponds to ca. 1,165 single $\{\text{Mo}_{154}\}$ wheels. This M_w value also suggests the presence of a hollow interior of the aggregates because a solid $\{\text{Mo}_{154}\}$ -type nanocrystal of 45-nm radius would contain a much larger number of individual $\{\text{Mo}_{154}\}$ macroions, i.e. more than 14,000. This means it would be much heavier. In our structural model [17], as shown schematically in Fig. 6.9, all the molecular giant wheels are homogeneously distributed to form a *single* layer on the surface of the “vesicles”, with their molecular isotropic xy plane parallel to the surface. Whereas the term *vesicle* is widely used for bilayer-type hollow spherical assemblies due to the close packing of surfactants or biolipids, our current supramolecular structure is fundamentally different. The water components inside our unprecedented structures do not contribute to the scattered intensity so that the measured M_w does not include them, otherwise their actual M_w would be >10 times greater. Our model can reasonably explain how such giant wheels can form uniform, spherical, higher-level-type aggregates. Based on the mentioned M_w value, it is estimated that the average closest center-to-center distance between two adjacent $\{\text{Mo}_{154}\}$ anions is ca. 4.9 nm. Considering that the diameter of the $\{\text{Mo}_{154}\}$ anion is ca. 3.6 nm [7, 12], it follows that the cluster anions are not touching each other in the vesicles.

High-resolution transmission electron microscopy (TEM) studies directly confirm these results [17]. Figure 6.10a shows a typical TEM image of the $\{\text{Mo}_{154}\}$ -type

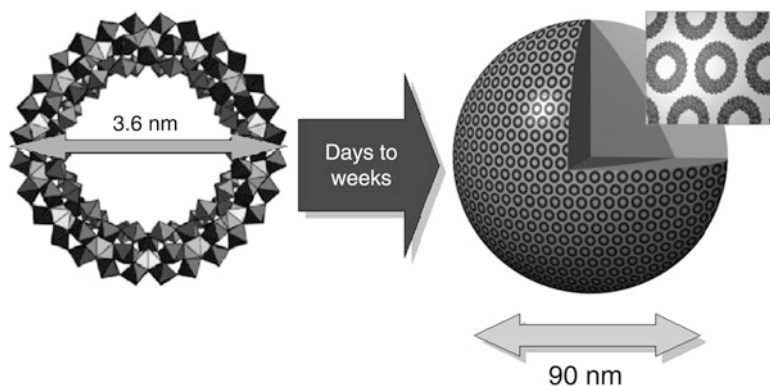


Fig. 6.9 Structural model of the 90-nm spherical vesicles formed from single $\{\text{Mo}_{154}\}$ giant wheels

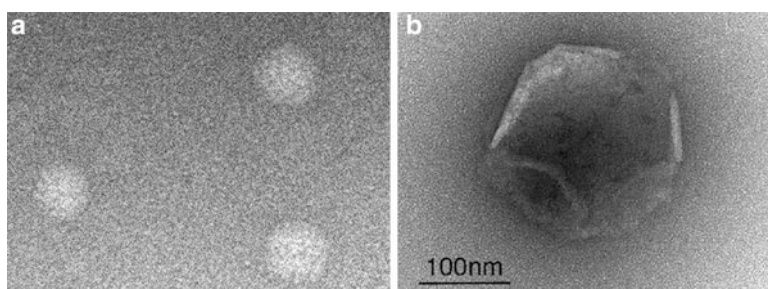


Fig. 6.10 (a) Transmission electron micrograph of some vesicles and (b) a larger, broken one showing the thin-walled hollow nature

vesicles as obtained in aqueous solution. Figure 6.10b displays a broken sphere, which clearly shows that the vesicle wall is thin and hollow inside. Figure 6.11a is a magnification from a patch of a broken vesicle wall flattened on the support carbon film. No long-range ordered packing of $\{\text{Mo}_{154}\}$ wheels on the burst vesicle surface was found, but some ordered packing was observed in small local areas (Fig. 6.11b,c). The lattice spacings are in the range of 3.6–4.2 nm, similar to the size of $\{\text{Mo}_{154}\}$, suggesting that indeed the wheels form the vesicle surface.

6.2.2 Dielectric Relaxation Studies to Get Information on the Role of Water

One of the few methods for obtaining information directly on the state of water at surfaces of the present type of species is dielectric relaxation, a technique used for investigating hydration structures and dynamics in simple aqueous systems and now

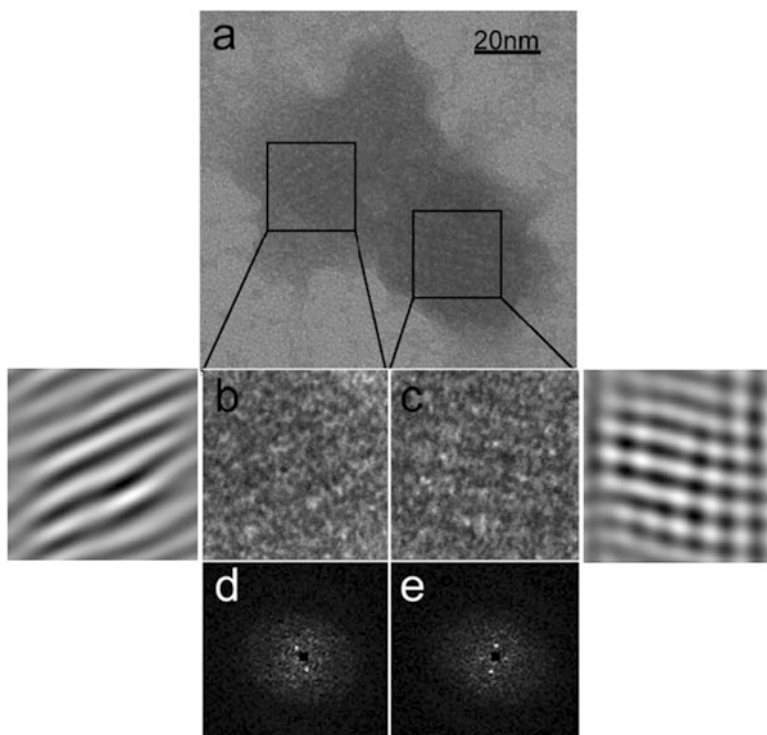
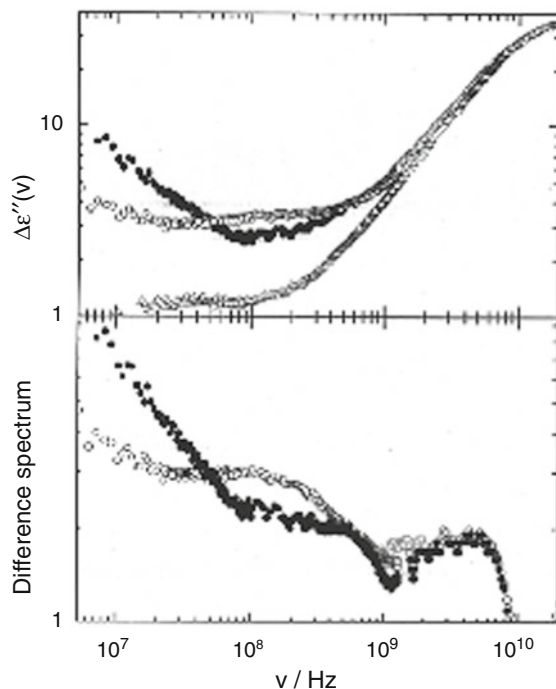


Fig. 6.11 (a) TEM from a broken vesicle flattened surface; (b) and (c) show two magnified areas from this flake displaying some structure in the noise. The left-most and right-most pictures were obtained by Fourier filtering, (d) and (e) are the corresponding power spectra indicating some degree of order

also increasingly applied in studies of more complex systems, such as proteins and micellar aggregates [18]. Dielectric spectra were recorded in the frequency range $300 \text{ kHz} < \nu < 20 \text{ GHz}$. The dielectric absorption of an electrically conductive sample reflects a superposition of a relaxation term and of a contribution caused by the conventional static (direct current) electrical conductance. We are interested in the relaxation spectrum, which can be obtained by subtracting the “trivial” conductance term from the initial experimental spectrum (Fig. 6.12). This has been done both for fresh and aged solutions containing the wheel-shaped $\{\text{Mo}_{154}\}$ species [19]. For comparison, we also investigated the dielectric relaxation of a saturated aqueous solution of the much less hydrophilic, spherical molybdenum-iron-oxide based clusters of the type $\{\text{Mo}_{72}\text{Fe}_{30}\}$, which also show self-assembly processes, but of a different type and much slower.

The electrical conductance σ of the initial solution, obtained as a by-product of dielectric spectroscopy, is of some interest in itself. The observed value of σ for a fresh 1.82 mmol solution roughly corresponds to the conductance of a 0.05 m NaCl

Fig. 6.12 Conductance-corrected dielectric spectra (*top*) and difference spectra (*bottom*) of aqueous solutions of the $\{\text{Mo}_{154}\}$ type cluster in the freshly prepared (*open circles*) and aged state (after 2 weeks; *full circles*). The spectrum of the $\{\text{Mo}_{72}\text{Fe}_{30}\}$ type cluster (*triangles in the lower part of the top spectra*) is shown for comparison



solution in water. Important in this context is that the solution contains an average of 15 Na^+ and 14 H^+ ions per cluster anion (this refers to the Na salt (not containing NO groups) in which two anions occur with charges 14- and 16-; see formula of the former one in the legend to Fig. 6.5 and also refs. [7, 10]), giving rise to a pH value of about 2.3. The observed conductance implies that by far not all Na^+ and H^+ ions are mobile while their interactions with the anionic Mo clusters even get stronger when the assembly process is in progress [19].

Assuming that there are no processes below the frequency window of our experiments, the resulting dielectric spectrum implies that the features obtained for the fresh and aged solutions of $\{\text{Mo}_{154}\}$ are associated with shells of confined water attached to the “assemblies”. The spectra are dominated by an intense absorption near 20 GHz with a Lorentzian lineshape due to bulk water. Spectral analysis shows that its wing superimposes absorptions at lower frequencies. We therefore subtracted this mode from the total spectrum, thereby generating the difference spectra as shown in the lower part of Fig. 6.12, which accentuates the low-frequency processes. The difference spectrum of the freshly prepared state indicates a distinct mode near 4 GHz, a broad absorption regime smeared out from 50 MHz to 1 GHz, and an intense mode centred at 7 MHz, which is only partially sampled owing to the frequency cut-off of our experimental range. The intermediate regime between 50 MHz and 1 GHz can be approximately parameterized by two modes. The resulting five-term parameterization of the total spectrum, as summarized in

Table 6.2 Spectral parameterization of the dielectric absorption spectrum of an aqueous solution of $\{\text{Mo}_{154}\}$ before ageing

	Water type assigned relaxation time t (ns) amplitude	
1	22 (7.2 MHz)	7.1
2	1.7 (94 MHz)	4.4
3	0.2 (800 MHz)	2.6
4	0.04 (4,000 MHz)	2.8
Bulk	0.00822 (19,400 MHz)	68

Table 6.2, assumes that different kinds of confined water assemblies are associated with each single $\{\text{Mo}_{154}\}$ type cluster anion.

On “ageing” of the solution, that is, after 2 weeks, which corresponds to the above mentioned vesicle formation, the following tendencies are observed: The first peak at 7.2 MHz almost doubles, the second at ca. 90 MHz decreases to less than the half, the third shifts from 800 to 450 MHz (this means that the related water shell gets more strongly bound) and decreases by about 40%; the fourth peak keeps position and amplitude and, finally, the bulk water peak at about 20 GHz is approximately constant. Together this indicates that the strength of the hydration extends as cluster aggregation takes place with more water molecules being more strongly bound between the wheels and the presence of relatively fewer less strongly bound water molecules. This change clearly shows that the different types of confined water assemblies in fact play a significant role in the formation and stabilization of the finally resulting vesicle (see also next section).

6.3 What Is the Driving Force Behind This Self-Assembly?

The term self-assembly suggests that such processes can occur spontaneously, that is, are favored by negative free energy changes. However, assembling species leading to a homogeneous distribution is usually an entropy-loss process. Therefore, some driving forces must exist in the self-assembly process to compensate for the loss of entropy. For example, hydrophobic interactions are important in assembling amphiphilic surfactant-micelle and bilayer-vesicle structures [20]. The hydrophobic interaction is a short-range force; therefore, we can – in case of regular lipid vesicles – always observe closely packed hydrophobic regions and outside hydrophilic parts. But in the present scenario, each molybdenum blue-type cluster ion is covered with a “layer” of H_2O ligands that make it strongly hydrophilic. Therefore the mechanism of this self-assembly must be substantially different from those of amphiphilic ones. In any case it is obvious that a delicate balance between attractive and repulsive forces makes the vesicles stable. The repulsive force is due to the electrostatic interaction between the negatively charged giant anions while the attractive forces are more complicated. Besides the unlikely hydrophobic interaction, the contribution from attractive van der Waals forces cannot predominantly account for the attraction [21]. We believe that a counterion effect, besides a strong contribution of hydrogen bonding (the water shell between

the macroions should formally act as glue) could be an important factor. The strong attraction among giant anions leading to the vesicle formation occurs only when the macroions carry charges, although not too many (polyoxometalates are naturally repulsive towards each other). However, when counterions stay close enough to the macroions the repulsion decreases and helps to keep the two macroions at a shorter distance from each other. Recall that conductivity measurements indicated that a fraction of the counterions cannot move freely, even in very dilute solutions. They are closely associated with POM macroions, leading to a lower solution conductance value than expected [19]. (The decrease can not only be explained by the macroion assembly.)

In Fig. 6.10, the burst vesicle exhibits a wrinkle feature and a high contrast around the edge (typical for an empty sphere, e.g., lipid vesicles) that indicates the biomembrane-like soft nature of its surface. Considering that the present $\{\text{Mo}_{154}\}$ -type wheels are rather “hard” inorganic species, the soft nature of the vesicle surface clearly favours the assumption of the presence of additional linking materials/glue between adjacent macroions, i.e. the existence of highly structured water nanoassemblies because “free” water molecules will not hold the isolated giant wheels to form the fairly stable supramolecular structure. It is known that the viscosity of water can increase several orders of magnitude in a nanoscale confinement [22], which means in the present case that water molecules linked with hydrogen bonds should act as “viscous glue” to form the whole supramolecular assembly.

Our previous understanding of soluble inorganic ions in diluted solutions was straightforward: they should homogeneously distribute in a solvent and exist as single ions, reaching the minimum free energy (ΔG) and the maximum entropy (ΔS) simultaneously. However, this general solute state for inorganic ions is not valid for the hydrophilic macroions described here. These macroions have two different states: an entropy favored first (general) state, in which the solutes distribute homogeneously, and a more important thermodynamically favored second state, in which the solutes self-associate into supramolecular structures owing to strong inter-solute interactions.

This is certainly not the end of this centuries-lasting story. There are several questions left open, among them the further aggregation of our vesicles into even larger, grape-like structures (cf. Figs. 6.7 and 6.13). This seems to be a textbook example for a process related to the term “From simple to complex systems” [23].

In summary, after more than 200 years of continuous explorations, scientists have reached a better understanding of the longtime puzzle of “molybdenum blue solutions” [24] and it turned out to be really complex. Furthermore, with the discovery of various other structurally well-defined, giant, hydrophilic molybdenum-oxide based species, inorganic chemists have successfully pushed the size limit of inorganic ions into the nanometer scale. Consequently, this progress provides new challenges in different fields, for example, the physical chemistry of solutions. The giant anions show totally different solution behaviour when compared to regular inorganic ions, owing to their sizes and especially their surface properties. In any case even the chemistry of the discrete molecular wheels is still an actual research topic [25].

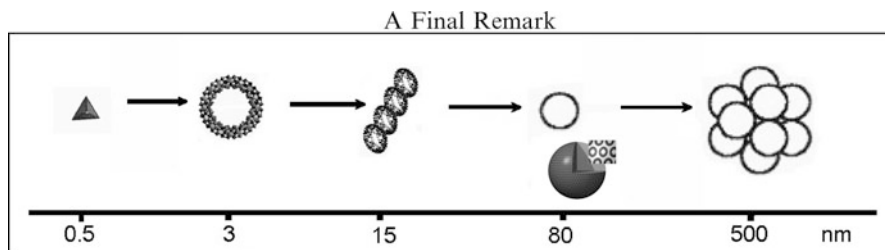


Fig. 6.13 Hierarchical Patterning – The old and well known “molybdenum blue” test tube reaction [24] covers a size range of more than three orders of magnitude

Acknowledgments We thank the Deutsche Forschungsgemeinschaft, the Fonds der Chemischen Industrie, the European Union, the German-Israeli Foundation for Scientific Research & Development (GIF) and the Volkswagen Foundation for continuous support of our work. We also gratefully acknowledge the contributions of Tianbo Liu (Lehigh) who performed a series of investigations on the assembly processes of the giant molybdenum-oxide based clusters, and furthermore Andreas Dress (ICB Shanghai), Martin Chaplin (SBU London), Hermann Weingärtner (RUB Bochum) and their respective groups to this work (cf. references cited).

References

- Schwarzenbach G (1950) *Allgemeine und Anorganische Chemie*, 4th edn. Thieme, Stuttgart, p 117
- Scheele CW (1793) *Sämtliche Physische und Chemische Werke*. In: Hermbstädt DSF (ed) vol 1. Sändig, Niederwalluf, pp 185–200 reprint 1971
- Schuffe JA (1985) *Torbern Bergman: a man before his time*. Coronado Press, Lawrence
- For the older literature cf. Gmelins *Handbuch der Anorganischen Chemie* (1935) System-Nr 53, 8th edn. Verlag Chemie, Berlin, and references cited therein
- Berzelius JJ (1826) *Poggend Ann Phys Chem* 6:369
- Müller A, Krickemeyer E, Meyer J, Bögge H, Peters F, Plass W, Diemann E, Dillinger S, Nonnenbruch F, Randerath M, Menke C (1995) *Angew Chem Int Ed* 34: 2122; See also Müller A, Peters F, Pope MT, Gatteschi D (1998) *Chem Rev* 98:239
- Müller A, Serain C (2000) *Acc Chem Res* 33:2
- (a) Müller A, Roy S (2003) *Coord Chem Rev* 245: 153; (b) Müller A, Koop M, Bögge H, Schmidtman M, Peters F, Kögerler P (1999) *Chem Commun* 1885; (c) Müller A, Roy S (2004) In: Rao CNR, Müller A, Cheetham AK (eds) *The chemistry of nanomaterials: synthesis, properties and applications*. Wiley-VCH, Weinheim, chapter 14, pp 452–475; (d) Müller A, Koop M, Bögge H, Schmidtman M, Beugholt C (1998) *Chem Commun* 1501 (in that paper the problem of the charge determination of the $\{Mo_{154}\}$ and $\{Mo_{176}\}$ type species has been discussed)
- Müller A, Das SK, Fedin VP, Krickemeyer E, Beugholt C, Bögge H, Schmidtman M, Hauptfleisch B (1999) *Anorg Allg Chem* 625:1187
- (a) Müller A, Das SK, Krickemeyer E, Kuhlmann C (2004) In: Shapley JR (ed) *Inorganic synthesis*, vol 34. Wiley, New York, pp 191–200; (b) Müller A, Roy S (2005) *Eur J Inorg Chem* 3561; (c) Cronin L, Diemann E, Müller A (2003) In: Woollins JD (ed) *Inorganic experiments*. Wiley-VCH, Weinheim, pp 340–346

11. (a) Müller A, Krickemeyer E, Bögge H, Schmidtman M, Peters F, Menke C, Meyer J (1997) *Angew Chem Int Ed* 36:483; (b) Müller A, Krickemeyer E, Bögge H, Schmidtman M, Beugholt C, Das SK, Peters F (1999) *Chem Eur J* 5:1496; (c) Cronin L, Kögerler P, Müller A (2000) *J Solid State Chem* 152:57 (a review)
12. (a) Müller A, Kögerler P, Dress A (2001) *Coord Chem Rev* 222: 193; (b) Müller A, Kögerler P, Kuhlmann C (1999) *Chem Commun* 1347; (c) Müller A, Kögerler P, Bögge H (2000) *Struct Bond* 96:203
13. Müller A, Beckmann E, Bögge H, Schmidtman M, Dress A (2002) *Angew Chem Int Ed* 41:1162
14. Müller A, Diemann E, Kuhlmann C, Eimer W, Serain C, Tak T, Knöchel A, Pranzas PK (2001) *Chem Commun* 1928; See also ref. 7
15. Chu B (1991) *Laser light scattering*, 2nd edn. Academic, New York
16. Provencher SW (1976) *Biophys J* 16:27
17. Liu T, Diemann E, Li H, Dress AWM, Müller A (2003) *Nature* 426:59
18. (a) Nandi N, Bhattacharyya K, Bagchi B (2000) *Chem Rev* 100:2013; (b) Oleinikova A, Sasisanker P, Weingärtner H (2004) *J Phys Chem B* 108:8467; (c) Baar C, Buchner R, Kunz W (2001) *J Phys Chem B* 105:2906 and 2914
19. Oleinikova A, Weingärtner H, Chaplin M, Diemann E, Bögge H, Müller A (2007) *Chem Phys Chem* 8:646, and references cited therein
20. Jung HT, Coldren B, Zasadzinski JA, Iampietro DJ, Kaler EW (2001) *Proc Natl Acad Sci USA* 98:1353
21. (a) Liu G, Liu T (2005) *J Am Chem Soc* 127:6942; (b) Liu T, Imber B, Diemann E, Liu G, Cokleski K, Li H, Chen Z, Müller A (2006) *J Am Chem Soc* 128:15914
22. Israelachvili J, Gourdon D (2001) *Science* 292:867
23. See also articles referring to dissipative and non-dissipative systems in: Müller A, Dress A, Vögtle F (eds) (1996) *From simplicity to complexity in chemistry – and beyond*, Part I. Vieweg, Wiesbaden, as well as Mainzer K, Müller A, Saltzer WG (eds) (1998) *From simplicity to complexity*, Part II. information – interaction – emergence, Vieweg, Wiesbaden
24. See for instance the book Emsley J (2001) *Nature's building blocks: an A – Z guide to the elements*. Oxford University Press, Oxford, chapter: Molybdenum, section: Element of history, p 263. There we read: About this time (1781) Scheele discovered a simple and specific test for molybdenum. [...] (molybdate) would form an intense blue colour on adding a reducing agent to the solution. [...]. The test was used for almost 200 years, despite the fact that chemists could not identify the agent responsible for the colour. In 1996 the puzzle was solved by a group of German chemists at the University of Bielefeld who showed it to consist of a cyclical cluster made up of 154 molybdenum atoms interlinked with oxygen atoms.; (b) Gouzerh P, Che M (2006) From Scheele and Berzelius to Müller: Polyoxometalates (POMs) revisited and the “missing link” between the bottom up and top down approaches, *L'Actualité Chimique*, June Issue, No. 298, 9
25. Shishido S, Ozeki T (2008) *J Am Chem Soc* 130:10588

Chapter 7

Encapsulated Water Molecules in Polyoxometalates: Insights from Molecular Dynamics

Pere Miró and Carles Bo

Abstract We demonstrated that classical molecular dynamic simulations are an attractive tool for studying water clusters encapsulated in polyoxometalate nanocapsules by fully confirming the structures determined experimentally, $(\text{H}_2\text{O})_{12}$ in Mo_{57}V_6 and $(\text{H}_2\text{O})_{100}$ in Mo_{132} . The polyhedral shape of $(\text{H}_2\text{O})_{100}$ water cluster and the effect of the inner ligands in the generation of high density ($\text{Mo}_{132}\text{-SO}_4$) and low density ($\text{Mo}_{132}\text{-HCO}_2$) water clusters have been demonstrated. In the case of $\text{Mo}_{132}\text{-SO}_4$ and $\text{Mo}_{132}\text{-HCO}_2$, our simulations showed that encapsulated water molecules self-assemble dynamically in shell structures, which are strongly affected by slightly increasing the volume of the capsule. Water in the cavities is structurally closer to ice water than to liquid water, as it is unable to diffuse as liquid water does.

7.1 Introduction

Complexity is a concept often invoked for describing chemical phenomena that escape our current understanding, either because the inherent complication of the systems, or because the undetermined number of coupled parameters. Here we can include the structure of very large molecules, supramolecular assemblies [1], non-linear processes, and even the origin of life. Complexity can be also found

P. Miró

Institute of Chemical Research of Catalonia (ICIQ), Av. Països Catalans 16,
43007 Tarragona, Spain
e-mail: pmr@ICIQ.ES

C. Bo (✉)

Institute of Chemical Research of Catalonia (ICIQ), Av. Països Catalans 16,
43007 Tarragona, Spain

Departament de Química Física i Química Inorgànica, Universitat Rovira i Virgili,
Marcel·lí Domingo s/n, 43007 Tarragona, Spain
e-mail: cbo@iciq.es

in one of the simplest but curious materials, water. The structure and behaviour of water molecules encapsulated in confined spaces are of capital interest because they are of relevance to several aspects of molecular biology, for example, protein folding and activity [2, 3]. However, while the properties of confined water are rather peculiar and their computational description is not easy, the structure and properties of bulk liquid water has deserved attention too. Regarding the problem of understanding the structure of bulk liquid water [4–15] the so-called two-structure models were developed, while with reference to biological scenarios it is assumed in the literature that the liquid consists of rapidly exchanging high density water (HDW) and low density water (LDW) microdomains differing in their physical and chemical properties because of their different strength of hydrogen bonds. It is worth mentioning here a paper related to biological aspects entitled “Life depends upon two kinds of water” [16, 17], which states that “[...] protein conformations demanding greater hydration are favoured by more active water (as high density water containing many weak bent and/or broken hydrogen bonds) and conformations are relatively favoured by lower activity water (as low-density water containing many strong intra-molecular aqueous hydrogen bonds)”. In any case it is generally accepted that networks of hydrogen-bonded water assemblies, especially high density water, control protein folding, structures, and activities.

One possible way to investigate confined water assemblies systematically is by trapping them in structurally well defined and differently sized as well as functionalized nanosized capsule cavities. The use of nanosized carbon tubes [18] or, in particular, metal oxide based capsules has advantages as it allows work under a variety of experimental conditions. The first reported POM with an internal cavity was the Preysler anion [19], however its internal cavity just allows the encapsulation of one cation and only one water molecule. The group in Bielefeld mainly lead the synthesis of new POMs with internal cavities such as the donut-shaped $[\text{H}_3\text{Mo}_{57}\text{V}_6(\text{NO})_6\text{O}_{183}(\text{H}_2\text{O})_{18}]^{21-}$ (Mo_{57}V_6) [20] and the spherical $[(\text{Mo}_6\text{O}_{21}(\text{H}_2\text{O})_6)_{12}(\text{Mo}_2\text{O}_4(\text{L}^{n-}))_{30}]^{(12+n)-}$ (Mo_{132}) nanocapsules (Fig. 7.1) [21, 22].

In one hand, Mo_{57}V_6 has two different cavities, three external where three $(\text{H}_2\text{O})_2$ are trapped and the internal one where a $(\text{H}_2\text{O})_{12}$ water cluster is present. On the other hand, the Mo_{132} structure is a soluble spherical porous capsule of the type $[(\text{pentagonal unit})_{12}(\text{metal linker unit})_{30}]^{n-}$ as $[(\text{Mo})\text{Mo}_5\text{O}_{21}(\text{H}_2\text{O})_6]_{12}(\text{Mo}_2\text{O}_4(\text{L}))_{30}]^{n-}$, which is stable in solution under well defined conditions with a cavity where a large quantity of water molecules can be confined. An important aspect of Mo_{132} is the pores that can be closed upon the correct choice of the counterions in a stepwise manner. They have been described as artificial cells [23]. These capsules, which may be considered as coordination polymers with spherical periodicity, can be constructed with differently sized cavities based on the choice of internal ligands.

The compound $[(\text{Mo}_6\text{O}_{21}(\text{H}_2\text{O})_6)_{12}(\text{Mo}_2\text{O}_4(\text{HCO}_2))_{30}]^{42-}(\text{Mo}_{132}\text{-HCO}_2)$, which contains the Mo_{132} -type capsules with the largest possible cavity, was prepared and was characterized by different techniques (IR, Raman and X-Ray diffraction.) [21]. The anionic capsule $\text{Mo}_{132}\text{-HCO}_2$ contains 12 pentagonal units

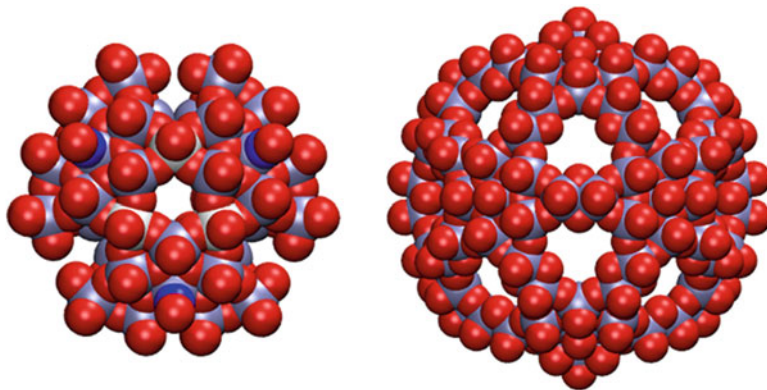


Fig. 7.1 Structures for $[\text{H}_3\text{Mo}_{57}\text{V}_6(\text{NO})_6\text{O}_{183}(\text{H}_2\text{O})_{18}]^{21-}$ (Mo_{57}V_6) and $[(\text{Mo}_6\text{O}_{21}(\text{H}_2\text{O})_6)_{12}(\text{Mo}_2\text{O}_4(\text{L}^{n-}))_{30}]^{(12+n)-}$ (Mo_{132}) nanocapsules

$[(\text{Mo})\text{Mo}_5\text{O}_{21}(\text{H}_2\text{O})_6]^{6-}$ placed at the 12 vertices of an icosahedron and linked by 30 dinuclear $[\text{Mo}_2\text{O}_4(\text{HCO}_2)]^+$ units. The construction principle automatically leads to capsules with 20 Mo_9O_9 pores. Since the 20 pores remained open during the synthesis of $\text{Mo}_{132}\text{-HCO}_2$ the structure of the water molecules encapsulated in its cavity are influenced. The cavity of $\text{Mo}_{132}\text{-HCO}_2$ hosts a $(\text{H}_2\text{O})_{80}$ water cluster [22] consisting of a $(\text{H}_2\text{O})_{60}$ shell that is embedded into a peripheral dodecahedral $(\text{H}_2\text{O})_{20}$ shell (Fig. 7.2, top right), while the two shells interact via hydrogen bonds. However the cavity should not be completely free of NH_4^+ ions that disorder the water cluster.

To study the nature of a pure encapsulated water molecule assembly in the cavity of $\text{Mo}_{132}\text{-HCO}_2$, that is, in the absence of inorganic cations, a derivative compound was synthesized in Müller's group replacing the ammonium by formamidinium cations [24]. This new compound was also structurally characterized by different techniques and has the same skeleton as the previously presented $\text{Mo}_{132}\text{-HCO}_2$ but with closed pores due to the presence of the new cations. Formamidinium cations are too large to pass through the Mo_9O_9 pores but can close them as mentioned above (Fig. 7.2, top left). The new scenario showed as expected a cation-free water cluster integrated in the capsule cavity. Also in contraposition with the open pore compound, a large number of water molecules were encapsulated and a $(\text{H}_2\text{O})_{100}$ water cluster laid inside $\text{Mo}_{132}\text{-HCO}_2$ when the pores are closed.

The encapsulated water molecules in $\text{Mo}_{132}\text{-HCO}_2$ were found arranged in a well-defined and unprecedented structure that can be described by a four concentric shell arrangement with radii of 3.92–4.13, 6.72–6.78, 7.59–7.78, and 8.31–8.70 Å (Fig. 7.3, top). The water molecules in these shells are structured in a polyhedral shape, with water oxygens in the vertex of the polyhedra. They have the following structures in the same sequence as before: $(\text{H}_2\text{O})_{20}$ dodecahedron, $(\text{H}_2\text{O})_{20/2}$ dodecahedron, $(\text{H}_2\text{O})_{60}$ distorted rhombicosidodecahedron, and $(\text{H}_2\text{O})_{20/2}$ dodecahedron (Fig. 7.3, bottom left), while the two $(\text{H}_2\text{O})_{20/2}$ shells are not separated enough from each other (related O...O distances on the C_3 axes < 2 Å) to allow a

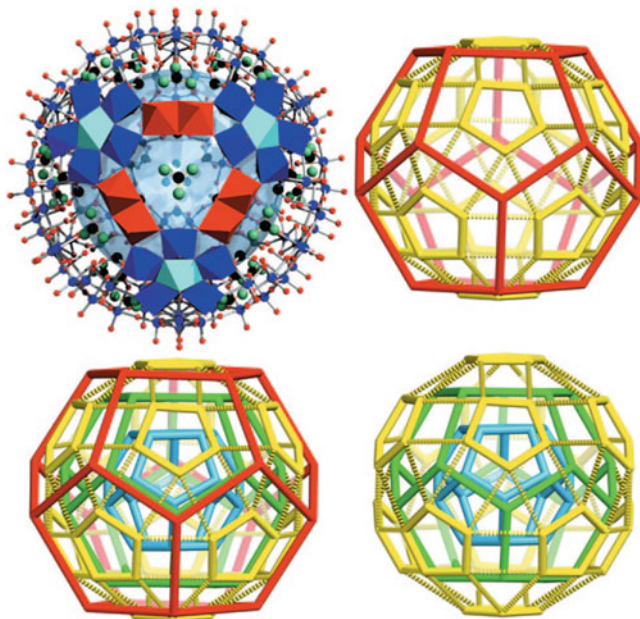


Fig. 7.2 Structure of the different water molecule assemblies (in wireframe representation showing only the water oxygen atoms) occurring within the cavities of the three different spherical porous (Mo_{132})-type POMs while hydrogen bonds between the shells are not shown. *Top right:* Scenario in open $\text{Mo}_{132}\text{-HCO}_2$ a showing the peripheral (H_2O)₂₀ (red) and the inner (H_2O)₆₀ shell, while highlighting the 12 (H_2O)₅ pentagons (yellow, like for $\text{Mo}_{132}\text{-SO}_4$). *Bottom left:* The situation in $\text{Mo}_{132}\text{-HCO}_2$ a showing the three dodecahedra, that is, one fully occupied (light blue) and the two underoccupied (H_2O)_{20/2} types (red and green), as well as the (H_2O)₆₀ shell (yellow). *Bottom right:* Shown is the three-shell water assembly in $\text{Mo}_{132}\text{-SO}_4$; the central (blue) and the peripheral (yellow) shells correspond to those in $\text{Mo}_{132}\text{-HCO}_2$. Additionally shown (top left) is the $\text{Mo}_{132}\text{-HCO}_2$ structure highlighting one pore (in polyhedral representation with the pentagonal units in blue and dinuclear linkers in red) and showing the noncovalently bonded formamidinium cations. The large blue sphere highlights the cavity in which the water molecules are encapsulated. Carbon in black, nitrogen and hydrogen in green, molybdenum in blue and oxygen in red [24] (Color figure online)

complete occupation. As a consequence of this, the water molecules are distributed statistically at the vertices of the two dodecahedra, while both show occupancies of 50%. If a H_2O molecule occurs in one of the two dodecahedra the position of the second dodecahedron on the same C_3 axis is vacant.

Remarkably, the same number of water molecules as in $\text{Mo}_{132}\text{-HCO}_2$ was also found in $[(\text{Mo}_6\text{O}_{21}(\text{H}_2\text{O})_6)_{12}(\text{Mo}_2\text{O}_4(\text{SO}_2))_{30}]^{72-}$ ($\text{Mo}_{132}\text{-SO}_4$) nanocapsule [25,26]. But in that case three concentric fully occupied shells were present, which are organized in the form of two (H_2O)₂₀ dodecahedra and one strongly distorted (H_2O)₆₀ rhombicosidodecahedron (Fig. 7.2, bottom right). The radii of the shells are 3.84–4.04, 6.51–6.83, and 7.56–7.88 Å, respectively (Fig. 7.3, bottom). The important comparison between $\text{Mo}_{132}\text{-HCO}_2$ and $\text{Mo}_{132}\text{-SO}_4$ reveals that the larger

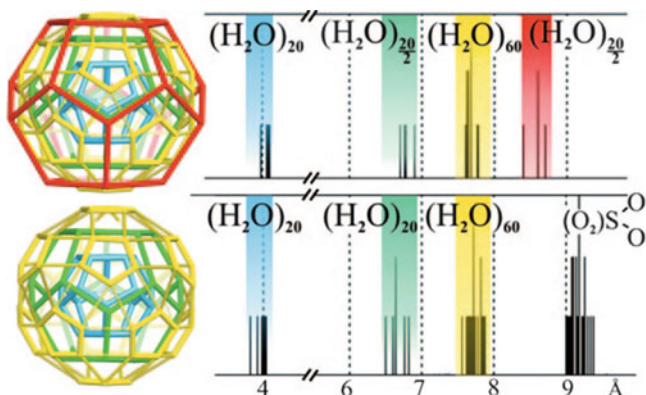


Fig. 7.3 The distance histograms related to capsules $\text{Mo}_{132}\text{-HCO}_2^-$ (*top*) and $\text{Mo}_{132}\text{-SO}_4$ (*bottom*): Shown are the distributions of oxygen atoms of the water molecules at the different distances from the center of the cavities. Color code as in Fig. 7.2 [24] (Color figure online)

ligands (SO_4^{2-}) block more space in the internal cavity than smaller ones (HCO_2^-). This difference has as a consequence the different structures of the two $(\text{H}_2\text{O})_{100}$ assemblies. Therefore, this scenario can be described as “high and low density” water molecule assemblies, while the terms HDW/LDW are considered relative to each other, that is, related to the present system and not in general consideration.

In this chapter, we report the results of a computational study aimed at simulating the long-time collective behaviour of water clusters inside POM nanocapsules. Firstly, we will describe the donut-shaped Mo_{57}V_6 structure, which has one internal cavity with 12 water molecules, and three external cavities with two water molecules each. Our objective was to use this system to set up a methodology and compare the simulation results with the available neutron scattering data, and also to get then hints about the behaviour of the confined water molecules, whether they exchange with the bulk or not, or with cations. Next we studied the giant Mo_{132} considering two different inner ligands, SO_4^{2-} and HCO_2^- . The structure of the confined $(\text{H}_2\text{O})_{100}$ water cluster in both cases was studied in detail. Our final goal was to reproduce the experimental results, to demonstrate the spontaneous self-assembly of the water molecules inside POM nanocapsules and study the effect of the inner ligand into the layered structures.

7.2 Computational Details

We used a large number of explicit solvent molecules to describe high dilution conditions for the POMs. The methodology employed is based on classical molecular dynamics MD simulations that were carried out using the DLPOLY package [27–29]. The simulations of $[\text{H}_3\text{Mo}_{57}\text{V}_6(\text{NO})_6\text{O}_{183}(\text{H}_2\text{O})_{18}]^{21-}$ anion contained 9,018 water molecules (9,000 solvent water molecules, 6 water molecules in

the external cavities and 12 water molecules in the internal cavity), 1 anion and 21 cations (Li^+ or Na^+) in order to keep the system electro neutral. The simulations were performed at different temperatures: 100, 200 and 300 K. The simulations for the $[(\text{Mo}_6\text{O}_{21}(\text{H}_2\text{O})_6)_{12}(\text{Mo}_2\text{O}_4(\text{SO}_4))_{30}]^{72-}$ ($\text{Mo}_{132}\text{-SO}_4$) anion contained 9,073 molecules (8,828 solvent water molecules, 100 water molecules in the internal cavity and 72 molybdenum-coordinated water molecules), one anion and 72 Na^+ cations in order to maintain the system electro neutral; the $[(\text{Mo}_6\text{O}_{21}(\text{H}_2\text{O})_6)_{12}(\text{Mo}_2\text{O}_4(\text{HCO}_2))_{30}]^{42-}$ ($\text{Mo}_{132}\text{-HCO}_2$) anion contained 9,043 molecules (8,828 solvent water molecules, 100 water molecules in the internal cavity and 72 molybdenum coordination waters), one anion and 42 guanidinium cations in order to maintain the electroneutrality of the system. Twenty of the counterions were placed as plugs nearby the pores.

For $\text{Mo}_{132}\text{-SO}_4$ and $\text{Mo}_{132}\text{-HCO}_2$, independent runs of 1 ns, with total length of 10 ns, were carried out at 298 K and 198 K, which permitted us to obtain statistically reliable results. The POM has been kept rigid during the simulations, neglecting bonding parameters. The set of Lennard-Jones parameters of the anions was taken from previous work [30–32]. The atomic charges for Mo_57V_6 species the charges were taken from a density functional calculation (quadrupolar charges) and for Mo_{132} nanocapsule from a Qeq method [33]. The parameter set used for water molecules corresponds to that of the SPC/E model [34]. The monovalent cations used are Li^+ and Na^+ whose models are described in the work of Lee and Rasaiah [35].

7.3 Encapsulated $(\text{H}_2\text{O})_{12}$ and $(\text{H}_2\text{O})_2$ Clusters in Mo_{57}V_6

The neutron scattering structure determination of Mo_{57}V_6 revealed that the internal cavity contains twelve water molecules [20, 36], that are structured in two rings with six molecules each, one ring atop the other like a water sandwich (Fig. 7.4).

The internal water molecules act as ligands too: six bonded to the six vanadium atoms and six bonded to molybdenum atoms. The structure determined by neutron diffraction showed a local pseudo- C_{3h} symmetry. The 12 water molecules form two 12-membered rings consisting of six $\text{O}\cdots\text{H}\cdots\text{O}$ hydrogen bonds each.

The whole system was studied by means of classical MD simulations in explicit solvent. Energy minimization of the 12 water clusters inside the cavity skeleton, which was kept frozen, converged rapidly to the structure shown on the left hand side of Fig. 7.5. Note that water molecules are disposed in such a way as to maximize hydrogen bond interactions and that this arrangement matches precisely the structure determined by neutron diffraction.

Hydrogen bond distances between neighbouring water molecules measured in the minimum energy structure (1.711 Å) were in good agreement with experimental values from neutron diffraction (1.765 Å), and also with the distances found in ice subtype I_h (1.746 Å) (Fig. 7.5, right). By using the trajectories obtained from the MD simulations, the spatial distribution function (SDF) of oxygen and hydrogen

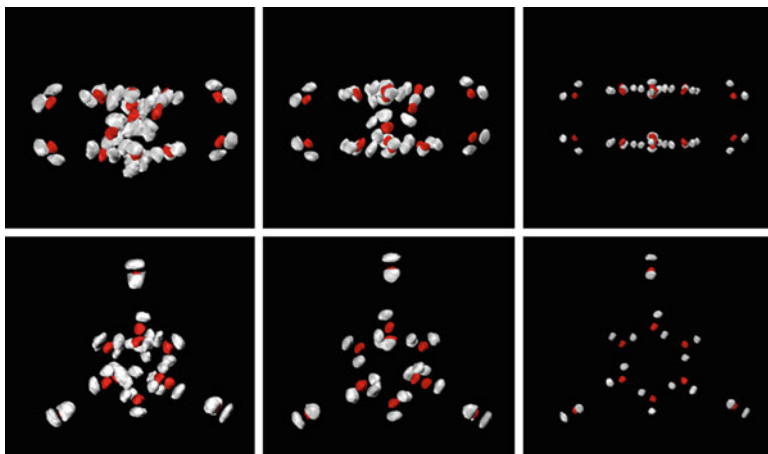


Fig. 7.6 Side (*top*) and axial (*bottom*) view of the oxygen (*red*) and hydrogen (*white*) atoms spatial distribution function (*SDF*) of the encapsulated water molecules at different temperatures: 300 K (*left*), 200 K (*center*) and 100 K (*right*). The POM structure is omitted for clarity (Color figure online)

As it can be seen in Fig. 7.6, at low temperature the isosurfaces indicate that all the 18 water molecules (6 in the three external cavities and 12 in the inner cavity) remained rather stable at their equilibrium positions. When temperature was increased, the volume enclosed by the isosurfaces was clearly larger than at low temperature, indicating that the mobility of those molecules increased. Also, Fig. 7.6 shows that some water molecules, precisely those in the two rings had enough kinetic energy for breaking some hydrogen bonds and diffuse inside the cavity. Although exchange between the two rings is observed, the water cluster basic structure still remains even at room temperature. The water molecules located at the three external cavities even at room temperature stay quite fixed. The narrow shape of these cavities, which does not allow full rotation of the water molecules inside, limits their motion. In all the cases, the lateral apertures and the pore of the cavity seem to be small enough to prevent any water molecule to be released. Although it could be a consequence of the lack of flexibility of the pore imposed in the simulations, neither water molecules nor cation exchange between the cavity and the bulk were observed.

7.4 Encapsulated (H₂O)₁₀₀ Cluster in Mo₁₃₂

To gain more insight into the nature and formation of the (H₂O)₁₀₀ water assemblies in the Mo₁₃₂ capsules, a series of classical MD simulations on Mo₁₃₂-SO₄ and Mo₁₃₂-HCO₂ were carried out. The simulations were started from a randomly

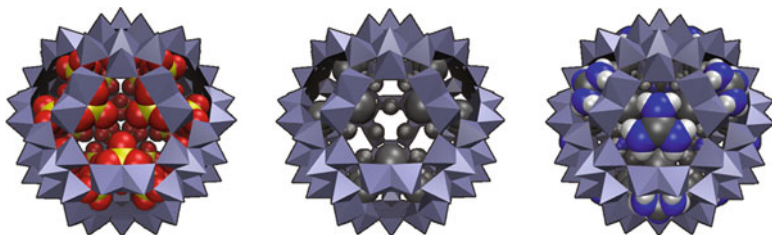


Fig. 7.7 Pores of $\text{Mo}_{132}\text{-SO}_4$ (left) and $\text{Mo}_{132}\text{-HCO}_2$ (center and middle). The right pore has been closed with guanidinium counterions. Molybdenum polyhedra in ice blue, oxygen in red, nitrogen in blue, carbon in grey and hydrogen in white (Color figure online)

generated configuration, solvent water molecules and counterions (Na^+ in the case of $\text{Mo}_{132}\text{-SO}_4$ and guanidinium cations in the case of $\text{Mo}_{132}\text{-HCO}_2$) were allowed to diffuse freely in the simulation box, while the geometry of the capsule including that of the normally flexible ligands was kept frozen. Assumed capsule rigidity causes the channel diameters to be too small to allow the entrance of hydrated Na^+ counterions into capsule $\text{Mo}_{132}\text{-SO}_4$, in contrast to the situation for the real $\text{Mo}_{132}\text{-SO}_4$ in solution. Thus, in our simulations $\text{Mo}_{132}\text{-SO}_4$ behaves in that respect as a closed capsule. However, when the sulfate ligands were substituted by formate ligands, the related enlarged channels allowed Na^+ ions to pass through. Therefore, plugs had to be present in $\text{Mo}_{132}\text{-HCO}_2$ to avoid cation uptake. The guanidinium ions were chosen as the plugs to avoid the entrance of the counterions in the inner POM cavity. Consequently, 20 guanidinium ions were placed in the pores and fixed to the Mo_{132} structure (Fig. 7.7).

Initially, counterions were distributed randomly around the nanocapsule, which was filled and surrounded by water. In the internal cavity of the POM 172 water molecules were placed; 72 waters fulfilling the molybdenum coordination sphere of the pentagonal $\text{Mo}(\text{Mo})_5$ units and a structureless 100 H_2O cluster. Following a standard protocol [24], a large number of configurations were collected through the MD trajectory and analyzed. Then, the radial (RDF) and spatial (SDF) distribution functions of the centers of the capsule-oxygen water atoms were computed.

For the $\text{Mo}_{132}\text{-SO}_4$ capsule, the computed RDFs showed three significant peaks and a residual inner peak, pointing a three-shell structure. A very nice agreement of the main features with the experimentally determined distances between the capsule center and the capsule–water oxygen atoms was found (Table 7.1). As the RDF in Fig. 7.8 reveal, there are three main peaks in the RDF located at 4.4, 6.7, and 7.4 Å. This result means that although during the simulations water molecules can diffuse inside the capsule continuously, a layered shell type structure is obtained. In other words, the dynamic structure matches the static experimental data reasonably well.

When the space distribution function (SDF) was plotted it revealed a clear polyhedral-type structure. The highest probability regions of finding water molecules inside the capsule (red areas in Fig. 7.9) correspond to water ligands coordinated to the metal atoms of the 12 pentagonal moieties. In total there are 72

Table 7.1 Experimental versus computed distances from the center of the capsule (in Å) to oxygen atoms of water molecules

	Mo ₁₃₂ -SO ₄		Mo ₁₃₂ -HCO ₂	
	Experimental	Calculated	Experimental	Calculated
Peak 1	3.84–4.04	4.4	4.02–4.08	4.4
Peak 2	6.51–6.83	6.7	6.62–6.72	6.9
Peak 3	7.56–7.88	7.4	7.66–7.78	7.9
Peak 4	–	–	8.52–8.79	8.8

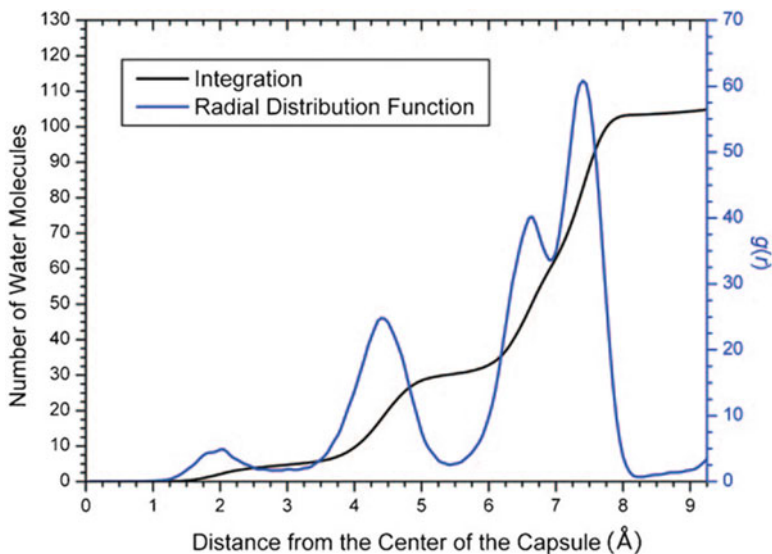


Fig. 7.8 Radial distribution function from the center of the Mo₁₃₂-SO₄ capsule (*blue*) and the integration of the number of water molecules (*black*) [24] (Color figure online)

water molecules coordinated to the molybdenum. These ligand type water molecules remain, as expected, fixed at their locations of maximum probability. The RDF peak of this shell is located at about 10 Å from the center of the capsule but it is not shown in Fig. 7.8. The two shells at 7.4 and 6.7 Å form the same polyhedra as were found crystallographically, that is, a distorted (H₂O)₆₀ rhombicosidodecahedron and a (H₂O)₂₀ dodecahedron (Fig. 7.10).

In these nodes, the grey isosurface extends towards the edges that connect the vertices of the polyhedra, thus suggesting that water molecules in these shells are rather mobile and can exchange their locations. The exchange seems to occur through the edges and not through the faces of the polyhedra. This phenomenon was of course not observed in the crystals since they were measured at low temperatures.

Visual inspection of the trajectories indicates a stepwise motion with molecules frequently switching between the shells and in a synchronous way, between the

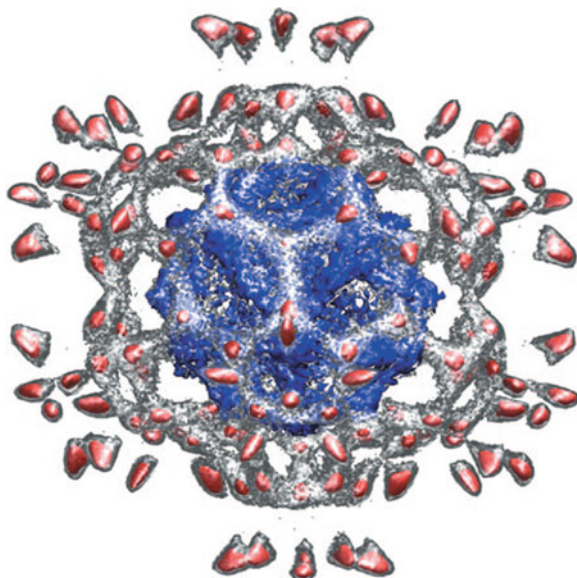


Fig. 7.9 Isosurfaces of the spatial distribution function (*SDF*) for water oxygen atoms inside capsule $\text{Mo}_{132}\text{-SO}_4$. Two isosurfaces are shown: one colored *red* and the other colored either *gray-transparent* or *blue*, for clarity. The *red* isosurface corresponds to the regions of maximum probability of finding water oxygen atoms. We found 152 *red* nodes, which are located precisely at the same positions that we found in the X-ray structure: the dodecahedral *second layer* (20), the distorted rhombicosidodecahedron *third layer* (60), and the twelve centered-pentagons of the coordinated water molecules (72). The *gray-transparent* isosurface corresponds to a probability one order of magnitude lower than the *red* isosurface, and indicates exchange between the second and third layer. The *blue* isosurface (same *SDF* value as the *gray* one) shows the inner shell [24] (Color figure online)

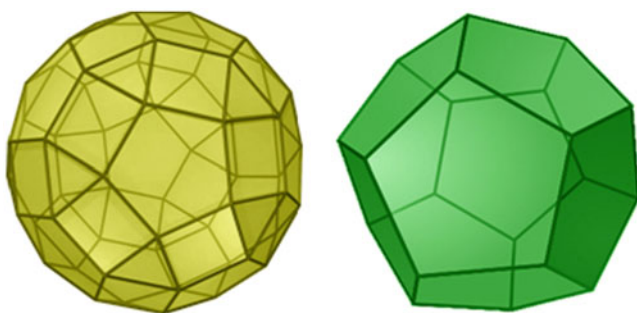


Fig. 7.10 Rhombicosidodecahedron and dodecahedron polyhedras

peaks 2 and 3. The result corresponds especially to the non-negligible overlap between these peaks at 6.7 and 7.4 Å in the RDF in Fig. 7.8. Furthermore, the blue isosurface depicted in Fig. 7.9 is not connected with the second and third shells, as a result of the zero overlap between the corresponding peaks in the RDF. In this inner

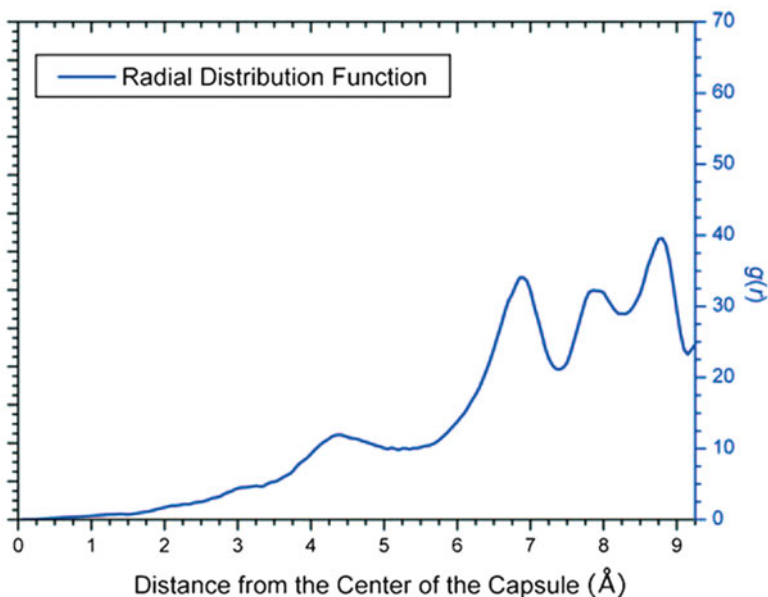


Fig. 7.11 Radial distribution function from the center of the $\text{Mo}_{132}\text{-HCO}_2$ capsule [24]

layer, water molecules are much more mobile than those in the two outer layers, and consequently, is rather difficult to determine regions of high probability. But a dodecahedron $(\text{H}_2\text{O})_{16}$ and a tetrahedron $(\text{H}_2\text{O})_4$ lay in the core of the $(\text{H}_2\text{O})_{100}$ water cluster in our simulations. Although water behaves more liquid-like in this inner part, the polyhedral shape of the SDF blue isosurface suggests a constrained motion imposed by the symmetry of the upper layers in contact with the capsule surface (Fig. 7.10).

When a model for $\text{Mo}_{132}\text{-HCO}_2$ was considered, a lower temperature (198 K) had to be used since at room temperature the water cluster was structureless. The RDF plot, as shown in Fig. 7.11, displayed a rather different behavior. Instead of the three main peaks found for $\text{Mo}_{132}\text{-SO}_4$ a fourth peak appeared at 8.8 Å, in good agreement with the experiment (Table 7.1). But the additional space available inside the capsule allowed water molecules to be more mobile in agreement, in line with the existence of a lower density water 100 cluster. Water mobility and exchange between layers is clearly indicated by the strongly overlapped RDF peaks. Contrary to the case of $\text{Mo}_{132}\text{-SO}_4$, the SDF function for $\text{Mo}_{132}\text{-HCO}_2$ did not reveal any clear image since the diffusion during the simulation was rather important because the large cavity, the lower negative charge of the capsule, and the occurrence of the formate ligands.

7.5 Conclusions

The results presented above demonstrate that classical molecular dynamic simulations are attractive for studying water clusters encapsulated in polyoxometalate nanocapsules. The structures determined experimentally, $(\text{H}_2\text{O})_{12}$ in Mo_{57}V_6 and $(\text{H}_2\text{O})_{100}$ in Mo_{132} were fully confirmed computationally. In the later case, the number and location of the RDF peaks agree perfectly well with the shell structure. Moreover, the polyhedral shape of $(\text{H}_2\text{O})_{100}$ water cluster and the effect of the inner ligands in the generation of high density ($\text{Mo}_{132}\text{-SO}_4$) and low density ($\text{Mo}_{132}\text{-HCO}_2$) water clusters have been demonstrated. In the case of $\text{Mo}_{132}\text{-SO}_4$ and $\text{Mo}_{132}\text{-HCO}_2$, our simulations showed that encapsulated water molecules self-assemble dynamically in shell structures, which are strongly affected by a slightly increasing volume of the capsule. Water in the cavities is structurally closer to ice water than to liquid water, as is unable to diffuse as liquid water does. Further studies on related systems are currently under development in our laboratory.

Acknowledgements Research supported by the MICINN of Spain (CTQ2008-06549-C02-02/BQU and Consolider Ingenio 2010 CSD2006-0003), the Generalitat de Catalunya (2009SGR-00462 and XRQTC) and the ICIQ Foundation. Computer resources provided by the BSC-CNS. P.M. thanks the Generalitat de Catalunya for a FI fellowship (2009FIC00026). We thank Prof. Achim Müller (University of Bielefeld) for inspiring discussions.

References

1. Whitesides GM, Ismagilov RF (1999) *Science* 284(5411):89–92
2. Ball P (2001) *Cell Mol Biol* 47(5):717–720
3. Stumpff-Kane AW, Maksimiak K, Lee MS, Feig M (2008) *Protein Struct Funct Bioinformatics* 70(4):1345–1356
4. Benson SW, Siebert ED (1992) *J Am Chem Soc* 114(11):4269–4276
5. Bondybey VE, Beyer MK (2002) *Int Rev Phys Chem* 21(2):277–306
6. Bukowski R, Szalewicz K, Groenenboom GC, van der Avoird A (2007) *Science* 315(5816):1249–1252
7. Keutsch FN, Saykally RJ (2001) *Proc Natl Acad Sci USA* 98(19):10533–10540
8. Mishima O, Stanley HE (1998) *Nature* 396(6709):329–335
9. Robertson WH, Diken EG, Johnson MA (2003) *Science* 301(5631):320–321
10. Robinson GW, Cho CH (1999) *Biophys J* 77(6):3311–3318
11. Smith JD, Cappa CD, Messer BM, Cohen RC, Saykally RJ (2004) *Science* 306:851
12. Stanley HE, Buldyrev SV, Giovambattista N, La Nave E, Scala A, Sciortino F, Starr FW (2002) *Physica A (Amsterdam)* 306(1–4):230–242
13. Vedamuthu M, Singh S, Robinson GW (1994) *J Phys Chem* 98(9):2222–2230
14. Wernet P, Nordlund D, Bergmann U, Cavalleri M, Odelius M, Ogasawara H, Naslund LA, Hirsch TK, Ojamae L, Glatzel P, Pettersson LGM, Nilsson A (2004) *Science* 304(5673):995–999
15. Zubavicus Y, Grunze M (2004) *Science* 304(5673):974–976
16. Wiggins PM (1990) *Microbiol Rev* 54(4):432–449
17. Wiggins PM (2001) *Cell Mol Biol* 47(5):735–744

18. Britz DA, Khlobystov AN, Porfyrakis K, Ardavan A, Briggs GAD (2005) *Chem Commun* 1:37–39
19. Preyssler C (1970) *Bulletin De La Societe Chimique De France* 1:30
20. Muller A, Krickemeyer E, Dillinger S, Bogge H, Plass W, Proust A, Dloczik L, Menke C, Meyer J, Rohlfing R (1994) *Zeitschrift Fur Anorganische Und Allgemeine Chemie* 620(4):599–619
21. Muller A, Sarkar S, Shah SQN, Bogge H, Schmidtman M, Sarkar S, Kogerler P, Hauptfleisch B, Trautwein AX, Schunemann V (1999) *Angew Chem Int Ed* 38(21):3238–3241
22. Muller A, Fedin VP, Kuhlmann C, Bogge H, Schmidtman M (1999) *Chem Commun* 10: 927–928
23. Muller A, Das SK, Talismanov S, Roy S, Beckmann E, Bogge H, Schmidtman M, Merca A, Berkle A, Allouche L, Zhou YS, Zhang LJ (2003) *Angew Chem Int Ed* 42(41):5039–5044
24. Mitra T, Miró P, Tomsa AR, Merca A, Bögge H, Ávalos JB, Poblet JM, Bo C, Müller A (2009) *Chem A Eur J* 15(8):1844–1852
25. Müller A, Krickemeyer E, Bögge H, Schmidtman M, Botar B, Talismanova MO (2003) *Angew Chem Int Ed* 42(18):2085–2090
26. Müller A, Bögge H, Diemann E (2003) *Inorg Chem Commun* 6(3):329
27. Smith W, Forester TR (1996) *J Mol Graph* 14(3):136–141
28. Smith W, Yong CW, Rodger PM (2002) *Mol Simul* 28(5):385–471
29. Smith W (2006) *Mol Simul* 32(12–13):933–1121
30. López X, Nieto-Draghi C, Bo C, Ávalos JB, Poblet JM (2005) *J Phys Chem A* 109(6): 1216–1222
31. Leroy F, Miró P, Poblet JM, Bo C, Ávalos JB (2008) 112(29) 8591
32. Miró P, Poblet JM, Ávalos JB, Bo C (2009) *Can J Chem* 87(10):1296–1301
33. Rappe AK, Goddard WA (1991) *J Phys Chem* 95(8):3358–3363
34. Berendsen HJC, Grigera JR, Straatsma TP (1987) *J Phys Chem* 91(24):6269–6271
35. Lee SH, Rasaiah JC (1996) *J Phys Chem* 100(4):1420–1425
36. Lutz HD, Nagel R, Mason SA, Müller A, Bögge H, Krickemeyer E (2002) *J Solid State Chem* 165(1):199–205

Chapter 8

Organometallic Dendrimers: Design, Redox Properties and Catalytic Functions

Didier Astruc, Catiá Ornelas, and Jaime Ruiz

Abstract The divergent synthesis, properties and functions of dendrimers terminated by metallocenyl redox groups are briefly illustrated in this micro-review, with emphasis on molecular electronics, sensing with regenerable derivatized Pt electrodes and efficient catalysis with dendrimer-stabilized Pd nanoparticles.

8.1 Introduction

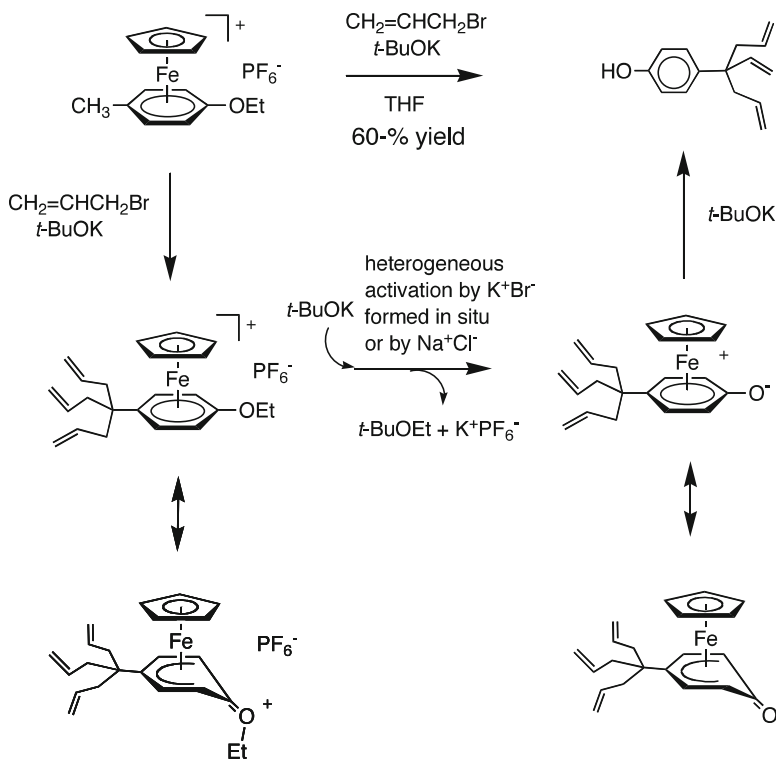
Dendrimers have attracted considerable attention since their discovery three decades ago [1–43]. Potential applications involve supramolecular properties [11] in the fields of nanomedicine [29], materials science [4–13] and catalysis [16, 30, 38–43]. Since the late 1980s, we have focused our attention on metallodendrimers [14, 44] with the aim to develop knowledge concerning redox properties that are useful for redox sensing and catalysis as well as for the design of molecular batteries. In this microreview article, we will illustrate the design of our recent series of metallodendrimers and some of their properties and applications.

8.2 The Complexes $[\text{FeCp}(\eta^6\text{-arene})][\text{PF}_6]$ as a Source of Dendritic Core, Dendrons and Dendrimers

In the complexes, $[\text{FeCp}(\eta^6\text{-arene})][\text{PF}_6]$, the arene ligand undergoes reactions resulting from “Umpolung” of the arene reactivity [45], i.e. the benzylic groups are easily deprotonated [46], the chloride arene substituent is easily substituted by

D. Astruc (✉) • C. Ornelas • J. Ruiz

Institut des Sciences Moléculaires, UMR CNRS N°5255, Université Bordeaux I,
351 Cours de la Liberation, 33405 Talence Cedex, France
e-mail: D.Astruc@ism.u-bordeaux1.fr



Scheme 8.1 Mechanism of the one-pot eight-step synthesis of the phenoltriallyl dendron

nucleophiles such as alkoxyde [45] and the aryl ethers are heterolytically cleaved by *t*-BuOK in THF below room temperature in the presence of an inorganic salt such as KBr [47]. Moreover, these organometallic cations can be reduced to 19-electron Fe^I complexes that have a specific radical- and electron-transfer reactivity [48]. The removal of the arene ligand from the complex can easily proceed either via the 19-electron complexes or using visible photolysis of the 18-electron cations [49].

Using these properties, dendritic cores are quantitatively synthesized under ambient conditions from the mesitylene complex, whereas a simple tripodal dendron is prepared in a one-pot eight-step synthesis from the *p*-ethoxytoluene complex (Scheme 8.1). With a nona-allyl arene core and the “phenoltriallyl” brick, dendrimers containing 3^{*n*+2} terminal allyl tethers (*n* = generation number) could be constructed [15] using the 1 → 3 C connectivity pioneered by Newkome with arborols [50] by a series of hydrosilylation-Williamson reactions. The hydrosilylation was carried out using chloromethyldimethylsilane [51] and Karstedt catalyst at 40°C whereas the Williamson step was performed between the chloromethyl-terminated dendrimers and phenoltriallyl using a catalytic amount of NaI and K₂CO₃ in DMF at 80°C. Each step was checked by ¹H, ¹³C and ²⁹Si NMR and gave virtually pure dendrimers at the accuracy of NMR. MALDI TOF mass spectra show, however, that if the molecular peak largely predominates for

the second generation 81-allyl dendrimer, the defects predominate in the spectrum of the 3rd generation 243-allyl dendrimer and the molecular peak is not even seen in that of the 4th generation 729-allyl dendrimer which shows massifs near the molecular peak (Scheme 8.2).

The dendrimers were characterized by size exclusion chromatography until generation five showing a polydispersity between 1.00 and 1.02, atomic force microscopy showing the progression of the height of the monolayer from the first to the 9th generation and transmission electron microscopy of the polyiodo derivative of the last generation. Although the number of defects becomes larger and larger as the generation number increases, it may be estimated that the last generation reaches a number of terminal tethers of the order of 10^5 . Beyond generation 5 (theoretical number: $3^7 = 2187$ terminal tethers), it is compulsory that further dendritic construction reactions occur inside the dendrimers interior because the small termini must back fold toward the center in order to avoid the bulk at the periphery and fill the interior cavities. Thus the dendrimer construction becomes limited by the volume rather than by the surface. The reactions become slower and slower and the yields are lower as the generation number increases beyond generation 5.

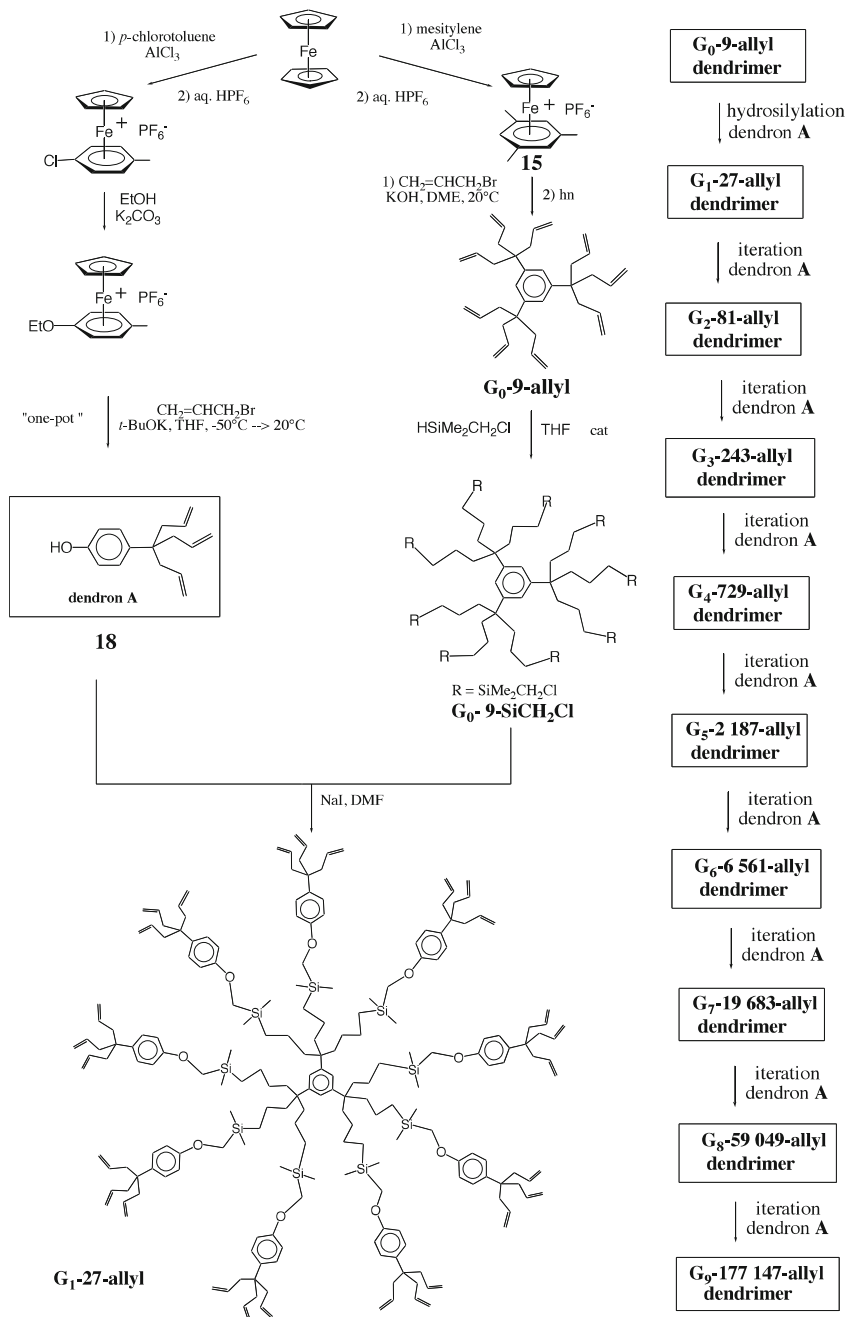
A challenge is the one-pot synthesis of dendrimers using such a strategy [52]. This was shown to be possible if chlorodimethylsilane [53] is used instead of the chloromethyldimethylsilane in the construction scheme. Indeed, the terminal Si-Cl bonds formed at the periphery of the dendrimer subsequent to hydrosilylation are much more reactive in the Williamson reaction with phenolates than the chloromethylsilyl termini, which permits the one-pot synthesis of up to the 243-allyl G_3 dendrimer. The Si-phenolate link is less robust than the Si-CH₂-phenolate link, but stable enough for extensive characterization. Such fragile dendrimers might be useful for applications requiring the decomposition of the dendrimer interior after using it as a template, for instance in materials chemistry (Scheme 8.3) [52].

8.3 Ferrocenyl Dendrimers

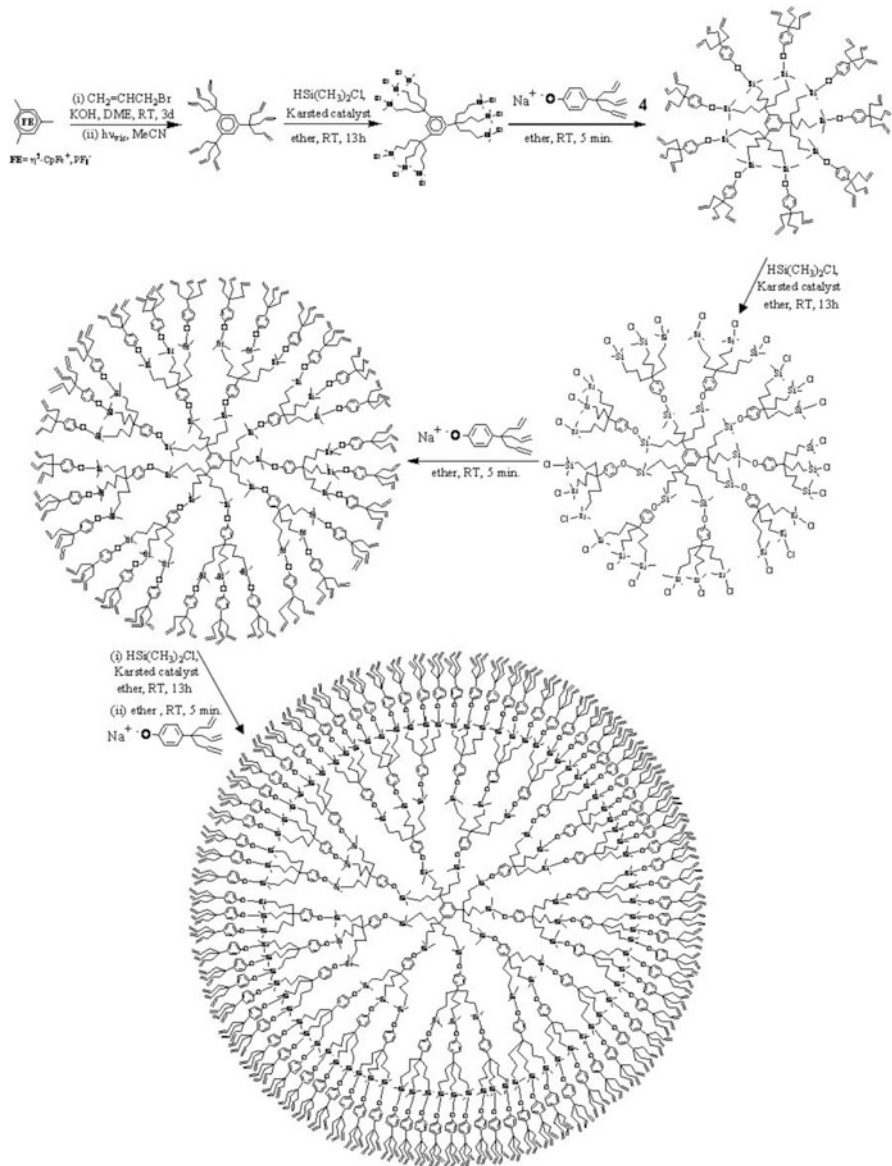
The first ferrocenyl dendrimers designed for function were synthesized by reaction of amine-terminated dendrimers with ferrocenoyl chloride, which yielded amidoferrocenyl dendrimers that were redox exo-receptors of oxo-anions [54]. It was subsequently found that silylferrocenylation of polyolefin dendrimers yielded polysilylferrocenyl dendrimers (Scheme 8.4).

Likewise, the silylferrocenylation of the “phenoltriallyl” brick yielded triferrocenyl dendrons that could be condensed onto a polyhalogeno core to form polyferrocenyl dendrimers (Scheme 8.5) [55].

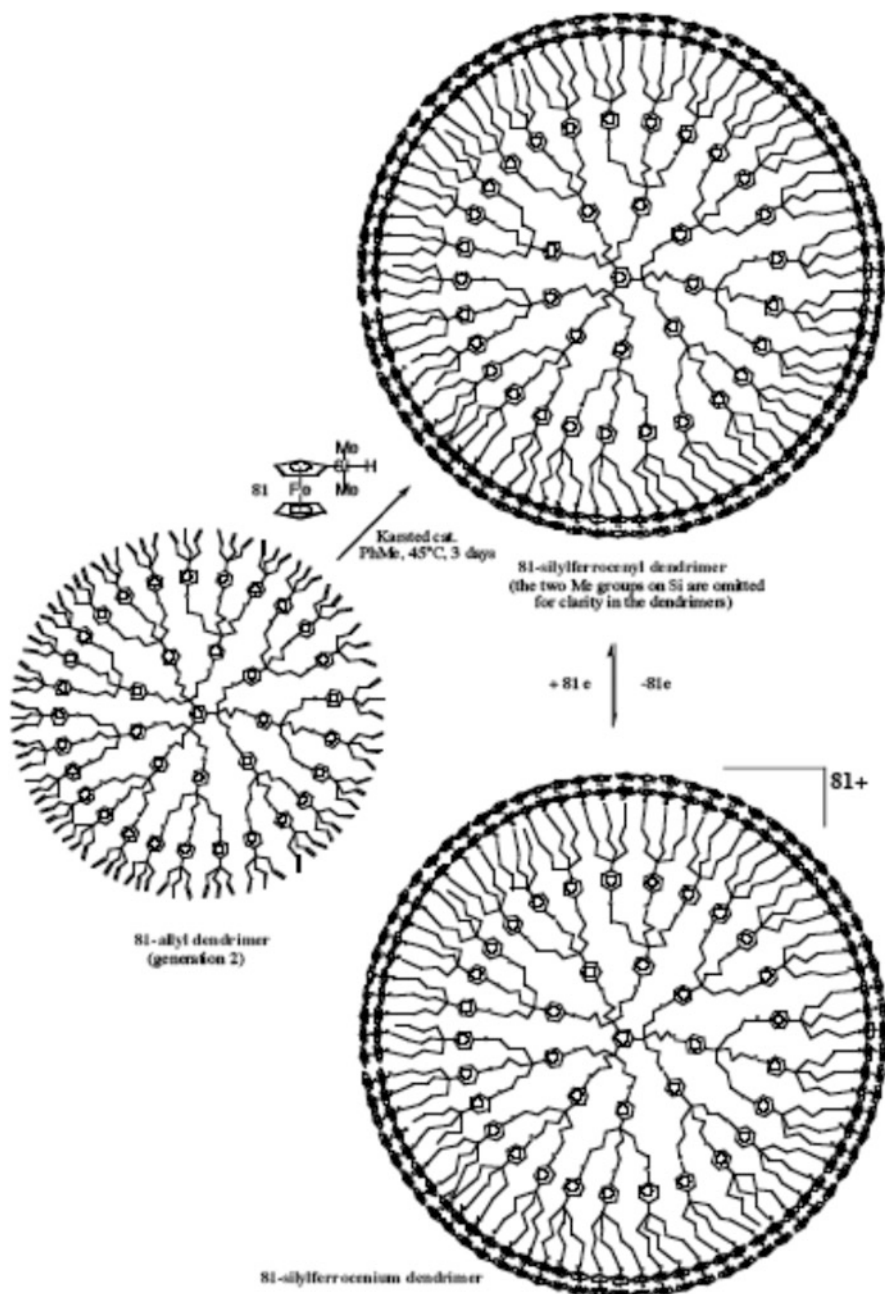
With gold-nanoparticle-cored dendrimers, it was found that the silyl group was an excellent alternative to the amido group when it was attached to the ferrocenyl termini for the recognition of oxo-anions including ATP [56]. The factors involved in the redox recognition are the electrostatic attraction between the anion and the ferrocenium cation upon anodic oxidation and the supramolecular bonding between the amido group (hydrogen bonding) of the silyl group (Si hypervalence).



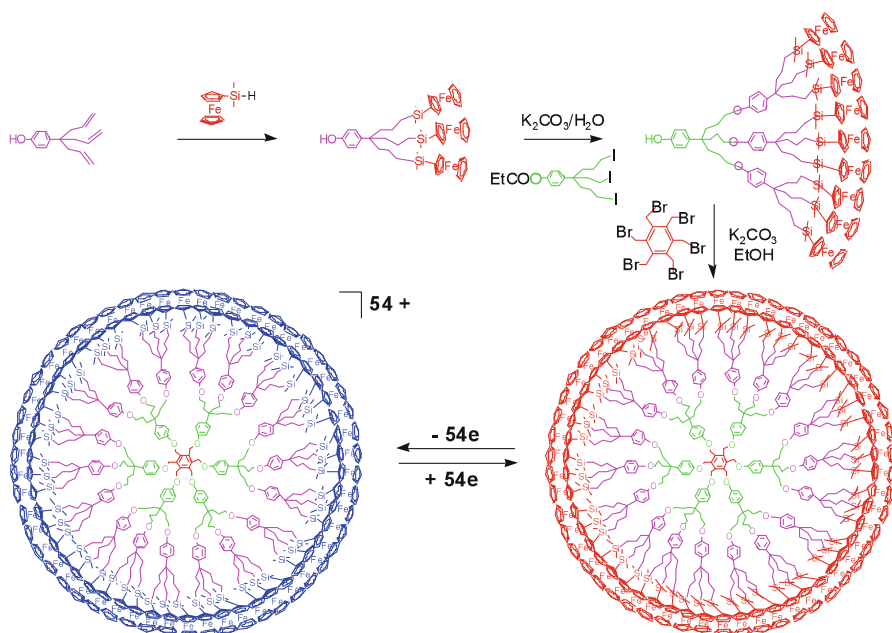
Scheme 8.2 Construction of giant dendrimers starting from ferrocene with 3^{n+2} terminal tethers (n = generation number) until G₉ (theoretical number of 3^{11} terminal tethers). Each dendrimer along the construction was characterized by ¹H, ¹³C and ²⁹Si NMR (till G₉), MALDI TOF mass spectrometry (till G₄), SEC (PI = 1.00 to 1.02 till G₅), TEM and AFM (till G₉) showing the steady size increase



Scheme 8.3 One-pot synthesis of polyolefin dendrimers till G_3 ($3^5 = 243$ terminal allyl groups) using the silane HSiMe_2Cl



Scheme 8.4 Ferrocenyl-silylation of the “phenoltriallyl” dendron for the construction of ferrocenyl-terminated dendrimers

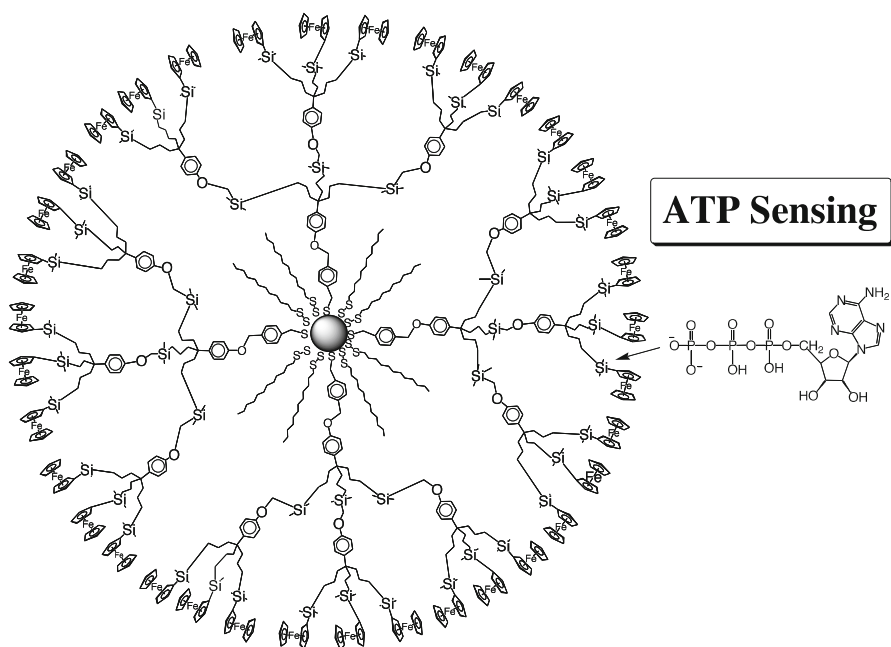


Scheme 8.5 Ferrocenylsilylation of the 81-allyl G_2 dendrimer for the synthesis of ferrocenyl-terminated dendrimers

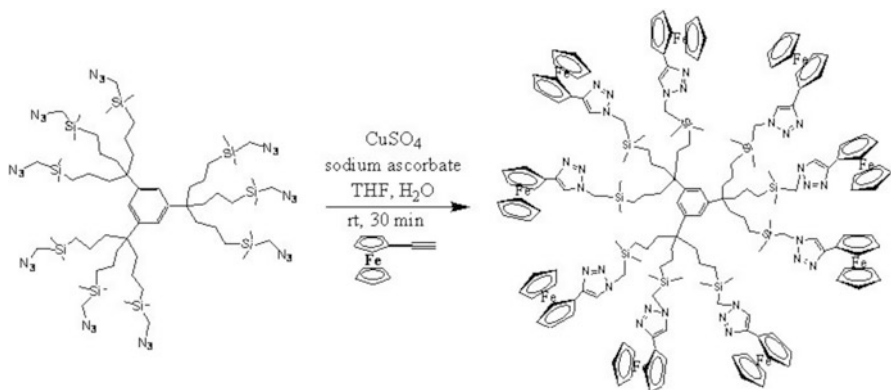
The amidoferrocenyl or silylferrocenyl monomers do not show any effect, however. Therefore, the dendrimer topology is important for recognition of oxo-anions. The appropriate encapsulation of the anionic host between the dendritic tethers is a key factor that very much increases the interaction between the functional ferrocenyl termini and the guest (Scheme 8.6).

8.4 Engineering the Dendrimer Family with Peripheral Ferrocenyltriazole Ligands: “Click” Dendrimers and Metallodendrimers for Oxo-Anion and Transition-Metal Cation Sensing

The 1,2,3-triazole is an ideal choice for the interaction with many substrates that have Brönsted or Lewis acid properties including transition metals and their complexes. Thus the encapsulation of such guests should prove feasible by introducing such triazole groups on the dendrimer tethers. The 1,2,3-triazole group is readily formed by “Click” chemistry recently reported by Sharpless to catalyze with Cu^{I} the regioselective Huisgens reaction between azido derivatives and terminal alkynes [57]. We used the dendrimer family that was constructed as indicated above and substituted the terminal halogeno group by azido upon reaction with NaN_3 . These

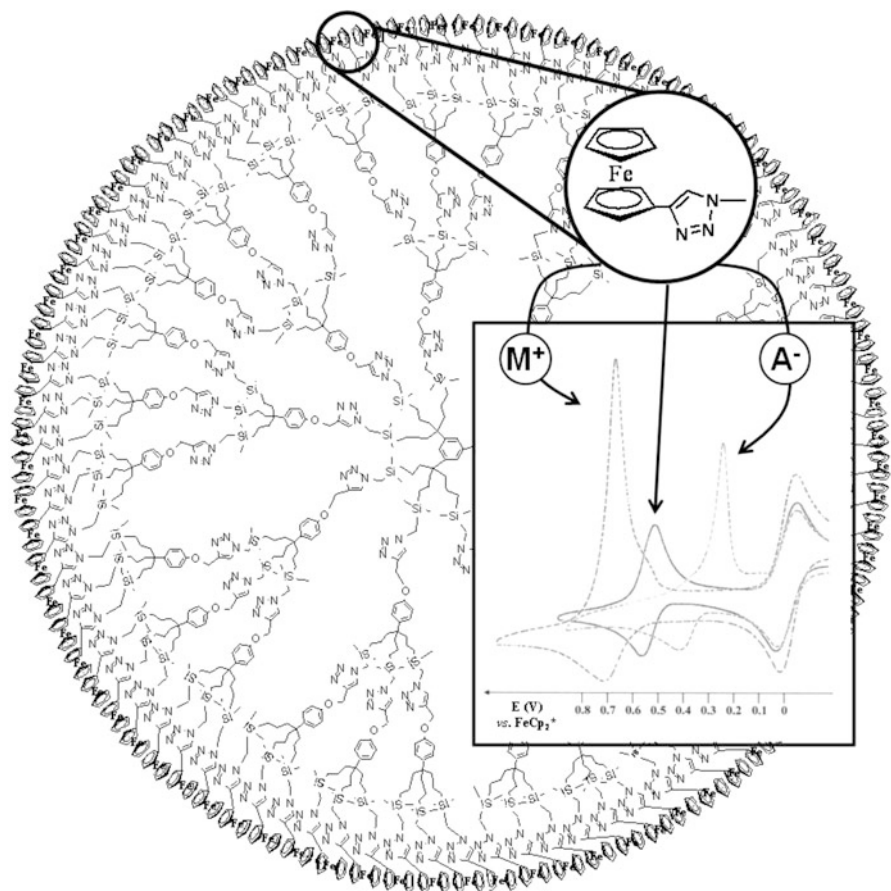


Scheme 8.6 Gold-nanoparticle-cored dendrimer terminated by ferrocenylsilyl group that recognize and sense oxo-anions such as H_2PO_4^- and ATP



Scheme 8.7 Synthesis of a “click” ferrocenyl dendrimer (G0)

azido-terminated dendrimers were engaged in reactions with ferrocenyl acetylene in order to locate the redox sensor directly on the triazole ring for adequate sensing of the interaction of guests with the triazole heterocycle by perturbation of the redox potential of the ferrocenyl system (Scheme 8.7).



Scheme 8.8 Second-generation “click” ferrocenyl dendrimer (81 terminal ferrocenyltriazolyl groups) that recognizes both oxo-anions including ATP and transition-metal dications (Cu^{I} , Cu^{II} , Pd^{II} , Pt^{II}) with positive dendritic effect (i.e. recognition, characterized by the shift of potential of the ferrocenyl CV wave, works all the better as the dendrimer generation is higher)

Ferrocenyl terminated dendrimers are known as very good sensors of oxo-anions with positive dendritic effects, i.e. the magnitude of the recognition effect increases together with generation number, because the dendrimer topology of higher generations involves narrower channels for a better interaction with the dendritic site on the tethers. Thus oxo-anions including ATP, a DNA fragment, are well recognized by the “Click” ferrocenyltriazolyl dendrimers. The additional electron density brought by the oxo-anions makes the ferrocenyl oxidation easier, i.e. at less positive oxidation potentials. On the other hand, the interaction with acetonitrile complexes of several transition metals (Cu^{I} , Cu^{II} , Pd^{II} , Pt^{II}) withdraws electron density from the ferrocenyltriazolyl system, the ferrocenyl oxidation is rendered more difficult, and its wave is found at more positive potentials (Scheme 8.8) [58].

8.5 The Click Reaction as a Useful Iterative Method for Dendrimer Construction

In the preceding example, the “click” reaction was used for peripheral dendrimer functionalization. We then addressed the challenge of using the “click” reaction iteratively for divergent dendrimer construction. For this purpose, the “phenoltriallyl” brick used above was propargylated at the focal point before “click” reaction with an azido-terminated dendritic core as above. After the “click” reaction, the polyolefin dendrimer formed in which the number of terminal tethers has been multiplied by three is submitted to hydrosilylation with chloromethyldimethylsilane as in our classic dendrimer construction, then the terminal chloro groups are substituted by azido groups for further iteration of the “Click” reaction with the propargylated dendron (Scheme 8.9) [59].

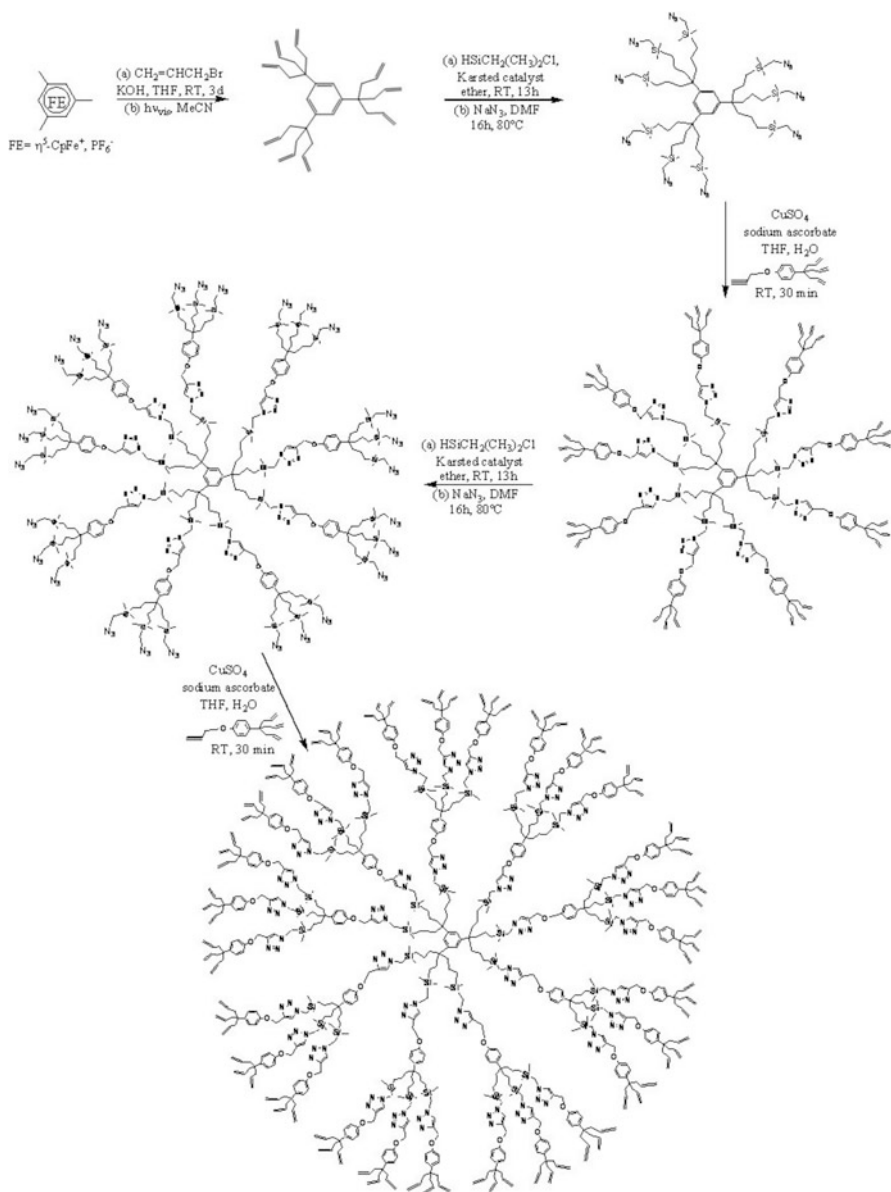
8.6 Dendrimers Containing Triazole Ligands and Ferrocenyl Termini as Useful Templates for Transition-Metal Ions and Transition-Metal Nanoparticles

The triazole ligands were introduced in these dendrimers in order to bind transition-metal cations before their reduction to metal (0) to form nanoparticles that are either stabilized inside the dendrimer or, if the dendrimer is too small, that are stabilized by the dendrimer without encapsulation. The ferrocenyl groups located at the dendrimer periphery just near the triazole rings allow titrating the metal cations that interact herewith. Palladium (II) was coordinated to the triazole ligands in the dendrimer interior using $\text{Pd}(\text{OAc})_2$, then reduced to Pd(0) using NaBH_4 or methanol. The coordination of $\text{Pd}(\text{OAc})_2$ onto the triazole ligands was monitored by cyclic voltammetry, showing the appearance of a new wave corresponding to the ferrocenyl groups attached to Pd(II)-coordinated triazoles.

The outcome was a one-to-one stoichiometry that allowed designing a given number of Pd atoms in the Pd nanoparticles if the dendrimer is large enough for nanoparticle encapsulation. This aspect is very important for applications (Scheme 8.10) [59].

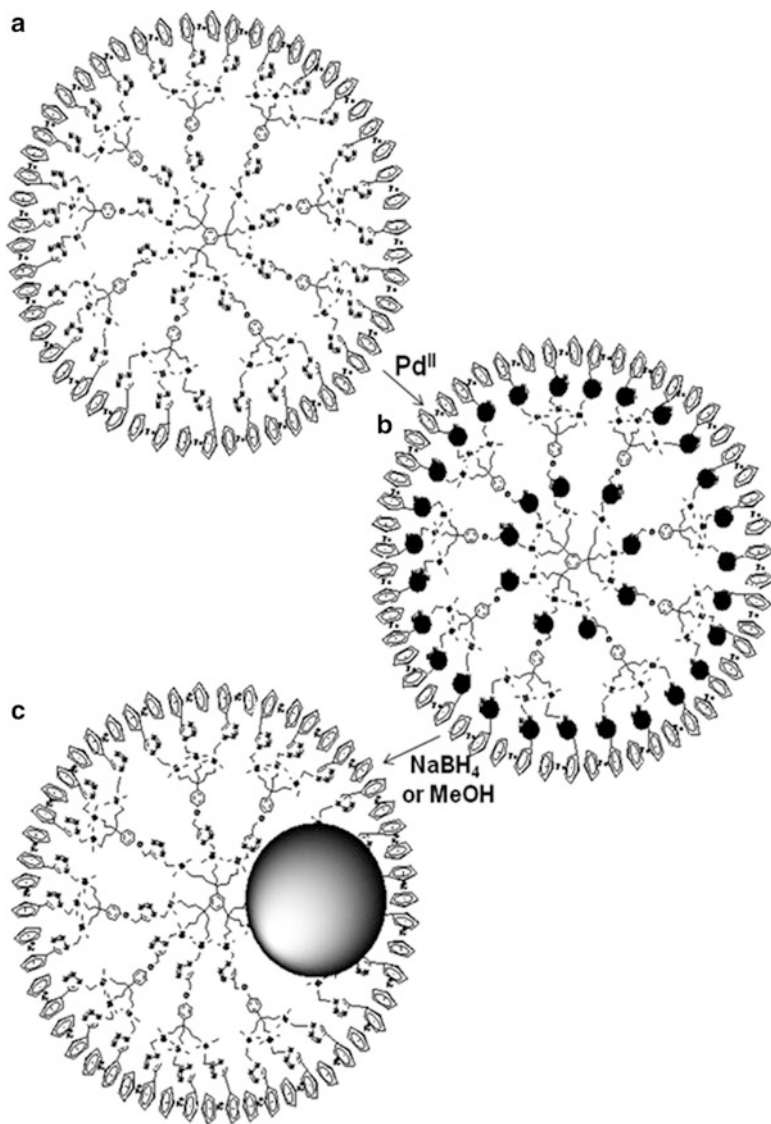
8.7 Application in Catalysis of “Click” Dendrimers and Dendrimer-Stabilized Nanoparticles

Nanoparticles are attracting increasing attention as catalysts from both the homogeneous- and heterogeneous catalysis communities, because they are “ligandless” catalysts avoiding toxic phosphines, and they show remarkable activities and selectivities [60].



Scheme 8.9 Iterative construction of a G_2 "click" dendrimer using a hydrosilylation-click-reaction sequence

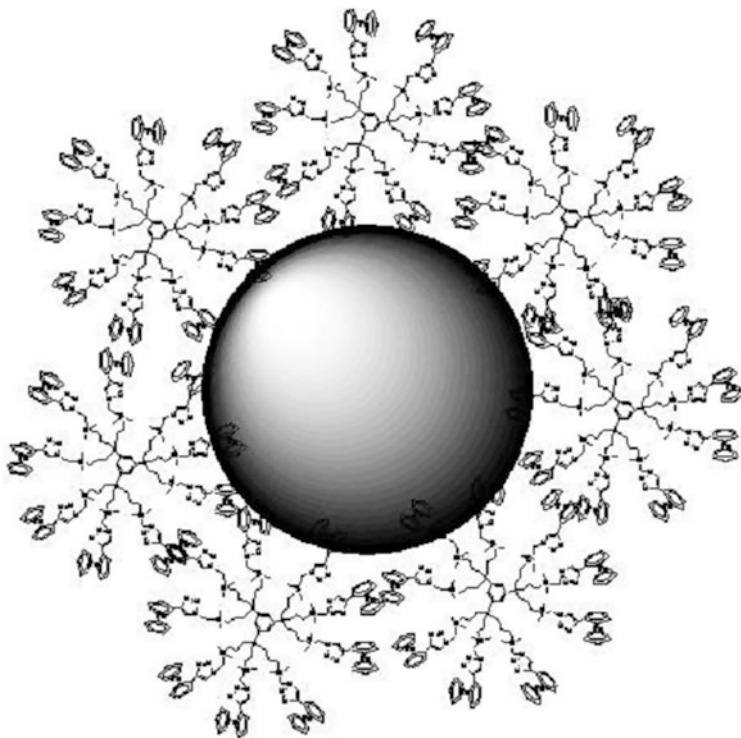
Nanoparticles can be stabilized by an extremely large variety of supports from organic to inorganic [61]. Polymers have been among the most popular supports for nanoparticle catalysts, [62] thus dendrimers also stabilize them, and dendrimer stabilization can proceed either by encapsulation [63] or, if the dendrimer is too



Scheme 8.10 Coordination of the triazole ligand by $\text{Pd}(\text{OAc})_2$ monitored by ferrocenyl redox sensing followed by Pd(II) reduction to dendrimer-encapsulated Pd(0) nanoparticles used further in catalysis. The variety of nanoparticle sizes obtained with this strategy is crucial for catalyst optimization and mechanistic investigation

small, by peripheral stabilization of the nanoparticle surrounded by a number of dendrimers [64]. Thus commercial polyamidoamine and polypropylene imine have been extensively used to stabilize nanoparticle catalysts [65].

Click-dendrimer-stabilized nanoparticles are a new family of dendrimer-stabilized nanoparticles that is particularly suitable for catalytic studies [59, 66].



Scheme 8.11 Pd nanoparticle surrounded and stabilized by several *small* G_0 dendrimers

Different Pd nanoparticles were synthesized from the dendrimers of generations 0 (9 tethers) to 2 (81 tethers). Transmission electron microscopy shows that generations G_1 and G_2 form dendrimer-encapsulated nanoparticles whose sizes correspond to Pd nanoparticles that contain the same number of Pd^0 atoms as that of Pd^{II} ions initially coordinated to the triazoles inside the dendrimer, whereas G_0 is too small to encapsulate the nanoparticle formed. In this case, the nanoparticle is surrounded by a number of dendrimers that provide stabilization (Scheme 8.11).

The collection of different nanoparticles having different designed sizes is crucial to the study of the mechanisms in nanoparticle catalysis. These “click” dendrimer-stabilized nanoparticles are efficient catalysts for selective olefin hydrogenation under ambient conditions, and the turnover frequencies, turnover numbers and yields depend on the nanoparticle size. The smallest nanoparticles (from G_1) are the most active ones, in agreement with a classic hydrogenation mechanism entirely proceeding at the nanoparticle surface [66]. On the other hand, the turnover numbers, turnover frequencies and yields are independent on the type of nanoparticle stabilization and sizes of the nanoparticles for the Suzuki cross coupling reaction between chlorobenzene or bromobenzene and PhB(OH)_2 . Moreover, the

TON increases when the amount of nanoparticle catalyst is decreased or when the solution is diluted. The efficiency reaches 54% yield using 1 ppm Pd nanoparticles, i.e. the amount of nanoparticle catalyst is homeopathic. On the other hand, with high loading of catalyst, the yield is not quantitative, reaching only 70% at 1% Pd atom catalyst. These phenomena are taken into account by a leaching mechanism whereby one or two Pd atoms escape from the nanoparticle surface subsequent to the oxidative addition of the aryl halide onto the nanoparticle surface, then become extremely active in solution until it is quenched by the mother nanoparticle [66]. A similar mechanism had been proposed earlier by de Vries for the Heck reaction at high temperature (150–170°C) [67–69].

8.8 Conclusion and Outlook

The synthesis of high-generation dendrimers starting from organoiron activation provided suitable nanomaterials for molecular electronics, catalysis and sensing. In molecular electronics, the property of fast electron transfer (electrochemical reversibility) with metallocenyl-terminated dendrimers and the single wave of multi-ferrocenyl dendrimers in cyclic voltammetry leads to useful electrocatalytic and sensing properties. For sensing, the compared performances of the functional groups attached to the peripheral groups as exo-receptors offered flexibility of substrates using specific termini. Using the most recent “click” dendrimers with which the recognition can be achieved for both oxo-anions and transition-metal cations, redox recognition was very useful to determine the number of Pd^{II} ions coordinated into the dendrimer on the triazole ligands. The precise sizes of Pd nanoparticles designed in this way led to delineation of mechanistic experiments and catalyst optimization that significantly contribute to the knowledge and performances of Pd nanoparticle catalysis. This approach of dendrimer catalysis is complementary to the one introducing inorganic or organometallic catalysts at the core or periphery of dendrimers that was more classic and involved leaching and limited possibilities of catalyst recovery [70]. Studies are ongoing along this line to use suitable dendrimers for efficient “Green” catalysis [71].

Acknowledgements The valuable efforts and contributions of students and colleagues cited in the references to the subject of this micro-review and financial assistance from the Institut Universitaire de France (IUF), the Université Bordeaux I, the Centre National de la Recherche Scientifique (CNRS) and the Agence Nationale de la Recherche (ANR) are gratefully acknowledged.

References

1. Newkome GR, Yao Z, Baker GR, Gupta VK (1985) Micelles. *J Org Chem* 50:2003–2004
2. Tomalia DA, Naylor AM, Goddard WA III (1990) *Angew Chem Int* 29:138–175
3. Jansen JFGA, de Brabander-van den Berg EMM, Meijer EW (1999) *Science* 266:1226

4. (a) Newkome GR, Moorefield CN, Vögtle F (2001) *Dendrimers and dendrons. Concepts, syntheses, applications*. Wiley, Weinheim; (b) Newkome GR (ed) (1994, 1995, 1996, 1999, 2002) *Advances in dendritic molecules*, vols 1, 2, 3, 4, 5. JAI Press, Greenwich
5. Tomalia DA, Fréchet JMJ (eds) (2003) *Dendrimers and other dendritic polymers*. Wiley, Amsterdam
6. (a) Vögtle F, Richardt G, Werner N (2007) *Dendritische Moleküle – Konzepte, Synthesen, Eigenschaften, Anwendungen*. B. G. Teubner-Verlag, Stuttgart; (b) Vögtle F (ed) (1998, 2000, 2001) *Dendrimer I, II and III*. Springer, Berlin
7. (a) Newkome GR, Moorefield CN (1992) *Aldrichim Acta* 25:31; (b) Newkome GR (1998) *Pure Appl Chem* 70:2337
8. (a) Tomalia DA, Dupont Durst H (1993) In: Weber E (ed) *Topics Curr Chem, Supramolecular chemistry, directed synthesis and molecular recognition*. vol 165. Springer, Berlin, 193; (b) Tomalia DA (2005) *Mater Today* 34
9. Balzani V, Campagna S, Denti G, Juris A, Serroni S, Venturi M (1998) *Acc Chem Res* 31:26
10. Moore JS (1997) *Acc Chem Res* 30:402
11. Zeng F, Zimmermann SC (1997) *Chem Rev* 97:1681–1712
12. Bauer RE, Grimsdale AC, Müllen K (2005) *Top Curr Chem* 245:253–286
13. Percec V (1995) *Pure Appl Chem* 67:2031–2038
14. (a) Ardoin, N, Astruc, D (1995) *Bull Soc Chim Fr* 132:875–909; (b) Astruc D (1996) *C. R. Acad. Sci* 322: Sér. II b, 757–766
15. Matthews OA, Shipway AN, Stoddart JF (1998) *Prog Polym Sci* 23:1–56
16. Newkome GR, He E, Moorefield CN (1999) *Chem Rev* 99:1689–1746
17. Bosman AW, Janssen HM, Meijer EW (1999) *Chem Rev* 99:1665–1688
18. (a) Hawker C, Fréchet JMJ (1990) *Chem Commun* 1010–1011; (1990) *J Am Chem Soc* 112:7638–7643; (b) Miller TM, Neeman TX (1990) *Mater Chem* 2:346–350
19. Fréchet JMJ (1994) *Science* 263:1710–1715
20. Fréchet JMJ (1995) *Science* 269:1080–1082
21. Hecht S, Fréchet JMJ (2001) *Angew Chem Int Ed Engl* 40:74–77
22. Grayson SM, Fréchet JMJ (2001) *Chem Rev* 101:3819–3867
23. Fréchet JMJ (1999) *Pure Appl Chem* A33:1399–1407
24. Issberner J, Moors R, Vögtle F (1994) *Angew Chem Int Ed* 33:2413–2420; Fischer M, Vögtle F (1999) *Angew Chem Int Ed* 38:884–890
25. Friedhofen J, Vögtle F (2006) *New J Chem* 30:32–43
26. Chow H-F, Mong K-K, Nongrum MF, Wan C-W (1998) *Tetrahedron* 54:8543–8660
27. Gorman C (1998) *Adv Mat* 10:295–309
28. Reviews on phosphorus- and silicon-based dendrimers: (a) Gudat D (1997) *Angew Chem Int Ed Engl* 36:1951–1958; (b) Caminade A-M, Majoral J-P (1999) *Chem Rev* 99:845–863
29. Astruc D (2003) *Pure Appl Chem* 75:461–481
30. Astruc D (ed) (2003) *Dendrimers and nanoscience* C. R. Chimie 6
31. (a) Tomalia DA (1994) *Adv Mat* 6:529–539; (b) Tomalia DA, Dvornic PR (1994) *Nature* 372:617–618
32. Tomalia DA (2005) *Mater Today* 8:34–46
33. (a) Meltzer AD, Tirrel DA, Jones AA, Inglefield PT, Hedstrand DM, Tomalia DA (1992) *Macromolecules* 25:4541; (b) Mijovic J, Ristic S, Kenny J (2007) *Macromolecules* 40:5212
34. Chase PA, Gebbink RJ, Klein M, van Koten G (2004) *J Organomet Chem* 689:4016–4054
35. Schlüter AD, Rabe PJ (2000) *Angew Chem Int Ed Engl* 39:864
36. Flory PJ (1953) *Principles of polymer chemistry*. Cornell University Press, Ithaca
37. Voit BI (2003) *C R Chimie* 6:821–832
38. Oosterom GE, Reek JNH, Kamer PCJ, van Leeuwen PWNM (2001) *Angew Chem Int Ed* 40:1828–1849
39. Kreiter R, Kleij AW, Klein Gebbink RJM, van Koten G (2001) In: Vögtle F, Schalley CA (eds). *Dendrimers IV: metal coordination, self assembly, catalysis*, vol 217. *Top Curr Chem*, Springer, Berlin, 163

40. (a) Astruc D, Chardac F (2001) *Chem Rev* 101:2991–3024; (b) van Heerbeek R, Kamer PCJ, van Leeuwen PWNM, Reek JNH (2002) *Chem Rev* 102:3717–3756
41. Méry D, Astruc D (2006) *Coord Chem Rev* 250:1965–1979
42. Moorefield CN, Newkome GR (2007) *New J Chem* 31:1192–1217
43. Crooks RM, Zhao M, Sun L, Chechik V, Yeung LK (2001) *Acc Chem Res* 34:181–190
44. Scott RWJ, Wilson OM, Crooks RM (2005) *J Phys Chem B* 109:692–704
45. Moulines F, Astruc D (1988) *Angew Chem Int Ed Engl* 27:1347–1349
46. (a) Astruc D (1983) *Tetrahedron* 39:4027–4095; (b) Trujillo HA, Casado C, Ruiz J, Astruc, D (1999) *J Am Chem Soc* 121:5674–5686
47. Astruc D, Hamon J-R, Román E, Michaud P (1981) *J Am Chem Soc* 103:7502–7514
48. Sartor V, Djakovitch L, Fillaut J-L, Moulines F, Neveu F, Marvaud V, Guittard J, Blais J-C, Astruc D (1999) *J Am Chem Soc* 121:2929–2930
49. (a) Hamon J-R, Astruc D, Michaud P (1981) *J Am Chem Soc* 103:758–766; (b) Desbois M-H, Astruc D, Guillin J, Varret F, Trautwein AX, Villeneuve G (1989) *J Am Chem Soc* 111:5800–5809; (c) Lacoste M, Rabaa H, Astruc D, Le Beuze A, Saillard J-Y, Précigoux G, Courseille C, Ardoin N, Bowyer W (1989) *Organometallics* 8:2233–2242
50. (a) Catheline D, Astruc D (1983) *J Organometal Chem* 248:C9-C12; (b) Catheline D, Astruc D (1984) *Organometallics* 3:1094–1100; (d) Ruiz J, Astruc D (2008) *Inorg Chim Acta* 361:1–4
51. (a) Newkome GR, Yao Z, Baker GR, Gupta VK (1983) *J Org Chem* 50:2003; (b) Newkome GR (1998) *Pure Appl Chem* 70:2337; (c) Narayanan VV, Newkome GR (1998) *Top Curr Chem* 197:19
52. Krsda SW, Seyferth D (1998) *J Am Chem Soc* 120:3604
53. Ornelas C, Ruiz J, Astruc D (2006) *Org Lett* 8:2751
54. van der Made AW, van Leeuwen PWNM, Brandes RAC (1993) *Adv Mater* 5:466
55. (a) Valério C, Fillaut J-L, Ruiz J, Guittard J, Blais J-C, Astruc D (1997) *J. Am Chem Soc* 119:2588; (b) Ruiz J, Ruiz-Medel M-J, Daniel M-C, Blais J-C, Astruc D (2003) *Chem Commun* 464; (c) Daniel M-C, Ruiz J, Blais J-C, Daro N, Astruc D (2003) *Chemistry. Eur J* 9:4371; (d) Daniel M-C, Ruiz J, Astruc D (2003) *J Am Chem Soc* 125:1150; (e) Daniel M-C, Ba F, Ruiz J, Astruc D (2004) *Inorg Chem* 43:8649
56. (a) Nlate S, Ruiz J, Blais J-C, Astruc D (2000) *Chem Commun* 417; (b) Nlate S, Ruiz J, Sartor V, Navarro R, Blais J-C, Astruc D (2000) *Chem Eur J* 6:2544
57. (a) Daniel M-C, Ruiz J, Nlate S, Palumbo J, Blais J-C, Astruc D (2000) *Chem Commun* 2001; (b) Daniel M-C, Ruiz J, Nlate S, Blais J-C, Astruc D (2003) *J Am Chem Soc* 125:2617; (c) Daniel M-C, Astruc D (2004) *Chem Rev* 104:293; (d) Astruc D, Daniel M-C, Ruiz J (2004) *Chem Commun* 2637
58. (a) Kolb HC, Finn MG, Sharpless KB (2001) *Angew Chem Int Ed* 40:2004; (b) Bock VD, Hiemstra H, van Maarseveen JH (2006) *Eur J Org Chem* 51
59. Ornelas C, Ruiz J, Cloutet E, Alves S, Astruc D (2007) *Angew Chem Int Ed Engl* 46:872
60. (a) Ornelas C, Salmon L, Ruiz J, Astruc D (2007) *Chem Commun* 4946–4948; (b) Ornelas C, Salmon L, Ruiz J, Astruc D (2008) *Chem Eur J* 14:50–64
61. Bönnemann H, Nagabushana KS (2004) In: Nalwa HS (ed) *Encyclopedia of nanoscience and nanotechnology*, vol 1. ASP, Stevenson Ranch p 777
62. Toshima N, Yonezawa Y (1998) *New J Chem* 22:1179
63. (a) Astruc D, Lu F, Ruiz J (2005) *Angew Chem Int Ed* 44:7852; (b) Astruc D (2007) *Inorg Chem* 46:1884
64. (a) Zhao M, Sun L, Crooks RM (1998) *J Am Chem Soc* 120:4877; (b) Balogh L, Tomalia DA (1998) *J Am Chem Soc* 120:7355
65. Esumi K, Suzuki A, Aihara N, Usui K, Torigoe K (1998) *Langmuir* 14:3157
66. (a) Crooks RM, Zhao M, Sun L, Chechik V, Yeung LK (2001) *Acc Chem Res* 34:181; (b) Scott RWJ, Wilson OM, Crooks RMJ (2005) *Phys Chem B* 109:692; (c) Chandler BD, Gilbertson JD (2006) *Top Organomet Chem* 20:97
67. Diallo A, Ornelas C, Ruiz J, Salmon L, Astruc D (2007) *Angew Chem Int Ed* 46:8644–8648
68. de Vries AHM, Parlevliet FJ, Schmeder-van de Vondervoort L, Mommers JHM, Henderickx HJW, Walet MAN, de Vries AHM (2002) *Adv Synth Catal* 344:996

69. de Vries AHM, Mulders JMCA, Mommers JHM, Hendericks HJW, de Vries JG (2003) *Org Lett* 5:3285
70. de Vries JG (2006) *Dalton Trans* 421
71. (a) Plault L, Hauseler A, Nlate S, Astruc D, Gatard S, Neumann R (2004) *Angew Chem Int Ed* 43:2924–2928; (b) Heuze K, Méry D, Gauss D, Astruc D (2003) *Chem Commun* 2274–2275; (c) Heuze K, Méry D, Gauss D, Blais J-C, Astruc D (2004) *Chem Eur J* 10:3936–3944

Chapter 9

Antioxidants of Hydrocarbons: From Simplicity to Complexity

Vagif Farzaliyev

Abstract One of the most important yet complex chemistries is the spontaneous reaction of oxygen with organic matter, generally referred to as autoxidation. Suppressing this chemistry is important in many industries and critical when it comes to the performance of lubricants. The chapter summarizes kinetic parameters for reaction of the potent sulphur-containing antioxidants with both cumylperoxide radicals and cumene hydroperoxide. It also demonstrates that antioxidants can be formulated that have synergistic activity. One example of this phenomenon is the combination in one molecule of phenolsulphide and aminosulphide moieties, which results in an antioxidant with superior activity for the critical hydroperoxide decomposition process compared to molecules containing either moiety alone.

9.1 Introduction

Oxidative stability is one of the most important operational properties of lubricants, inasmuch as a great many undesirable phenomena take place in engines and mechanisms in the process of their operation are associated with formation of various oxidation products. Therefore the development of highly effective antioxidants is an actual problem of the chemistry of additives.

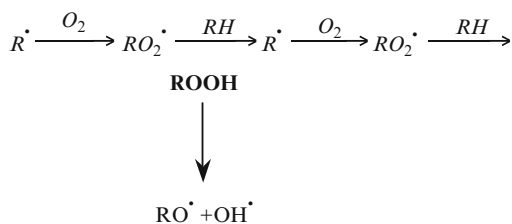
One of the requirements for promising lubricants is a low content of metals, since in the course of operation of lubricants in engines, the metal-containing compounds form high-ash deposits. In addition, the application of zinc dithiophosphate as an antioxidant in present engine oils is considered to be undesirable because the

V. Farzaliyev (✉)

Institute of Chemistry of Additives, Azerbaijan National Academy of Sciences, 2062 block,
Beyukshor shosse, Baku 370029, Azerbaijan
e-mail: chemistry@science.az

phosphorus contained in it poisons the combustion catalyst for exhaust gases. Thus the development of highly efficient ashless antioxidants that are free of phosphorus is noteworthy.

Oxidation of hydrocarbons is known to be a degenerate-branched radical-chain process, which may be represented simply as

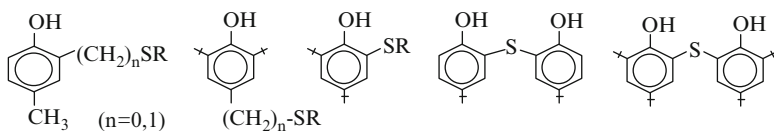


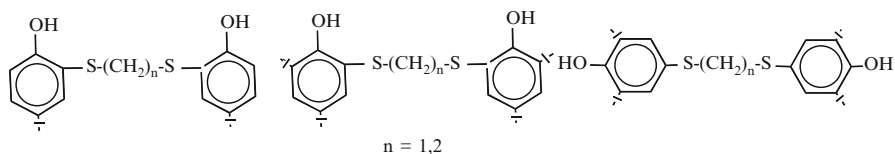
To inhibit this process it is necessary to introduce compounds that react rapidly with radicals formed (R^{\cdot} or RO_2^{\cdot}) or destroy hydroperoxide without generating free radicals.

At present, the most widely used chain-terminating antioxidants that react with peroxide radicals are substituted phenols, aromatic amines, and additives that decompose hydroperoxides into molecular products – sulphides and others.

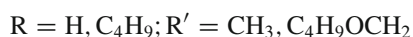
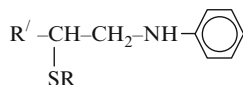
Because the antioxidant properties of additives are related to certain functional groups in their structures, it is of considerable interest to synthesize and investigate the mechanism of action of organic compounds containing two or more effective functional groups en route to realizing new and more effective types of antioxidants. On this basis, research has been carried out on the synthesis, mechanism of action, and establishment of structure-efficiency relationships of sulphur-containing multifunctional antioxidants.

In the choice of sulphur-containing multifunctional antioxidants it was decided to combine in one molecule the properties of two types of antioxidants: those that terminate chains by reacting with peroxide radicals and those that decompose hydroperoxides. Generally phenols and aromatic amines exhibit the first type of activity and sulphides, etc. exhibit the second type. Therefore, compounds that contain both a sulphur atom and a phenolic fragment such as phenolsulphides, aromatic amine – aminosulphides, and aminophenolsulphides are of interest. Some of the phenolsulphides we targeted contain a sulphur atom and one phenolic fragment (monophenolsulphides) or two phenolic fragments (bis-phenolsulphides) but differ in the mutual arrangement of sulphur atom and hydroxy groups and other parameters as follows:

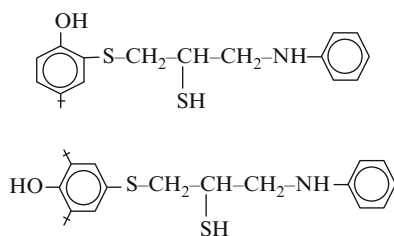




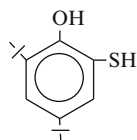
Some aminosulphides we synthesized and studied are of the following structural motif bearing both a sulphur atom and an aniline fragment:



To investigate the antioxidant activity of compounds where phenolsulphide and aminosulphide fragments are combined, aminophenolsulphides were prepared:

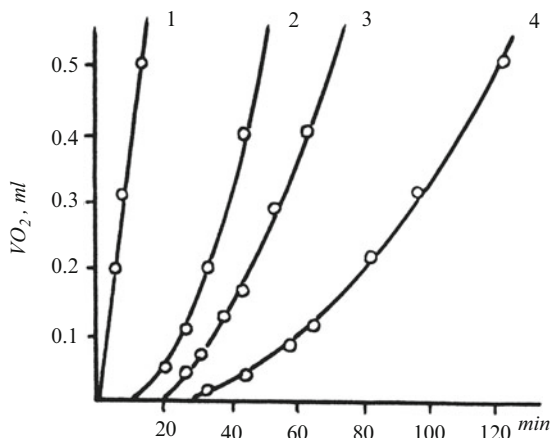


The action mechanism of sulphur-containing antioxidants was studied by the well-established method of following O_2 uptake with time as a function of added inhibitor (antioxidant). The effect of antioxidants that inhibit chain termination and also ones exhibit hydroperoxide decomposition activity were evaluated. Isopropylbenzene (cumene) was used as the representative organic reactant (e.g. Fig. 9.1) and the reaction was initiated by azodiisobutyronitrile in the presence of the other reactants at 60°C .



The concentration of an initiator was 2×10^{-2} M and the concentration of antioxidants was varied in the range $0.5\text{--}10.0 \times 10^{-4}$ M. All the antioxidants studied inhibit initiation of cumene oxidation by reacting with cumylperoxide radicals. Figure 9.1 presents the typical kinetic curves for cumene oxidation in the presence of sulphur-containing antioxidants. The rate constants for reaction of the antioxidants with cumylperoxide radicals (k_7) was calculated by absorption kinetics of oxygen,

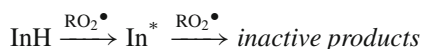
Fig. 9.1 Kinetic curves of initiated oxidation of cumene in the presence of monophenolsulphide
 $[InH] = 0$ (1); 3×10^{-4} (2);
 4×10^{-4} (3);
 5×10^{-4} mol/l (4)



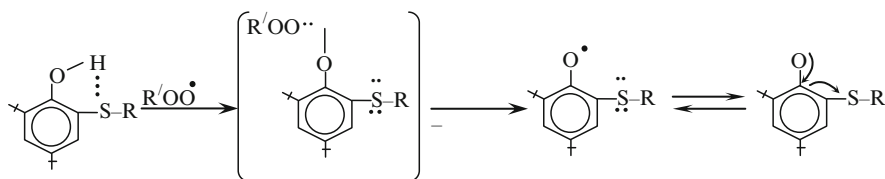
and by induction period: the stoichiometric inhibition coefficient (f) is equal to the number of oxidation chains terminating from one molecule of the antioxidant and its transformation products. Figure 9.1 shows that the oxidation rate in the presence of antioxidant after an induction period (curves 2–4) is less than the oxidation rate in the absence of antioxidant (curve 1).

Table 9.1 indicates the average values of the kinetic parameters for reaction of the sulphur-containing antioxidants studied with cumylperoxide radicals. One can see that for monophenolsulphides with sulfur groups bound directly to the arene core, regardless of the location of the SR group (*o*- or *p*-position) with respect to the OH group, give a stoichiometric coefficient of inhibition (f) of ~ 1 . For compounds where the sulphur atom is connected to the benzene ring through a methylene bridge, then $f = 2$.

It is known that for alkyl phenols $f = 2$, i.e. they terminate two oxidation chains:



It may be assumed that the termination of one oxidation chain by monophenolsulphides, with a sulphur atom directly connected to the benzene ring, is due to stabilization of the forming phenoxyl radical by the sulphur atom:



In the case of monophenolsulphides with a methylene bridge between benzene ring and sulphur atom, such conjugation is excluded. As a result, the phenoxyl radical formed is able to react with the second peroxide radical.

Table 9.1 Kinetic parameters of the reaction of sulphur-containing antioxidants with cumylperoxide radicals

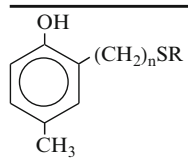
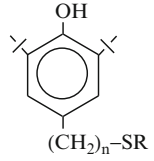
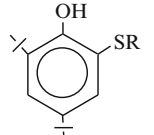
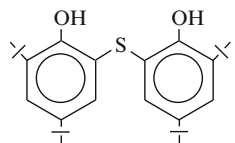
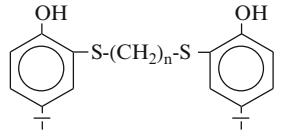
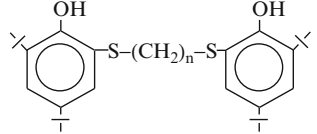
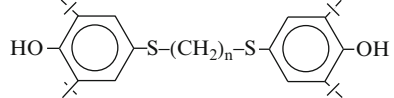
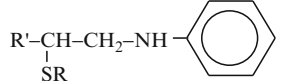
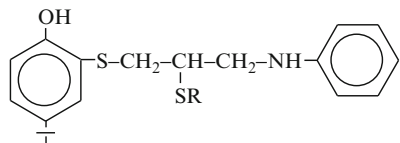
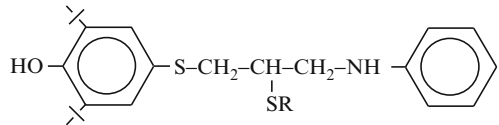
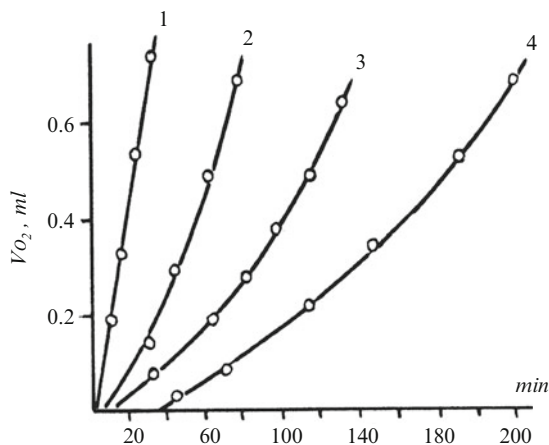
Antioxidant	f	$k_7 \times 10^{-4} \text{ (M}^{-1} \text{ s)}$
	2	2-6
	2	2-6
	1	1-2
	2	2
	2	4
	2	2
	2	2
	1	2
	1	2
	2	3

Fig. 9.2 Kinetic curves of initiated oxidation of cumene in the presence of aminosulphide. $[InH] = 0$ (1); 2×10^{-4} (2); 4×10^{-4} (3); 7×10^{-4} mol/l (4)



The rate constants for reaction of monophenolsulphides with cumylperoxide radicals (k_7) are in the range $2-6 \times 10^4 \text{ M}^{-1} \text{ s}$ that somewhat exceed the values for known alkylphenolic antioxidants.

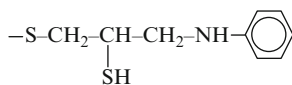
It is established that in monophenolsulphides, electron-donating substituents at sulphur atom increase k_7 and electron-accepting ones decrease it.

The kinetic parameters of reaction of bisphenolsulphides with cumylperoxide radicals are consistent with the termination of two oxidation chains ($f \approx 2$). It is known that for bisphenolic antioxidants, $f \approx 4$. This may be explained by an analogous mechanism of reaction with peroxide radicals proposed for monophenolsulphides that have the sulphur atom connected directly to the benzene ring. k_7 values for bisphenolsulphides are also in the range $2-6 \times 10^4 \text{ M}^{-1} \text{ s}$.

Aminosulphides terminate one oxidation chain ($f = 1$), and from the rate constant for reaction with cumylperoxide radicals, are somewhat inferior to phenolsulphides ($k_7 = 1-2 \times 10^4 \text{ M}^{-1} \text{ s}$.) The degree of inhibition of the transformation products of aminosulphides in reaction with cumylperoxide radicals, indicate they are superior to those in the phenolsulphide reactions (Fig. 9.2).

Figure 9.3 illustrates kinetic curves for oxygen absorption in the initiated oxidation of cumene in the presence of aminophenolsulphides.

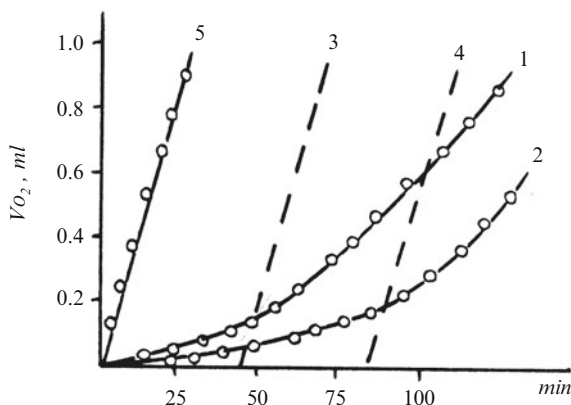
Comparison of the curves 1 and 2 shows that at the same initial concentration of aminophenolsulphide in which fragment



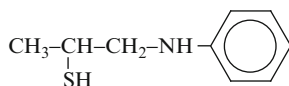
is in the *p*-position with respect to the phenolic hydroxyl group is several times more effective than aminophenolsulphide where the fragment is in the *o*-position.

Comparison of the experimental curves 1 and 2 with theoretical curves 5 and 4 (Fig. 9.3) for inhibitors, accordingly terminating chains 1 and 2 and taken

Fig. 9.3 Kinetic curves of initiated oxidation of cumene in the presence of *o*- (1) and *p*-aminophenolsulphides (2). $[\text{InH}] = 5 \times 10^{-4}$ M. Curves 3–5 are addressed in the text



at the concentration equal to that of aminophenolsulphides, indicates that for *o*-aminophenolsulphide $f \approx 1$ and that *p*-phenolsulphide also have a high k_7 value. Aminophenolsulphides exhibit a high degree of “secondary inhibition”.



Thus, the kinetic investigations show that the sulphur-containing antioxidants synthesized efficiently terminate oxidation chains by reaction with peroxide radicals.

The presence of the sulphide function in the antioxidants synthesized implied their reaction with hydroperoxides. Early investigations of the reaction of phenolsulphides with cumyl hydroperoxide indicated that their hydroperoxide decomposition activity is far higher than that of sulphides and other types of compounds established to react rapidly with hydroperoxides. This was the rationale for a more detailed investigation of the reactions of sulphur-containing antioxidants with hydroperoxides.

Reactions of the above inhibitors with cumyl hydroperoxide were carried out in chlorobenzene solution under a nitrogen or argon atmosphere at 90–110°C with various ratios of reactants. Under these conditions, cumyl hydroperoxide (CHP) was essentially stable in the absence of any added antioxidant.

It is established that all sulphur-containing antioxidants decompose cumyl hydroperoxide. The kinetic curves of decomposition of cumyl hydroperoxide under the action of these antioxidants are S shaped (Fig. 9.4, curve 1), which is indicative of autocatalysis. There is always some induction period during which a negligible amount of CHP is consumed, followed by a rapid catalytic decomposition of CHP and then a decrease in this rate as the CHP concentration approaches zero. This indicates that catalytic decomposition of CHP in the presence of the antioxidants studied here proceeds not by reaction with the initial antioxidant but with its transformation products formed during the induction period.

Fig. 9.4 Kinetic curves for decomposition of CHP in the presence of monophenolsulphide: 110°C; [InH] = 5×10^{-4} M. 1: reaction with the first portion of CHP; 2: reaction after addition of a fresh portion of CHP

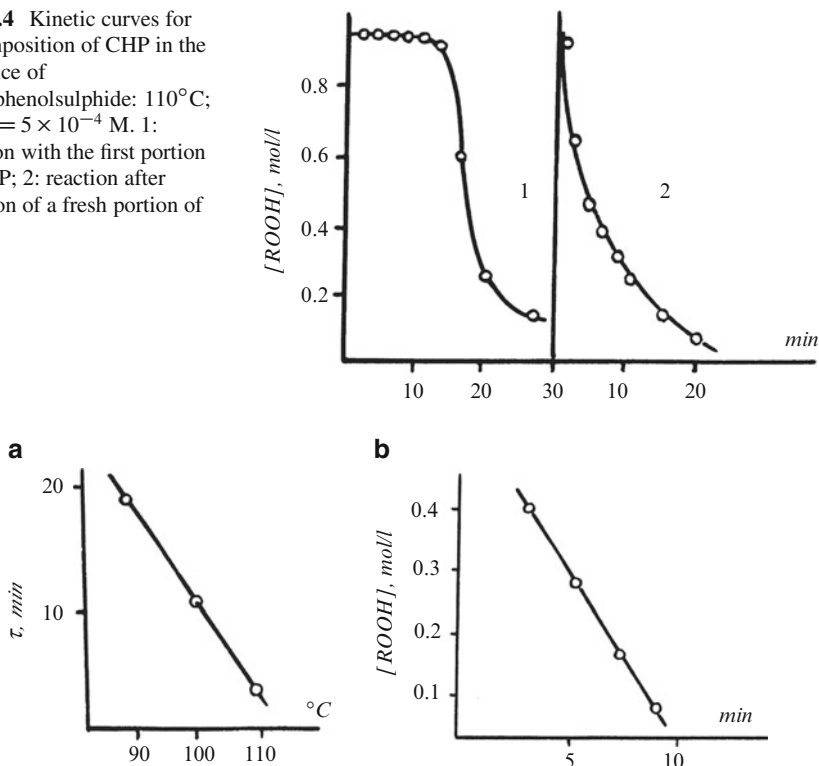
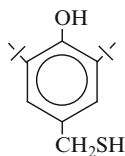


Fig. 9.5 Dependence of induction period for CHP decomposition in the presence of bisphenolsulphide on temperature (a) ([InH] = 5×10^{-4} M) and on the concentration of CHP (b) ([InH] = 5×10^{-4} M)

To confirm this, a fresh portion of CHP was added to the products of a completed CHP + antioxidant reaction. This time no induction period was observed (Fig. 9.4, curve 2).

It was also established that increasing reaction temperature leads to a decrease in induction period, and that this relationship is almost linear (Fig. 9.5a).



The increase of CHP concentration at constant temperature and constant antioxidant concentration also results in the decrease of induction period (Fig. 9.5b). The inverse dependence of induction period on initial concentration of CHP proves that the formation of products with high catalytic activity takes place under the action of CHP and not as a result of thermal conversions of sulphur-containing antioxidants.

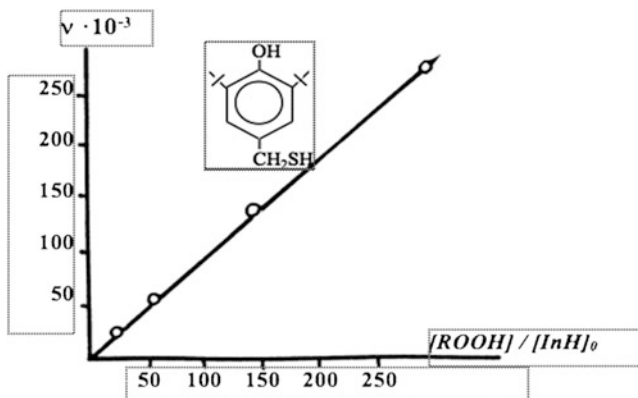


Fig. 9.6 Dependence of the catalytic factor (ν) on the ratio of initial concentration of CHP and mono-phenolsulphide

The value of an induction period doesn't depend on the concentration of the antioxidants investigated.

The kinetic parameters of antioxidants reacting with CHP were calculated for the catalytic decomposition stage.

The concentration of CHP molecules (ν) decomposing under the effect of one molecule of sulphur-containing antioxidant was calculated using the formula:

$$\nu = \frac{[\text{CHP}]_0 - [\text{CHP}]_\infty}{[\text{InH}]_0}$$

where: $[\text{CHP}]_0$ and $[\text{CHP}]_\infty$ are, accordingly, the initial and final concentrations of CHP; $[\text{InH}]_0$ – initial concentration of the antioxidant.

The values of a catalytic factor ν showed that the transformation products of one molecule of antioxidant, depending on the structure, are able to decompose from several hundred to several thousand CHP molecules. The value ν increases directly proportional to the increase of the ratio of CHP and the initial antioxidant concentrations (Fig. 9.6). This indicates that the antioxidants studied are more efficient in the decomposition of hydroperoxides than other known organic compounds.

It was established that for all sulphur-containing antioxidants, the reaction with CHP is of first order with respect to both the antioxidant and CHP; and an initial reaction rate of catalytic decomposition of CHP is represented by the equation: $W_0 = k[\text{InH}] \cdot [\text{CHP}]$

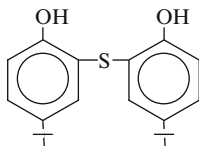
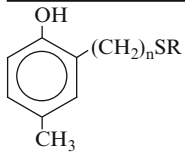
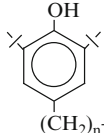
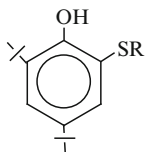
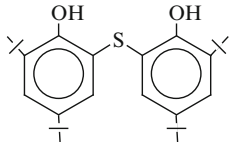
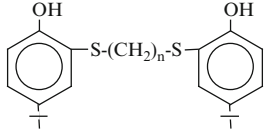
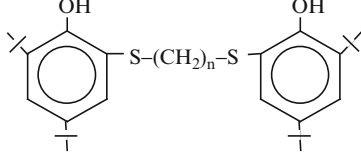
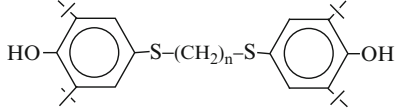


Table 9.2 Kinetic parameters of the reaction of sulphur-containing antioxidants with cumene hydroperoxide (110°C)

Antioxidant	K ($M^{-1} s$)	$\nu \times 10^{-3}$
	3–5	3–9
	2–10	4–10
	2–14	2–6
	10	18
	8–13	3–8
	14	11
	16	23

(continued)

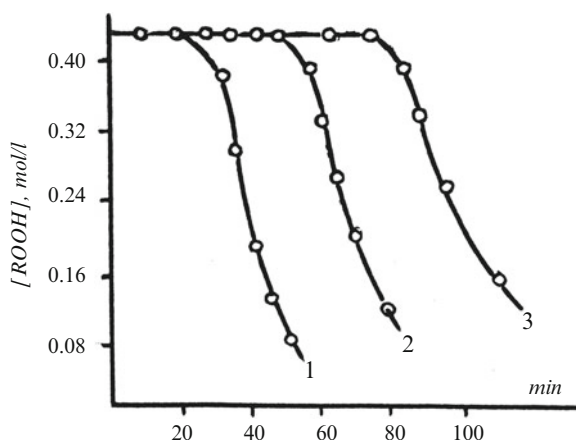
Measurement of the reaction rate constant at various temperatures facilitated determination of the activation energy for the catalytic decomposition of CHP by the antioxidants studied. Depending on the structure of sulphur-containing antioxidant, the activation energy values varied in the range 40–90 kJ/mol.

Table 9.2 lists the averaged values of kinetic parameters for the catalytic decomposition of CHP affected by sulphur-containing antioxidants. The data indicate that

Table 9.2 (continued)

Antioxidant	K ($M^{-1} s$)	$\nu \times 10^{-3}$
$R'-\underset{\substack{ \\ SR}}{CH}-CH_2-NH-\text{C}_6\text{H}_5$	6-7	27-45
$\text{C}_6\text{H}_4(\text{OH})-\text{S}-CH_2-\underset{\substack{ \\ SR}}{CH}-CH_2-NH-\text{C}_6\text{H}_5$	0,5	54
$\text{C}_6\text{H}_3(\text{OH}, \text{t-Bu})-\text{S}-CH_2-\underset{\substack{ \\ SR}}{CH}-CH_2-NH-\text{C}_6\text{H}_5$	14	55

Fig. 9.7 Kinetic curves of decomposition of CHP in the presence of monophenolsulphide (InH_1) and 2,6-di-*tert*-butyl-4-methyl-phenol (InH_2).
 $[\text{InH}_1] = 1 \times 10^{-3} \text{ M}$;
 $[\text{InH}_2] = 0$ (1); 1×10^{-3} (2);
 $2 \times 10^{-3} \text{ M}$ (3)

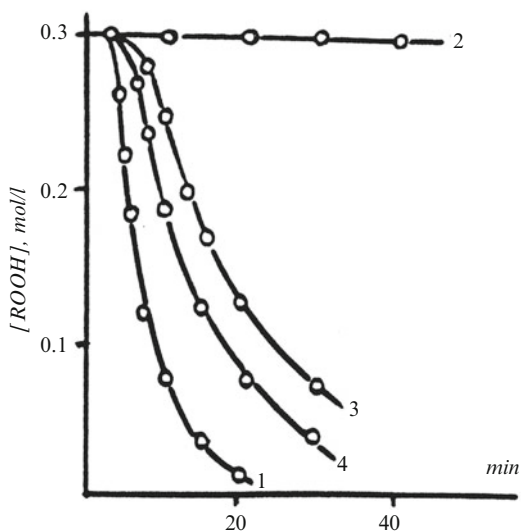


the greatest activity for catalytic CHP decomposition is exhibited by the transformation products of aminophenolsulphide with a hindered phenolic fragment.

Thus, the combination in one molecule of phenolsulphide and aminosulphide fragments results in a compound with superior activity to either fragment alone with respect to its catalytic hydroperoxide decomposition activity.

The reaction of antioxidants with CHP in the presence of the radical acceptor (scavenger), 2,6-di-*tert*-butyl-4-methylphenol, showed that its addition at the beginning of reaction results in inhibition of CHP decomposition, and that the duration of this inhibition increases with the increase of its concentration (Fig. 9.7). Addition of the radical acceptor mentioned at the catalytic decomposition stage of CHP has no effect on the reaction rate. Therefore, in the first stage of the reaction of CHP with antioxidants the formation of their transformation products and the resulting catalytic decomposition of CHP, is a free radical process.

Fig. 9.8 Kinetic curves for decomposition of CHP in the presence of monophenolsulphide at 110°C ; $[\text{InH}] = 3 \times 10^{-3} \text{ M}$; without preliminary treatment (1); after the reaction with RO_2 (2), R (3) and oxidation by oxygen (4)



In using the sulphur-containing compounds in this overview as antioxidants, it must be borne in mind that in the course of their inhibition of the oxidation process they are simultaneously attacked by oxygen-based free radicals and other products that form during the oxidation of hydrocarbons. As a result, the activity of the antioxidants in the decomposition of hydroperoxides change with time, an example of complex kinetics, one theme of this volume.

It was established that the sulphur-containing antioxidants completely lose their catalytic activity in the decomposition of CHP reacting with peroxide radicals. However, their activity is not significantly decreased in the reaction with alkyl radicals and oxygen (Fig. 9.8).

It was known that the reaction of phenolic and amine antioxidants with peroxide radicals proceeds in the presence of hydroxy and amine groups. The fact that the reaction products of sulphur-containing antioxidants studied with peroxide radicals do not catalytically decompose CHP indicates that participation of hydroxy and amine groups in the formation of an effective catalyst for the decomposition of hydroperoxides.

Based on above studies, the initial stage of the reaction of phenolsulphides with CHP can be expressed by the scheme leading to the formation of sulfoxide.

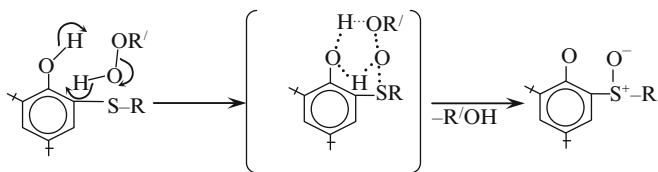
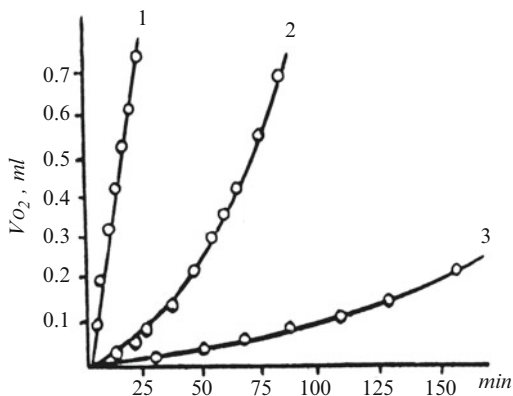
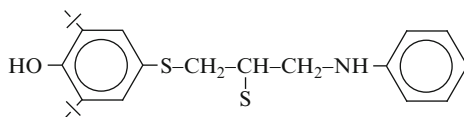


Fig. 9.9 Kinetic curves of initiated oxidation of cumene (1) in the presence of aminophenolsulphide (InH_1) (2) and its reaction products with CHP (InH_2) (3).
 $[\text{InH}_1] = 1 \times 10^{-4} \text{ M}$;
 $[\text{InH}_2] = 1 \times 10^{-5} \text{ M}$

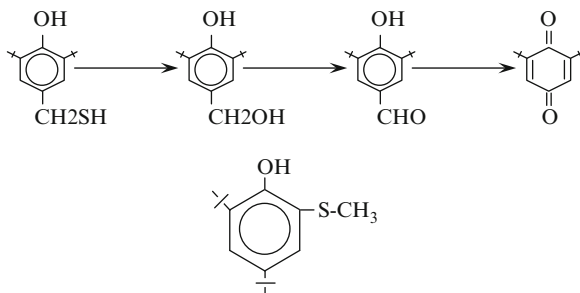


The investigations showed that the introduction of pyridine either at the beginning of the process or at the stage of catalytic CHP decomposition, fully inhibits the reaction of sulphur-containing antioxidants studied with CHP. Hence, the transformation products of the antioxidants catalytically decomposing CHP are acidic in character.

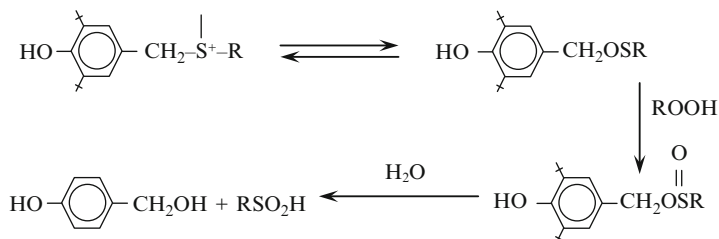
It was established that the transformation products of sulphur-containing antioxidants in reaction with CHP efficiently and even repeatedly ($f \geq 10$) terminate the oxidation chains by reaction with peroxide radicals (Fig. 9.9).



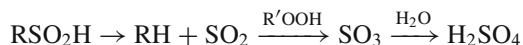
Investigation of the transformation products from the reaction of CHP with hindered phenolsulphides containing a sulphur atom connected to the arene ring through a methylene bridge indicated the formation of 4-hydroxy-3,5-di-*tert*-butylbenzyl alcohol as the main product of its further oxidation:



Taking into account the results of studying the character and structure of transformation products of phenol sulphides from the reaction with CHP, the following scheme for transformation of the sulfoxide may be suggested:



The sulphinic acid that forms efficiently destroys the hydroperoxides and is able to repeatedly terminate oxidation chains by reacting with peroxide radicals. At higher temperatures sulphinic acid may also eliminate sulphurous-acid anhydride leading to the formation of sulphuric acid, which also effectively destroys hydroperoxides:



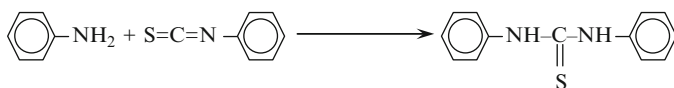
A similar mechanism may be suggested for the transformation products of aminosulphides involving participation of the hydrogen atom of the imine group.

The results of investigating the antioxidant activity of a series of compounds synthesized in lubricants confirmed their high efficiency.

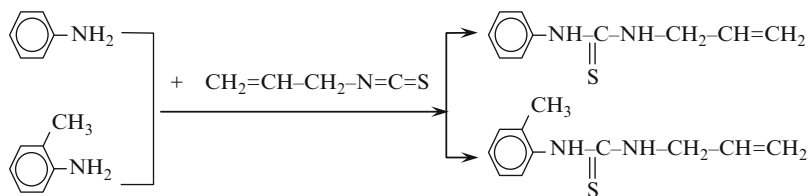
Thus, the sulphur-containing compounds studied are antioxidants of combined action: they terminate oxidation chains by direct reaction with peroxide radicals, and they are oxidized by hydroperoxides to form products that catalytically convert hydroperoxide into molecular products while actively reacting with peroxide radicals. Synergy is seen in inhibiting hydrocarbon oxidation by addition of antioxidants containing sulphur atoms in combination with a phenolic or aniline fragment.

To obtain new antioxidants of combined action a number of nitrogen-containing compounds such as thiocarbamide derivatives with substituents of different character at nitrogen atom were synthesized.

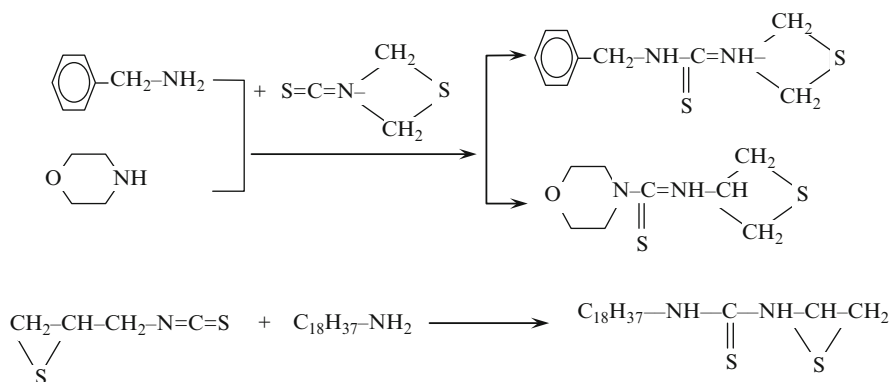
By addition of phenylisothiocyanate to aniline, *N-N'*-diphenylthiocarbamide was synthesized:



Accordingly, reaction of allylisothiocyanate with aniline and *o*-toluidine produces *N*-phenyl-*N'*-allylthiocarbamide and *N*-(*o*-methylphenyl)-*N'*-allylthiocarbamide:



Addition of 3-thiethanylisothiocyanate to benzylamine and morpholine accordingly yields *N*-benzyl-*N'*-(3-thiethanyl)thiocarbamide and *N*-morphonyl-*N'*-(3-thiethanyl)thiocarbamide, and addition of 1,2-epithio-3-isothiocyanatopropane to octadecylamine yields *N*-octadiene-*N'*-(1,2-epithiopropyl)thiocarbamide:



Investigation of the reactions of these compounds with cumylperoxide radicals and cumyl hydroperoxide showed that the mechanism of antioxidant action of these compounds is similar to that of previously studied sulphur-containing phenol and amine derivatives, namely, they efficiently terminate oxidation chains by reacting with peroxide radicals (Fig. 9.10) and catalytically convert hydroperoxides into molecular products (Fig. 9.11).

Table 9.3 gives the kinetic parameters for the reactions of the thiocarbamides above with cumylperoxide radicals and cumyl hydroperoxide as well as the induction periods for cumene autooxidation in the presence of the given antioxidants. These thiocarbamides terminate oxidation chains fairly effectively by reacting with peroxide radicals. The reactivity of the derivative containing benzene and thiethanyl fragments at the nitrogen atom is quite distinct from the other thiocarbamides in the efficiency of its reaction with cumylperoxide radicals. High values of reaction rate constant (k_7) and stoichiometric coefficient (f) are characteristics of the reaction of *N*-benzyl-*N'*-(3-thiethanyl)-thiocarbamide with cumylperoxide radicals: multiple termination of oxidation chains are observed.

Fig. 9.10 Kinetic curves for the initiation of cumene autoxidation in the presence of *N*-benzyl-*N'*-(3-thiethanyl)thiocarbamide ($T = 60^\circ\text{C}$, $[\text{InH}] = 5 \times 10^{-6} \text{ M}$)

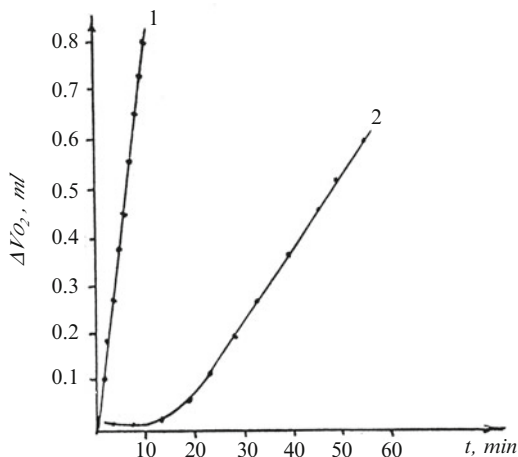
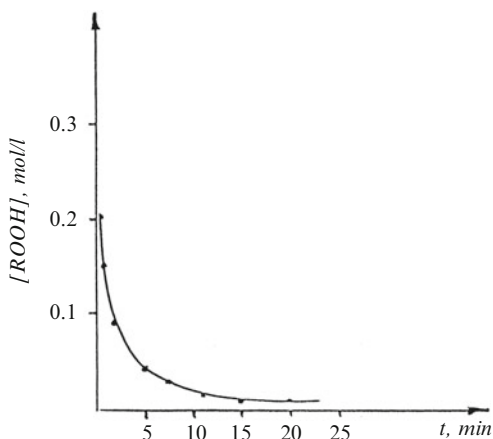


Fig. 9.11 Kinetic curves for decomposition of CHP in the presence of *N*-benzyl-*N'*-(3-thiethanyl)thiocarbamide ($T = 110^\circ\text{C}$, $[\text{InH}] = 5 \times 10^{-6} \text{ M}$, $[\text{CHP}] = 0.2 \text{ M}$)

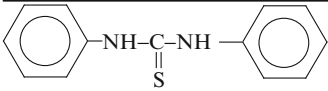
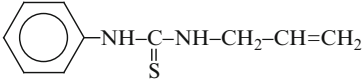
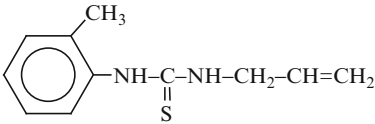
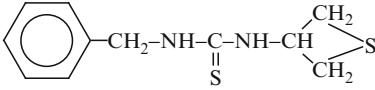
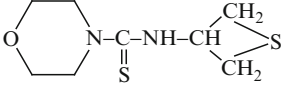


The reaction products of thiocarbamide derivatives with cumylperoxide radicals exhibit a secondary inhibiting effect.

The thiocarbamides with an aryl fragment at one nitrogen atom and α -allylic and thietanyl fragments at the other have the highest activity with cumyl hydroperoxide, and among these compounds, *N*-(*o*-methyl-phenyl)-*N'*-allylthiocarbamide, has the highest stoichiometric coefficient (ν) and markedly differs in its activity.

The kinetic parameters for reaction of the thiocarbamides with cumylperoxide radicals and cumyl hydroperoxide are also consistent with *N*-benzyl-*N'*-(3-thiethanyl) thiocarbamide being faster in both oxidation chain termination (reacting with cumylperoxide radicals) and in catalytic decomposition of cumyl hydroperoxide. It was also shown that *N*-benzyl-*N'*-(3-thiethanyl) thiocarbamide inhibits cumene autoxidation better than the other thiocarbamide derivatives when used in lower concentrations than the latter.

Table 9.3 Kinetic parameters for the reaction of thiocarbamide derivatives with cumylperoxide radicals and cumyl hydroperoxide as well as the induction periods in cumyl autoxidation in presence of given antioxidants

Antioxidant	$k_7 \times 10^{-4}$ ($M^{-1} s$)	f	$K \times 10^{-1}$ ($M^{-1} s$)	$\nu \times 10^{-3}$	τ (min)
	2.33	2.4	4.7	82	100
	2.31	2.2	30	560	110
	3.19	2.2	30	860	138
	7.05	34	12.5	526	250 ^a
	2.0	1.9	2.4	69	86
$C_{18}H_{37}$ -NH-C(=S)-NH-CH(CH ₂) ₂ S	3.27	2.1	2.3	58	120

^a [InH] = 5×10^{-6} M

The research allows one to draw several conclusions. First, these thiocarbamides function as combined-action antioxidants, and some of them strongly inhibit hydrocarbon oxidation. Second, as shown in Fig. 9.8, some of the traditional inhibitors we have synthesized after their reaction with peroxide radicals are unable to catalytically decompose hydroperoxides. Third, in the process of hydrocarbon oxidation, peroxide radicals are earlier oxidation products than hydroperoxides, hence these antioxidants will be consumed following the reaction with peroxide radicals.

In addition, to retain these antioxidants prior to hydroperoxide formation, we originally prepared a synergic mixture with ionol. So far, k_7 for ionol is higher than for our antioxidants, therefore the latter will persist prior to hydroperoxide formation and then function with combined action. Figure 9.12 indicates the efficiency of a synergic mixture ionol + aminophenylsulfide. Inasmuch as the transformation products of our antioxidants in reaction with hydroperoxides are more active than parent ones, we tried to add hydroperoxide to our antioxidants in advance. The curves in Figs. 9.12 and 9.13 illustrate high efficiency

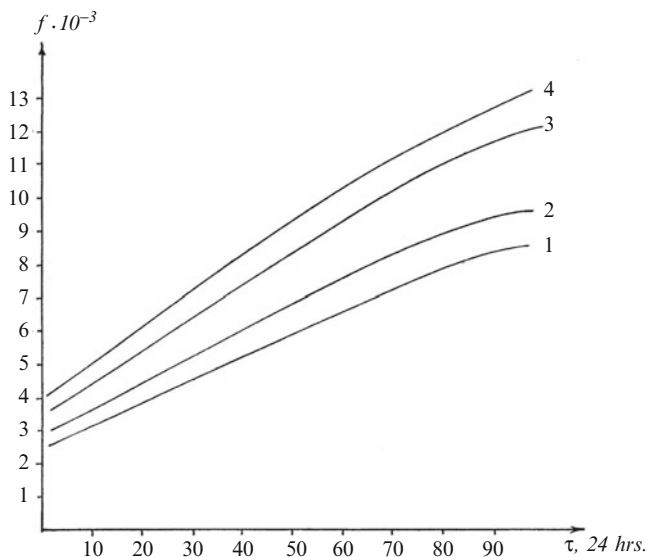


Fig. 9.12 Dependence of stoichiometric coefficient (f) of the reaction of cumylperoxide radicals with interaction products of *N*-benzyl-*N'*-thiethanylthiocarbamide (InH) with cumyl hydroperoxide (ROOH) on the ratio of InH:ROOH and the incubation time of the InH + ROOH mixture ($T = 60^\circ\text{C}$; $[\text{InH}] = 5 \times 10^{-7} \text{ M}$). InH:ROOH = 1:0.25 (1); 1:0.5 (2); 1:1 (3); 1:2 (4).

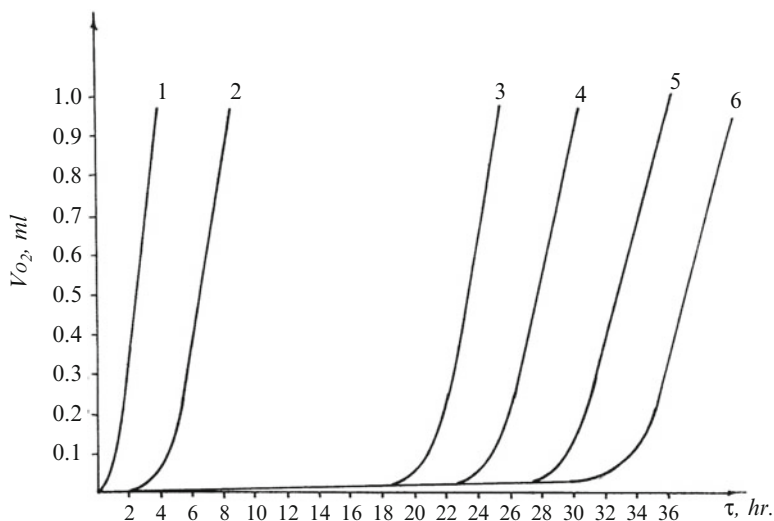


Fig. 9.13 Kinetic absorption curves for consumption of O_2 during cumene autoxidation (1) in the presence of *N*-benzyl-*N'*-thiethanylthiocarbamide (InH) (2) and in the presence of its transformation products from reaction with cumyl hydroperoxide (ROOH) at various ratios of InH:ROOH (3–6). $T = 110^\circ\text{C}$; $[\text{InH}] = 5 \times 10^{-6} \text{ M}$. InH:ROOH = 1:0.25 (3); 1:0.5 (4); 1:1 (5); 1:2 (6)

of *N*-benzyl-*N'*-thiethanylthiocarbamide transformation products on treatment with cumyl hydroperoxide both in reaction with cumylperoxide radicals (very high *f* values) and in autooxidation of cumene (high values of induction periods). Thus, in passing from simple antioxidants to complex ones, we can obtain highly efficient hydrocarbon antioxidants.

Chapter 10

Structural and Electronic Features of Wells-Dawson Polyoxometalates

Laia Vilà-Nadal, Susanna Romo, Xavier López, and Josep M. Poble

Abstract Density functional theory approach is used to study structural and electronic features of $X_2M_{18}O_{62}^{q-}$ Wells-Dawson (or simply ‘Dawson’) polyoxometalates (POM). We deeply concentrated on the isomerism in this family of POMs because isomerism is related to the possibility of tuning some properties with controlled geometrical changes, such as the different location of a given atom (*positional isomerism*) or a rotation of a fragment of the molecule (*rotational isomerism*). We have evaluated the relative stability of the isomers considering only the $[W_{18}O_{54}]$ cage with and without the internal anions $[(XO_4)_2]^{q-}$.

10.1 Introduction

Polyoxometalates (POMs) [1–4] are metal oxide clusters formed upon the assembly of early transition metal ions and oxo ligands. Most POMs known to date are molecular (zero dimensional), and due to their structure and composition, they are in general soluble in water and some organic solvents [5]. This fact is very important in the chemistry of POMs because they present some solid-state properties at the molecular level, which makes them unique for homogeneous catalysis, for example. From the structural point of view, POMs are highly ordered clusters with an additional richness arising from the existence of various isomeric forms in some cases, notably in the common $XM_{12}O_{40}^{q-}$ Keggin and $X_2M_{18}O_{62}^{q-}$ Wells-Dawson (or simply ‘Dawson’) structures. Isomerism in POMs has been largely studied

L. Vilà-Nadal • S. Romo • X. López • J.M. Poble (✉)
Departament de Química Física i Inorgànica, Universitat Rovira i Virgili,
Marcel·li Domingo s/n, 43007 Tarragona, Spain
e-mail: joosepmaria.poble@urv.cat

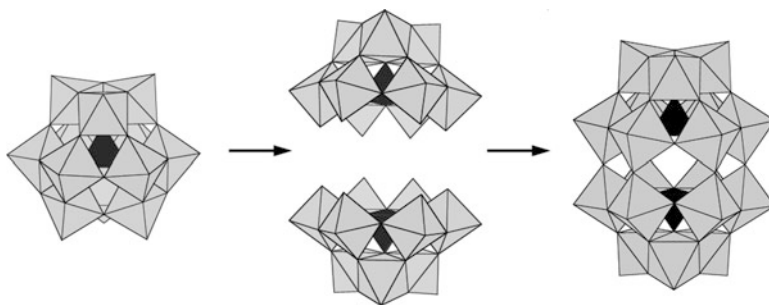


Fig. 10.1 Building-up process from the α -Keggin to the A- α -Dawson structure. Gray octahedra are MO_6 units ($M = \text{W}, \text{Mo}$), and black tetrahedra are XO_4 anions (Color figure online)

and their properties deeply analyzed experimentally and computationally, although some basic points are still not completely clear. The main interest on isomerism is related to the possibility of tuning some properties with controlled geometrical changes, such as the different location of a given atom (*positional isomerism*) or a rotation of a fragment of the molecule (*rotational isomerism*).

The Dawson structure [6] is based on the truncated XM_9O_{34} Keggin unit (XM_9 in short): two of these fragments can be assembled symmetrically to form the X_2M_{18} cluster, as shown in Fig. 10.1. The most typical compositions associated to the Dawson structure derive from the phosphotungstate and -molybdate anions, $[\text{P}_2\text{M}_{18}\text{O}_{62}]^{6-}$ (P_2M_{18} , $M = \text{W}, \text{Mo}$). Compounds containing As or S instead of phosphorus have also been reported [7]. In P_2M_{18} , as in the other derivatives of the Dawson structure, the eighteen metal atoms, in local pseudo-octahedral environment, are organized in four parallel rings of 3, 6, 6, and 3 metal ions each. At variance to the highly symmetric Keggin anion, the structure presents two distinct positions: the M_3 rings, located at the polar regions, are also called *caps*, and the two M_6 rings are located at the equatorial region, forming the *belt*. These features derive in some chemically different behaviors. The electronic structure of the Dawson anion is such that the first unoccupied molecular orbital (LUMO) is delocalized over the equatorial region, whereas the first virtual orbital located on the *cap* region has been computed to be 0.85 eV higher in energy [8–10]. Multiple metal substitutions can be carried out on the original structure.

Theoretical studies on POMs started in the early 1990s with the pioneering work of Rohmer, Bénard and coworkers [11]. Ever since, computational works have focused on the interpretation of diverse observed phenomena [12], among which the relative stability or the features associated to different isomers. Satisfactory explanations for observed stabilities and redox properties were reported for the cases of Keggin [13] and Dawson [8, 10] anions. In the present chapter we discuss the two types of isomerism in Dawson structures, stressing its effects on the electronic properties and applications.

10.2 Positional Isomers

Metal atoms can be removed and replaced from the complete Dawson structure, and the position at which this process occurs defines the α_1 and α_2 isomers (shaded octahedra in Fig. 10.2). These two isomers are chemically different at some effects despite being structurally very similar. In both the mono-vacant P_2W_{17} and the metal substituted $P_2W_{17}M$ forms, α_1 and α_2 have, for instance, different redox responses [14–19], basicities and binding energies to M, which also derive in different relative stabilities [20]. It is worth stressing that the nature of the substituting atom determines the new properties of the compound, although the final position it occupies within the cluster is also important. In the present section we will sketch the main features related to the positional isomerism in the Dawson structure, especially the redox chemistry.

The present section discusses the results obtained with density functional theory (DFT) calculations performed on the α_1 and α_2 isomers of P_2MW_{17} with $M = Mo, V$ and Re in various oxidation states, for which experimental data are also available. Many other metal elements have been incorporated to the Dawson structure such as Ti [21], Nb, Ta [22], etc. In the present work, we carried out geometry optimizations on the series of compounds stated. It is worth pointing out that in other cases not discussed here, such as $P_2Ti^{IV}W_{17}$ or $P_2Ta^VW_{17}$, the extra electrons are not trapped at the substituted position but at the W framework because these two ions are less electronegative than W^{VI} in this cluster. The electrochemical behavior of α_1 relative to α_2 is similar in these cases and thus resembles the unsubstituted P_2W_{18} form. This fact emphasizes that some metal ions have a minor electronic effect and thus could be *not interesting* for some goals.

In what concerns the monovacant α_1 - and α_2 - P_2W_{17} systems, after geometry optimization we found that the energy difference $\Delta E(\alpha_2 - \alpha_1) = -6.0 \text{ kcal mol}^{-1}$ in favor of α_2 . This significant difference arises from the dissimilar geometrical and electronic environment of the vacancies in each isomer. Contant and coworkers [20] proposed that the orientation of the internal tetrahedra PO_4^{3-} with respect to the

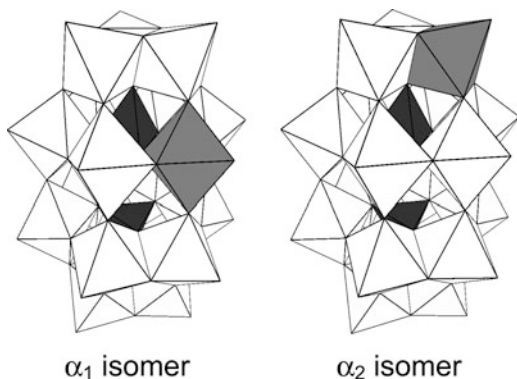


Fig. 10.2 The two positional isomers of the monosubstituted Dawson anion. Replacement occurs in the *belt* and *cap* regions to give the α_1 and α_2 isomers, respectively

Table 10.1 Computed energy differences (in kcal mol⁻¹) between α_1 and α_2 isomers vs the number d of electrons added to M, for [P₂W₁₇O₆₁MO]^{q-} compounds

M	q	d	$\Delta E(\alpha_2-\alpha_1)$
W(VI)	6	0	0.0
W(V) ^a	7	1	+6.6
Mo(VI)	6	0	-1.6
Mo(V)	7	1	+3.0
V(V)	7	0	+1.0
V(IV)	8	1	+4.4
Re(VII)	5	0	-2.2
Re(VI)	6	1	+2.5
Re(V)	7	2	+8.2
Re(IV)	8	3	+16.4

^a For M = W, only one isomer exists, so the energy difference arises from reducing either at the belt or at the cap sites

cavity generated by the removal of a [W^{VI}O]⁴⁺ fragment determines the relative stability of the positional isomers. In the lacunary structure α_1 -[P₂W₁₇O₆₁]¹⁰⁻, one of the internal oxygens remains bonded to P and one W atom, whereas in α_2 it is bonded to P and two W atoms. It is expected that the former destabilize further the system favoring the stability of α_2 . Introducing a [Re^{VII}O]⁵⁺ unit in either isomer, for example, stabilizes them differently, α_2 being still more stable than α_1 by 2.2 kcal mol⁻¹. The larger nucleophilicity of the α_1 vacancy explains the reduction of the energy gap between both forms.

Table 10.1 collects the energy differences obtained at the DFT level between the two isomers of each compound in several oxidation states.

A single pattern is observed for all the compounds, that is, as electrons are added, the α_1 isomer gains stability relative to α_2 , so the α_1/α_2 relative stability depends on the oxidation state of the system.

It comes out that the first electrons added to the fully oxidized POMs occupy d_{xy}-like orbitals, particularly belonging to the substituting M ion in the present case. This orbital is mainly nonbonding and populating it with one or two electrons has minor structural changes. The origin of the differences observed may be understood from the energies and compositions of the molecular orbitals involved in the process of reduction (see Fig. 10.3 for P₂V^VW₁₇ as an example). The energy of a reduction process changes as a function of the region (*cap* or *belt*) accepting the incoming electron. In the series herein discussed, for the fully oxidized compounds (d⁰ metals), the energy differences between isomers, $\Delta E(\alpha_2-\alpha_1)$, range from -2.2 for Re^{VII} to +1.0 kcal mol⁻¹ for V^V. Other d⁰ compounds feature intermediate $\Delta E(\alpha_2-\alpha_1)$ values. In general, the fully oxidized α_1 and α_2 structures containing M ions are quasi degenerate (as for P₂V^VW₁₇) or slightly favor the α_1 isomer (the case of Re^{VII} and Mo^{VI} ions).

To compare or predict experimental redox potentials using theoretical methods, absolute reduction potentials have to be first computed and made relative to the normal hydrogen electrode (NHE). The absolute reduction potential for this process

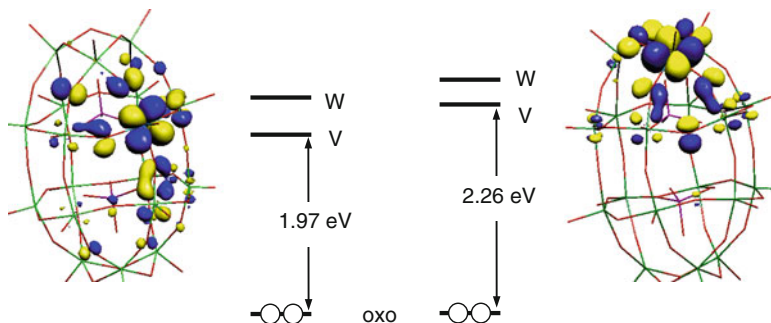


Fig. 10.3 Sequence of molecular orbitals involved in the redox processes, and the highest occupied oxo-like orbital, together with a 3D representation of the lowest unoccupied molecular orbital (LUMO) for α_1 - (left) and α_2 -P₂V^VW₁₇. The atomic symbol represents the main character of the orbitals. The region where the orbital representations take larger values denotes the position of substitution

($H^+ + e^- \rightarrow \frac{1}{2}H_2$) has been estimated to be +4.28 eV [23], and is related to its free energy change ΔG° by the Nernst equation. So, to predict the reduction potential of a given process we need to compute the free energy change, and then combine it with that of NHE [24]. We have computed the reduction energies taking into account the solvation effects computationally. For the present case, we calculated the energies for the process $POM(ox)_{aq} + e^-_{gas} \rightarrow POM(red)_{aq}$, where the free electron is considered in the gas phase since its energy can be taken as zero.

As electrons are successively added to the structures, α_1 isomers are progressively stabilized relative to α_2 since the former isomer invariably feature lower accepting orbitals. After the first reduction (d^1 compounds), only the Re^{VI} derivative of α_1 gets more stable than α_1 by 2.5 kcal mol⁻¹. The V^{IV} derivative presents the largest $\Delta E(\alpha_2-\alpha_1)$ with +4.4 kcal mol⁻¹ after the first reduction step. From the fully oxidized forms, all the $\Delta E(\alpha_2-\alpha_1)$ values have shifted to more positive values. For the d^2 compound computed, Re^V, $\Delta E(\alpha_2-\alpha_1) = +8.2$ kcal mol⁻¹. In d^3 configuration (P₂Re^{IV}W₁₇), the energy difference achieves +16.4 kcal mol⁻¹. If we compare different compounds with a given number of d electrons we find that total higher negative charges of the Dawson anion favor α_1 isomers. That is, the relative stability of α_1 augments in the order Re^{VI} < Mo^V < V^{IV}.

The trends found in the relative stability of the isomers have been rationalized in base to the electronic structure of each compound. As expected from the orbital energies and compositions, all the compounds are reduced in a $d(M)$ orbital. When electrons occupy an empty orbital belonging to the substituting M atom, the reduction energy (RE), as occurs in V, Mo or Re derivatives, depends on the position of M. The reduction energy can be considered as $-EA$ (electron affinity) of the anion in solution. The nature of cap and belt positions makes all α_1 isomers be more oxidant than α_2 . The REs are always more exothermic in substituted α_1 forms by ca. 180–250 meV (DFT) and by ca. 85–200 meV (experiments), as shown in Table 10.2. The energy difference between isomers tends to be overestimated

Table 10.2 Computed reduction energies (REs) and experimental reduction free energies, ΔG_{red} , in eV, $\Delta\text{RE}(\alpha_2-\alpha_1)$ and $\Delta\Delta G_{\text{red}}(\alpha_2-\alpha_1)$, in meV, for α_1/α_2 -[P₂W₁₇O₆₁MO]⁹⁻ compounds

M		DFT		Experimental		Ref.
		RE	$\Delta\text{RE}(\alpha_2-\alpha_1)$	ΔG_{red}	$\Delta\Delta G_{\text{red}}(\alpha_2-\alpha_1)$	
W ^{VI}	α_1	-4.40	+290	-4.58		[25]
	α_2	-4.12				
Mo ^{VI}	α_1	-4.55	+196	-4.92	+170	[26]
	α_2	-4.35	-4.75			
V ^V	α_1	-4.40	+180	-5.00	+85	[27]
	α_2	-4.22	-4.92			
Re ^{VII}	α_1	-4.88	+200	-5.26	+170	[28]
	α_2	-4.68	-5.09			
Re ^{VI}	α_1	-4.65	+250	-4.92	+200	[28]
	α_2	-4.40	-4.72			

at the DFT level – remarkably for the vanadate in the present study – but the trends are correct. The ranges shown are quite small (70 and 115 meV for DFT and CVs, respectively) indicating that the computed $\Delta\text{RE}(\alpha_2-\alpha_1)$ and its experimental homologue $\Delta\Delta G_{\text{red}}(\alpha_2-\alpha_1)$ are hardly affected by the substituting metal, M. On the other hand, the absolute REs (theoretical and experimental) are much more dependent on M, varying in a range of 500 meV, and especially on their oxidation states. For instance, reduction of the V^VW₁₇ derivative gives -4.40 vs. -4.88 eV for Re^{VII}W₁₇ at the DFT level. Given that the overall molecular charge depends on the oxidation state of M, the absolute REs are mainly governed by the substituting metal ion. It must be stressed again that these differences are, in general, smaller in CVs compared to DFT.

10.3 Rotational Isomers

Six isomers for the [X₂M₁₈O₆₂]⁶⁻ anion (X = As^V, P^V; M = Mo^{VI}, W^{VI}) were postulated in 1970 by Baker and Figgis, depicted in Fig. 10.4 and named α , β , γ and α^* , β^* , γ^* [29].

The α -[X₂M₁₈O₆₂]⁶⁻ anion is built up from two A- α -XM₉O₃₄ halves connected by six common oxygen atoms lying on a mirror plane. The whole anion belongs to the *D*_{3h} point group [30]. The β anion is formally related to the α isomer by a $\pi/3$ rotation of a polar M₃O₁₃ group, then the symmetry is lowered to *C*_{3v}. A second $\pi/3$ rotation of another polar M₃O₁₃ group restores the plane of symmetry and the *D*_{3h} symmetry for the γ isomer. In all these anions the hexagonal belts of both XM₉ moieties appear in eclipsed conformation along the direction of the *C*₃ axis. If the two A- α -XM₉O₃₄ subunits are related through an inversion center, as postulated by Wells [31] in 1945 for P₂W₁₈O₆₂, the resulting anion named α^* would belong to

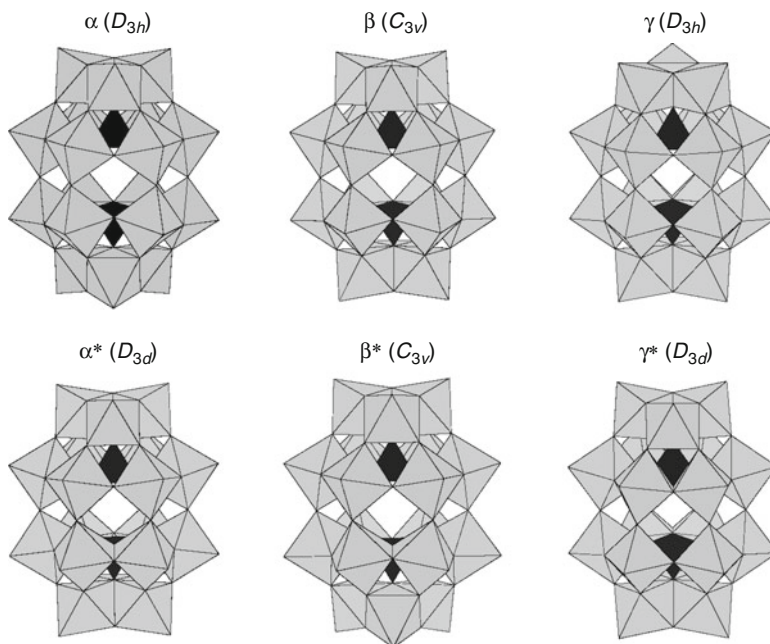


Fig. 10.4 The six rotational isomers of the Dawson structure. *Top:* α , β , γ . *Bottom:* α^* , β^* , γ^*

Table 10.3 Experimentally detected Dawson $[X_2M_{18}O_{62}]^{q-}$ isomers

Isomer	M = Mo	M = W	Ref.
α	P, As, S	P, As	[33, 34]
β		P, As	[35]
γ		P, As	[36]
α^*			
β^*			
γ^*		As, S	[37]

the D_{3d} point group. Rotation of one or both polar M_3O_{13} groups of the α^* anion generates the two remaining isomers, β^* (C_{3v}) and γ^* (D_{3d}), respectively. In that case the hexagonal belts of both XM_9 moieties are staggered along the direction of the C_3 axis. As depicted in Table 10.3, only α , β , γ and γ^* isomers have been detected and crystallographically resolved [32].

In a previous study we used DFT calculations to analyze the relative stability of the α and β isomers of the Dawson heteropolyanions [10]. Here, as an expansion of that previous work, we extend the investigation towards γ and α^* , β^* , γ^* isomers. We will discuss the structural and stability properties of α , β , γ and α^* , β^* , γ^* isomers of the $[As_2W_{18}O_{62}]^{6-}$ anion. All the isomers were computed under each correspondent symmetry constraints. For instance, α isomer of As_2W_{18} was computed under the constraints of D_{3h} symmetry group, whereas for the corresponding β isomer the symmetry of the molecule is C_{3v} , etc. The results in

Table 10.4 Relative energies with respect to the most stable $[\text{As}_2\text{W}_{18}\text{O}_{62}]^{6-}$ isomer

Isomer	Symmetry	Solvent (kcal mol ⁻¹)	In vacuum (kcal mol ⁻¹)
α	D_{3h}	1.1	3.5
β	C_{3v}	2.4	3.9
γ	D_{3h}	0.6	1.2
α^*	D_{3d}	16.5	17.5
β^*	C_{3v}	6.5	6.9
γ^*	D_{3d}	0.0	0.0

Table 10.5 Relative energies for $[\text{W}_{18}\text{O}_{54}(\text{XO}_4)_2]^{q-}$ where X = As, P and S and for the $[\text{W}_{18}\text{O}_{54}]$ box

Isomer	Symmetry	$[\text{W}_{18}\text{O}_{54}]$	$[\text{W}_{18}\text{O}_{54}(\text{AsO}_4)_2]^{6-}$ (kcal mol ⁻¹)	$[\text{W}_{18}\text{O}_{54}(\text{PO}_4)_2]^{6-}$ (kcal mol ⁻¹)	$[\text{W}_{18}\text{O}_{54}(\text{SO}_4)_2]^{4-}$ (kcal mol ⁻¹)
α	D_{3h}	0.3	1.1	0.0	0.0
β	C_{3v}	3.3	2.4	5.2	3.6
γ	D_{3h}	0.0	0.6	5.4	3.7
α^*	D_{3d}	3.3	16.5	22.1	16.7
β^*	C_{3v}	0.1	6.5	12.6	7.0
γ^*	D_{3d}	3.3	0.0	7.5	1.9

Table 10.4 are relative to the most stable isomer *in vacuum* and also including the effect of the solvent through a continuum model. In both cases we have obtained the same stability trend being γ^* the most stable isomer and α^* the less stable. These results are consistent with the experimental observed species: γ^* isomer has been detected while isomers α^* and β^* have not.

We have also studied how the stability of the isomer can be modulated by the presence of different heteroatoms. As a first step, we have evaluated the relative stability of the isomers considering only the $[\text{W}_{18}\text{O}_{54}]$ cage without the internal anions $[(\text{XO}_4)_2]^{q-}$. As shown in Table 10.4, there are two groups with different stability order: isomers α , γ , β^* and around 3 kcal mol⁻¹ less stable we have isomers β , α^* and γ^* . The relative stability of the polyoxometalate isomers is significantly altered after encapsulating the two $[\text{XO}_4]$ anions.

When X = As, the relative energy of the four isomers γ^* , γ , α and β was found to differ in less than 2.5 kcal mol⁻¹. Indeed, these four isomers have been characterized experimentally (see Table 10.3). Isomer β^* appears at 6.5 kcal mol⁻¹ above the lowest-energy isomer (γ^*) (Table 10.5).

For $[\text{P}_2\text{W}_{18}\text{O}_{62}]^{6-}$ the results are slightly different: here the most stable isomer is α , that is around 5 kcal mol⁻¹ more stable than isomers β and γ . In this case the stability order is $\alpha > \beta > \gamma$. Again this agrees with the experimentally obtained isomers. Finally, for the case X = S, we have found that the stability order is $\alpha > \gamma^* > \beta > \gamma$. In fact, γ^* is the only isomer experimentally resolved for the Dawson anion $[\text{S}_2\text{W}_{18}\text{O}_{62}]^{4-}$. Knowing that isomers α and γ^* have a difference of only 1.9 kcal mol⁻¹, we can expect a thermodynamically favorable synthesis of α - $[\text{S}_2\text{W}_{18}\text{O}_{62}]^{4-}$. A graphical representation of the relative isomer energies is given in Fig. 10.5.

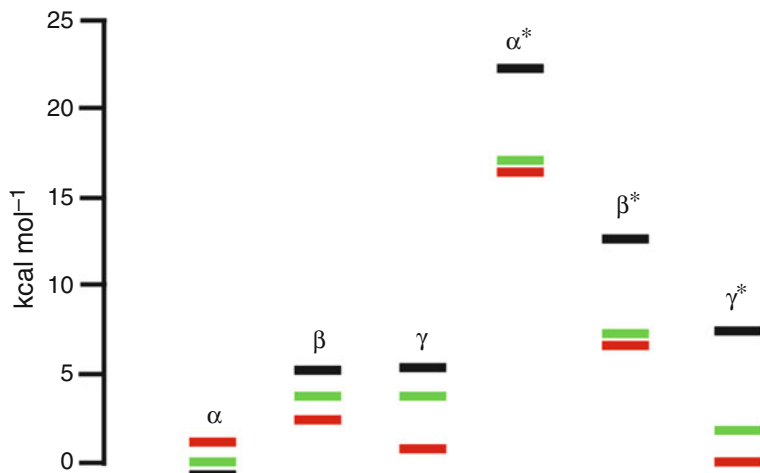


Fig. 10.5 Graphical representation of relative energies with respect to the most stable isomer for $[W_{18}O_{54}(XO_4)_2]^{9-}$ where X = As (red), P (black) and S (green) (Color figure online)

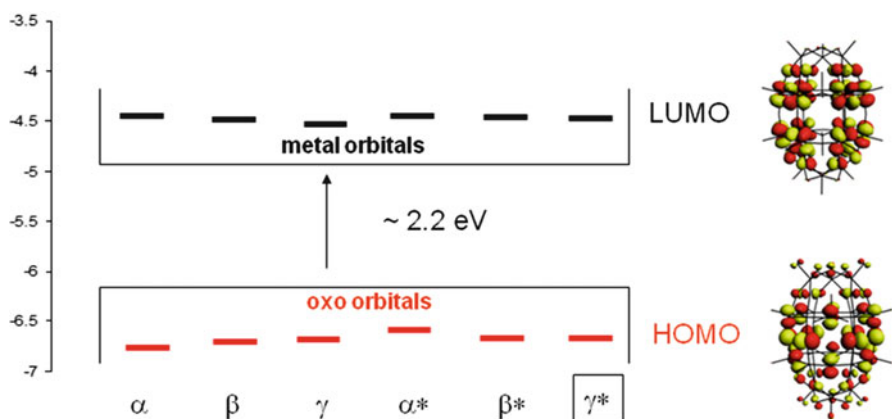


Fig. 10.6 Graphical representation of orbital energies HOMO-LUMO for the six isomers α , β , γ , α^* , β^* , γ^* when X = As, $[As_2W_{18}O_{62}]^{6-}$. As an example, we have also depicted 3D orbitals for isomer γ^* (D_{3d}): HOMO (orbital of symmetry A_{2u} , mainly composed of p-oxygen orbitals delocalized over oxygen bridge, belt and terminal atoms) and LUMO (orbital of A_{1u} symmetry, mainly composed of d-metal orbitals delocalized over the metal belt atoms)

The structural differences among isomers are not significant: we have obtained differences $<29.9^\circ$ for angles and $<0.8 \text{ \AA}$ for distances. As a final point, we have also compared the HOMO-LUMO gaps for several isomers, as shown in Fig. 10.6 for the case of $[As_2W_{18}O_{62}]^{6-}$. As it is common for POMs the HOMO orbitals correspond to oxygen atoms and LUMO orbitals correspond to metal atoms. When X = As the HOMO-LUMO gap is around 2.2 eV for all isomers, the same trend was observed when X = P and S, the results are not presented here.

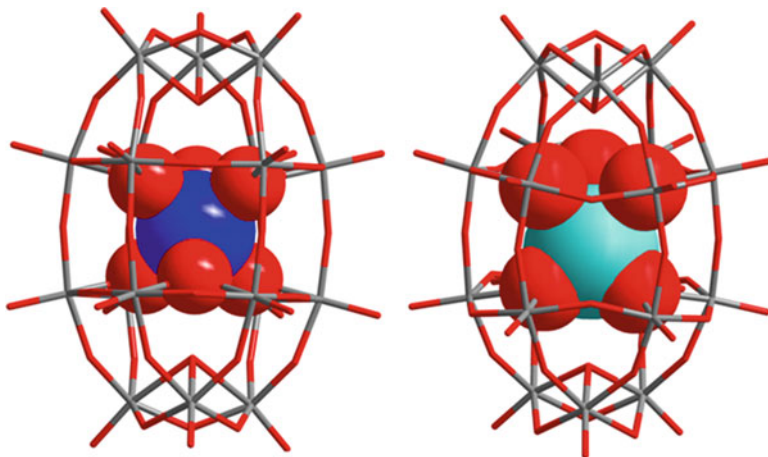


Fig. 10.7 Structures of the new Dawson-like $\{W_{18}X\}$ POM type, the $\{W_{18}\}$ cages are shown as *sticks* and the central $\{XO_6\}$ group is represented as space filling model. *Left:* $\gamma^*-[W_{18}O_{56}(XO_6)]^{10-}$ $X = W^{VI}$ and Te^{VI} . *Right:* $\beta^*-[W_{18}O_{56}(IO_6)]^{9-}$ being the first example of β^* isomer

Conventionally, redox-inactive anions, such as SO_4^{2-} and PO_4^{3-} , are often used as templating anions in the formation of many POM clusters. A strategy to create new functional POMs involves the encapsulation of redox-active templates instead. By utilizing sulfite, selenite, tellurite, and periodate anions as templates, several new types of redox-active heteropolyoxometallates have been isolated. The POM cluster $[M_{18}O_{54}(SO_3)_2]^{3-}$ ($M = W, Mo$), which contains two embedded redox-active sulfite templates, can be activated by a metallic surface and can reversibly interconvert between two electronic states [38]. Both templates can be replaced by a single template located in the centre of the cluster to give a Dawson-like $\{W_{18}X\}$ POM [39]. The first member of this family to be discovered was actually an isopolyanion $\{W_{19}\}$ with a Dawson-type cage; the nineteenth tungsten is located at the centre of the cluster instead of the two tetrahedral heteroatoms that are usually found inside conventional Dawson clusters [40]. Structural analysis of the cluster shows that the internal tungsten ion could be replaced by other elements, such as Pt^{IV} , Sb^V , Te^{VI} , or I^{VII} . The POMs $\beta^*-[H_3W_{18}O_{56}(IO_6)]^{6-}$, with an embedded high-valent iodine [37], and $\gamma^*-[H_3W_{18}O_{56}(TeO_6)]^{7-}$, that captures the tellurate anion TeO_6^{6-} , were discovered thereafter (Fig. 10.7) [41].

It is worth mentioning that the presence of the $[IO_6]$ unit inside the $\{W_{18}\}$ cage is able to stabilize the β^* cage, which was found rather high in energy in conventional Dawson anions. The full analysis of isomerism in these Dawson-like anions is much more complex because of the presence of protons. Redox properties and their influence in the isomerism stability is also an interesting issue that should be understood from experiments and theory in incoming years.

Acknowledgements This work was supported by the Spanish MCINN (CTQ2008-06549-C02-01/BQU), the Generalitat de Catalunya (2009SGR-00462) and the XRTQC. X. L. thanks the Ramón y Cajal program (RYC-2008-02493).

References

1. Pope MT, Müller A (1991) Polyoxometalate chemistry: an old field with new dimensions in several disciplines. *Angew Chem Int Ed* 30:34–48
2. Hill CL (ed) (1998) Introduction: polyoxometalates—multicomponent molecular vehicles to probe fundamental issues and practical problems. *Chem Rev* 98:1–390
3. Long D-L, Burkholder E, Cronin L (2007) Polyoxometalate clusters, nanostructures and materials: from self assembly to designer materials and devices. *Chem Soc Rev* 36:105–121
4. Long D-L, Tsunashima R, Cronin L (2010) Polyoxometalates: building blocks for functional nanoscale systems. *Angew Chem Int Ed* 49:1736–1578
5. Pope MT (1983) *Heteropoly and isopolyoxometalates*. Springer, Berlin
6. (a) Dawson B (1953) The structure of the 9(18)-heteropoly anion in potassium 9(18)-tungstophosphate, $K_6(P_2W_{18}O_{62}) \cdot 14H_2O$. *Acta Crystallogr* 6:113–126; (b) D'Amour H (1976) Vergleich der heteropolyanionen $[PMo_9O_{31}(H_2O)_3]^{3-}$, $[P_2Mo_{18}O_{62}]^{6-}$ und $[P_2W_{18}O_{62}]^{6-}$. *Acta Crystallogr B Struct Crystallogr Cryst Chem* 32:729–740
7. See, for example, (a) Wells AF (1947) *Structural inorganic chemistry*, 1st ed, Clarendon Press, Oxford; (b) Hori T, Tamada O, Himeno S (1989) The structure of 18-molybdo-disulphate(VI)(4-) ion in $(NEt_4)_4S_2Mo_{18}O_{62} \cdot CH_3CN$. *J Chem Soc Dalton Trans* 8:1491–1497; (c) Contant R, Thouvenot R (1991) Hétéropolyanions de type Dawson. 2. Synthèses de polyoxotungstoarsénates lacunaires dérivant de l'octadécaturstodiansénate. Étude structurale par RMN du tungstène-183 des octadéca(molybdotungstovanado)diarsénates apparentés. *Can J Chem* 69:1498–1506; (d) Contant R, Thouvenot R (1993) A reinvestigation of isomerism in the Dawson structure: syntheses and ^{183}W NMR structural characterization of three new polyoxotungstates $[X_2W_{18}O_{62}]^{6-}$ ($X=P^V, As^V$). *Inorg Chim Acta* 212:41–50; (e) Himeno S, Tatewaki H, Hashimoto M (2001) Synthesis, structure, and characterization of an alpha-Dawson-type $[S_2W_{18}O_{62}]^{4-}$ complex. *Bull Chem Soc Jpn* 64:1623–1631; (f) Contant R, Fruchart J-M (1974) Investigation, in solution, of reduced 18-molybdo-2-arsenates and 18-molybdo-2-phosphates (alpha and beta) *Rev Chim Miner* 11:123–140; (g) Richardt PJS, Gable RW, Bond AM, Wedd AG (2001) Synthesis and redox characterization of the polyoxo anion, $\gamma^*-[S_2W_{18}O_{62}]^{4-}$: a unique fast oxidation pathway determines the characteristic reversible electrochemical behavior of polyoxometalate anions in acidic media. *Inorg Chem* 40:703–709
8. López X, Bo C, Poblet JM (2002) Electronic properties of polyoxometalates: electron and proton affinity of mixed-Addenda Keggin and Wells-Dawson anions. *J Am Chem Soc* 124:12574–12582
9. Keita B, Levy B, Nadjo L, Contant R (2002) Toward a qualitative understanding of the initial electron transfer site in Dawson-type heteropolyanions. *New J Chem* 26:1314–1319
10. López X, Bo C, Poblet JM (2003) Relative Stability in α - and β -Wells–Dawson heteropolyanions: a DFT study of $[P_2M_{18}O_{62}]^{n-}$ ($M = W$ and Mo) and $[P_2W_{15}V_3O_{62}]^{n-}$. *Inorg Chem* 42:2634–2638
11. (a) Rohmer M-M, Ermenwein R, Ulmschneider M, Wiest R, Bénard M (1991) Ab initio SCF calculations on $[V_{10}O_{28}]^{6-}$: a benchmark for the classical calculation and processing of molecular integrals on large Gaussian basis sets. *Int J Quantum Chem* 40:723–743; (b) Kempf JY, Rohmer M-M, Poblet JM, Bo C, Bénard M (1992) Relative basicities of the oxygen sites in $[V_{10}O_{28}]^{6-}$. *J Am Chem Soc* 114:1136–1146; (c) Rohmer M-M, Bénard M (1994) An interpretation of the structure of the inclusion complexes $[RCN.cntnd.(V_{12}O_{32})^{4-}]$ ($R = CH_3, C_6H_5$) from electrostatic potentials. *J Am Chem Soc* 116:6959–6960

12. Poblet JM, López X, Bo C (2003) Ab initio and DFT modelling of complex materials: towards the understanding of electronic and magnetic properties of polyoxometalates. *Chem Soc Rev* 32:297–308
13. López X, Maestre JM, Bo C, Poblet JM (2001) Electronic properties of polyoxometalates: a DFT study of α/β - $[\text{XM}_{12}\text{O}_{40}]^{n-}$ Relative stability (M=W, Mo and X=main group elements). *J Am Chem Soc* 123:9571–9576
14. Kozik M, Hammer CF, Baker LCW (1986) Direct determination by ^{183}W NMR of the locations of added electrons in ESR-silent heteropoly blues. Chemical shifts and relaxation times in polysite mixed-valence transition-metal species. *J Am Chem Soc* 108:2748–2749
15. Kozik M, Baker LCW (1990) Electron exchange reactions between heteropoly anions: comparison of experimental rate constants with theoretically predicted values. *J Am Chem Soc* 112:7604–7611
16. Acerete R, Harmalker S, Hammer CF, Pope MT, Baker LCW (1979) Concerning isomerisms and interconversions of 2:18 and 2:17 heteropoly complexes and their derivatives. *J C S Chem Commun* 777–779
17. Ciabrini JP, Contant R, Fruchart JM (1983) Heteropolyblues: relationship between metal-oxygen-metal bridges and reduction behaviour of octadeca(molybdotungsto)diphosphate anions. *Polyhedron* 2:1229–1233
18. (a) Contant R, Abbessi M, Canny J, Belhouari A, Keita B, Nadjo L (1997) Iron-substituted Dawson-type tungstodiphosphates: synthesis, characterization, and single or multiple initial electronation due to the substituent nature or position. *Inorg Chem* 36:4961–4967; (b) Keita B, Belhouari A, Nadjo L, Contant R (1998) New electroactive metal oxides electrodeposited from selected Keggin and Dawson-type heteropolyanions. *J Electroanal Chem* 442:49–57; (c) Contant R, Richet M, Lu YW, Keita B, Nadjo L (2002) Isomerically pure alpha(1)-monosubstituted tungstodiphosphates: synthesis, characterization and stability in aqueous solutions. *Eur J Inorg Chem* 2587–2593 263
19. Keita B, Girard F, Nadjo L, Contant R, Canny J, Richet M (1999) Metal ion complexes derived from the alpha(1) isomer of (P2W17O61)(10-): comparison with the corresponding alpha(1) species. *J Electroanal Chem* 478:76–82
20. Ciabrini J-P, Contant R (1993) Mixed heteropolyanions. Synthesis and formation constants of Cerium(III) and Cerium(IV) complexes with lacunary tungstophosphates. *J Chem Res (M)* 2720–2744
21. Qu LY, Shan QJ, Gong J, Lu RQ, Wang DR (1997) Synthesis, properties and characterization of Dawson-type tungstophosphate heteropoly complexes substituted by titanium and peroxotitanium. *J Chem Soc Dalton Trans* 23:4525–4528
22. Park DR, Park S, Choi JH, Song IK (2010) Acidity of group 5 metal (V, Nb, Ta)-substituted Keggin and Wells-Dawson heteropolyacid (HPA) catalysts and their application to esterification of acetic acid with ethanol. *Catal Lett* 135:269–274
23. Lewis A, Bumpus JA, Truhlar DG, Cramer CJ (2004) Molecular modeling of environmentally important processes: reduction potentials. *J Chem Edu* 81:596–603 and corrections in 2007, 84:934
24. Fernández JA, López X, Bo C, de Graaf C, Baerends EJ, Poblet JM (2007) Polyoxometalates with internal cavities: redox activity, basicity and cation encapsulation in $[\text{X}^{n+}\text{P}_5\text{W}_{30}\text{O}_{110}]^{(15-n)-}$ Preyssler complexes, with $\text{X}=\text{Na}^+$, Ca^{2+} , Y^{3+} , La^{3+} , Ce^{3+} and Th^{4+} . *J Am Chem Soc* 129:12244–12253
25. Pope MT, Papaconstantinou E (1967) Heteropoly blues. II. Reduction of 2:18-tungstates. *Inorg Chem* 6:1147–1152
26. Himeno S, Takamoto M (2002) Difference in voltammetric properties between the Keggin-type $[\text{XW}_{12}\text{O}_{40}]^{(n-)}$ and $[\text{XMo}_{12}\text{O}_{40}]^{(n-)}$ complexes. *J Electroanal Chem* 528:170–174
27. Harmalker SP, Leparulo MA, Pope MT (1983) Mixed-valence chemistry of adjacent vanadium centers in heteropolytungstate anions. I. Synthesis and electronic structures of mono-, di-, and trisubstituted derivatives of α - $[\text{P}_2\text{W}_{18}\text{O}_{62}]^{6-}$. *J Am Chem Soc* 105:4286–4292

28. Venturelli A, Nilges MJ, Smirnov A, Belford RL, Francesconi LC (1999) Synthesis and characterization of Re^{V} , Re^{VI} and Re^{VII} complexes of the α_2 - $[\text{P}_2\text{W}_{17}\text{O}_{61}]^{10-}$ isomer. *J Chem Soc Dalton Trans* 3:301–310
29. Baker LCW, Figgis JS (1970) New fundamental type of inorganic complex: hybrid between heteropoly and conventional coordination complexes. Possibilities for geometrical isomerisms in 11-, 12-, 17-, and 18-heteropoly derivatives. *J Am Chem Soc* 92:3794–3797
30. Herve G, Tézé A (1977) Study of α - and β -enneatungstosilicates and germanetes. *Inorg Chem* 6:2115–2117
31. Wells AF (1945) *Structural inorganic chemistry*. Oxford University Press, Oxford
32. Pope MT (2003) *Comprehensive coordination chemistry II*. Pergamon, Oxford
33. Himeno S, Hori T, Saito A (1989) Spectroscopic and electrochemical characterization of 18-molybdodisulfate(VI)(4-), $\text{S}_2\text{Mo}_{18}\text{O}_{62}^{4-}$. *Bull Chem Soc Jpn* 62:2184–2188
34. Hori T, Tamada O, Himeno S (1989) The structure of 18-molybdodisulphate (VI) (4-) ion in $(\text{NET}_4)_4\text{S}_2\text{Mo}_{18}\text{O}_{63}\text{CH}_3\text{CN}$. *J Chem Soc Dalton Trans* 8:1491–1497
35. (a) Maksimovskaya RI, Maksimov GM (1995) Thermal transformations of heteropoly acid α - $\text{H}_6\text{P}_2\text{W}_{18}\text{O}_{62}$ center dot NH_2O by P^{31} NMR. *Russ J Inorg Chem* 40:1363–1368; (b) Maksimovskaya RI, Maksimov GM (1995) Identification of γ -isomer of heteropoly anion $\text{P}_2\text{W}_{18}\text{O}_{62}^{6-}$ BY P^{31} , W^{183} , and O^{17} NMR. *Russ J Inorg Chem* 40:1369–1371
36. Contant R, Thouvenot R (1993) A reinvestigation of isomerism in the Dawson structure: syntheses and ^{183}W NMR structural characterization of three new polyoxotungstates $[\text{X}_2\text{W}_{18}\text{O}_{62}]^{6-}$ ($\text{X}=\text{P}^{\text{V}}$, As^{V}). *Inorg Chem Acta* 212:41–50
37. (a) Acerte R, Hammer C, Baker LC (1984) Reinterpretations, based on tungsten-183 NMR spectra, of several heteropolytungstates derived from the Wells-Dawson “2:18” structure. Preparation and structure proof for the first γ -Isomer of a 2:18 complex. *Inorg Chem* 23:1478–1482; (b) Neubert H, Fuchs JZ (1987) Crystal structures and vibrational spectra of two isomers of octadecatungsto-diarsenate $(\text{NH}_4)_6\text{As}_2\text{W}_{18}\text{O}_{62}\cdot n\text{H}_2\text{O}$. *Z Naturforsch B Chem Sci* 42:951–958; (c) Richardt PJS, Gable RW, Bond AM, Wedd AG (2001) Synthesis and redox characterization of the polyoxo anion, γ^* - $[\text{S}_2\text{W}_{18}\text{O}_{62}]^{4-}$: a unique fast oxidation pathway determines the characteristic reversible electrochemical behavior of polyoxometalate anions in acidic media. *Inorg Chem* 40:703–705
38. (a) Fleming C, Long D-L, McMillan N, Johnston J, Bovet N, Dhanak V, Gadegaard N, Kögerler P, Cronin L, Kadodwala M (2008) Reversible electron-transfer reactions within a nanoscale metal oxide cage mediated by metallic substrates. *Nat Nanotechnol* 3:229–233; (b) Fay N, Bond AM, Baffert C, Boas JF, Pilbrow JR, Long D-L, Cronin L (2007) Structural, electrochemical, and spectroscopic characterization of a redox pair of sulfite-based polyoxotungstates: a - $[\text{W}_{18}\text{O}_{54}(\text{SO}_3)_2]^{4-}$ and a - $[\text{W}_{18}\text{O}_{54}(\text{SO}_3)_2]^{5-}$. *Inorg Chem* 46:3502–3510
39. Long D-L, Song YF, Wilson EF, Kögerler P, Guo SX, Bond AM, Hargreaves JSJ, Cronin L (2008) Capture of periodate in a $\{\text{W}_{18}\text{O}_{54}\}$ cluster cage yielding a catalytically active polyoxometalate $[\text{H}_3\text{W}_{18}\text{O}_{56}(\text{IO}_6)]^{6-}$ embedded with high valent iodine. *Angew Chem Int Ed* 47:4384–4387
40. Long DL, Kögerler P, Parenty ADC, Fielden J, Cronin L (2006) Discovery of a fundamentally new family of isopolyoxo-tungstates, $[\text{H}_4\text{W}_{19}\text{O}_{62}]^{6-}$, encapsulating a $\{\text{WO}_6\}$ moiety within a $\{\text{W}_{18}\}$ Dawson-like cluster cage. *Angew Chem Int Ed* 45:4798–4803
41. Yan J, Long D-L, Wilson EF, Cronin L (2009) Discovery of heteroatom ‘embedded’ Te $\{\text{W}_{18}\text{O}_{54}\}$ Nano- functional polyoxometalates using cryospray mass spectrometry. *Angew Chem Int Ed* 48:4376–4380

Chapter 11

Homogeneous Computational Catalysis: The Mechanism for Cross-Coupling and Other C-C Bond Formation Processes

Christophe Gourlaouen, Ataulpa A.C. Braga, Gregori Ujaque,
and Feliu Maseras

Abstract The application of modern density functional theory techniques to the computational study of palladium-catalyzed C-C formation reactions has led to a better mechanistic understanding of these processes of fundamental interest in organic chemistry. This chapter reviews the main contributions to the topic, analyzing the current knowledge on the different reaction steps: oxidative addition, transmetalation, metalation, reductive elimination and isomerization. A special emphasis is placed on the metalation step, which is specific of C-C bond formation processes.

11.1 Introduction

The construction of complex organic molecules from simple building fragments is based in the availability of simple and reliable processes leading to the formation of carbon-carbon bonds. Cross-coupling reactions are among the most widely used

C. Gourlaouen • A.A.C. Braga
Institute of Chemical Research of Catalonia (ICRC), Av. Països Catalans, 16, 43007 Tarragona,
Catalonia, Spain

G. Ujaque
Unitat de Química Física, Edifici Cn, Universitat Autònoma de Barcelona, 08193 Bellaterra,
Catalonia, Spain

F. Maseras (✉)
Institute of Chemical Research of Catalonia (ICRC), Av. Països Catalans, 16, 43007 Tarragona,
Catalonia, Spain

Unitat de Química Física, Edifici Cn, Universitat Autònoma de Barcelona, 08193 Bellaterra,
Catalonia, Spain
e-mail: fmaseras@icq.es

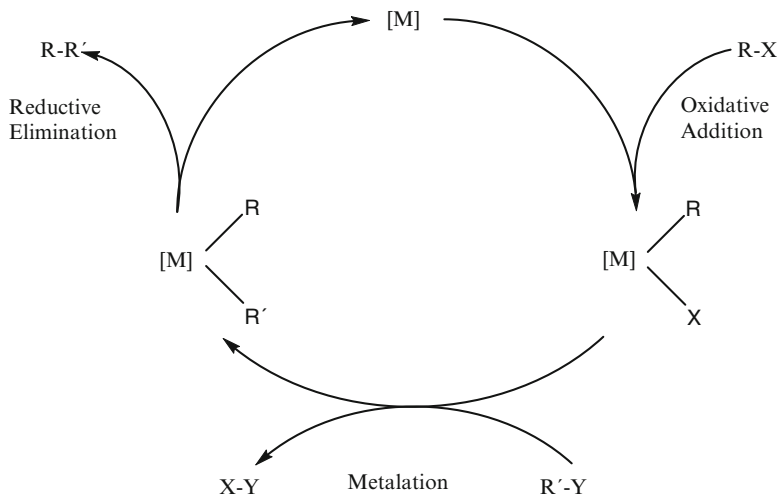
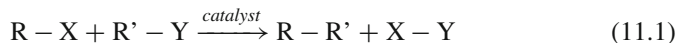


Fig. 11.1 Generally accepted overall mechanism for cross-coupling and arylation reactions

methods for the formation of carbon-carbon bonds, and are thus a fundamental tool in organic synthesis [1]. Most cross-coupling processes respond to the general formula:



where R and R' are organic groups (often at least one of them is an aryl), X is a good leaving group (often halide or triflate), and the catalyst is a transition metal complex (often a palladium species with phosphine ligands). The Y group is usually attached to R' through an electropositive atom. The nature of Y decides the particular name of the cross-coupling reaction. In the Suzuki-Miyaura reaction, Y is an organoboronic acid [2]; in the Stille reaction is an organotin compound [3]; in the Negishi reaction is an organozinc compound [4], and there are other reactions where the electropositive atom is Al, Mg, Si, Cu, etc. Other related processes not responding exactly to the formula above are also classified as cross-coupling: the Heck reaction, where R'-Y is an alkene [5]; the Sonogashira reaction, where R'-Y is a terminal alkyne [6]; and the Buchwald-Hartwig reaction, where a carbon-nitrogen bond is formed [7, 8]. The direct arylation reactions [9, 10], usually not included under the cross-coupling label, would in contrast fulfill Eq. 11.1, with the particularity that R' must be an aryl, and Y must be H.

Cross-coupling reactions share this general label because of the use of similar catalysts and because they are considered to respond to the same general mechanism, shown in Fig. 11.1. The R-X molecule is first oxidatively added to the metal. Then the transmetalation step follows, where the R' group is transferred from Y to the metal, and the X group leaves the metal coordination sphere. The final step is the reductive elimination, where R and R' are bound, and the metal catalyst

recovers its initial state. Direct arylation processes follow the same general scheme, with the particularity that the intermediate step must be referred to as metalation, because hydrogen is not a metal. The existence of this general scheme does not explain all the mechanistic details. Additional species not indicated in Fig. 11.1 are often required, among them bases and salts. The catalyst is usually formed *in situ*, and its precise form is often unknown, in particular concerning the number and nature of ligands. The optimization of catalytic systems has often relied heavily in a trial-and-error approach, and a better mechanistic knowledge would be very helpful for a more rational design that would allow to better tackle a number of remaining challenges. There are still some substrates (aryl chlorides, alkyl halides) difficult to activate [11], and the topic of enantioselective cross-coupling remains largely unexplored. A number of experimental studies on the mechanism of cross-coupling reactions have been carried out [12–14], although they are limited because of the multistep nature of the reactions and the elusiveness of the intermediates. It is, in any case, clear that different behaviors seem to be present for different reactions, the role of the Y group being thus critical.

The contribution of computational chemistry to this field is relatively recent. Some calculations of full catalytic cycles have appeared in the last years for the Suzuki-Miyaura and Stille cross-coupling processes. The full catalytic cycle for the Suzuki-Miyaura reaction has been analyzed by Goossen, Thiel and co-workers for the coupling between acetic anhydride with phenylboronic acid [15, 16], and we have studied the coupling between vinyl bromide and vinylboronic acid [17]. The full catalytic cycle for the Stille reaction, assuming an associative cross-coupling, has been studied by Alvarez, de Lera and co-workers [18]. These works show complex mechanistic pictures, often with close energy competing parallel pathways. As an example, we present in Fig. 11.2 the simplified scheme obtained from our calculations for the cross-coupling between vinyl bromide and vinylboronic acid catalyzed by a palladium monophosphine species. Most of the steps shown in the scheme consist in fact of several microsteps, with different intermediates and transition states. And this scheme neglects the presence of (bis)phosphine species, which have a scheme of their own, interconnected with that presented in Fig. 11.2.

Because of the complexity of the full mechanism, most theoretical studies concentrate on particular steps of the catalytic cycle. This chapter is thus organized by the different steps of the mechanism, rather than by reaction. Oxidative addition and reduction elimination have been studied also in the context of other organometallic reactions. Transmetalation is on the other hand specific of C-C bond formation processes, and because of this, it will be discussed in more detail. Our intention in this contribution is to review the present state of the research in the area. As will be seen, a significant part of the articles mentioned have been published after 2003, indicating the current high activity on the topic. Because of this, it is impossible to provide a definitive mechanistic picture. This is rather a progress report on a very active research field. This paper complements a recent review by some of us that focused on cross-coupling [19].

Several of the articles that will be discussed occupy more than ten pages in a scientific journal. It is therefore out of question to present a detailed description of each of the intermediates and transition states that were computed. Such a

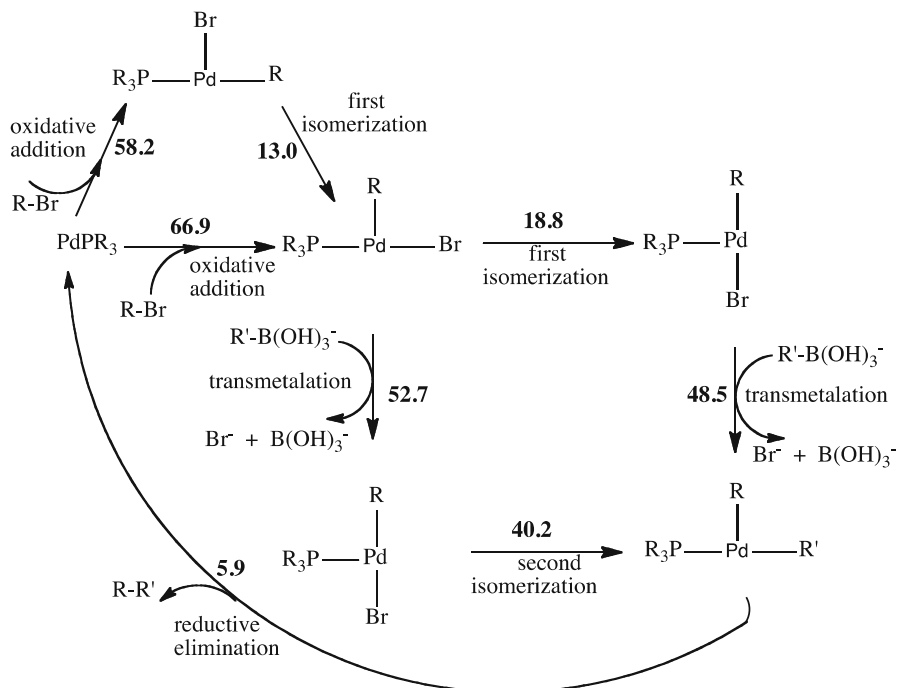
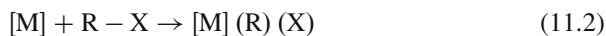


Fig. 11.2 Computed mechanism for the cross-coupling between vinyl bromide and vinyl boronic acid catalyzed by a monophosphine palladium species. The highest energy barrier involved in each reaction step is indicated in kJ/mol

description should be obtained directly from the source articles. The computational methods applied were not identical, but quite similar. The validity of the results do not seem to depend on the methodological details. The energy was in almost all cases computed using density functional theory (DFT), with a generalized gradient approach (GGA). The functional applied more often was B3LYP, although some calculations also used BP86. Basis sets had at least a valence double- ζ plus polarization quality. Solvent effects were introduced when mentioned with the polarized continuum model (PCM).

11.2 Oxidative Addition

In the oxidative addition step, the bond between the organic R group and the leaving X group breaks, and two new bonds are formed with the metal, whose oxidation state increases by two units. This is shown in Eq. 11.2:



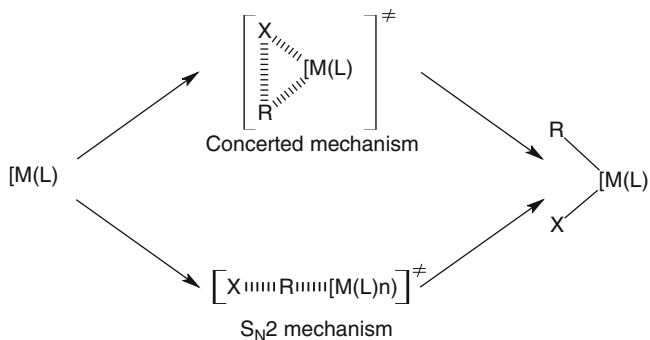


Fig. 11.3 Concerted and S_N2 transition states for oxidative addition

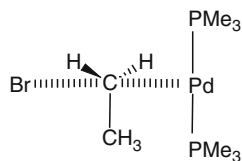
The oxidative addition of non-polar sigma bonds (H-H, C-C, C-H) to d^{10} ML_2 transition metal complexes was among the first organometallic reactions computationally studied [20–22], and was already established in the 1980s to take place in a concerted way with a mostly symmetric transition state. More recent studies on C-Ge, C-Si, Si-C, Si-H bonds confirm a similar picture [23, 24].

The specific case of polar sigma bonds, like that of aryl halides typically present in most of cross-coupling processes has been the subject of a number of recent studies. The focus of computational attention is probably related to the fact that oxidative addition has been postulated to be the rate limiting step in a number of cross-coupling reactions, although not in all of them. The final configuration of the carbon, in the case Csp^3-X , is also a critical feature for this step. This configuration is highly sensitive to experimental conditions as highlighted by Stille and Lau [25].

Theoretical calculations by Senn and Ziegler [26] discuss the existence of the two mechanisms suggested by Stille, shown in Fig. 11.3. The concerted path is similar to that involving non-polar sigma bonds and features simultaneous formation of the Pd-C and Pd-X bonds in the transition state. This is the only transition state that can be located in gas phase calculations for sp^2-X species [27]. This path leads to retention of configuration for alkyl halides. The second pathway is dissociative, and has two steps: first, the carbon is attacked by the metal and the halide anion is expelled, leaving a cationic palladium species; after, the two charged species collapse to the product. This mechanism leads to inversion of configuration of the carbon centre for alkyl halide. This second pathway has consequently been labeled as S_N2 the transition state being assumed to be similar to that reaction.

Senn and Ziegler find the dissociative pathway to be the preferred one in their calculations in THF solution of the oxidative addition of chloro-, bromo- and iodobenzene to Pd(P-P) complexes, where P-P is a chelating diphosphine ligand of the type 1,2-bis(dimethylphosphino)ethane or (P)-2,2'-bis(dimethylphosphino)-1,1'-biphenyl. The barriers from the prereaction complex are in fact quite low: 31, 12 and 5 kJ/mol for the chloro, bromo and iodo species, respectively. For methyl-(1S,5R)-5-chlorocyclohex-3-ene-1-carboxylate in presence of neutral palladium, Espinet and Echavarren observed retention of configuration in apolar solvent (benzene) and inversion in polar solvent (acetonitrile) [13].

Fig. 11.4 Transition state for S_N2 pathway in the oxidative addition of $\text{CH}_3\text{CH}_2\text{Br}$ to $\text{Pd}(\text{PMe}_3)_2$



The preference for one of the two pathways seems to depend on the particular nature of the catalyst and of the substrate. The role of anionic additive has been analyzed by different authors. Jutand and co-workers [14, 28] have provided a significant amount of experimental evidence suggesting an anionic form for the catalyst, $[\text{PdL}_n(\text{Cl})]^-$. Calculations by Bickelhaupt and co-workers [29] have shown that naked Pd favors a concerted path for the oxidative addition of Cl-CH_3 , while $[\text{PdCl}]^-$ favors the dissociative path even in gas phase. Goossen, Thiel and co-workers [30] have explored the reaction of $[\text{Pd}(\text{PMe}_3)_2(\text{OAc})]^-$ with Ph-I. The mechanism in this case is quite subtle. The acetate ligand moves away from palladium when iodobenzene coordinates and returns afterwards to the metal to displace another ligand. Two different paths of similar energies are characterized for this process. The most favored of them ends up with departure of iodide, and resembles the dissociative pathway. The least favored pathway displaces a phosphine, and the transition state associated to C-I cleavage is of a concerted type.

The nature of the substrate also influences the reaction. As mentioned in the introduction, the prototypical substrates for oxidative addition are aryl halides, but fragments different from aryl are also relevant. In fact, alkyl groups are known to be less active, and there is considerable interest in the design of catalytic systems suitable for them. Ariafard and Lin have recently carried [31] out calculations on the oxidative addition of different Br-R groups to $\text{Pd}(\text{PH}_3)_2$ and $\text{Pd}(\text{PPh}_3)_2$. Methyl, benzyl, phenyl, vinyl have been used for R group. The barriers relative to the separate fragments are lower for the systems involving sp^2 carbons than for those involving sp^3 carbons. The potential energy values are 39, 56, 77, 99 kJ/mol for vinyl, phenyl, benzyl and methyl, respectively. This result is explained by the existence of low-lying C-Br π^* orbitals in the unsaturated systems.

The use of alkyl halides has given rise to the question of control of the carbon stereochemistry configuration. The concerted mechanism (CM) would lead to retention of configuration whereas the dissociative pathway being assimilated to a S_N2 would lead to inversion. The experimental conditions (nature of the halide, solvent, steric congestion) have a major influence on the S_N2 mechanism [32]. The nature of the nucleophile, namely the donating character of the phosphines bound to the metal must also be considered.

We have recently examined these topics in a computational study [33]. Our reference system is the oxidative addition of $\text{CH}_3\text{CH}_2\text{Br}$ on $\text{Pd}(\text{PMe}_3)_2$. For this model, we found that even in the gas phase the S_N2 mechanism has a lower barrier (77 kJ/mol), than the concerted mechanism (117 kJ/mol). The structure presents the typical structure for S_N2 transition states (see Fig. 11.4), with a nearly linear arrangement of the Pd...C...Br atoms.

The effect of the solvent on the gas phase results is substantial. The S_N2 mechanism leads to ionic species whereas in the concerted mechanism the system remains neutral. Solvation in a polar solvent contributes to stabilization of the S_N2 path. This resulted for our model in a significant lowering of the S_N2 barrier from 77 to 31 kJ/mol. On the contrary the barrier for CM path arises slightly from 117 to 129 kJ/mol. The next parameter studied for the S_N2 /CM competition was the effect of substituents on the alkyl bromide. Starting from CH_3Br we analyzed the evolution of the gas phase barrier of both mechanisms when replacing sequentially each hydrogen atom by a methyl group. For the S_N2 path, the barrier increases from 77 (CH_3CH_2Br) to 92 ($(CH_3)_2CHBr$) and to 153 kJ/mol for $(CH_3)_3CBr$. In contrast, the barrier was barely affected for CM path: it changed from 106 (CH_3Br) to 117 (CH_3CH_2Br) and to 113 kJ/mol for $(CH_3)_2CHBr$.

We finally analyzed the influence of the nature of the phosphine spectator ligand. PMe_3 is a relatively electron rich phosphine. We compared its behavior with that of the less donating PH_3 phosphine and the electron deficient PF_3 group. Again, the effect was substantial for the S_N2 path. The barrier to the TS arises from 117 for PMe_3 to 144 for PH_3 and 178 kJ/mol for PF_3 . The effect on the CM path was smaller and in the opposite direction. The barrier was lowered from 117 for PMe_3 to 101 for PH_3 and to 74 kJ/mol (PF_3). Another influence of the phosphine is related to its bulkiness. In the transition state of S_N2 path, the P-Pd-P angle remains close to 180° (164° for $Pd(PMe_3)_2$ with $CH_3CHBrCH_3$), but is more closed for CM path (126°). In the presence of bulky phosphines there will be repulsion between the phosphine and the substrate (especially for S_N2) and between the phosphines themselves (mainly in the CM path). With triphenyl phosphine both angles are tighter (160° for S_N2 and 121° for CM) and the barrier is lower for CM than for S_N2 , 74 vs. 81 kJ/mol.

In summary, most of the parameters considered have a substantial effect, and the S_N2 path seems to be particularly sensitive to these influences.

Another factor affecting the oxidative addition is the number of phosphine ligands attached to the metal in the active form of the catalyst. In the case of palladium systems, the catalyst is introduced as a precursor, often as $Pd_2(dba)_3$ (dba = dibenzylideneacetone) or $[Pd(PPh_3)_4]$, however this is clearly not the active form. The diphosphine form discussed above has been postulated in most experimental proposals, and consequently used in calculations, because of the well established stability of $d^{10} ML_2$ complexes, but the monophosphine form ML can be also envisaged. On the one hand, its presence has been in fact proposed from experimental results on the activation of usually inert substrates by catalytic systems involving bulky phosphines [34, 35]. On the other hand, in a mass spectrometry study of Stille reaction [36] no monophosphine species were identified and only $Pd(P(C_6H_5)_3)_2$ containing moieties were observed on the spectrum. However, computational studies have shown that the barrier to oxidative addition of aryl bromide is lower for $Pd(PR_3)$ than for $Pd(PR_3)_2$ [37]. Norrby and co-workers have gone one step further and evaluated oxidative addition for the systems with a single ligand, either a phosphine or an anion [38, 39]. They compare the barriers for the oxidative addition of I-Ph to four different systems: $Pd(PPh_3)_2$, $Pd(PPh_3)$, $[PdCl]^-$

and $[\text{Pd}(\text{OAc})]^-$. The result is conclusive in favor of the monocoordinated species, that present barriers of 2 kJ/mol at most, in contrast with a barrier of 13 kJ/mol for $\text{Pd}(\text{PPh}_3)_2$. The precise estimation of the energy required to access these more reactive catalytic forms, however, is not trivial.

In summary, the calculations carried out on the oxidative addition step show a large variety of mechanistic possibilities, all with reasonable energy barriers. The bond cleavage itself may take place through two different competitive pathways, either concerted or dissociative. The catalyst may be in different forms concerning the number of ligands and the presence of additional anionic ligands. Finally, the nature of the organic group and the halide affect also the mechanism. The emerging global picture is that different mechanisms are likely to operate for different systems, and that there is no unequivocal choice of the oxidative addition path for cross-coupling reactions. We could in particular identify some general trends for the oxidative addition of alkyl halide species. From our results, conditions that electronically enrich the metal (donating phosphines) or stabilize the charge-separated transition state (polar solvent) will favor the $\text{S}_{\text{N}}2$ path. In contrast, substituent bulk seems to favor the concerted path.

11.3 Transmetalation

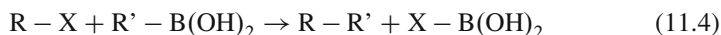
Transmetalation is the most characteristic process of the C–C cross-coupling reactions. This is the stage where the organic group R' bound to an electropositive group Y is transferred to the palladium complex, as shown in Eq. 11.3:



The comprehension of this process has been computationally addressed in recent years by several research groups. The following two subsections will summarize the available results on the Suzuki-Miyaura and Stille reactions, which are those studied in more detail. More limited studies have been also carried out in related processes, like the Heck reaction [40] and direct arylation [41, 42].

11.3.1 The Suzuki-Miyaura Reaction

The Suzuki-Miyaura reaction is one of the most used reactions in organic synthesis [1, 2]. The reaction takes place between an organic halide (or triflate), R-X , and a boronic acid, $\text{R}'\text{-B}(\text{OH})_2$, as shown in Eq. 11.4:



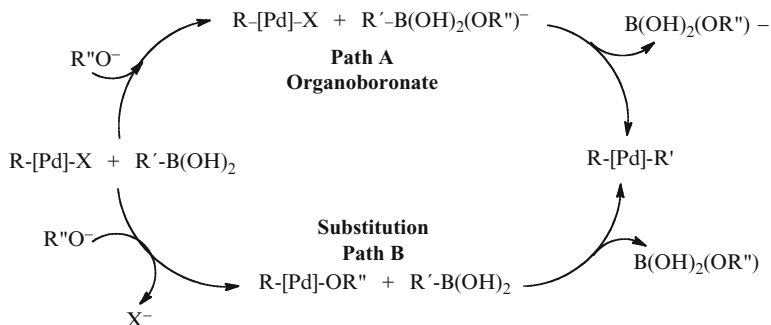


Fig. 11.5 Proposed pathways for the role of the base in the transmetalation step of the Suzuki-Miyaura cross-coupling

The key challenge for computational chemistry with respect to the transmetalation step of the Suzuki-Miyaura cross-coupling was to understand the role of the external base. It is certainly well known from experiment that the presence of a base in solution is required for the reaction to take place. Several proposals have been put forward for the role of this base from experimental studies. Most of this information was summarized by Miyaura in a very clarifying paper [43]. Two main pathways are proposed (Fig. 11.5): either the base binds the boronic acid to form the organoboronate species (path A), or the base substitutes the halide ligand in the coordination sphere of the catalyst (path B). These two proposed pathways were theoretically evaluated by us on a model system, using *trans*-PdBr(CH₂ = CH)(PH₃)₂, CH₂ = CH-B(OH)₂ and OH⁻ species as reactants [44].

In the pathway labeled as path A (shown in Fig. 11.6), the transmetalation process takes place between the organoboronate species (obtained from the reaction between the boronic acid and OH⁻) and the square planar palladium catalyst that comes from the oxidative addition of R-X to the PdL₂ catalyst. The reaction takes place in three steps: in the first step the organoboronate replaces the halide in the coordination sphere of the catalyst, subsequently there is an intramolecular substitution process where the vinyl group of the boronate replaces the OH group in the coordination sphere of the catalyst, and in the last step the proper transmetalation process takes place generating the *trans*-Pd(CH₂ = CH)₂(PH₃)₂ intermediate and the B(OH)₃ species. The energy difference between the lowest energy (-67.9 kJ/mol below reactants) and highest energy (17.6 kJ/mol above reactants) points is around 85 kJ/mol, therefore becoming a suitable pathway explaining the role of the base.

In the other proposed mechanism, labeled as path B, the base directly replaces the halide in the coordination sphere of the catalyst. Despite the computational effort devoted to look for a transition state accounting for the direct replacement of the halide by the hydroxyl group, all the attempts were fruitless. This unsuccessful search was unexpected because the ligand substitution mechanism for a square-planar complex is a generally accepted mechanism going through a trigonal bipyramid structure [45]. All the different optimizations produced either

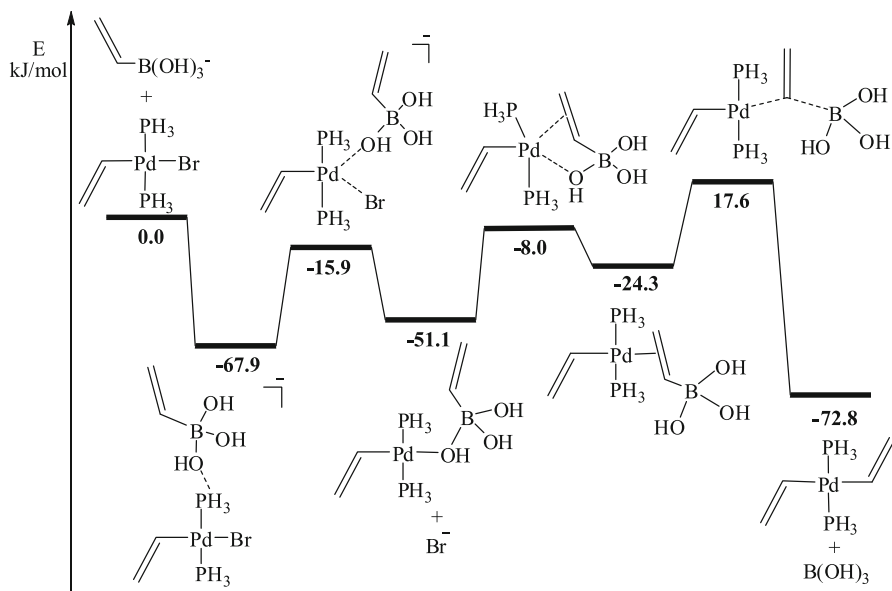


Fig. 11.6 Energy profile of reaction path A for the transmetalation step in Suzuki-Miyaura cross-coupling

high-energy chemically unreasonable structures or two different structures: one with the OH⁻ oxidizing one of the phosphine ligands, or the other where the phosphine was replaced by the hydroxyl group. Further analysis of the potential energy surface around this region allowed us to find an alternative pathway, labeled as path B'. In this new pathway the intermediate formed by reaction of the base with a coordinated phosphine forms the *trans*-[Pd(CH₂=CH)Br(PH₃OH)(PH₃)]⁻ complex, and this intermediate can evolve to replace the halide ligand by the hydroxo group by migration of the OH from the phosphine to the Pd center; this complex could, in principle, give rise to the transmetalation process with the organoboronic acid (vide infra, path C). This pathway could be an alternative to path A, nevertheless, the presence of an oxidized phosphorus group makes the existence of this species in the reaction cycle quite unlikely. Indeed, phosphine oxidation is one of the known causes of catalyst destruction, and it seems to be connected to this compound (Fig. 11.7).

A related experimental result is that transmetalation takes place in absence of the base if the halide is replaced by a hydroxo or alkoxy group in the starting palladium complex [46]. The reaction mechanism for this process (labeled as path C) was computationally studied, and the energy profile was found to be smooth. The highest energy barrier is quite low, around 80 kJ/mol. Path C is in fact identical to path A from the point where the organoboronate species is coordinated to the catalyst. Hence, computational results reproduce the experimental observation of

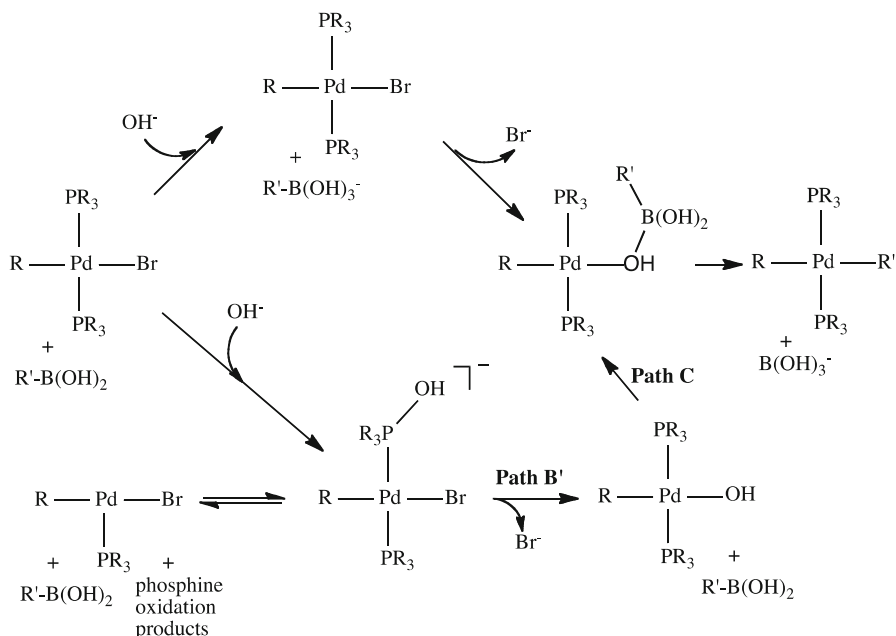


Fig. 11.7 Schematic representation of the pathways accounting for the role of the base in the transmetalation step of the Suzuki-Miyaura reaction, being path A the most feasible one

a low energy path C, and furthermore relate it to path A. The overall mechanistic picture resulting from these calculations is presented in Fig. 11.7.

These computational results were found to remain qualitatively valid when the PH_3 phosphine is replaced by PPh_3 and when vinyl groups are replaced by phenyl groups [47].

The collection of these results indicates that, in the Suzuki-Miyaura reaction, one of the key problems of the transmetalation step is the displacement of the bromide ligand from the metal coordination sphere. The boronic acid itself is not able to undertake this replacement, as shown in the direct mechanism. A base is therefore necessary for the transmetalation to take place. The direct replacement of the halide (Br^-) by the base (OH^-) is not feasible (path B). Nevertheless, the base may attack the boronic acid (path A) or the phosphine ligand (path B'). The latter must be discarded as the main mechanism because it easily leads to ligand oxidation and destruction of the catalyst. Therefore, the main catalytic cycle should proceed through path A, which has low-energy barriers and no obvious undesired products. Initial proposals about the transmetalation process suggested that it takes place through a four-center transition state [48], with two bridging group ligands (the halide and the base) between the two metal atoms. These results show that the transmetalation process does not take place in one concerted step, but several steps are needed.

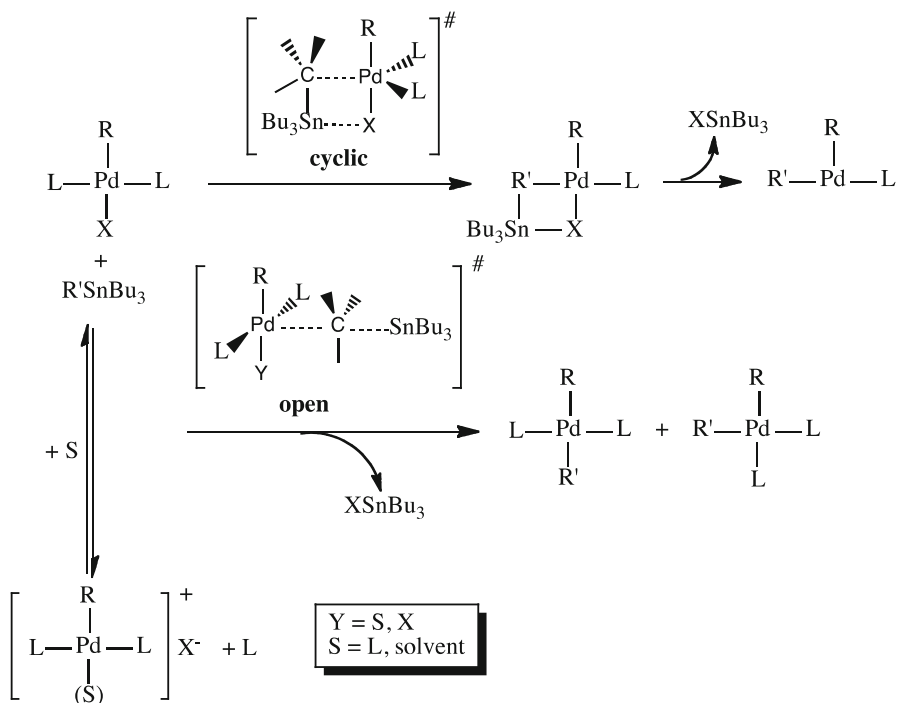
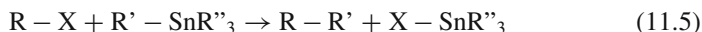


Fig. 11.8 Schematic representation of the proposed cyclic and open pathways for the transmetalation in the Stille reaction

11.3.2 The Stille Reaction

The Stille reaction is a general Pd-catalyzed cross-coupling reaction [3, 13], that owes its popularity in part to the easy preparation of organotin compounds and their tolerance toward most functional groups (Eq. 11.5).



In this case, two different transmetalation mechanisms, labeled as *cyclic* and *open*, have been proposed to explain the experimental data, and they are both shown in Fig. 11.8. The existence of the cyclic mechanism was proposed by Espinet and coworkers [49] to account for the evidence that some Stille processes take place with retention of configuration at the transmetalated carbon atom. This retention of configuration implies a transition state, or intermediate, where the X and R' ligands are bridging the two metal atoms (see Fig. 11.8, upper pathway). The open mechanism was proposed for those cases where the product presents inversion of configuration. This mechanism can produce either *cis* or *trans* geometries of the $L_2Pd(R)(R')$ species (Fig. 11.8, lower pathway). The open pathway seems to be

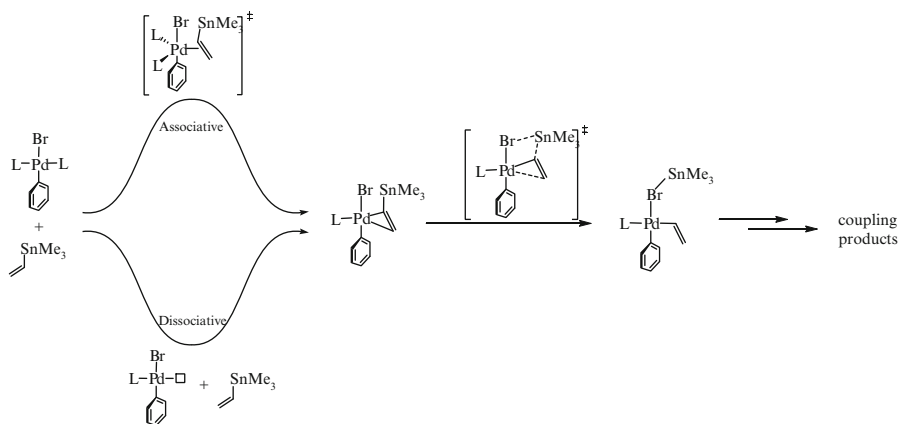


Fig. 11.9 Schematic representation of the associative and dissociative pathways for the cyclic alternative of the transmetalation step in the Stille reaction

more common and is expected to be favored for more electrophilic Pd centers, as in species with bad coordinating anions (like triflate) which are easily substituted by a neutral molecule (such as solvent or the ligand used in excess) [50–52].

Both mechanisms (cyclic and open) have been computationally analyzed by some of us, and the cyclic mechanism had been also studied by other authors. Our computational study [53] used a model system where the coupling takes place between Br-Ph and $CH_2 = CH-SnMe_3$, and is catalyzed by $Pd(PH_3)_2$ or $Pd(AsH_3)_2$. The effect of THF and C_6H_5 solvents were considered. In this work, we found that the cyclic mechanism did not take place in a concerted way. It was impossible to locate the proposed structure either as an intermediate or as a transition state. Instead, it was found that the transmetalation takes place in two steps (Fig. 11.9). In the first one, with a barrier below 40 kJ/mol, there is a substitution of an L ligand by the incoming vinyl group of the stannane; whereas in the second, the proper transmetalation takes place through a cyclic transition state. The cyclic four-member ring transition state corresponding to the second step has the highest energy barrier, with a value between 62 and 102 kJ/mol depending on L and the solvent, therefore becoming the rate determining step. These results were in concordance with other studies previously published by Napolitano and coworkers for alkynyl stannanes [54], and by Álvarez, coworkers [18] for alkenyl stannanes. All these studies also agreed that this process takes place in an associative way: the departure of the L ligand is coupled with the entry of the stannane in the palladium coordination sphere. Lin and co-workers [55] studied the effect of changing the halide ligand on the cyclic transmetalation step. Their results show that the activation barriers increase in the order $Cl < Br < I$. This trend is rationalized by observing that the Sn-X bond energy increases faster than the Pd-X bond energy in the order $I < Br < Cl$.

For the open mechanism, the most characteristic features are the absence of a cyclic species, and the formation of a cationic palladium complex. Experimentally

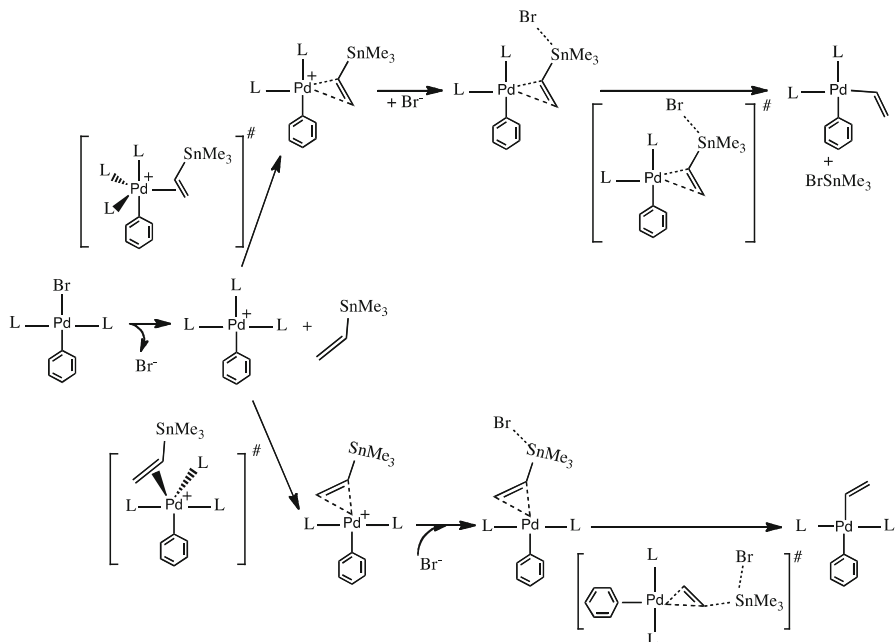


Fig. 11.10 Schematic representation of the *cis* and *trans* pathways for the open alternative of the transmetalation step in the Stille reaction

the *trans*- $[PdL_2XR]$ complexes formed after the initial oxidative addition are found to be in equilibrium with other species such as *trans*- $[PdL_2SR]^+$ or $[PdL_3R]^+$, depending on the reaction conditions, especially on the nature of the X group (bad coordinating ligands are better leaving groups) and the solvent. In our theoretical study on the Stille reaction [53], we analyzed the formation of a cationic species by substitution of the X ligand (bromide or triflate) by a neutral species as a phosphine or arsine ligand or a solvent molecule. This ligand substitution is found to be, as expected, much more favorable (by about 60 kJ/mol) for the case of triflate than for the case of bromide.

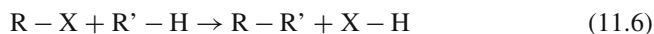
The following steps on the transmetalation process were studied starting from the cationic species, $[PdL_3R]^+$. Hence, the next step corresponds to the replacement of one of the L ligands by the incoming stannane, an R-for-L substitution step. This step may follow two different competitive pathways, depending on whether the stannane group goes *cis* or *trans* to the R substituent (see Fig. 11.10). Both possibilities were explored, and the energy barriers found for both pathways were quite similar, with values between 30 and 40 kJ/mol in solution. Once the stannane is coordinated to the palladium catalyst, a S_N2 substitution of the R group by a halide at the Sn center should follow. The energy barrier of this step for both the *cis* and the *trans* pathways is quite low. This process produces an intermediate with both organic groups attached to the palladium center, therefore ready to undergo the reductive

elimination. The comparison of the two steps for the open mechanism shows that the barrier in the R-for-L substitution is higher than for the transmetalation itself, which represents an interesting difference with respect to the case of the cyclic mechanism.

The transmetalation step for the Stille reaction is thus quite different from that in the Suzuki cross-coupling. No base is required, and a Br-Sn bond is in fact formed after the transmetalation. However, the transmetalation step in the Stille reaction is also complex, with two major mechanisms being possible, one leading to retention of configuration, and the other leading to inversion of configuration in the R' group. The specific mechanism taking place for a given catalytic system is mainly affected by the X group and the solvent, while the L ligand exerts a smaller (although kinetically significant) effect.

11.3.3 Direct Arylation

Direct arylation [9, 10], is a reaction formally similar to cross-coupling, with the key difference that one of the carbons involved in the process is not bound to a heteroatom, but to hydrogen (Eq. 11.6).



From a theoretical point of view, the key issue has been the basic nature of the metalation step, where the R' groups moves from a R'-H bond to a M-R' bond. C-H activation is very common in organic chemistry as it allows the formation of functionalized hydrocarbons. Different mechanisms had been proposed for this metalation step, including electrophilic aromatic substitution, σ -bond metathesis, oxidative addition/reductive elimination and Heck-like insertion. Theoretical studies have facilitated narrowing the mechanistic possibilities to two main options: oxidative addition/reductive elimination and proton abstraction by a base. In the oxidative addition/reductive elimination process the metal is inserted in the C-H bond with formal increase in the oxidation state of the metal, and the hydride leaves the metal coordination sphere of the metal afterwards. In the proton abstraction mechanism, the metal does not interact directly with the proton, which is captured by a base, with simultaneous formal creation of a carbanion that binds to the metal center. The mechanism of the reaction will depend on the presence of a base able to abstract the proton and of the existence of an energetically accessible oxidation state for the metal.

Various elements have been used for arylation reactions, mainly transition metals [56, 57] from columns 6 to 10. The great versatility of this method had led to its use in many syntheses. We will discuss here mainly cases involving two different metals: palladium and ruthenium.

Arylation with palladium involves the metal in its divalent state. It has been applied in ring closure reactions [58, 59] and intermolecular arylation [60]. In these cases, the mechanism is of the second type, the proton is abstracted by a base

Fig. 11.11 Transition state of H-abstraction with Pd(II) assisted by HCO_3^-

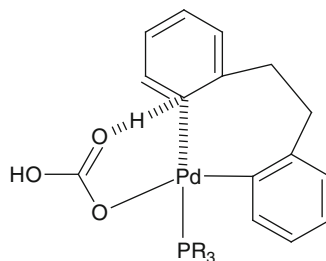


Fig. 11.12 Intermediate for Pd(IV) path (*left*) and transition state for Pd(II) path (*right*) in the vinyl to aryl shift

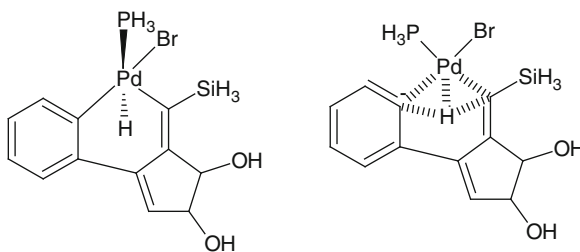
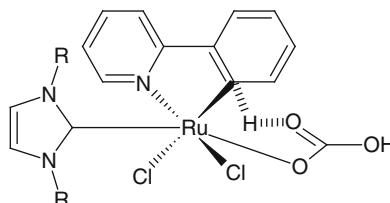


Fig. 11.13 Transition state for Ru-catalyzed proton abstraction mechanism of arylation



(typically carbonate or hydrogen carbonate) (see Fig. 11.11). The computed barrier for this reaction is 98 kJ/mol. This barrier is sensitive to the presence of substituents on the phenyl ring. With three fluorine atoms, the barrier is reduced to 55 kJ/mol, the reaction is thus favored by electron acceptors.

A related process involving C-H activation in palladium center is the shift of a hydrogen between two different sites of an organic ligand, coupled with a shift of the metal from a vinyl site to an aryl site [61–63]. In this case, two different processes were found to be feasible (Fig. 11.12). The oxidative path is composed of two steps with the highest barrier of 140 kJ/mol. The one step migration with a constant oxidation state has a lower barrier of 95 kJ/mol.

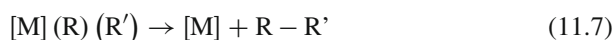
Ruthenium-catalyzed arylation seems to favor the proton abstraction mechanism. We studied the coupling of an aryl group to a phenylpyridine moiety [64]. The first step consists of cleavage of a C-H bond to form a Ru-C bond. The two mechanisms, oxidative addition on the ruthenium or H-abstraction, were evaluated. As for palladium, the oxidation of Ru(II) to Ru(IV) is energetically disfavored with a barrier of 133 kJ/mol. The H-abstraction possesses a much lower barrier, 35 kJ/mol with HCO_3^- as proton abstractor (Fig. 11.13). The barrier of H-abstraction is sensitive to the nature of the base: it is only of 22 kJ/mol with acetate.

Similar results have been found in the computational study of an iridium complex [65]. Again the abstraction of the proton by the base has a lower barrier (67 kJ/mol) than insertion of the metal in the C-H bond (158 kJ/mol).

Thus the proton abstraction mechanism seems to be the favored pathway in the metalation step of transition-metal-catalyzed arylations. This may seem surprising because a relatively weak base as carbonate is taking away an aryl proton, which has very low acidity. The presence of the metal is in this case key to stabilize the development of a negative charge in the carbon center, as proved by the structure of the transition states, where the metal-carbon bond is practically already formed. It is worth mentioning that external bases are key in both direct arylation and the Suzuki-Miyaura cross-coupling, but their roles are completely different.

11.4 Reductive Elimination

In the reductive elimination step, a bond between the two organic groups attached to the metal is made, and the two previously existing bonds with the metal are lost resulting in a decrease in the metal oxide state by two units (Eq. 11.7).



Reductive elimination is of course the microscopic reverse of oxidative addition, and the general studies mentioned above on the oxidative addition of non-polar sigma bonds (H-H, C-C, C-H) to d^{10} ML_2 transition metal complexes also apply. The transition state is in particular concerted, with simultaneous breaking of the two M-C bonds.

Computational studies of the reductive elimination in systems related to cross-coupling have been recently reviewed by Ananikov, Musaev and Morokuma [66]. Studies on this step are more scarce than those concerned with oxidative addition. This, in part, is explained by the dominance of the concerted mechanism and the lack of the alternative dissociative path shown in Fig. 11.2. The dissociative mechanism is associated to the existence of a polar sigma bond. The bond in R-X is polar, but that in R-R' is not. Moreover, there are no experimental reports where reductive elimination is considered to be the rate determining step, which also decreases the computational attention given to this process. The theoretical studies on the full catalytic cycle seem to confirm a lower barrier for reductive elimination than for oxidative addition. For instance, in our work on the Suzuki-Miyaura catalytic cycle, we found barriers in the range 55–85 kJ/mol for oxidative addition and barriers in the range 5–20 kJ/mol for reductive elimination. These results were obtained for the reaction between vinylbromide and vinylboronic acid, and may not be general.

The computational studies by Ananikov, Musaev and Morokuma on C-C coupling in palladium and platinum bis(phosphine) complexes address the dependence of the barrier on the nature of the organic groups being reductively eliminated [67–69]. In their calculations on reductive elimination from

$\text{Pd}(\text{PH}_3)_2(\text{R})_2$ complexes, they found the following order in potential energy barriers as a function of the group: vinyl (28 kJ/mol) < phenyl (49 kJ/mol) < ethynyl (61 kJ/mol) < methyl (105 kJ/mol). The values are low for the unsaturated substrates, but the value for the sp^3 methyl system may be competitive with that of other reaction steps, and may be even related to the low reactivity of alkyl systems. They have recently extended the work to $\text{Pd}(\text{PR}'_3)_n(\text{R}_2)$ ($\text{R}' = \text{H, Me, Ph, Cy}$; $n = 1, 2$) systems, and found that the ordering of kinetic barriers with respect to the nature of the phosphine substituents is different in (bis)phosphine than in monophosphine complexes.

Reductive elimination may thus be a relevant step in some cross-coupling processes. It may be affected by some of the factors that have been discussed above for oxidative addition of R-X , like anionic additives and the number of ligands attached to the active form. However, the analysis of these topics from a computational point of view is still limited. The main results can in fact be found in works not focusing on cross-coupling. Macgregor and co-workers analyzed the reductive elimination process in a series of $\text{M}(\text{PH}_3)_2(\text{CH}_3)(\text{R})$ and $\text{M}(\text{PH}_3)(\text{CH}_3)(\text{R})$ complexes ($\text{M} = \text{Ni, Pd, Pt}$; $\text{R} = \text{CH}_3, \text{NH}_2, \text{OH}$) [70]. The focus of the work was the effect on the process of the nature of the metal and the R group, but it is worth mentioning that they found the barrier for reductive elimination of $\text{CH}_3\text{-CH}_3$ is lower for the monophosphine system than for the (bis)phosphine system. A similar result has been found by us in the reductive elimination of two vinyl groups from $\text{Pd}(\text{PH}_3)_2(\text{vinyl})_2$ [17]. Bo and co-workers [71] have analyzed the effect of the P-Pd-P bite angle on the reductive elimination of acetonitrile in a series of diphosphine systems $(\text{R}_2\text{PXPdR}_2)\text{Pd}(\text{CH}_3)(\text{CN})$ ($\text{R} = \text{H, Me, Ph}$; $\text{X} = (\text{CH}_2)_n$). Their work confirms that larger bite angles favor reductive elimination, and it is because of orbital, not steric, effects.

Reductive elimination thus seems to be a mechanistically simpler step than the oxidative addition and transmetalation processes discussed in the previous section. However, a better understanding of some details in reductive elimination would be welcome, and further computational work in this area seems necessary.

11.5 Isomerization

The intermediates obtained after the oxidative addition have been usually observed as *trans*- $[\text{PdL}_2(\text{R})(\text{X})]$ complexes [2]. Consequently, it has been proposed that the catalytic cycle goes through this type of *trans* complex. This does not pose any complication to the transmetalation step, and in fact a number of the calculations presented above use this *trans* arrangement. However, things are different for oxidative addition and reductive elimination. Both reactions require a *cis* arrangement of the ligands involved, as discussed in previous sections. Therefore, the isomerization steps shown in Eqs. 11.8 and 11.9 must be postulated in order to close the catalytic cycle in some cases. The *cis-trans* isomerization process has been studied

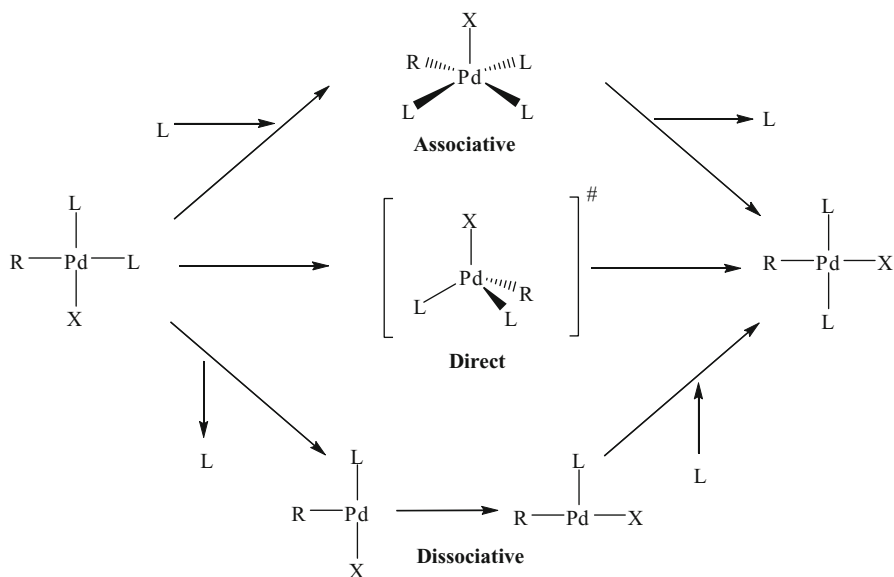
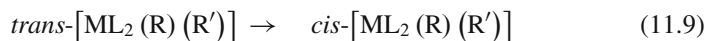
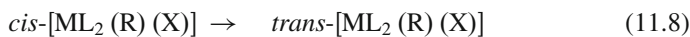


Fig. 11.14 Three possible pathways for *cis-trans* isomerization in a $PdL_2(R)(X)$ complex



experimentally by Casado and Espinet [72] in the case where the complex is that formed by the oxidative addition of $C_6Cl_2F_3I$ to $[Pd(PPh_3)_4]$. They found up to four parallel pathways were operable, but concluded that isomerization was always faster than transmetalation, and therefore not mechanistically relevant.

This step has been computationally analyzed in the studies of the full catalytic cycles. In particular, in our study of the Suzuki-Miyaura cross-coupling [17] we considered the three possible pathways depicted in Fig. 11.14. They differ in the coordination number of the intermediate/transition states involved.

The direct path is formally the simplest, with coordination number four being unchanged throughout the process. However, it has the highest barrier, 85 kJ/mol above the *trans* complex in the case of our particular set of PH_3 ligands and vinyl and bromide substituents. The barrier is even higher (142 kJ/mol) when bromide is replaced by vinyl for the isomerization step prior to reductive elimination. These high barriers are consistent with the tetrahedral nature of the transition states, a geometry heavily disfavored for low spin d^8 ML_4 species due to the population of antibonding orbitals.

The two alternative paths, associative and dissociative, avoid the problem of the tetrahedral transition state through a change in the coordination number. In the

associative path, a new ligand is attached, and the resulting five-coordinate complex rearranges through Berry pseudorotation. In the dissociative path, a phosphine ligand is lost, and the resulting T-shape three-coordinate species rearranges through a Y-shape transition state. For the species with bromide and vinyl, our calculations showed both isomerization paths proceed smoothly, with barriers of 23 kJ/mol at most. For the bis(vinyl)complexes, only the dissociative path was feasible, with a barrier of 50 kJ/mol.

Calculations are conclusive indicating that the isomerization steps often proposed in some cross-coupling processes happen through low barrier mechanisms, and that these mechanisms can be diverse. This result is in agreement with the experimental observations, and confirms the view that this step seems to have minor mechanistic relevance.

11.6 Concluding Remarks

Palladium catalyzed cross-coupling and direct arylation reactions follow a common general scheme encompassing oxidative addition, metalation and reductive elimination steps. However, substantial differences exist with regard to significant mechanistic aspects for different catalytic systems. The experimental observations are confirmed and refined by the computational studies. These show for example that transmetalation follows substantially different paths depending on whether organoboron (Suzuki-Miyaura) or organotin (Stille) reactants are involved. The metalation step of direct arylation follows the same general pattern, but it has also some nuances. It seems thus that it is not appropriate to talk about *the* mechanism of cross-coupling and arylation reactions, or even of a given type of cross-coupling reaction, but rather of a manifold of mechanisms accessible to certain types of system.

The processes for C-C bond formation lie at the basis of the chemical tools to achieve complex molecules from simple fragments. Yet even in this seemingly simple process, complexity arises in the form of multistep reactions affected by a lot of different factors. Computational chemistry, always in hand with experiment, is already a very useful tool for the understanding and optimization of these fundamental catalytic systems.

References

1. De Meijere A, Diederich F (eds) (2004) Metal-catalyzed cross-coupling reactions, 2nd edn. Wiley, Weinheim
2. Miyaura N, Suzuki A (1995) Chem Rev 95:2457–2483
3. Stille JK (1986) Angew Chem Int Ed Engl 25:508–524
4. Negishi E, Anastasia L (2003) Chem Rev 103:1979–2017
5. Beletskaya IP, Cheprakov AV (2000) Chem Rev 100:3009–3066

6. Sonogashira K (2002) *J Organomet Chem* 653:46–49
7. Hartwig JF, Kawatsura M, Hauck SI, Shaughnessy KH, Alcazar-Roman LM (1999) *J Org Chem* 64:5575–5580
8. Muci AR, Buchwald SL (2002) *Top Curr Chem* 219:131–209
9. Campeau LC, Fagnou K (2006) *Chem Commun* 1253–1264
10. Alberico D, Scott ME, Lautens M (2007) *Chem Rev* 107:174–238
11. Littke AF, Fu GC (2002) *Angew Chem Int Ed* 22:4176–4221
12. Echavarren AM, Cárdenas DJ (2004) *Metal-catalyzed cross-coupling reactions*. 2nd edn. In: De Meijere A, Diederich F (eds) Wiley, Weinheim, pp 1–39
13. Espinet P, Echavarren AM (2004) *Angew Chem Int Ed* 43:4704–4734
14. Amatore C, Jutand A (2000) *Acc Chem Res* 33:314–321
15. Goossen LJ, Koley D, Hermann HL, Thiel W (2005) *J Am Chem Soc* 125:11102–11114
16. Goossen LJ, Koley D, Hermann HL, Thiel W (2006) *Organometallics* 25:54–67
17. Braga AAC, Ujaque G, Maseras F (2006) *Organometallics* 25:3647–3658
18. Alvarez R, Faza ON, López CS, de Lera AR (2006) *Org Lett* 8:35–38
19. Braga AAC, Ujaque G, Maseras F (2008) In: Morokuma K, Musaev DG (eds) *Computational modeling for homogeneous and enzymatic catalysis*, Wiley, Weinheim, pp 109–130
20. Noell JO, Hay PJ (1982) *J Am Chem Soc* 104:4578–4584
21. Low JJ, Goddard WA (1984) *J Am Chem Soc* 106:6928–6937
22. Obara S, Kitaura K, Morokuma K (1984) *J Am Chem Soc* 106:7482–7492
23. Sakaki S, Mizoe N, Musahi Y, Biswas B, Sugimoto MJ (1998) *J Phys Chem A* 102:8027–8036
24. Matsubara T, Hirao K (2002) *Organometallics* 21:4482–4489
25. Stille JK, Lau KSY (1976) *J Am Chem Soc* 98:5841–5849
26. Senn HM, Ziegler T (2004) *Organometallics* 23:2980–2988
27. Sundermann A, Martin JML (2001) *Chem Eur J* 7:1703–1711
28. Kozuch S, Amatore C, Jutand A, Shaik S (2005) *Organometallics* 24:2319–2330
29. Diefenbach A, de Jong GT, Bickelhaupt FM (2005) *J Chem Theory Comput* 1:286–298
30. Goossen LJ, Koley D, Hermann HL, Thiel W (2005) *Organometallics* 24:2398–2410
31. Ariafard A, Lin Z (2006) *Organometallics* 25:403–4033
32. Smith M, March J (2007) *March's advanced organic chemistry: reactions, mechanisms, and structures*, 6th edn. Wiley, Weinheim
33. Besora M, Gourlaouen C, Yates B, Moseras F (2011) *Dalton Trans* 40:11089–11094
34. Hartwig JF, Paul F (1995) *J Am Chem Soc* 117:5373–5374
35. Littke AG, Dai CY, Fu GC (2000) *J Am Chem Soc* 122:4020–4028
36. Santos LS, Rosso GB, Pilli RA, Marcos MN (2007) *J Org Chem* 72:5809–5812
37. Cundari TR, Deng J (2005) *J Phys Org Chem* 18:417–425
38. Ahlquist M, Fristrup P, Tanner D, Norrby P-O (2006) *Organometallics* 25:2066–2073
39. Ahlquist M, Norrby P-O (2007) *Organometallics* 26:550–553
40. Balcells D, Maseras F, Keay BA, Ziegler T (2004) *Organometallics* 23:2784–2796
41. Davies DL, Donald SMA, Macgregor SA (2005) *J Am Chem Soc* 127:13754–13755
42. García-Cuadrado D, Braga AAC, Maseras F, Echavarren AM (2006) *J Am Chem Soc* 128:1066–1067
43. Miyaura N (2002) *J Organomet Chem* 653:54–57
44. Braga AAC, Morgon NH, Ujaque G, Maseras F (2005) *J Am Chem Soc* 127:9298–9307
45. Hegedus LS (1994) *Transition metals in the synthesis of complex organic molecules*. University Science, Mill Valley
46. Miyaura N, Yamada Y, Suginome H, Suzuki A (1985) *J Am Chem Soc* 107:972–980
47. Braga AAC, Morgon NH, Ujaque G, Lledós A, Maseras F (2006) *J Organomet Chem* 691:4459–4466
48. Osakada K (2003) *Fundamentals of molecular catalysis*. In: Kurosawa H, Yamamoto A (eds), Elsevier, Amsterdam, pp 233–292
49. Casado AL, Espinet P (1998) *J Am Chem Soc* 120:8978–8985
50. Casado AL, Espinet P, Gallego AM (2000) *J Am Chem Soc* 122:11771–11782
51. Farina V, Krishnan B, Marshall DR, Roth GP (1993) *J Org Chem* 58:5434–5444

52. Casado AL, Espinet P, Gallego AM, Martínez-Irarduya JM (2001) *Chem Commun* pp 339–340
53. Nova A, Ujaque G, Maseras F, Lledós A, Espinet P (2006) *J Am Chem Soc* 128:14571–14578
54. Napolitano E, Farina V, Persico M (2003) *Organometallics* 22:4030–4037
55. Ariafard A, Lin Z, Fairlamb IJS (2006) *Organometallics* 25:5788–5794
56. Arndsten BA, Bergman RG, Mobely TA, Peterson TH (1995) *Acc Chem Res* 28:154–162
57. Shilov AE, Shulpin GB (1997) *Chem Rev* 97:2879–2932
58. Pascual S, De Mendoza P, Braga AAC, Maseras F, Echavarren AM (2008) *Tetrahedron* 64:6021–6029
59. Garcia-Cuadrado D, De Mendoza P, Braga AAC, Maseras F, Echavarren AM (2007) *J Am Chem Soc* 129:6880–6886
60. Lafrance M, Rowley CN, Woo TK, Fagnou K (2006) *J Am Chem Soc* 128:8754–8756
61. Mota AJ, Dedieu A (2007) *J Org Chem* 72:9669–9678
62. Mota AJ, Dedieu A (2006) *Organometallics* 25:3130–3142
63. Mota AJ, Dedieu A (2005) *J Am Chem Soc* 127:7171–7182
64. Ozdemir I, Demir S, Cetinkaya B, Gourlaouen C, Maseras F, Bruneau C, Dixneuf PH (2008) *J Am Chem Soc* 130:1156–1157
65. Davies DL, Donald SMA, Ar-Duaij O, Macgregor SA, Pölleth M (2006) *J Am Chem Soc* 128:4210–4211
66. Ananikov VP, Musaev DG, Morokuma K (2008) In: Morokuma K, Musaev DG (eds) *Computational modeling for homogeneous and enzymatic catalysis*, Wiley, Weinheim, pp 131–148
67. Ananikov VP, Musaev DG, Morokuma K (2002) *J Am Chem Soc* 124:2839–2852
68. Ananikov VP, Musaev DG, Morokuma K (2005) *Organometallics* 24:715–723
69. Ananikov VP, Musaev DG, Morokuma K (2007) *Eur J Inorg Chem* 34:5390–5399
70. Macgregor SA, Neave GW, Smith C (2003) *Faraday Discuss* 124:111–127
71. Zuidema E, van Leeuwen PWNM, Bo C (2005) *Organometallics* 24:3703–3710
72. Casado AL, Espinet P (1998) *Organometallics* 17:954–959

Chapter 12

Electron Transfer to Dioxygen by Keggin Heteropolytungstate Cluster Anions

Ophir Snir and Ira A. Weinstock

Abstract This chapter describes recent developments in understanding electron transfer to dioxygen (O_2) and the outer-sphere oxidation of the superoxide radical anion, $O_2^{\bullet-}$, by metal complexes. The following topics, of broad spectrum value in the complex chemistry of polyoxometalate (POM) systems and quantitative electron transfer are addressed: the nature of electron self-exchange between POMs; electron self-exchange between O_2 and $O_2^{\bullet-}$ (including the problem of size differences between O_2 or $O_2^{\bullet-}$ and their typical metal-complex electron donors or acceptors); and reactions of the one-electron-reduced POMs with O_2 . Electron transfer from Keggin POMs to O_2 occurs by an outer-sphere mechanism; the effect of POM charge on rate constants for the reduction of O_2 is significant and attributable to anion–anion repulsion within the successor-complex ion pairs formed between the negatively charged POM anions and $O_2^{\bullet-}$. These findings were followed by the discovery of a concerted proton–electron (CPET) pathway for electron transfer to O_2 at lower pH values (<1).

12.1 Introduction

Dioxygen is a strong oxidant, with a standard reduction potential of 1.23 V (Eq. 12.1).



Most organisms and organic matter on earth are unstable relative to the main products of their oxidation by O_2 : H_2O and CO_2 . Fortunately, however, the ground

O. Snir • I.A. Weinstock (✉)

Department of Chemistry, Ben Gurion University of the Negev, Beer Sheva 84105, Israel
e-mail: iraw@bgu.ac.il

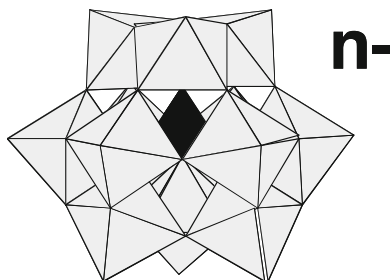


Fig. 12.1 The α -Keggin anions, shown in coordination-polyhedron notation, are 1.12 nm in diameter, and possess tetrahedral (T_d) symmetry. In each polyanion, 12 W addendum atoms are at the *center* of WO_6 polyhedra, which each possess C_{4v} symmetry and have O atoms at their vertices. At the *center* of this cluster (*shaded*) is a tetrahedral metalate oxoanion, $\text{X}^{n+}\text{O}_4^{(8-n)-}$

electronic state of molecular oxygen is a triplet (it is a diradical), whereas most organic compounds found in nature are closed-shell (non-radical) species. As a result, electronic interactions between ground-state dioxygen and most organic compound are spin forbidden, such that the barriers for electron transfer to O_2 are large, and kinetically unfavorable (slow). Moreover, the changes in Gibbs free energies associated with most one-electron reductions of O_2 to superoxide radical anion, $\text{O}_2^{\bullet-}$, are large and positive, i.e., unfavorable. For these reasons, O_2 in its triplet ground state is relatively inert, and its (typically reductive) activation has been, and still is, a major mechanistic challenge [1–12]. Once activated, however, autoxidation reactions that can then ensue are mechanistically complex, difficult to control and usually highly nonselective. And, the multiple elementary steps involved in these reactions occur at rates that vary with reaction conditions. Given this complexity, the acquisition of fundamental information about the reduction of dioxygen bears directly on advances in chemical biology [13–18] and sustainable-energy technologies [19, 20].

Many polymeric metal-oxide cluster anions (polyoxometalates, or POMs) are entirely inorganic, and contain (primarily) V, Mo, and W in their highest-valent (d^0) electronic states. As a result, and unlike metallo-organic complexes, these POMs are remarkably stable in even strongly oxidizing conditions. Moreover, they possess reversible redox chemistries, are well-defined molecular species, and are stable in both organic solvents and water (over easily determined pH ranges). As a result, POMs are frequently used to control the reactions of O_2 [21–28], and are attractive candidates for use as physicochemical probes for elucidating the mechanisms of electron-transfer reactions. One class of tungsten-based POM, the “heteropolytungstates”, and specifically those with a Keggin structure (Fig. 12.1), are outer-sphere complexes; oxide exchange with solvent (often water) is very slow [29], and they undergo electron-transfer reactions only via outer-sphere processes. Hence, by accurately measuring the kinetic and thermodynamic parameters associated with these processes (i.e., electron self-exchange rate constants, k_{11} , reorganization energies—both outer- and inner-sphere, λ_{out} and λ_{in} , respectively—corrected Gibbs

free energies of the Marcus model, ΔG° , work terms for the formation of precursor complexes, w_{ij} , or dissociation of successor complexes, w_{ji} , and more), these heteropolytungstates can be used to study reductions of O_2 in water, or any other solvent in which salts of these POMs are soluble. With options for controlling reduction potentials, charges and basicities of the reducing agents, and other factors that might affect the kinetics and thermodynamics of the reaction, mechanistic studies using POM probes have shed new light on fundamental aspects of the first one-electron reduction of O_2 .

In this chapter the focus is on recent findings related to the mechanism(s) of the first one-electron reduction of O_2 in water by reduced Keggin heteropolytungstate electron donors. We will first discuss electron self-exchange reactions between these POMs, followed by an introduction to the mechanism of electron self-exchange between O_2 and its one-electron reduced form, $O_2^{\cdot-}$. A simple and elegant quantitative resolution to disparities between published rate constants (from Marcus treatments), ultimately attributable to size differences between metal complexes and either O_2 or $O_2^{\cdot-}$, will then be presented. The mechanisms of electron transfer from reduced Keggin heteropolytungstates to O_2 in water will then be summarized. Finally, an important new role for pH will be discussed. This involves the emergence of a fundamentally new type of concerted proton–electron transfer (CPET) to O_2 at low pH values in water.

12.2 Electron Self-Exchange Between Keggin Heteropolytungstates

This section will focus exclusively on self-exchange reactions between the isostructural series of Keggin-type heteropolytungstates, $X^{n+}W_{12}O_{40}^{(y-n)-}$, $X^{n+} = P^{5+}$ (anion **1**), Si^{4+} (anion **2**), Al^{3+} (anion **3**) and $y = 8, 9, 10$ for the fully oxidized, one- and two-electron reduced species, respectively. These electronic states are indicated by subscripts, e.g., $\mathbf{1}_{ox}$, $\mathbf{1}_{1e}$ and $\mathbf{1}_{2e}$.

In 1990, Kozik and Baker [30, 31] published experimental and theoretical information concerning the rate constants for electron self-exchange (k_{11}) between fully oxidized Keggin-type polyoxometalates (POMs), $\alpha\text{-PW}_{12}\text{O}_{40}^{3-}$ ($\mathbf{1}_{ox}$) and their one-electron reduced analogs, $\alpha\text{-PW}_{12}\text{O}_{40}^{4-}$ ($\mathbf{1}_{1e}$), and between $\alpha\text{-PW}_{12}\text{O}_{40}^{4-}$ ($\mathbf{1}_{1e}$) and the two-electron reduced anion $\alpha\text{-PW}_{12}\text{O}_{40}^{5-}$ ($\mathbf{1}_{2e}$). In that work, line broadening of [31]P NMR signals of the anions in water at 25 °C was used to determine self-exchange rate constants as a function of ionic strength, μ , at the fast-exchange limit of the NMR time scale. The ionic strength was varied from 0.026 to 0.616 M, and 6 rate constants, k , were determined over that range of ionic-strength values. Those values are much larger than 0.01 M, for which the Debye-Hückel theory was derived. Nevertheless, the six k values could be fitted to the extended Debye-Hückel equation (Eq. 12.2, which is valid up to 0.1 M ionic strength) to give a straight line ($R^2 = 0.998$) and a slope that yielded a charge product z_1z_2 of 14.2

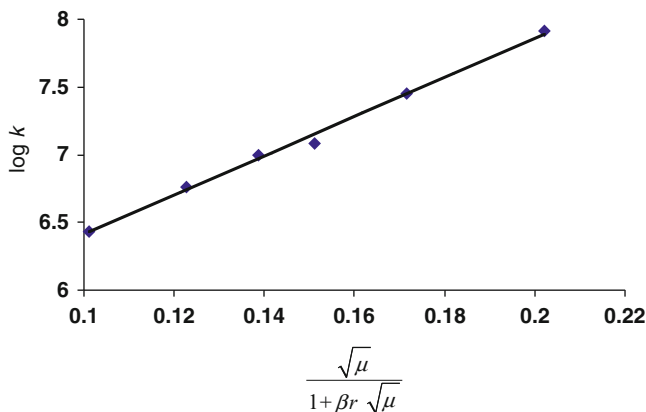


Fig. 12.2 Plot of $\log k$ versus $\mu^{1/2}/[1 + \beta r(\mu)^{1/2}]$ for the electron exchange reaction between α -PW₁₂O₄₀³⁻(**1**_{ox}) and α -PW₁₂O₄₀⁴⁻(**1**_{1e}). The line is a linear fit of the data ($R^2 = 0.998$) (Plotted from data in ref. [30])

(Fig. 12.2), close to the theoretical value of 12, the product of the negative charges of **1**_{ox} and **1**_{1e} (3- and 4-, respectively).

$$\log k = \log k_o + 2z_1z_2\alpha\mu^{1/2} / (1 + \beta r\mu^{1/2}) \quad (12.2)$$

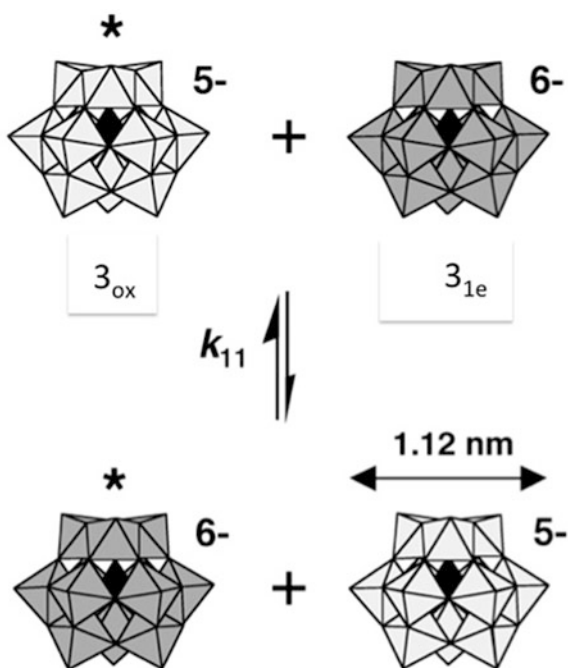
In Eq. 12.2, $\alpha = 0.509$ and $\beta = 0.329 \times 10^8 \text{ mol}^{-1/2} \text{ cm}^{1/2}$ are constants of the theory, and r is the hard-sphere collision distance.

The behavior of the Keggin heteropolytungstates at the high ionic strengths used by Kozik and Baker was ascribed to the “fact that heteropoly anions, owing to the very pronounced inward polarization of their exterior oxygen atoms, have extremely low solvation energies and very low van der Waals attractions for one another.” An additional important factor is that [32, 33] the negative charges of the POM anions are shared between many atoms (e.g., 53 in the Keggin structure) and are therefore highly diffused. This makes the POMs even less coordinating than typical “noncoordinating” anions, such as perchlorate (ClO₄⁻). The negative charge of that anion is distributed over 5 atoms, which leads to a charge-to-atom ratio of 0.2 (1:5), whereas the same ratio for **1**_{1e} (with a charge of 4-) is only 0.07.

Using Sutin’s semi-classical form of the Marcus model [34], Kozik and Baker predicted (calculated) a rate constant for the self-exchange reaction between **1**_{ox} and **1**_{1e} of $(3.6 \pm 0.1) \times 10^5 \text{ M}^{-1} \text{ s}^{-1}$ (at zero ionic strength), which was in close agreement with their experimental (measured) value of $(1.1 \pm 0.2) \times 10^5 \text{ M}^{-1} \text{ s}^{-1}$, after extrapolation to zero ionic strength.

Weinstock and co-workers [32, 33] used a similar [27]Al NMR experiment to determine rate constants as a function of ionic strength in water for electron self-exchange between a series of AlW₁₂O₄₀ⁿ⁻ (α and β isomers of fully oxidized, one- and two-electron reduced ions), at the slow-exchange limit of the NMR time scale. Figure 12.3 shows a representative self-exchange reaction between α -AlW₁₂O₄₀⁵⁻ (**3**_{ox}) and α -AlW₁₂O₄₀⁶⁻ (**3**_{1e}) couple.

Fig. 12.3 Electron exchange between $\alpha\text{-AlW}_{12}\text{O}_{40}^{5-}(\mathbf{3}_{\text{ox}})$ and $\alpha\text{-AlW}_{12}\text{O}_{40}^{6-}(\mathbf{3}_{1\text{e}})$. At the center of each cluster (shaded) is a tetrahedral aluminate oxoanion, $\text{Al}^{\text{III}}\text{O}_4^{5-}$ (Reprinted from ref. [32] with permission from the American Chemical Society)



As was done by Kozik and Baker, a reaction (hard-sphere collision) distance of 1.12 nm was used, which corresponds to twice the hydrodynamic radius of a fully oxidized Keggin-type $\text{X}^{n+}\text{W}_{12}\text{O}_{40}^{(8-n)-}$ anion (the hydrodynamic radius remains effectively constant upon one- or two-electron reduction of the anion) [35, 36]. Values of z_1z_2 charge-products obtained from slopes of linear fittings to the extended Debye-Hückel equation (Eq. 12.2) were within experimental uncertainties of those calculated from the actual charges of the reacting anions. Aqueous solution chemistries were most extensively defined for $\alpha\text{-AlW}_{12}\text{O}_{40}^{5-}(\mathbf{3}_{\text{ox}})$ and $\alpha\text{-AlW}_{12}\text{O}_{40}^{6-}(\mathbf{3}_{1\text{e}})$, for who's self-exchange, the experimental charge product z_1z_2 was 29 ± 2 , statistically identical to the theoretical value of 30. The electron self-exchange rate constant (extrapolated to $\mu = 0$) was found to be $k_{11} = (6.5 \pm 1.5) \times 10^{-3} \text{ M}^{-1} \text{ s}^{-1}$, which is more than seven orders of magnitudes smaller than the $(1.1 \pm 0.2) \times 10^5 \text{ M}^{-1} \text{ s}^{-1}$ value of Kozik and Baker for reactions of $\mathbf{1}_{\text{ox}}$ and $\mathbf{1}_{1\text{e}}$. Use of Sutin's semiclassical model showed this striking difference to be a consequence of (primarily) the large negative charges of $\mathbf{3}_{\text{ox}}$ and $\mathbf{3}_{1\text{e}}$ (5- and 6-, respectively), and to a lesser extent of a slight increase of the inner-sphere reorganization energy, λ_{in} for reactions of $\mathbf{3}$ relative to those of $\mathbf{1}$. Both these contributions are shown in Fig. 12.4. The dotted line indicates the decrease in rate due to increase in total reorganization energy; the dashed line shows the effect of increasing charge product z_1z_2 from 12 for reaction between $\mathbf{1}_{1\text{e}}$ and $\mathbf{1}_{\text{ox}}$, to 30 for $\mathbf{3}_{1\text{e}}$ and $\mathbf{3}_{\text{ox}}$.

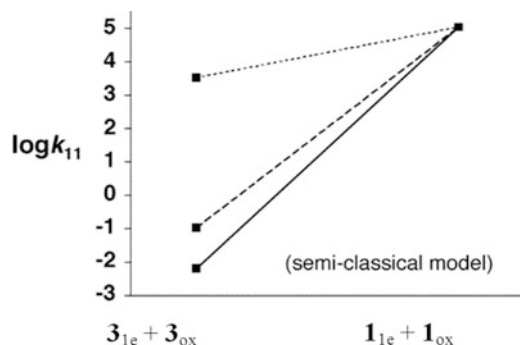


Fig. 12.4 Zero-ionic-strength self-exchange rate constants for electron transfer between α - $\text{AlW}_{12}\text{O}_{40}^{6-}$ and α - $\text{AlW}_{12}\text{O}_{40}^{5-}$ (3_{1e} and 3_{ox}) and between α - $\text{PW}_{12}\text{O}_{40}^{4-}$ and α - $\text{PW}_{12}\text{O}_{40}^{3-}$ (1_{1e} and 1_{ox}). The rate constant for self-exchange between 1_{1e} and 1_{ox} is at the *upper right* ($k_{11} = 1.1 \times 10^5 \text{ M}^{-1} \text{ s}^{-1}$; $\log k_{11} = 5.04$), and that for self-exchange between 3_{1e} and 3_{ox} is at the *lower left* ($k_{11} = 6.5 \times 10^{-3} \text{ M}^{-1} \text{ s}^{-1}$; $\log k_{11} = -2.19$). See the text for descriptions of the *three lines* shown (Reprinted from ref. [32] with permission from the American Chemical Society)

The above studies, and the data in Fig. 12.4, provide the information needed to use 3_{1e} to study the first one-electron step in the reduction of O_2 to H_2O ; [37] see discussion in Sect. 12.3.1.

Swaddle and co-workers [38] had studied the effect of cation (alkali metal or triflate supporting electrolytes) catalysis on the self-exchange reaction between the $3_{ox}/3_{1e}$ couple. Rate accelerations were found to depend specifically on the identity and concentrations of the cations, and the authors suggest that these could be more important than ionic-strength.

The zero ionic strength rate constant for electron self-exchange between Keggin anions, α - $\text{SiW}_{12}\text{O}_{40}^{4-}$ (2_{ox}) and α - $\text{SiW}_{12}\text{O}_{40}^{5-}$ (2_{1e}) was also estimated [37]. This was done by first setting the inner-sphere reorganization energy, λ_{in} [39, 40], for this self-exchange reaction equal to 12.2 kcal mol $^{-1}$, the mean of λ_{in} for **1** and **3** (15.5 and 8.85 kcal mol $^{-1}$, respectively). Sutin's semiclassical method [34], then gave a k_{11} value at $\mu = 0$ of $1.6 \times 10^2 \text{ M}^{-1} \text{ s}^{-1}$, which lies between the experimentally established values for self-exchange between the $1_{ox}/1_{1e}$ and $3_{ox}/3_{1e}$ pairs.

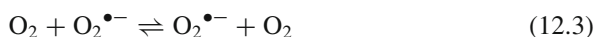
12.3 Outer-Sphere Electron Transfer to O_2 and from $\text{O}_2^{\bullet-}$

12.3.1 Electron Self-Exchange Between O_2 and $\text{O}_2^{\bullet-}$

Application of the Marcus cross relation (MCR) to reductions of dioxygen by metal complexes, and to its reverse, oxidations of the superoxide radical anion, $\text{O}_2^{\bullet-}$, supports an outer-sphere mechanism [41–48]. O_2 oxidations of organic electron

donors such as hydroquinones [49] and phenols [50], and the reverse reactions that involve oxidations of $\text{O}_2^{\bullet-}$, gave $\log K$ vs $\log k$ relationships expected for a Marcus (outer-sphere) process [39, 40, 51]. However, while relatively early applications of the MCR to O_2 oxidations by metal complexes clearly supported an outer-sphere mechanism, this was not the case for $\text{O}_2^{\bullet-}$ reductions of metal complexes which, until recently [52], were believed to involve some complex interactions that were not yet fully understood.

The works cited in refs. [41–47] and [49] were published before an *experimentally* determined value for the self-exchange rate constant, k_{22} , for reaction between O_2 and $\text{O}_2^{\bullet-}$ (Eq. 12.3) was available.



Without an experimental value for k_{22} , theoretical values for k_{22} were estimated using the MCR, e.g., as was done in refs. [41–47] and [49]. However, the calculated rate constants did not agree with one another and, in fact, spanned several orders of magnitude.

In 1989, Lind and Merényi measured k_{22} directly using $^{32}\text{O}_2$ and $^{36}\text{O}_2^{\bullet-}$ [53]. A value of $k_{22} = 450 \pm 160 \text{ M}^{-1} \text{ s}^{-1}$ was reported. This appeared to supply the missing piece of information needed to accurately predict—using the MCR—bimolecular rate constants, k_{12} , for O_2 oxidations of metal complexes, and k_{21} for reductions of metal complexes by the superoxide radical anion. Nevertheless, when kinetic data for electron transfer from “outer-sphere” metallo-organic complexes to O_2 were analyzed using the MCR [47], an “effective” rate constant for self-exchange between O_2 and $\text{O}_2^{\bullet-}$ of between 1 and $10 \text{ M}^{-1} \text{ s}^{-1}$ was obtained. When organic electron donors with radii of between 5 and 7 Å, similar to that of Keggin-type POMs (see Sect. 12.3.1), were reacted with O_2 , the MCR gave $k_{22} \approx 2 \text{ M}^{-1} \text{ s}^{-1}$ [54, 55]. In general, estimated k_{22} values obtained by using the MCR to analyze kinetic data for outer-sphere reductions of O_2 by electron-donor complexes, are consistently 1–3 orders of magnitude too small [37, 46, 47]. This *consistency*, however, supported the outer-sphere nature of these reactions [37]. On the other hand, when the MCR was used to calculate k_{22} from kinetic data for reactions between otherwise outer-sphere electron-*acceptor* complexes and $\text{O}_2^{\bullet-}$, calculated k_{22} values spanned 13 orders of magnitude.

The discrepancies between the experimental value of k_{22} and the smaller values calculated from the Marcus theory have been attributed to the small size of O_2 (bond length = 1.21 Å [56]), relative to many electron donors, whose typical sizes are ca. 7–13 Å [55]. This size difference has been noted as a significant contributor to differences between experimental values and those obtained using the MCR, whose derivation assumes the reactants are ideal spheres of the same size. In 1993, Ebersson [48] further noted that the large variation in kinetic parameters associated with electron transfers to O_2 or from $\text{O}_2^{\bullet-}$ might be “due to the fact that the small oxygen/superoxide species easily can come close enough to the second reactant for significant electronic overlap to develop in the transition state”. In other words, the reactions are not truly outer-sphere in nature because electronic coupling between

the reactants is too large (i.e., >1 kcal mol⁻¹). Bakac and Espenson [46] suggested that differences between the solvation energies of the non-polar O₂ molecule and the strongly hydrogen-bonded O₂^{•-} might lead to failure of the MCR to predict k_{22} values from kinetic data. They argued that such differences in solvation energies might cause solvent reorganization energies (λ_{out}) to change dramatically with changes in the nature of the metal complex: “Depending on the local chemical environment of the redox partner, each reaction “prepares for” electron transfer in a different way, particularly as regards the extent of desolvation of O₂(H₂O)_n^{•-}”. In a later publication [47], Bakac and Espenson noted that “the reaction of Fe(cp)₂⁺ with O₂ is apparently nonadiabatic in CH₃CN, and the same might be true in aqueous solutions.” Furthermore, “strong ion pairing with the counterions might well influence the kinetics of the reactions of Fe(CN)₆³⁻ and Mo(CN)₈³⁻”. As pointed out above, k_{22} values calculated from rates of reductions of O₂ by metal complexes were in fairly good agreement with one other, while the problematic reactions were those involving oxidations of O₂^{•-}. To explain this, it was suggested that O₂^{•-}, with an O–O distance of 1.33 Å [57], is specifically solvated in water, such that its effective size is much larger than that of O₂ [46, 47, 56, 57].

12.3.2 General Outer-Sphere Redox Reactions of O₂ and O₂^{•-}

In 2008, Weinstock [52] proposed a modification for the Marcus cross relation, which takes into account the relatively small size of O₂^{•-}, and provides a correction that could, in principle, be applied to any homogeneous electron transfer process characterized by significant differences in size between the donors and acceptors. For this, a single experimentally accessible term was introduced into the general form of the MCR. This term quantitatively accounts for differences in size between electron donors and acceptors.

In the familiar form of the MCR [39, 40], it is assumed that the reorganization energy for the cross reaction, λ_{12} , is the mean of the reorganization energies associated with the self-exchange reactions of each component, i.e., $\lambda_{12} = 1/2 (\lambda_{11} + \lambda_{22})$ [39, 40]. In the case of $r_1 \neq r_2$ the *inner-sphere* reorganization energy, λ_{in} (internal changes in bond lengths, dihedral and torsion angles, etc.), of the cross reaction can still be estimated from the average of the individual self-exchanges: $\lambda_{12(\text{in})} = 1/2 (\lambda_{11(\text{in})} + \lambda_{22(\text{in})})$. However, the *outer-sphere* component of the reorganization energy, λ_{out} , of the cross reaction (external changes in solvent coordinates around the reacting pair), is a function of the radii r_1 and r_2 of the donor and acceptor, respectively (Eq. 12.4). Therefore, when $r_1 \neq r_2$, it can not be expressed in the same manner, i.e., $\lambda_{12(\text{out})} \neq 1/2 (\lambda_{11(\text{out})} + \lambda_{22(\text{out})})$.

$$\lambda_{12(\text{out})} = (ne^2) \left(\frac{1}{r_1} + \frac{1}{r_2} - \frac{1}{r_1 + r_2} \right) \left(\frac{1}{\eta^2} - \frac{1}{D_s} \right) \quad (12.4)$$

In Eq. 12.4, ne^2 is the charge transferred from one reactant to the other, η is the refractive index and D_s is the static dielectric constant.

The modified MCR was obtained by defining the reorganization energy of the cross reaction as shown in Eq. 12.5, using the addition of the single term, Δ , defined in Eq. 12.6.

$$\lambda_{12} = \frac{1}{2}(\lambda_{11} + \lambda_{22} + 2\Delta) \quad (12.5)$$

$$\Delta = (ne^2) \left(\frac{1}{2r_1} + \frac{1}{2r_2} - \frac{1}{r_1 + r_2} \right) \left(\frac{1}{\eta^2} - \frac{1}{D_s} \right) - \frac{1}{2}(\lambda_{11(out)} + \lambda_{22(out)}) \quad (12.6)$$

Equation 12.5 effectively removes the outer-sphere components of the reorganization energies of the self-exchange reactions, $\lambda_{11(out)}$ and $\lambda_{22(out)}$, and replaces them by Eq. 12.4, which explicitly accounts for the difference in size between the two reacting species. When Eq. 12.5 is used to derive the MCR, it retains its familiar form (Eq. 12.7). The expressions for $\ln f_{12}$ and W_{12} , however, now include Δ (Eqs. 12.8 and 12.9) as an additional term.

$$k_{12} = (k_{11}k_{22}K_{12}f_{12})^{1/2}W_{12} \quad (12.7)$$

$$\ln f_{12} = \frac{[\ln K_{12} + (w_{12} - w_{21})/RT]^2}{4 \ln(k_{11}k_{22}/Z^2) + (w_{11} + w_{22} - \frac{\Delta}{2})/RT} \quad (12.8)$$

$$W_{12} = \exp \left[- \left(w_{12} + w_{21} - w_{11} - w_{22} + \frac{\Delta}{2} \right) \right] / 2RT \quad (12.9)$$

Equations 12.6, 12.7, 12.8 and 12.9 were then used together with Lind and Merényi's experimentally determined value of $450 \text{ M}^{-1} \text{ s}^{-1}$, the rate constant, k_{22} , for the self-exchange reaction in Eq. 12.3, to calculate rate constants, k_{12} , for the 14 reactions between inorganic complexes and O_2 listed in Table 12.1. Previous MCR analyses of these reactions either gave estimated k_{22} values of between 1 and $10 \text{ M}^{-1} \text{ s}^{-1}$ (much smaller than $450 \text{ M}^{-1} \text{ s}^{-1}$), or based on the difference in size between the reactants, were carried out using a k_{22} value of ca. $2 \text{ M}^{-1} \text{ s}^{-1}$ in order to obtain accurate rate constants, k_{12} , for the cross reactions [37, 46, 47].

Calculated cross-reaction k_{12} values for one-electron reductions of O_2 by the complexes listed in Table 12.1 were then obtained using the modified MCR (Eqs. 12.6, 12.7, 12.8 and 12.9) using a *single value* of r_2 (specific to outer-sphere electron transfer reactions of O_2). This was done by fitting calculated k_{12} values to *observed* rate constants, k_{12} , using r_2 as *the only adjustable parameter*. A value of $r_2 = 2.5 \text{ \AA}$ gave the best fit, and the excellent agreement in Fig. 12.5. This provided, for the first time, a reliable method (Eqs. 12.6, 12.7, 12.8 and 12.9) for the accurate calculation of rate constants for outer-sphere electron transfer to O_2 .

The effective radius of 2.5 \AA was then used in Eqs. 12.6, 12.7, 12.8 and 12.9 to calculate k_{21} rate constants for reactions of outer-sphere metal complexes with $\text{O}_2^{\bullet-}$.

Table 12.1 Radii and rate constants for 14 electron donors

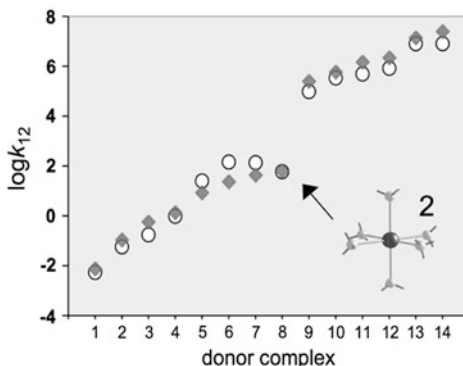
	Entry electron donor ^a	Eff. Radius ^b (Å)	k_{calc} ($\text{M}^{-1} \text{s}^{-1}$)	k_{obs} ($\text{M}^{-1} \text{s}^{-1}$)
1	$\text{Ru}^{\text{II}}(\text{NH}_3)_5\text{phen}^{2+}$	4.5	5.4×10^{-3}	7.7×10^{-3}
2	$\text{Ru}^{\text{II}}(\text{NH}_3)_5\text{isn}^{2+}$	4.5	5.8×10^{-2}	1.1×10^{-1}
3	$\text{Ru}^{\text{II}}(\text{NH}_3)_5(4\text{-vpy})^{2+}$	4.5	1.7×10^{-1}	5.7×10^{-1}
4	$\alpha\text{-PW}_{12}\text{O}_{40}^{4-}$	5.6	9.6×10^{-1}	1.4
5	$\alpha\text{-SiW}_{12}\text{O}_{40}^{5-}$	5.6	25	8.5
6	$\alpha\text{-AlW}_{12}\text{O}_{40}^{6-}$	5.6	1.4×10^2	24
7	$\text{Co}^{\text{II}}(\text{sep})^{2+}$	4.5	1.3×10^2	43
8	$\text{Ru}^{\text{II}}(\text{NH}_3)_6^{2+}$	3.4	59	63
9	$\text{Cr}^{\text{II}}(5\text{-Clphen})_3^{2+}$	6.8	9.7×10^4	2.5×10^5
10	$\text{Cr}^{\text{II}}(\text{bpy})_3^{2+}$	6.8	3.4×10^5	6.0×10^5
11	$\text{Cr}^{\text{II}}(\text{phen})_3^{2+}$	6.8	4.9×10^5	1.5×10^6
12	$\text{Cr}^{\text{II}}(5\text{-Mephen})_3^{2+}$	6.8	8.3×10^5	2.2×10^6
13	$\text{Cr}^{\text{II}}(4,4'\text{-Me}_2\text{bpy})_3^{2+}$	6.8	8.1×10^6	1.4×10^7
14	$\text{Cr}^{\text{II}}(4,7\text{-Me}_2\text{bpy})_3^{2+}$	6.8	8.1×10^6	2.5×10^7

Reproduced from ref. [51] with permission from the American Chemical Society

^aAbbreviations: phen = 1,10-phenanthroline; isn = isonicotinamide; vpy = vinyl pyridine; sep = sepulchrate; bpy = 2,2'-bipyridine

^bExcept for the Keggin anions (entries 4, 5 and 6), these are the “radii equivalent to the sphere of equal volume” [58] equal to $\frac{1}{2}(d_1d_2d_3)^{1/3}$, where d_1 , d_2 and d_3 are the diameters of the complexes along three orthogonal axis

Fig. 12.5 Observed (red diamond) and calculated (circles) rate constants for reactions of $\text{O}_2(\text{aq})$ with 14 one-electron donors. Complex 8 is highlighted (structure and arrow) because its outer-sphere character and kinetic parameters are well established (Reprinted from ref. [52] with permission from the American Chemical Society) (Color figure online)



All parameters, apart from r_2 , were literature values, including $k_{22} = 450 \text{ M}^{-1} \text{ s}^{-1}$. No adjustable parameters whatsoever were included in the set of calculations. These calculated rate constants are compared with experimentally determined ones in Fig. 12.6 [46, 47].

The results in Fig. 12.6 are even more striking than those in Fig. 12.5. This is because previously calculated values for these rate constants spanned 8 orders of magnitude! [46, 47] However, the agreement between experimental and calculated values in Fig. 12.6 provides strong evidence that one-electron oxidations of superoxide by “outer-sphere” oxidants occur via outer-sphere electron transfer. Finally, it should be mentioned that up until 1988, when Bakac and Espenson [46, 47] were

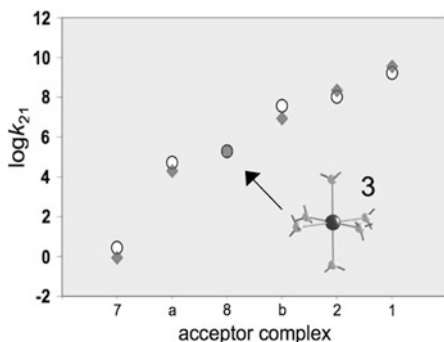


Fig. 12.6 Observed (red diamonds) and calculated (circles) rate constants for reactions of $\text{O}_2^{\bullet-}(\text{aq})$ with electron acceptors. The highlighted complex is the same one as in Fig. 12.5. The electron donors listed by letter and number in the figure are as follows: $\text{Co}^{\text{III}}(\text{sep})^{3+}$ (7'), $\text{Fe}^{\text{III}}(\text{edta})(\text{H}_2\text{O})^-$ (a) [59], $\text{Ru}^{\text{III}}(\text{NH}_3)_6^{3+}$ (8'), $\text{Fe}^{\text{III}}\text{Cp}_2^+$ (b), $\text{Ru}^{\text{III}}(\text{NH}_3)_5\text{isn}^{3+}$ (2'), $\text{Ru}^{\text{III}}(\text{NH}_3)_5\text{phen}^{3+}$ (1'). Rate data for one of these, a, was estimated from data for the reduction of O_2 (see ref. [59]). While this *estimated* value is consistent with an outer-sphere mechanism, experimental data [60] indicate this complex may behave as an inner-sphere oxidant of superoxide (Reprinted from ref. [52] with permission from the American Chemical Society) (Color figure online)

studying these reactions, the experimentally determined value of k_{22} —a key to the present analysis—had not yet been published by Lind and Merényi [53].

12.3.3 Outer-Sphere Electron Transfer from Heteropolytungstates to O_2

12.3.3.1 Marcus Adiabatic Sequential ET–PT Mechanism

Reactions of the iso-structural series of one-electron reduced heteropolytungstates, $\alpha\text{-X}^{n+}\text{W}_{12}\text{O}_{40}^{(9-n)-}$, $\text{X}^{n+} = \text{P}^{5+}$ (**1**_{1e}), Si^{4+} (**2**_{1e}) and Al^{3+} (**3**_{1e}), with O_2 at pH values from 2 to 7.2 in water [37] provided fundamental information regarding the mechanism of electron transfer to O_2 by this family of complexes. The effect of donor-ion charge on rate constants for reductions of O_2 to $\text{O}_2^{\bullet-}$ was also noted.

In reactions of all three POM donor-ions, O_2 was reduced to hydrogen peroxide (Eq. 12.10). In each case, the reactions were first order in both $[\text{donor}]$ and $[\text{O}_2]$, and rate-limiting outer-sphere electron transfer to O_2 was followed by rapid one-electron reduction of superoxide by a second equivalent of the reduced Keggin anion (**POM**_{1e}).



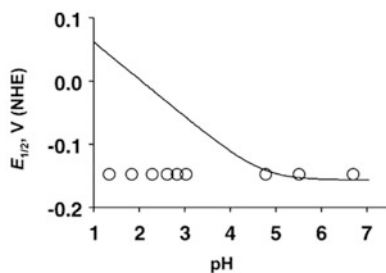


Fig. 12.7 Reduction potentials of the $3_{\text{ox}}/3_{1\text{e}}$ (circles) and $\text{O}_2(\text{aq})/\text{O}_2^{\bullet-}(\text{HO}_2^{\bullet})$ couples (solid line; calculated using published values). As the pH drops below the $\text{p}K_{\text{a}}$ of HO_2^{\bullet} (4.7), $E_{1/2}$ for the $\text{O}_2(\text{aq})/\text{O}_2^{\bullet-}(\text{HO}_2^{\bullet})$ couple becomes more positive, and ΔG° for electron transfer to O_2 becomes more favorable (Reprinted from ref. [37] with permission from the American Chemical Society)

At pH values below 4.7—the $\text{p}K_{\text{a}}$ of HO_2^{\bullet} —disproportionations of $\text{O}_2^{\bullet-}$ and HO_2^{\bullet} were orders of magnitude slower than reactions of superoxide anion or its protonated form with a second equivalent of $\text{POM}_{1\text{e}}$. This was true even at the lowest pH values studied, at which disproportionations of superoxide (and of protonated superoxide, HO_2^{\bullet}) are fast.

Anion **3** was used to study the $[\text{H}^+]$ dependence of the reaction between $3_{1\text{e}}$ and O_2 . For this, the bimolecular rate constant, k_{12} , for the rate-limiting electron transfer to O_2 , was determined at pH values from 2 to 7.2 at a constant ionic strength, μ , of 175 mM. Anion **3** is the only one of the three POM anions studied that is stable to hydrolysis at these pH values. Anions **1** and **2** begin to hydrolyze as the pH is raised above ca. 2 and 3, respectively. It was also shown from electrochemical experiments that neither anion 3_{ox} nor $3_{1\text{e}}$ are protonated between pH 2 and 7 (invariance of $E_{1/2}$ with pH). This means that if H^+ is involved in the reaction, it will *not* be due to protonation of the POM itself, but rather, to protonation of incipient $\text{O}_2^{\bullet-}$ (Fig. 12.7).

The rate constants, k_{12} , obtained at all pH values studied, were effectively identical. For anions $1_{1\text{e}}$ and $2_{1\text{e}}$, the rate of reactions with O_2 showed no significant change as the pH was decreased from 2 to 1. These were the first indications that the reaction is zero-order in $[\text{H}^+]$, namely, pH-independent. Solvent kinetic-isotope effect experiments were carried out in D_2O at D^+ concentrations corresponding to pH values of 2 and 7.2. The rate remained unchanged when the solvent H_2O was replaced by D_2O . That provided a second line of evidence that even at pH 2, well below the $\text{p}K_{\text{a}} = 4.7$ of protonated superoxide (HO_2^{\bullet}), proton transfer (PT) occurs *after* rate-limiting electron transfer to O_2 (ETPT mechanism), rather than via concerted proton–electron transfer (CPET) [61–65], in which an electron and proton are transferred simultaneously in a single elementary step—see Sect. 12.3.2.

Application of the regular form of the MCR (that work [37] was published before the modification of the MCR [52] was available) allowed comparison between measured and calculated values of k_{12} , the rate constants for reactions of one-electron reduced POM ions with O_2 . The experimental values obtained at pH 2

and $\mu = 175$ mM for reactions of anions $\mathbf{1}_{1e}$, $\mathbf{2}_{1e}$, and $\mathbf{3}_{1e}$ with O_2 , were 1.4 ± 0.2 , 8.5 ± 1 , and 24 ± 2 $\text{M}^{-1} \text{s}^{-1}$, respectively. When a k_{22} value of 450 $\text{M}^{-1} \text{s}^{-1}$ for the self-exchange reaction between O_2 and $\text{O}_2^{\bullet-}$ was used in the MCR to calculate k_{12} for the cross reaction with O_2 , estimated rate constants, $k_{12}(\text{calcd})$ were consistently larger than experimental values by 1 to 1.5 orders of magnitude (this was as expected: see Sects. 12.1 and 12.2). When an “effective” value of $k_{22} = 2$ $\text{M}^{-1} \text{s}^{-1}$ was used (as obtained by Lind and Merényi [54, 55] for reactions of organic electron donors, whose radii were between 5 and 7 Å, similar in size to the 5.6 Å radius of the Keggin anion), $k_{12}(\text{calcd})$ values fell into reasonable agreement with observed values, $k_{12}(\text{obs})$. This analysis provided strong evidence that the rate-limiting electron transfer to O_2 occurred via an outer-sphere mechanism.

The value of ΔG° for electron transfer to O_2 decreases by ca. 9 kcal mol⁻¹ (nearly 0.4 V more favorable) when the anion is changed from $\mathbf{1}_{1e}$ to $\mathbf{2}_{1e}$ to $\mathbf{3}_{1e}$. On the other hand, the associated increase in rates is modest (from 1.4 to 8.5 to 24 $\text{M}^{-1} \text{s}^{-1}$, respectively), significantly smaller than would be expected based on the decrease in ΔG° values. This is due to two phenomena: (1) a modest increase in the reorganization energies, λ , for self-exchange between one-electron-reduced and oxidized forms of the Keggin anions (from 25.2 to 30 to 32.2 kcal mol⁻¹, respectively, for $\mathbf{1}$, $\mathbf{2}$, and $\mathbf{3}$) [32], and (2) the effect of donor-anion charge. As the donor anion is varied from $\mathbf{1}_{1e}$ to $\mathbf{2}_{1e}$ to $\mathbf{3}_{1e}$, the corresponding successor-complex ion pairs $[(\mathbf{1}_{\text{ox}}^{3-})(\text{O}_2^{\bullet-})]^{4-}$, $[(\mathbf{2}_{\text{ox}}^{4-})(\text{O}_2^{\bullet-})]^{5-}$, $[(\mathbf{3}_{\text{ox}}^{5-})(\text{O}_2^{\bullet-})]^{6-}$ are subjected to larger anion–anion repulsions. More quantitatively, *corrected* Gibbs free energies, ΔG^{cor} (the difference in energy between the precursor and successor complexes, $[(\alpha\text{-X}^{n+}\text{W}_{12}\text{O}_{40}^{(9-n)-})(\text{O}_2)]^{(9-n)-}$ and $[(\alpha\text{-X}^{n+}\text{W}_{12}\text{O}_{40}^{(8-n)-})(\text{O}_2^{\bullet-})]^{(8-n)-}$) were shown to account for the attenuated increases in rate constants for electron transfer to O_2 as the POM anions became simultaneously better electron donors, and more negatively charged. This quantitative analysis of the kinetic effects of anion-anion repulsion within successor-complex ion pairs provided a second line of evidence that the ET reaction occurred via an outer-sphere mechanism.

12.3.3.2 Concerted Proton–Electron Transfer (CPET) to O_2 in Water

In a recent publication [66], we showed that at low pH values in water, the ETPT mechanism discussed in the previous section is accompanied by a parallel pathway: concerted proton–electron transfer (CPET; Fig. 12.8) [61–65].

This newly identified reaction is important from a fundamental perspective, as well as to environmental chemistry, technology (e.g., in sustainable energy), chemical biology and medicine. CPET is distinguished from the more general proton–coupled electron transfer (PCET) process, which refers to *all* the processes in which coupling involving successive transfers of protons and electrons occur. This term “PCET” *does not* define whether or not the proton and electron are transferred in a single elementary reaction step (CPET, simultaneous proton and electron transfer), or in two subsequent reactions, and therefore, two distinct

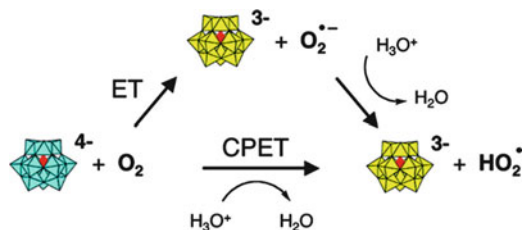
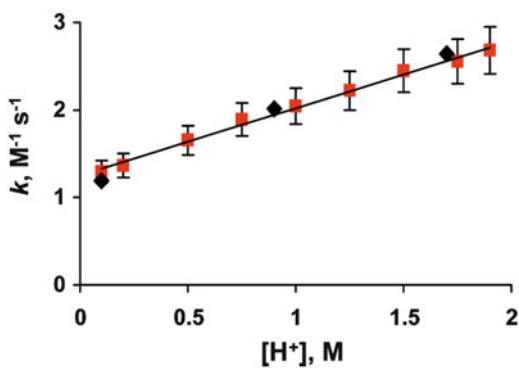


Fig. 12.8 Schematic representation of parallel ET and CPET pathways in reaction of 1_{1e} with O_2 . Water is not only the medium, but also serves as the source for protons (proton donor) (Reprinted from ref. [66] with permission from the American Chemical Society)

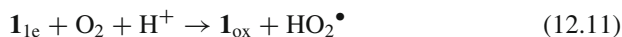
Fig. 12.9 Rate constants, k , for ET to O_2 as a function of $[H^+]$. Red squares are k values as a function of $[H^+]$ at constant ionic strength (2.0 M, by additions of LiCl; $R^2 = 0.994$). Black diamonds at 0.1, 0.9, and 1.7 M H^+ are k values obtained in the absence of added LiCl (Reprinted from ref. [66] with permission from the American Chemical Society) (Color figure online)



elementary steps (ET-PT, or in other cases involving reductions of more basic entities than O_2 or oxidations of acidic proton donors, PT-ET) [67–70].

CPET to dioxygen was documented [66] by reacting members from the isostructural series of one-electron reduced donor anions, 1_{1e} , 2_{1e} , and 3_{1e} , with O_2 at $[H^+]$ values from 0.1 to 1.9 M in water. Of the three donor-anions, 1_{1e} was the only POM anion to display a linear (first-order) dependence of observed rate constants, k_{obs} , on $[H^+]$ (Fig. 12.9). LiCl was used to maintain constant ionic strength, and several independent control experiments ruled out ion-association between Li^+ and 1_{1e} that could induce variations in k_{obs} value. (One representative set of control reactions is indicated by the black diamonds in Fig. 12.9; see caption for details).

Electrochemical measurements ruled out ion-association between 1_{1e} and H^+ (namely, protonation of the POM). Quantitative analysis of rate expressions for possible mechanisms then showed CPET to be the only plausible mechanism that could result in a linear dependence of rates on $[H^+]$. The CPET pathway was found to be first-order in $[H^+]$ (as well as in $[O_2]$ and $[1_{1e}]$), with the proton involved as a reactant (Eq. 12.11).



Linear regression and analysis of k_{obs} values provided rate constants for the ET and CPET pathways: $k_{\text{ET}} = 1.2 \text{ M}^{-1} \text{ s}^{-1}$ and $k_{\text{CPET}} = 0.8 \text{ M}^{-2} \text{ s}^{-1}$, respectively. As noted above, the rate of CPET is also a linear function of $[\text{H}^+]$, and the reaction stoichiometry of 2:1 ($\mathbf{1}_{1e}:\text{O}_2$, with H_2O_2 as the product) was identical to that previously established for ETPT reactions at less acidic pH values [37]. The rate expression is shown in Eq. 12.12.

$$\text{rate} = -1/2d[\mathbf{1}_{1e}]/dt = (k_{\text{ET}} + k_{\text{CPET}}[\text{H}^+])[\mathbf{1}_{1e}][\text{O}_2] \quad (12.12)$$

Kinetic-isotope effect (KIE) experiments (two independent sets) gave a KIE of $k_{\text{H}}/k_{\text{D}} = 1.7$, clearly indicating that PT is involved in the rate determining step of the reaction.

The relationship between Gibbs free energy of the reaction, ΔG° , and the kinetic significance of CPET, was then explored using the more negatively charged, Keggin-anions, $\mathbf{2}_{1e}$ and $\mathbf{3}_{1e}$. It was shown that, in line with theoretical predictions [12, 71–73], CPET becomes more competitive with ET (or with ETPT), and therefore more kinetically significant, as the parallel ET reaction becomes more endergonic. This correlation was more clearly established for $\mathbf{2}_{1e}$, which is less subject than $\mathbf{3}_{1e}$ to ion pairing with H^+ or Li^+ . The results emphasize the uniqueness of $\mathbf{1}_{1e}$, which is less subject to ion pairing than the more negatively charged donor anions, and whose reactions with O_2 are, at the same time, more endergonic. In this case, CPET is competitive with ET, and clearly observed.

Temperature dependence data were analyzed using a form of the Marcus model [68, 74, 75] that simultaneously takes into account the temperature dependence of the Gibbs free energy of the reaction, ΔG° . This modified form of the model allowed determination of accurate values for the reorganization energies for ET and CPET, λ_{ET} and λ_{CPET} , respectively. When the traditional adiabatic Marcus model was used, values of 29.7 and 48.2 kcal mol⁻¹ were calculated for λ_{ET} and λ_{CPET} , respectively, which implied that CPET is far less kinetically accessible. When the temperature dependence of ΔG° was accounted for, however, values of 41.5 and 52.4 kcal mol⁻¹ were obtained for λ_{ET} and λ_{CPET} , respectively, which corresponds to less dramatic difference in reorganization energies for the two pathways.

The CPET reaction is formally termolecular (Eq. 12.11), which might imply a simultaneous “three-body collision” involving all three reactants, $\mathbf{1}_{1e}$, O_2 and H^+ . This is highly unlikely in condensed phase. An alternative description of the three-body encounter was suggested, which relied upon a simple analytic result, combined with the unique nature of protons, and proton mobility, in water. Hence, rather than a single three-body collision, it was suggested that, at the relatively large $[\text{H}^+]$ values used to observe CPET, bimolecular collisions between the POM and O_2 take place *in close enough proximity* (i.e., within a reaction distance) to “excess” protons. Literature values for reaction distances associated with proton “hopping” in models of proton diffusion in water, are typically 2–3 hydrogen bonds, or $6 \pm 1 \text{ \AA}$ [76–87], and the situation described here is shown in Fig. 12.10.

The number of protons, P , within specific reaction distances of 5, 6 and 7 \AA from $[(\mathbf{1}_{1e}^{4-})(\text{O}_2)]^{4-}$ encounter pairs, was calculated using Eq. 12.13, and the results are

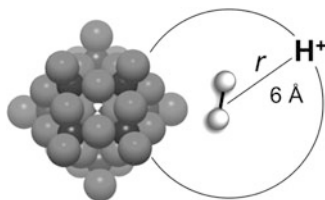


Fig. 12.10 Scale rendering of a $(1_{1e}, O_2)$ encounter pair (space-filling models), with the O_2 molecule located at a distance of $r = 6 \text{ \AA}$ from H^+ (Reprinted from ref. [66] with permission from the American Chemical Society)

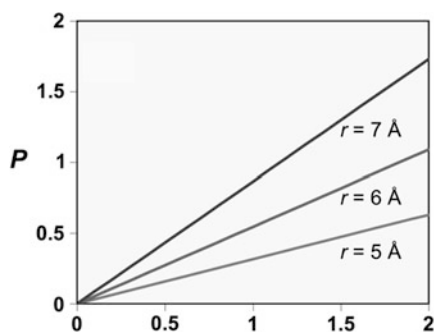


Fig. 12.11 Average numbers of H^+ ions (P) present within specific radii r from O_2 , plotted as a function of $[H^+]$ for $r = 5$ (green line), 6, and 7 \AA (blue line). The relative positions of the electron donor, 1_{1e} , are not included in the model, but see *below* for information about the “lifetimes” of the $(1_{1e}, O_2)$ pairs (Reprinted from ref. [66] with permission from the American Chemical Society) (Color figure online)

shown graphically in Fig. 12.11. At the pH values at which CPET is observed, large fraction of encounter pairs between POM and O_2 form within these plausible H^+ -diffusion reaction distances from the analytical loci of excess proton complexes.

$$P = \frac{4}{3}\pi r^3 N_A [H^+] \quad (12.13)$$

Figure 12.12 (red curve) shows the increase in rate constants for CPET (defined as $k_{\text{CPET}}[H^+]$) as the average distance between $(1_{1e}, O_2)$ encounter pairs and H^+ (x-axis) decreases with increasingly larger $[H^+]$ values. The black line corresponds to the pH-independent rate constant for the ET process; for more details see the figure caption.

The above descriptions are purely analytical. A more dynamic picture was obtained by considering the nature of proton diffusion in water, which is rapid compared to the lifetimes of the $(1_{1e}, O_2)$ encounter pairs. The lifetimes of these encounter pairs, τ , were calculated as the inverse of k_e ($\tau = 1/k_e$), the rate constant for diffusional “escape” from the solvent cage. Two different methods were used

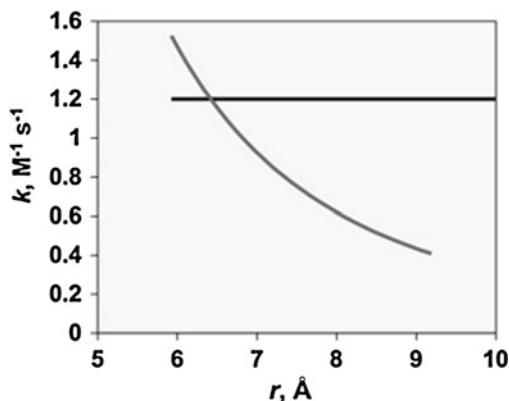


Fig. 12.12 Values for k_{ET} (black line) and $k_{CPET}[H^+]$ (red line), both in units of $M^{-1} s^{-1}$, as a function of the radii, r , of spherical volumes that each contain one proton. These radii indicate the average distance between O_2 molecules and the loci of H^+ ions in solvated proton complexes. The plot of $k_{CPET}[H^+]$ values (red line) begins at $r \approx 9 \text{ \AA}$, which corresponds to $[H^+] = 0.5 \text{ M}$, at which CPET values clearly exceed experimental uncertainties (see Fig. 12.9), and ends at the largest $[H^+]$ value studied (1.9 M) at which $r \approx 6 \text{ \AA}$. The two rate constants, k_{ET} and $k_{CPET}[H^+]$, reach parity ($1.2 \text{ M}^{-1} s^{-1}$) at $r \approx 6.5 \text{ \AA}$, within the commonly reported $5\text{--}7 \text{ \AA}$ “reaction distance” for proton diffusion in water (Reprinted from ref. [66] with permission from the American Chemical Society) (Color figure online)

[88–92], and a range of $\tau = 70\text{--}200 \text{ ps}$ was obtained. These times are approximately two orders of magnitudes longer than that required for proton dislocation over a single water molecule (i.e., the time required for a proton to “jump” a distance of ca. 2.5 \AA , which is ca. 1.5 ps [85, 93]). This raises the probability that protons initially farther than the typical $6 \pm 1 \text{ \AA}$ proton-diffusion reaction distance from ($\mathbf{1}_{1e}, O_2$) encounter pairs can diffuse much closer to O_2 prior to cage escape. It also allows for protons that are already within reaction distances of O_2 to repeatedly diffuse to within 1 or 2 \AA from O_2 , significantly increasing the probability of achieving positions and energies associated with the transition state for CPET. This dynamic situation is shown in Fig. 12.13, in which the excess proton is shown on the right-hand side as a proton complex in water, namely a proton “defect”. In theoretical models based on quantum nuclear path-integral simulations, these positively charged “defects” can become delocalized over $4\text{--}5 \text{ \AA}$ in roughly 10% of the configurations sampled, due mainly to zero-point effects on the PT free-energy profile [76, 82, 83]. The proton is initially located at the center of the water complex, 6 \AA from O_2 , and within the $70\text{--}200 \text{ ps}$ lifetime of ($\mathbf{1}_{1e}, O_2$) encounter pairs, it can easily diffuse through the water-chain network to a location much closer to O_2 .

Finally, the rate constant for CPET, k_{CPET} is still much smaller (orders of magnitude) than the diffusional cage escape rate constant, k_c (Fig. 12.14). Using a steady-state approximation, with $k_{CPET}[H^+] \ll k_c$, the rate expression for CPET reduces to Eq. 12.14.

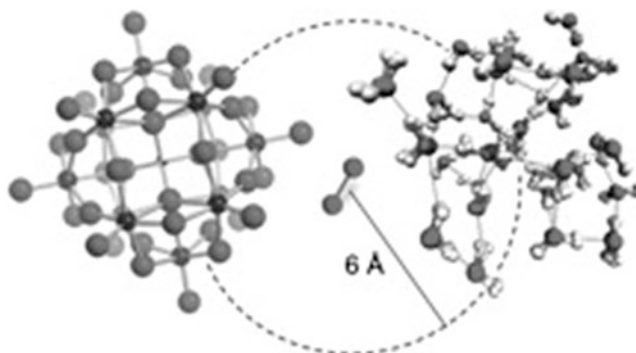


Fig. 12.13 Formation of a $(\mathbf{1}_{1e}, \text{O}_2)$ encounter pair (lifetime of 70–200 ps) close to an 11-Å-diameter fluxional hydrated-proton complex (*far right*; ball-and-stick structures are drawn to scale). As drawn, the dioxygen molecule is 6 Å from the positively charged “defect” initially located at the center of the hydrated-proton complex. There is a non-negligible probability for this defect becoming “quantum mechanically delocalized” to within 1 or 2 Å of O_2 , an event that occurs within a small fraction of the 70–200 ps lifetime of the $(\mathbf{1}_{1e}, \text{O}_2)$ pairs. The oxygen atoms over which the protonic defect is delocalized (from *center left* to *upper right*) are indicated by a partial covering of *blue*, which reflects the quantum mechanically probabilistic nature of the delocalization (Reprinted from ref. [66] with permission from the American Chemical Society) (Color figure online)

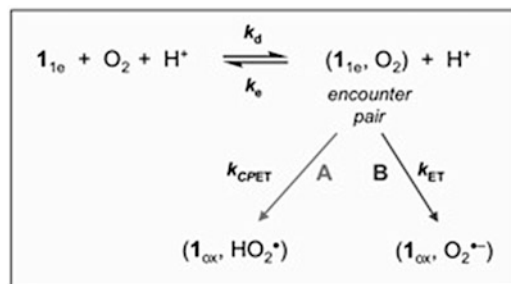


Fig. 12.14 Elementary steps for ET and CPET. Both reactions proceed via the formation of encounter pairs $(\mathbf{1}_{1e}, \text{O}_2)$. These form by diffusion at a rate equal to the bimolecular rate constant k_d , and dissociate from one another with a “cage-escape” rate constant, k_e . At large $[\text{H}^+]$, kinetically significant fractions of the $(\mathbf{1}_{1e}, \text{O}_2)$ encounter pairs form in close proximity to rapidly diffusing H^+ ions, and rates for CPET ($k_{\text{CPET}}[\text{H}^+]$) become competitive with those for ET (k_{ET}) (Reprinted from ref. [66] with permission from the American Chemical Society)

$$-\frac{1}{2}d[\mathbf{1}_{1e}]/dt = \frac{k_d}{k_e}k_{\text{CPET}}[\mathbf{1}_{1e}][\text{O}_2][\text{H}^+] \quad (12.14)$$

Taken together, the findings in refs [37] and [66] clearly show that CPET is observed only for the more endergonic reduction of O_2 by $\mathbf{1}_{1e}$, and only at sufficiently large H^+ concentrations. The authors [66] suggest that “the emergence of multisite CPET, with hydronium ion as the proton donor, may prove a general

feature of sufficiently endergonic reductions of dioxygen by otherwise “outer-sphere” complexes (or electrode reactions) at sufficiently low pH values in water.”

12.4 Concluding Comments

This chapter describes recent developments in understanding electron transfer to dioxygen (O_2) and the outer-sphere oxidation of the superoxide radical anion, $O_2^{\bullet-}$, by metal complexes. Many of the findings were obtained using polyoxometalates as physicochemical probes, and the nature of electron self-exchange between these cluster anions is discussed first. Self-exchange rate constants, k_{11} , were accurately determined for reactions between members of the iso-structural series of one-electron reduced heteropolytungstate anions, $X^{n+}W_{12}O_{40}^{(9-n)-}$, $X^{n+} = P^{5+}$ ($\mathbf{1}_{1e}$), Si^{4+} ($\mathbf{2}_{1e}$), and Al^{3+} ($\mathbf{3}_{1e}$), and their corresponding, fully oxidized forms. Data from those reactions provided fundamental parameters necessary to use the same POMs as mechanistic probes for studying electron transfer to O_2 .

Electron self-exchange reaction between O_2 and $O_2^{\bullet-}$ was then discussed, and developments before and after an experimentally determined rate constant for this reaction was published, were also summarized. Related to this, the problem of size differences between O_2 or $O_2^{\bullet-}$ and their typical metal-complex electron donors or acceptors was recently solved quantitatively by addition of a single experimentally accessible parameter, Δ , which corrected the outer-sphere reorganization energy used in the Marcus cross relation. When this was done, it was found that rate constants for one electron oxidations of the superoxide radical anion, $O_2^{\bullet-}$, by typical outer-sphere oxidants are successfully described by the Marcus model for adiabatic outer-sphere electron transfer.

Reaction between the one electron reduced POM anions and O_2 were then summarized. These studies demonstrated that at mildly acidic to neutral pH values in water, electron transfer from Keggin heteropolytungstates to O_2 occurs by an outer-sphere mechanism. In these cases, the effect of Keggin-ion charge on rate constants for the reduction of O_2 was shown to be significant, and was attributed to anion–anion repulsion within the successor-complex ion pairs formed between the negatively charged POM anions and $O_2^{\bullet-}$. This was followed by the discovery of a concerted proton–electron (CPET) pathway for electron transfer to O_2 at lower pH values (< 1).

The CPET reaction is termolecular, and is facilitated by the unique nature of proton diffusion in water. At the large $[H^+]$ at which CPET is observed, protons are present within the aqueous medium within typical proton-diffusion reaction distances from the encounter complexes formed by bimolecular collisions between $\mathbf{1}_{1e}$ and O_2 . Rapid proton diffusion in water then increases the probability of CPET occurring by allowing protons to repeatedly diffuse to within a few angstroms of the relatively long-lived ($\mathbf{1}_{1e}, O_2$) encounter complexes, whose lifetimes are estimated at 70 to 200 ps. These findings suggest that concerted proton-electron transfer may be

a common feature of many endergonic reductions of O₂ in acidic aqueous solutions by otherwise outer-sphere complexes or electrode reactions.

References

1. Tolman WB, Solomon EI (2010) Preface: forum on dioxygen activation and reduction. *Inorg Chem* 49:3555–3556
2. Gewirth AA, Thorum MS (2010) *Inorg Chem* 49:3557–3566
3. Smeets PJ, Woertink JS, Sels BF, Solomon EI, Schoonheydt RA (2010) *Inorg Chem* 49:3573–3583
4. Bakac A (2010) *Inorg Chem* 49:3584–3593
5. Neumann R (2010) *Inorg Chem* 49:3594–3601
6. Mukherjee A, Cranswick MA, Chakrabarti M, Paine TK, Fujisawa K, Münck E, Que L (2010) *Inorg Chem* 49:3618–3628
7. Halime Z, Kieber-Emmons MT, Qayyum MF, Mondal B, Gandhi T, Puiu SC, Chufan EE, Sarjeant AAN, Hodgson KO, Hedman B, Solomon EI, Karlin KD (2010) *Inorg Chem* 49:3629–3645
8. Shook RL, Borovik AS (2010) *Inorg Chem* 49:3646–3660
9. Ashley DC, Brinkley DW, Roth JP (2010) *Inorg Chem* 49:3661–3675
10. Zhang C, Fan F-RF, Bard AJ (2009) *J Am Chem Soc* 131:177–181
11. Shao M, Liu P, Adzic RR (2006) *J Am Chem Soc* 128:7408–7409
12. Anderson AB, Albu TV (1999) *J Am Chem Soc* 121:11855–11863
13. Humphreys KJ, Mirica LM, Wang Y, Klinman JP (2009) *J Am Chem Soc* 131:4657–4663
14. Roth JP (2009) *Acc Chem Res* 42:399–408
15. Meyer T, Huynh M, Thorp H (2007) *Angew Chem Int Ed* 46:5284–5304
16. Roth JP, Klinman JP (2003) *Proc Natl Acad Sci U S A* 100:62–67
17. Roth JP, Wincek R, Nodet G, Edmondson DE, McIntire WS, Klinman JP (2004) *J Am Chem Soc* 126:15120–15131
18. Tommos C, Babcock GT (1998) *Acc Chem Res* 31:18–25
19. Nocera DG, Guldi DM (Guest eds) (2009) Special issue on renewable energy. *Chem Soc Rev* 38:1–300
20. Eisenberg R, Nocera DG (Guest eds) (2005) Forum on solar and renewable energy. *Inorg Chem* 44:6799–7260
21. Kim WB, Voitl T, Rodriguez-Rivera GJ, Dumesic JA (2004) *Science* 305:1280–1283
22. Bar-Nahum I, Khenkin AM, Neumann R (2004) *J Am Chem Soc* 126:10236–10237
23. Kamata K, Yonehara K, Sumida Y, Yamaguchi K, Hikichi S, Mizuno N (2003) *Science* 300:964–966
24. Weinstock IA, Barbuzzi EMG, Wemple MW, Cowan JJ, Reiner RS, Sonnen DM, Heintz RA, Bond JS, Hill CL (2001) *Nature* 414:191–195
25. Weiner H, Finke RG (1999) *J Am Chem Soc* 121:9831–9842
26. Neumann R, Dahan M (1997) *Nature* 388:353–355
27. Hill CL, Weinstock IA (1997) *Nature* 388:332–333
28. Renneke RF, Hill CL (1986) *J Am Chem Soc* 108:3528–3529
29. Fedotov MA, Maksimovskaya RI, Begaliev DU, Il'yasova AK (1980) *Izv Akad Nauk SSSR Ser Khim* 7:1477–1480
30. Kozik M, Baker LCW (1990) *J Am Chem Soc* 112:7604–7611
31. Kozik M, Hammer CF, Baker LCW (1986) *J Am Chem Soc* 108:7627–7630
32. Geletii YV, Hill CL, Bailey AJ, Hardcastle KI, Atalla RH, Weinstock IA (2005) *Inorg Chem* 44:8955–8966
33. Geletii YV, Weinstock IA (2006) *J Mol Cat A Chem* 251:255–262

34. Sutin N (1982) *Acc Chem Res* 15:275–282
35. Grigoriev VA, Cheng D, Hill CL, Weinstock IA (2001) *J Am Chem Soc* 123:5292–5307
36. Grigoriev VA, Hill CL, Weinstock IA (2000) *J Am Chem Soc* 122:3544–3545
37. Geletii YV, Hill CL, Atalla RH, Weinstock IA (2006) *J Am Chem Soc* 128:17033–17042
38. Czap A, Neuman NI, Swaddle TW (2006) *Inorg Chem* 45:9518–9530
39. Snir O, Weinstock IA (2010) Electron transfer reactions. In: Bakac A (ed) *Physical inorganic chemistry applications*. Wiley, Hoboken
40. Marcus RA, Sutin N (1985) *Biochim Biophys Acta* 811:265–322
41. Pladziejewicz JR, Meyer TJ, Broomhead JA, Taube H (1973) *Inorg Chem* 12:639–643
42. Bakac A, Espenson JH, Creaser II, Sargeson AM (1983) *J Am Chem Soc* 105:7624–7628
43. Stanbury DM, Haas O, Taube H (1980) *Inorg Chem* 19:518–524
44. Creaser II, Geue RJ, Harrowfield JM, Herlt AJ, Sargeson AM, Snow MR, Springborg J (1982) *J Am Chem Soc* 104:6016–6025
45. Stanbury DM, Mulac WA, Sullivan JC, Taube H (1980) *Inorg Chem* 19:3735–3740
46. McDowell MS, Espenson JH, Bakac A (1984) *Inorg Chem* 23:2232–2236
47. Zahir K, Espenson JH, Bakac A (1988) *J Am Chem Soc* 110:5059–5063
48. Ebersson L, Gonzalez-Luque R, Lorentzon J, Merchan M, Roos BO (1993) *J Am Chem Soc* 115:2898–2902
49. Meisel D, Fessenden RW (1976) *J Am Chem Soc* 98:7505–7510
50. Jonsson M, Lind J, Reitberger T, Eriksen TE, Merenyi G (1993) *J Phys Chem* 97:8229–8233
51. Weinstock IA (1998) *Chem Rev* 98:113–170
52. Weinstock IA (2008) *Inorg Chem* 47:404–406
53. Lind J, Shen X, Merényi G, Jonsson BÖ (1989) *J Am Chem Soc* 111:7654–7655
54. Merenyi G, Lind J, Shen X, Eriksen TE (1990) *J Phys Chem* 94:748–752
55. Merényi G, Lind J, Jonsson M (1993) *J Am Chem Soc* 115:4945–4946
56. Hartnig C, Koper MTM (2002) *J Electroanal Chem* 532:165–170
57. Sawyer DT, Valentine JS (1981) *Acc Chem Res* 14:393–400
58. Brown GM, Sutin NA (1979) *J Am Chem Soc* 101:883–892
59. Bull C, McClune GJ, Fee JA (1983) *J Am Chem Soc* 105:5290–5300
60. Summers JS, Baker JB, Meyerstein D, Mizrahi A, Zilbermann I, Cohen H, Wilson CM, Jones JR (2008) *J Am Chem Soc* 130:1727–1734
61. Hammes-Schiffer S (2009) *Acc Chem Res* 42:1881–1889
62. Hammes-Schiffer S, Hatcher E, Ishikita H, Skone JH, Soudackov AV (2008) *Coord Chem Rev* 252:384–394
63. Costentin C (2008) *Chem Rev* 108:2145–2179
64. Huynh MHV, Meyer TJ (2007) *Chem Rev* 107:5004–5064
65. Mayer JM (2004) *Annu Rev Phys Chem* 55:363–390
66. Snir O, Wang Y, Tuckerman ME, Geletii YV, Weinstock IA (2010) *J Am Chem Soc* 132:11678–11691
67. Costentin C, Robert M, Savéant J-M (2007) *J Am Chem Soc* 129:5870–5879
68. Markle TF, Rhile IJ, DiPasquale AG, Mayer JM (2008) *Proc Nat Acad Sci U S A* 105:8185–8190
69. Hammes-Schiffer S, Soudackov AV (2008) *J Phys Chem B* 112:14108–14123
70. Irebo T, Reece SY, Sjodin M, Nocera DG, Hammarstrom L (2007) *J Am Chem Soc* 129:15462–15464
71. Anderson AB, Cai Y, Sidik RA, Kang DB (2005) *J Electroanal Chem* 580:17–22
72. Soudackov A, Hammes-Schiffer S (2000) *J Chem Phys* 113:2385–2396
73. Decornez H, Hammes-Schiffer S (2000) *J Phys Chem A* 104:9370–9384
74. Costentin C, Robert M, Savéant J-M (2007) *J Am Chem Soc* 129:9953–9963
75. Sjodin M, Polivka T, Pan J, Styling S, Sun L, Sundstrom V, Hammarstrom L (2004) *Phys Chem Chem Phys* 6:4851–4858
76. Marx D, Chandra A, Tuckerman ME (2010) *Chem Rev* 110:2174–2216
77. Stoyanov ES, Stoyanova IV, Reed CA (2010) *J Am Chem Soc* 132:1484–1485
78. Swanson JMJ, Simons J (2009) *J Phys Chem B* 113:5149–5161

79. Siwick BJ, Cox MJ, Bakker HJ (2007) *J Phys Chem B* 112:378–389
80. Marx D (2006) *Chemphyschem* 7:1848–1870
81. Mohammed OF, Pines D, Dreyer J, Pines E, Nibbering ETJ (2005) *Science* 310:83–86
82. Hynes JT (1999) *Nature* 397:565–566
83. Marx D, Tuckerman ME, Hutter J, Parrinello M (1999) *Nature* 397:601–604
84. Agmon N (1995) The Grotthuss mechanism. *Chem Phys Lett* 244:456–462
85. Eigen M (1964) *Angew Chem Int Ed* 3:1–19
86. Mohammed OF, Pines D, Pines E, Nibbering ETJ (2007) *Chem Phys* 341:240–257
87. Bell RP (1973) *The proton in chemistry*. Chapman & Hall, London
88. Yoshimura A, Uddin MJ, Amasaki N, Ohno T (2001) *J Phys Chem A* 105:10846–10853
89. Chiorboli C, Indelli MT, Rampi Scandola MA, Scandola F (1988) *J Phys Chem* 92:156–163
90. Eigen MZ (1954) *Phys Chem (Muenchen Ger)* 1:176–200
91. Stickrath AB, Carroll EC, Dai X, Harris DA, Rury A, Smith B, Tang K-C, Wert J, Sension RJ (2009) *J Phys Chem A* 113:8513–8522
92. Bagdasar'yan KS (1984) *Russ Chem Rev* 53:623
93. Meiboom S (1961) *J Chem Phys* 34:375–388

Chapter 13

Multi-electron Transfer Catalysts for Air-Based Organic Oxidations and Water Oxidation

Weiwei Guo, Zhen Luo, Jie Song, Guibo Zhu, Chongchao Zhao, Hongjin Lv, James W. Vickers, Yurii V. Geletii, Djamaladdin G. Musaev, and Craig L. Hill

Abstract Catalysts for multi-electron-transfer events are quite complicated just as the reactions they facilitate. Two classes of such catalysts, those for the air-based oxidation of organic compounds and those for the oxidation of water, are addressed in this chapter. Brief backgrounds in both these areas are provided followed by the ensemble of current challenges in each area illustrated by two ongoing cases in point. The efficient and sustained oxidation of water to dioxygen is critical to the production of solar fuels, which in turn may ultimately be necessary given the increasing cost of ever-less-accessible fossil fuels, the projected demographic trends, and the environmental consequences of fossil fuel use. Importantly, water oxidation catalysts must be connected with other functional units (light absorbers, reduction catalysts and key interfaces) to realize nanostructures or devices that efficiently produce solar fuels. Unfortunately these functional units are dependent on each other and also on several factors, thus predicting overall operation is a challenge in complexity.

W. Guo • Z. Luo • J. Song • G. Zhu • C. Zhao • H. Lv • J.W. Vickers • Y.V. Geletii • C.L. Hill (✉)
Department of Chemistry, Emory University, 1515 Dickey Drive, Atlanta, GA 30322, USA
e-mail: wguo8@emory.edu; zluo@emory.edu; jschem10@gmail.com; gzhu2@emory.edu;
czhao3@emory.edu; hongjin.lv@emory.edu; jamesw.vickers@gmail.com; iguelet@emory.edu;
chill@emory.edu

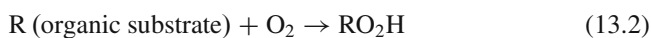
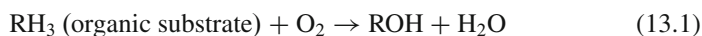
D.G. Musaev
Department of Chemistry, Cherry L. Emerson Center for Scientific Computation, Emory University, 1515 Dickey Drive, Atlanta, GA 30222, USA
e-mail: dmusaev@emory.edu

13.1 Introduction

Catalysts for the O₂-based oxidation of organic substrates and catalysts for the oxidation of water to O₂ are both of much current intellectual and practical interest. Both types of processes involve the transfer of multiple electrons and the catalysts themselves have both geometrical and electronic structures as well as mechanisms of action that are highly complex. The three usual requirements for optimal catalysts, namely fast turnover rates, high selectivity, and high stability, are certainly important for both these classes of catalytic processes. This overview article first provides general introductions to both areas of endeavor and then addresses recent significant advances in each area with an emphasis on the larger points that the community is learning in the course of investigating such complex systems.

13.1.1 Catalysts for Air-Based Oxidations

These processes are a main-stay in green synthetic organic chemistry because reagents and conditions are frequently simple and there are no deleterious oxygen-derived by-products: reactions taking place by the monooxygenase stoichiometry (Eq. 13.1) produce only H₂O as a by-product, and those taking place by a rare dioxygenase stoichiometry (Eq. 13.2) have no oxygen-derived by-product [1–4]. The environmental arguments for such processes alone are considerable and growing. These reactions result in the multi-electron reduction of O₂ and oxidation of the organic substrate (reactant).



Oxidation reactions that use ambient air as the oxidant are of additional value in that they can be used, in principle, to decontaminate a wide variety of toxic compounds in human environments, including toxic industrial chemicals (TICs), and do so very inexpensively and under mild conditions [5–11]. In addition, the availability of effective catalysts for air-based oxidation processes could be centrally valuable to the decontamination of chemical warfare agents (CWAs) [12, 13]. One of multiple reasons for this is that the logistic (and associated economic) burden for such decontamination technology is minimal. Most decontamination technology in military or civilian venues involves the use of highly reactive solutions, foams or powders that themselves have handling, transportation and safety challenges. This isn't the case if air and air only is the reactive decontaminating agent. In addition, no energy sources are needed for air-based decontamination because all air-based oxidations of organic substrates, including the TICs and CWAs, are thermodynamically favourable. The released energy sustains the reaction provided the catalytic

process is sufficiently rapid. In contrast, the organic substrate degradation reactions that proceed through hydrolysis or non-oxidation mechanisms frequently require an external energy source. Also, the safety concerns associated with the use of air-based oxidation processes are minimal: there is no toxic solution, gel or powder to deal with and no associated liquid or solid waste to remediate.

As attractive as rapid and controlled oxidations that require only ambient air are, such processes are very hard to realize. Dioxygen-based and in particular ambient-air-based oxidations are also unpredictable, a point that derives from the complex nature of autoxidation processes, both those that are facilitated by metals and those that are not [1, 14, 15]. A few years ago there were effectively no catalysts with sufficient reactivity to facilitate rapid oxidations of the usual organic substrates, including TICs and CWAs, using ambient air as the oxidant that proceeded at a satisfactory rate. Natural air-based oxidation processes of organic materials including rubber, plastics, metals, and biological structure are either extremely slow or, at high temperature, violently fast (fires and explosions). Designing and realizing catalytic systems that actually allow organic reactions with regular triplet oxygen to proceed at satisfactory rates were truly rare until recently.

13.1.2 Catalysts for Water Oxidation (Production of Solar Fuels)

The production of alternative and renewable energy to power the planet is a pressing international concern [16–19]. Two of the most critical points here are the accessibility of fossil fuels and the environmental cost of their continued and escalating use. Current projections indicate that we will run out of technologically accessible and thus economically viable fossil fuels (gas, petroleum and coal) quite shortly (3–5 decades) at the current rate of increasing energy demand. Also, the consensus of the research community, as reflected by reports by the U.S. National Academy of Science (NAS) and other credible research-based organizations, is that global climate change is real, caused by mankind's activities, and is already having a substantial and deleterious effect on world climate. The correctness of this assessment is time dependent and as time has moved forward and ever more experimental data have been accumulating, the human-activity origins of global climate change are becoming increasingly certain. One can argue against the consensus findings of the research community or take action that these findings might be or are correct. Fortunately, nearly all political and other leaders are increasingly embracing the scientific facts and starting to implement policy that reflects these facts. This has given rise to one of the largest and most active global research communities in memory: one focused on production of renewable energy. It is evident to all informed citizenries that if we run out of energy, it's not just the availability of fresh water in sub-Saharan Africa and other developing parts of the world that will be in jeopardy but virtually all our societal activities along with national and international security and global health.

The various forms of renewable energy (principally hydroelectric, geothermal, biofuels, wind, tides, and solar) constitute only about 10% of total energy consumption in most developed countries. Typically 5–10% of societally usable energy comes from nuclear and the remaining 80% comes from the burning of fossil fuels, which unavoidably produces CO₂ and H₂O. Critically, only solar has the capacity to power the planet given projected increases in the global population and standard of living [17]. (Developed societies consume far more energy than underdeveloped ones and the development of highly populated nations including China, India, Malaysia and Indonesia is rapid and substantial at present.) A consequence of technical realities (declining accessible fossil fuel availability and environmental changes), is that there are few governments not investing in renewable energy. As a result of this and the rapidly increasing technical information available, the worldwide research effort in this area has become commensurately substantial.

Energy must not only be generated but also stored in safe, viable and economical ways [20]. Of the ways to store energy, most prominently heat, electricity and fuel, it is latter which is critically needed [17, 19, 21]. Energy stored in the form of heat or electricity will likely never have the weight and volume density to power ships and aircraft. A very high percentage of the global economy depends on the commodities transported by ships. Thus the need for making not only electricity from ambient sunlight (photovoltaics, etc.) more efficiently and cheaply but more importantly, the need for making “solar fuel” is clear.

Four unit operations are needed to convert sunlight into solar fuel: (1) an efficient absorber of solar light; (2) a charge separation structure enabling the absorbed photon energy to be converted with high quantum yield into a charge-separated state (exciton); (3) harvesting the electron in this excited state and using it to reduce low-energy molecules, particularly CO₂ and H₂O, thus converting them into high energy molecules (reduced molecules or “fuels”); and (4) harvesting the hole (positive charge) in the excited state four times sequentially to oxidize water to oxygen [18]. Advances are needed in all four of the above unit operations but most experts write and state in current conferences that realizing catalysts for the multi-electron reduction of CO₂ and H₂O to fuels and the four-electron oxidation of H₂O to O₂, Eq. 13.3, is the greatest current challenge. Further, there is general consensus that the development of viable (very fast, selective and extremely stable) water oxidation catalysts (WOCs) is the real bottleneck [22].



A viable WOC is necessarily a complex structure because it must be multi-tasking: it must store up four oxidizing equivalents, facilitate removal of four electrons and enable the formation of the thermodynamically weak oxygen-oxygen single bond. The coupling of proton transfer with electron transfer is essential for having any multi-electron transfer process, and certainly for this four-electron one in Eq. 13.3, to proceed efficiently [23–27]. Proton coupled electron transfer (PCET) is itself a highly complex process as it is orchestrated and carried out in Nature and some synthetic systems alike [24, 28–31]. PCET is a principle

but not the only mechanism underlying the phenomenon of redox levelling, the observation that in some systems, multiple electrons can be removed or added to the catalyst with a minimal increase in the energy of the subsequent electron transfer events. In essence, for a multi-electron oxidation process, as exemplified by water oxidation, Eq. 13.3, the sequential oxidations of the catalyst (storing of four oxidizing equivalents needed) all proceed over a narrow potential range. Redox levelling is seen in catalytic water oxidation by the oxygen evolving center (OEC) in Nature (Photosystem II in green plants) [32] and in some synthetic WOCs.

A final note regarding renewable fuel production: when the sub-structures facilitating the four unit operations are physically joined, the rates of component processes, including electron transfer across the interfaces as well as catalytic fuel and oxygen production steps can be significantly altered. In short, rates and efficiencies are frequently dependent on device architecture as well as the characteristics of each separated unit. The full solar fuel generating nanostructures or devices and their operation are examples of nonlinear and complex systems. It is simplistic and unwise to formulate any functioning structural unit for artificial photosynthesis without real consideration of the impact that the new interfaces between this unit and the others and the effects the operating conditions will have on the thermodynamics and kinetics of the coupled processes.

13.2 Catalysts for Air-Based Oxidations

The first catalysts for O₂- or air-based oxidation that facilitate rates of serious interest were “nanogold” systems, a designation given to supported nanoparticles of Au(0) and, later, supported thin films [33, 34]. These systems are most effective for oxidation of CO to CO₂ [35–38] and don’t oxidize a wide spectrum of organic functions under mild conditions. This factor, in addition to potential cost and availability issues with gold, suggests these catalysts don’t appear to be optimal for use in decontamination and deodorization using ambient air on large scales. The second catalysts developed for air-based oxidations that are fast under ambient conditions (use air at room temperature) were polyoxometalate (POM) systems, and in particular polytungstates with 3d metals, including Cu, substituted in surface positions [39–43]. A general catalytic cycle that summarizes the general mechanism for these oxidations is shown in Fig. 13.1 [39]. Since POM redox potentials (and most other features that impact their redox reactions) can be systematically altered through synthesis, the rates of both the substrate (threat) oxidation step (at *right* in Fig. 13.1) and the air-based reduced-POM re-oxidation step (at *left* in Fig. 13.1) can be controlled to a considerable degree [39, 40].

More recently, co-catalysts, including iron bromide and nitrate complexes, were found for the catalytic air-based oxidation chemistry in Fig. 13.1 [44]. When these co-catalysts are combined with the appropriate POM (frequently [CuPW₁₁O₃₉]⁵⁻) potent redox cycles for organic oxidations in addition to the cycle given in Fig. 13.1 are introduced and overall air-based oxidation rates increase.

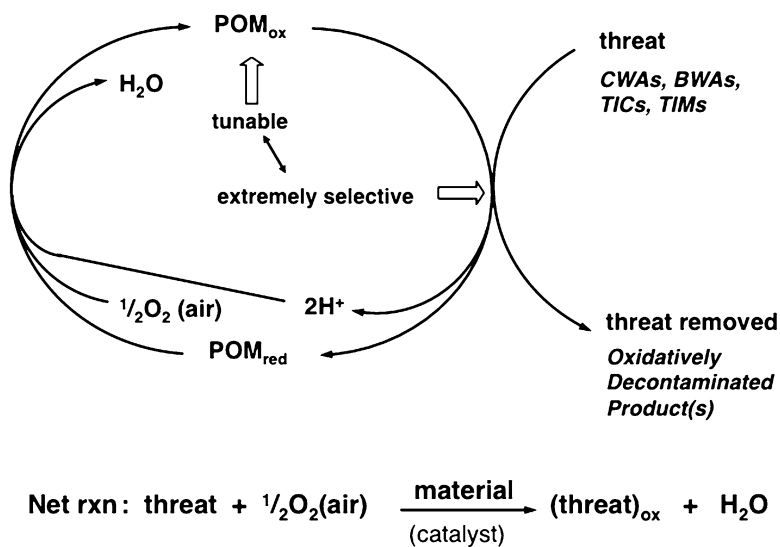


Fig. 13.1 The general two-step mechanism for POM-catalyzed O_2 -based oxidations of organic compounds

Iron bromide-catalyzed O_2 -based organic substrate oxidations have been noted by other groups [45, 46], but the mechanisms were not convincingly studied until recently [47]. These composite POM-iron bromide-nitrate catalysts are the fastest at present for air-based oxidation. They are multi-component systems that constitute some of the most complex synthetic systems known which have dynamic function. It is no surprise that attempts to heterogenize such multi-component catalysts while retaining their very high turnover rates for air-oxidation reaction have been challenging [48, 49]. Such work is ongoing in various laboratories.

Systematic efforts to combine the multiple attractive features of POM catalysts with the sorption and high-surface-area attributes of metal organic frameworks (MOFs) have produced several MOFs with POM units residing in the various pores. POMs in polymeric matrices, [50, 51] and most recently POMs in MOF pores that exhibit catalytic activity [52], have been recently reviewed. Research by Maksimchuk, Kholdeeva and co-workers [53, 54] and Gascon, Kapteijn and co-workers [55, 56] are noteworthy. Many of these hybrid (or composite) materials do display the catalytic attributes of the POMs and some of the selective uptake properties of the MOFs. Separate from this evident combining of attractive properties exhibited by both component structures, some POM-MOF type materials also are potential examples of complex behavior because the catalyzed reactions are far from equilibrium and the multiple features impacting catalyst turnover rates aren't related to each other in a simple way: they can change with time (conversion of the substrate) and conditions.

Recently, a POM-MOF catalyst was reported that demonstrates a dramatic synergy between the POM and MOF units in two respects: hydrolytic stability and catalytic turnover rate [11]. Whereas, the POM catalyst, $[\text{CuPW}_{11}\text{O}_{39}]^{5-}$, is only stable to hydrolysis over a narrow pH range, and the MOF is unstable to hydrolysis at all pH values, the POM-MOF conjugate is very stable in water over a wide pH range and can be recovered from extended incubation in highly basic solutions. In addition, the air-based oxidations (thiol + air forming disulfide + H_2O and H_2S + air forming S_8 + H_2O) catalyzed by the POM-MOF conjugate, $[\text{CuPW}_{11}\text{O}_{39}]^{5-}$ -MOF-199 (also known as HKUST-1 after the originators of this MOF) [57], is far faster than catalysis by the POM, $[\text{CuPW}_{11}\text{O}_{39}]^{5-}$, alone or by the MOF alone [11]. The origin of the dramatic increase in catalytic turnover rate when the POM is encapsulated is not obvious, but the X-ray structure of $[\text{CuPW}_{11}\text{O}_{39}]^{5-}$ -MOF-199 is consistent with one potential explanation for both the enhanced hydrolytic stability and the catalytic activity.

The X-ray structure of $[\text{CuPW}_{11}\text{O}_{39}]^{5-}$ -MOF-199 (Fig. 13.2) reveals that the catalytic $[\text{CuPW}_{11}\text{O}_{39}]^{5-}$ units are very tightly bound in some of the larger pores of MOF-199 (there is no evidence that even small molecules can diffuse into these POM-occupied sites). However, some of these larger pores are also empty giving this POM-MOF a high porosity which doubtless contributes to its catalytic properties (high turnovers and turnover rates for the air-based oxidations). The five counterions per $[\text{CuPW}_{11}\text{O}_{39}]^{5-}$ unit reside in smaller pores. The rate enhancements could derive from the tight fit of the $[\text{CuPW}_{11}\text{O}_{39}]^{5-}$ units in the pores and the consequent interactions between the 5-polyanion unit and the Cu(II) centers in the MOF-199 framework. These electrostatic interactions will increase the potential of the Cu center in the $[\text{CuPW}_{11}\text{O}_{39}]^{5-}$ which will, in turn, accelerate the substrate (e.g. thiol, H_2S) oxidation step (*right side* of Fig. 13.1).

Since this first step is frequently rate limiting in the overall POM catalyzed air-based oxidation processes, then this tight POM encapsulation in the MOF pores could explain the rate acceleration. The dramatically decreased hydrolytic decomposition of $[\text{CuPW}_{11}\text{O}_{39}]^{5-}$ -MOF-199 relative to either component alone likely reflects this stabilizing interaction between the highly negative POM units and the surrounding positive copper centers in the MOF framework.

Additional POM-MOF materials that display synergistic stabilization and catalysis have more recently been noted (unpublished work from our laboratory).

13.3 Catalysts for Water Oxidation (Production of Solar Fuels)

As noted in the introduction, the development of viable WOCs is central to the ultimate realization of useful devices for generating green fuel (solar fuels and others) [21, 22, 32, 58, 59]. “Viable” means fast, selective and extremely stable but also compatible with the other unit operations (light collection, exciton generation, and interfacial electron transfer) [60]. Given the central importance of WOCs, there

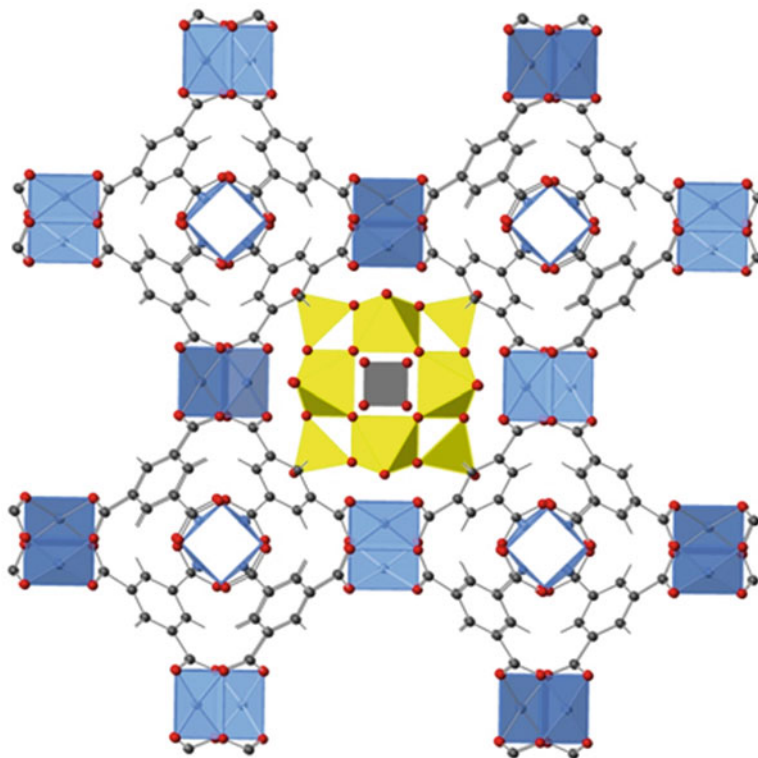


Fig. 13.2 X-ray crystal structure of $[\text{CuPW}_{11}\text{O}_{39}]^{5-}$ -MOF-199 in combined ball-and-stick and polyhedral representations. One of the large pores containing the *yellow* and *grey* Keggin-type POM is shown. This POM is orientationally disordered so that the Cu atom is statistically positioned over the 12 metal positions in the polyanion. The counterions in the smaller pores aren't shown for clarity. Color code: oxygen atoms are *red*; carbon atoms are *grey*; copper atoms are *blue-grey*; the PO_4 tetrahedron inside the POM is *grey*; and the WO_6 octahedra are *yellow*. (Color figure online)

have been many reports on both homogenous [61–77] and heterogeneous WOCs [78–89], with the number of reports of both types rapidly increasing as of mid-2012.

Homogeneous catalysts, including WOCs, are generally much faster than heterogeneous catalysts and their geometrical and electronic structures as well as the mechanisms of their reactions can be studied both experimentally and computationally more readily and with far more precision than for their heterogeneous counterparts. The principal advantage of heterogeneous catalysts is that they are generally much more robust (typically metal oxides for WOCs) and more easily prepared in quantity and at low cost. Our team's design concept and thrust was to use d^0 metal oxide cluster anions, and in particular polytungstates, as ligands to bind and stabilize multiple redox-active transition metals so that the latter could be sequentially oxidized by two or hopefully the four electrons that are needed for a viable WOC [90]. This concept was realized with the first POM-based WOC,

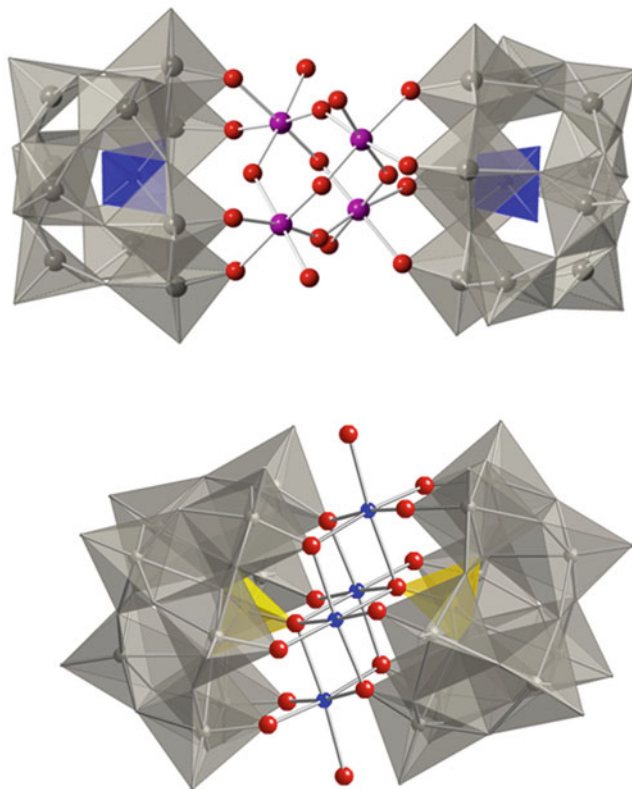


Fig. 13.3 X-ray crystal structures of polyanions $[\{\text{Ru}_4\text{O}_4(\text{OH})_2(\text{H}_2\text{O})_4\}(\gamma\text{-SiW}_{10}\text{O}_{36})_2]^{10-}$ (**Ru₄**) (top) and $[\{\text{Co}_4(\text{H}_2\text{O})_2(\text{PW}_9\text{O}_{34})_2\}]^{10-}$ (**Co₄**) (bottom) in combined ball-and-stick and polyhedral notation. Color code for **Ru₄**: oxygen is red; ruthenium is magenta; SiO_4 tetrahedra are blue; and WO_6 octahedra are gray. Color code for **Co₄**: oxygen is red; cobalt is blue; PO_4 tetrahedra are yellow; and WO_6 octahedra are gray (Color figure online)

$[\{\text{Ru}_4\text{O}_4(\text{OH})_2(\text{H}_2\text{O})_4\}(\gamma\text{-SiW}_{10}\text{O}_{36})_2]^{10-}$ (**Ru₄**), a complex that was also prepared via a different synthetic route by the group of Marcella Bonchio in Padova, Italy [91]. The X-ray crystal structure of **Ru₄** is shown in Fig. 13.3.

Since the initial papers on **Ru₄**, this complex has been extensively characterized and shown to function when immobilized on carbon nanotubes as a water electrooxidation catalyst [92], in solution as a homogeneous catalyst for visible-light-driven water oxidation [93], and when interfaced with $[\text{Ru}(\text{bpy})_3]^{2+}$ -sensitized TiO_2 surfaces [94]. **Ru₄** has shown no evidence of hydrolytic decomposition to the metal oxides (RuO_2 , WO_3) in any of these studies. The mechanism of water oxidation by $[\text{Ru}(\text{bpy})_3]^{3+}$ has also been probed in some depth and the principal catalytic cycle for water oxidation involves sequential oxidation of the resting oxidation state of **Ru₄**, which is $\text{Ru}(\text{IV})_4$, to the oxidation state $\text{Ru}(\text{V})_4$ [95], followed by O_2 evolution.

The availability and cost of ruthenium in **Ru₄** compelled us to prepare and evaluate several of the earth-abundant and inexpensive 3d metals in similar POM structural motifs, and specifically those bearing a core of multiple 3d metals bridged by oxygens that is sandwiched between multivalent polytungstate ligands. In 2010 we identified $[\text{Co}_4(\text{H}_2\text{O})_2(\text{PW}_9\text{O}_{34})_2]^{10-}$ (**Co₄**; X-ray structure in Fig. 13.3) as an effective water oxidation catalyst that was the fastest WOC known per active site metal at that time [96]. Subsequently, **Co₄** was demonstrated to catalyze efficient H₂O oxidation by persulfate using visible light and the standard photosensitizer $[\text{Ru}(\text{bpy})_3]^{2+}$ [97].

An intellectually but not necessarily practically important question pursued for decades is whether a soluble complex is the actual catalyst or an insoluble material (particles or film) arising from decomposition of this complex during turnover. This quandary first surfaced on the reducing side: were soluble organometallic complexes the catalysts or metal nanoparticles derived from breakdown of the complexes? A range of studies and techniques surfaced to address this issue [98, 99]. Most soluble complexes for reductive reactions (hydrogenations, metatheses, reductive couplings, etc.) remain homogeneous catalysts but many systems do, in fact, form metal particles that can't often be readily detected at the outset because the particle sizes are in the small nanometer size regime. Later this dilemma arose in context with oxidation catalysts. Specifically, do metal oxide cluster compounds, such as POMs, function as homogeneous oxidation catalysts, or do they simply serve as precursors to metal oxide particles or films, which are the true catalysts?

A recent publication reported that **Co₄** is simply a precatalyst for a cobalt oxide film which is the actual water oxidation catalyst under electrochemical conditions [100]. This publication didn't explicitly state that **Co₄** in our homogeneous catalytic studies [96] was not the actual catalyst and that insoluble cobalt oxide was but this was strongly implied. However, this implication is incorrect: our original paper reporting homogeneous water oxidation catalyzed by **Co₄** was under much different conditions than those in the subsequent study [100]. The original investigation used traditional (micromolar) concentrations of the POM WOC; whereas, the subsequent electrochemical study used catalyst concentrations two orders of magnitude higher. The solubility of polyoxometalates near their pH limits of thermodynamic hydrolytic stability is extremely sensitive to metal concentration. The original study used the soluble complex, $[\text{Ru}(\text{bpy})_3]^{3+}$, as the oxidant; whereas, the subsequent study used a highly oxidizing glassy carbon electrode as the oxidant. Also the two studies focused on different time regimes. It should be noted that the original study of water oxidation catalyzed by **Co₄** in solution provided seven different experiments that thoroughly established the stability of the **Co₄** under these conditions, including three techniques that directly ruled out the presence of cobalt oxide particles from decomposition of **Co₄** during catalysis [96]. All this data was effectively ignored in the subsequent electrochemical study. The original study (homogeneous water oxidation catalyzed by **Co₄**) has been reproduced by other research groups (work that has yet to be published). Finally, several other groups have used quite definitive techniques, including dynamic light scattering (DLS), to assess the presence of particles in homogeneous water oxidation

catalyzed by several different polyoxometalate complexes and none of these studies have shown POM decomposition to form metal oxide particles or films during catalysis [77, 101].

There is a key distinction between a soluble metal complex versus an insoluble product (particles or films) for the reductive versus oxidative domains. For reductive systems, generally, if not always, the metal is far more stable thermodynamically than the soluble complex. Thus once the metal forms, that's it; there is no going back to homogeneous catalysis. This is NOT the case for POMs (soluble metal-oxygen-cluster polyanions) and their corresponding metal oxide(s). POMs and metal oxide represent equilibrium systems in water over a wide range of pH values [102]. In other words, there are pH ranges where the POM is thermodynamically more stable than the metal oxide or hydroxide. Indeed, POMs are frequently made by heating up the metal oxide or hydroxide at a suitable pH in water: the metal oxide dissolves to form the POM [102]. This fact underlies our group's approach to develop multi-electron-transfer catalysts for solar fuel production because these catalysts must be extremely stable. (Projected turnover numbers, TONs, for the catalysts in viable solar fuel production devices range from 10^8 to more than 10^9 . . . and there are no known catalysts at present, synthetic or biological, that persist that long.) The dynamic behavior of metal oxides under catalytic water oxidation conditions is reflected not only in POM-metal oxide equilibration reactions but also in the evident equilibration chemistry of the Nocera catalyst (cobalt oxide phosphate film) under catalytic conditions [80, 103].

Since the development of Co_4 , another molecular WOC by Sun, Llobet, Privalov and co-workers is substantially faster but it contains organic ligands that are rapidly oxidized [104]. Most recently, a new carbon-free and thus oxidatively stable POM-based WOC has been developed in our group at Emory University. This one is more thermodynamically stable to hydrolysis than Co_4 in basic water, the desired medium for water oxidation. This new tetra-cobalt-containing polytungstate turns over at a rate of $>1,000$ O_2 molecules per second at pH 9, making it the fastest WOC, at least thus far.

But this brings one to a final point regarding solar fuel generation devices. What matters to the research community and to society is that such devices be efficient, fast and stable. It doesn't matter what form the catalysts, light absorber-charge separators or interfaces are as long as they exhibit these three attributes. If they do, they could well be viable.

We close by returning to a point noted above and related to the theme of this book: the oxidation of water and thus WOCs are very complicated, but in generating viable sunlight-driven solar fuel production systems, the WOC is only one component; interfacing the WOC with the light absorbing and charge separating components and these in turn with multi-electron-reduction catalysts can significantly perturb both the thermodynamics and kinetics of component steps in the overall process. Complete solar fuel generating entities are examples of complexity at a leading edge of scientific endeavor. At present it's not possible to predict the overall efficiency of solar fuel generating nanostructures or devices because the several component substructures affect each other's properties and in turn consequently partially control multiple charge transfer events. Complicating

matters further, these charge transfer events themselves may not necessarily depend linearly on the usual reaction parameters: local electronic structures, interface properties, external reaction conditions, and others.

Acknowledgements We thank the U.S. Department of Defense (the Army Research Office and the Defense Threat Reduction Agency (DTRA)) for funding complex catalysts for air-based oxidations and the Department of Energy, Office of Basic Energy Sciences for funding our research on catalytic water oxidation.

References

1. Sheldon RA, Kochi JK (1981) Metal-catalyzed oxidations of organic compounds. Academic Press, New York
2. Hill CL (1999) *Nature* 401:436
3. Neumann R (2004) Polyoxometalates as catalysts for oxidation with hydrogen peroxide and molecular oxygen. In: Beller M, Bolm C (eds) *Transition metals for organic synthesis*, 2nd edn., vol 2, Wiley, Weinheim, p 415
4. Neumann R (2004) *Mod Oxid Methods* 223
5. Boring E, Geletii YV, Hill CL (2001) *J Am Chem Soc* 123:1625
6. Boring E, Geletii YV, Hill CL (2003) In: Simandi LI (ed) *Advances in catalytic activation of dioxygen by metal complexes*, vol 26, Kluwer Academic Publishers, Dordrecht, p 227
7. Rhule JT, Neiwert WA, Hardcastle KI, Do BT, Hill CL (2001) *J Am Chem Soc* 123:12101
8. Okun NM, Anderson TM, Hill CL (2003) *J Mol Catal A Chem* 197:283
9. Kholdeeva OA, Timofeeva MN, Maksimov GM, Maksimovskaya RI, Neiwert WA, Hill CL (2005) *Inorg Chem* 44:666
10. Kholdeeva OA, Timofeeva MN, Maksimov, GM, Maksimovskaya RI, Rodionova AA, Hill CL (2005) Aerobic formaldehyde oxidation under mild conditions mediated by ce-containing polyoxometalates. In: Sowa JR Jr (ed) *Catalysis of organic reactions*, Marcel Dekker, Inc., New York, p 429
11. Song J, Luo Z, Britt D, Furukawa H, Yaghi OM, Hardcastle KI, Hill CL (2011) *J Am Chem Soc* 133:16839
12. Yang YC, Baker JA, Ward JR (1992) *Chem Rev* 92:1729
13. Hill CL, Okun NM, Hillesheim DA, Geletii YV (2007) In: Reynolds JG, Lawson GE, Koester CJ, (eds) *Anti-terrorism and homeland defense: polymers and materials*, ACS symposium series 980, chapter 12, American Chemical Society, Washington, DC, p 198
14. Black JF (1978) *Am Chem Soc* 100:527
15. Partenheimer W (1995) *Catal Today* 23:69
16. Chow J, Kopp RJ, Portney PR (2003) *Science* 302:1528
17. Lewis NS, Nocera DG (2006) *Proc Natl Acad Sci* 103(43):15729
18. Balzani V, Credi A, Venturi M (2008) *ChemSusChem* 1:26
19. Gray HB (2009) *Nat Chem* 1:7
20. Cook TR, Dogutan DK, Reece SY, Surendranath Y, Teets TS, Nocera DG (2010) *Chem Rev* 110:6474
21. Hammarstrom L, Hammes-Schiffer S (2009) *Acc Chem Res* 42:1859
22. Eisenberg R, Gray HB (2008) *Inorg Chem* 47:1697
23. Cukier RI, Nocera DG (1998) *Annu Rev Phys Chem* 49:337
24. Huynh MHV, Meyer TJ (2007) *Chem Rev* 107:5004
25. Hammes-Schiffer S (2009) *Acc Chem Res* 42:1881
26. Hammes-Schiffer S, Stuchebrukhov AA (2010) *Chem Rev* 110:6939
27. Warren JJ, Tronic TA, Mayer JM (2010) *Chem Rev* 110:6961

28. Kuhne H, Brudvig GW (2002) *J Phys Chem B* 106:8189
29. Carra C, Iordanova N, Hammes-Schiffer S (2003) *J Am Chem Soc* 125:10429
30. Kumar A, Sevilla MD (2010) *Chem Rev* 110:7002
31. Petek H, Zhao J (2010) *Chem Rev* 110:7082
32. Barber J (2009) *Chem Soc Rev* 38:185
33. Chen MS, Goodman DW (2004) *Science* 306:252
34. Chen M, Cai Y, Yan Z, Goodman DW (2006) *J Am Chem Soc* 128:6341
35. Guzman J, Gates BC (2004) *J Am Chem Soc* 126:2672
36. Kulkarni A, Lobo-Lapidus RJ, Gates BC (2010) *Chem Commun* 46:5997
37. Kim WB, Voitl T, Rodriguez-Rivera GJ, Dumesic JA (2004) *Science* 305:1280
38. Soares JMC, Bowker M (2005) *Appl Catal A* 291:136
39. Hill CL, Prosser-McCartha CM (1995) *Coord Chem Rev* 143:407
40. Neumann R (1998) *Prog Inorg Chem* 47:317
41. Mizuno N, Misono M (1998) *Chem Rev* 98:199
42. Okuhara T, Mizuno N, Misono M (2001) *Appl Catal A* 222:63
43. Nakagawa Y, Kamata K, Kotani M, Yamaguchi K, Mizuno N (2005) *Angew Chem Int Ed* 44:5136
44. Okun NM, Tarr JC, Hilleshiem DA, Zhang L, Hardcastle KI, Hill CLJ (2006) *Mol Catal A Chem* 246:11
45. Martín SE, Rossi LI (2001) *Tetrahedron Lett* 42:7147
46. Firouzbadi H, Iranpour N, Zolfigol MA (1998) *Synth Commun* 28:1179
47. Luo Z, Geletii YV, Hillesheim DA, Wang Y, Hill CL (2011) *ACS Catal* 1:1364
48. Okun NM, Anderson TM, Hill CL (2003) *J Am Chem Soc* 125:3194
49. Okun NM, Ritorto MD, Anderson TM, Apkarian RP, Hill CL (2004) *Chem Mater* 16:2551
50. Yu R, Kuang X-F, Wu X-Y, Lu C-Z, Donahue JP (2009) *Coord Chem Rev* 253:2872
51. Dolbecq A, Dumas E, Mayer CR, Mialane P (2010) *Chem Rev* 110:6009
52. Juan-Alcañiz J, Gascon J, Kapteijn F (2012) *J Mater Chem* 22:10102
53. Maksimchuk NV, Timofeeva MN, Melgunov MS, Shmakov AN, Chesalov YA, Dybtsev DN, Fedin VP, Kholdeeva OA (2008) *J Catal* 257:315
54. Maksimchuk NV, Kovalenko KA, Arzumanov SS, Chesalov YA, Melgunov MS, Stepanov AG, Fedin VP, Kholdeeva OA (2010) *Inorg Chem* 49:2920
55. Juan-Alcañiz J, Ramos-Fernandez EV, Lafont U, Gascon J, Kapteijn F (2010) *J Catal* 269:229
56. Juan-Alcañiz J, Goesten M, Martinez-Joaristi A, Stavitski E, Petukhov AV, Gascon J, Kapteijn F (2011) *Chem Commun* 47:8578
57. Chui SS-Y, Lo SM-F, Charmant JPH, Orpen AG, Williams ID (1999) *Science* 283:1148
58. Shevchenko D, Anderlund MF, Thapper A, Styring S (2011) *Energy Environ Sci* 4:1284
59. Inoue H, Shimada T, Kou Y, Nabetani Y, Masui D, Takagi S, Tachibana H (2011) *ChemSusChem* 4:173
60. Geletii YV, Yin Q, Hou Y, Huang Z, Ma H, Song J, Besson C, Luo Z, Cao R, O'Halloran KP, Zhu G, Zhao C, Vickers JW, Ding Y, Mohebbi S, Kuznetsov AE, Musaev DG, Lian T, Hill CL (2011) *Isr J Chem* 51:238
61. Gersten SW, Samuels GJ, Meyer TJ (1982) *J Am Chem Soc* 104:4029
62. Hurst JK (2005) *Coord Chem Rev* 249:313
63. McDaniel ND, Coughlin FJ, Tinker LL, Bernhard S (2008) *J Am Chem Soc* 130:210
64. Muckerman JT, Polyansky DE, Wada T, Tanaka K, Fujita E (2008) *Inorg Chem* 47:1787
65. Concepcion JJ, Jurss JW, Brennaman MK, Hoertz PG, Patrocínio AOT, Iha NYM, Templeton JL, Meyer TJ (2009) *Acc Chem Res* 42:1954
66. Hull JF, Balcells D, Blakemore JD, Incarvito CD, Eisenstein O, Brudvig GW, Crabtree RH (2009) *J Am Chem Soc* 131:8730
67. Masaoka S, Sakai K (2009) *Chem Lett* 38:182
68. McCool NS, Robinson DM, Sheats JE, Dismukes GC (2011) *J Am Chem Soc* 133:11446
69. Bernet L, Lalrempuia R, Ghattas W, Mueller-Bunz H, Vigara L, Llobet A, Albrecht M (2011) *Chem Commun* 47:8058
70. Chen Z, Concepcion JJ, Meyer TJ (2011) *Dalton Trans* 40:3789

71. Fillol JL, Codolà Z, Garcia-Bosch I, Gómez L, Pla JJ, Costas M (2011) *Nat Chem* 3:807
72. Murakami M, Hong D, Suenobu T, Yamaguchi S, Ogura T, Fukuzumi S (2011) *J Am Chem Soc* 133:11605
73. Wasylenko DJ, Ganesamoorthy C, Borau-Garcia J, Berlinguette CP (2011) *Chem Commun* 47:4249
74. Roeser S, Fàrrs P, Bozoglian F, Martínez-Belmonte M, Benet-Buchholz J, Llobet A (2011) *ChemSusChem* 4:197
75. An J, Duana L, Sun L (2012) *Faraday Discuss* 155:267
76. Kaveevivitchai N, Zong R, Tseng H-W, Chitta R, Thummel RP (2012) *Inorg Chem* 51:2930
77. Car P-E, Guttentag M, Baldrige KK, Alberto R, Patzke GR (2012) *Green Chem* 14:1680
78. Shafirovich VY, Khannanov NK, Strelets VV (1980) *Nouveau J Chim* 4:81
79. Harriman A, Pickering IJ, Thomas JM, Christensen PA (1988) *J Chem Soc Faraday Trans 1* 84:2795
80. Kanan MW, Nocera DG (2008) *Science* 321:1072
81. Youngblood WJ, Lee S-HA, Kobayashi Y, Hernandez-Pagan EA, Hoertz PG, Moore TA, Moore AL, Gust D, Mallouk TE (2009) *J Am Chem Soc* 131:926
82. Jiao F, Frei H (2009) *Angew Chem Int Ed* 48:1841
83. Robinson DM, Go YB, Greenblatt M, Dismukes GC (2010) *J Am Chem Soc* 132:11467
84. Carraro M, Sartorel A, Toma FM, Puntoriero F, Scandola F, Campagna S, Prato M, Bonchio M (2011) *Top Curr Chem* 303:121
85. Gerken JB, McAlpin JG, Chen JYC, Rigsby ML, Casey WH, Britt RD, Stahl SS (2011) *J Am Chem Soc* 133:14431
86. Pijpers JJH, Winkler MT, Surendranath Y, Buonassisi T, Nocera DG (2011) *Proc Natl Acad Sci* 108:10056
87. Sivasankar N, Weare WW, Frei H (2011) *J Am Chem Soc* 133:12976
88. Wang C, Xie Z, DeKrafft KE, Lin W (2011) *J Am Chem Soc* 133:13445
89. Wang D, Jiang H, Zong X, Xu Q, Ma Y, Li G, Li C (2011) *Chem Eur J* 17:1275
90. Geletii YV, Botar B, Kögerler P, Hillesheim DA, Musaev DG, Hill CL (2008) *Angew Chem Int Ed* 47:3896
91. Sartorel A, Carraro M, Scorrano G, Zorzi RD, Geremia S, McDaniel ND, Bernhard S, Bonchio M (2008) *J Am Chem Soc* 130:5006
92. Toma FM, Sartorel A, Iurlo M, Carraro M, Parisse P, Maccato C, Rapino S, Gonzalez BR, Amenitsch H, Ros TD, Casalis L, Goldoni A, Marcaccio M, Scorrano G, Scoles G, Paolucci F, Prato M, Bonchio M (2010) *Nat Chem* 2:826
93. Geletii YV, Huang Z, Hou Y, Musaev DG, Lian T, Hill CL (2009) *J Am Chem Soc* 131:7522
94. Orlandi M, Argazzi R, Sartorel A, Carraro M, Scorrano G, Bonchio M, Scandola F (2010) *Chem Commun* 46:3152
95. Geletii YV, Besson C, Hou Y, Yin Q, Musaev DG, Quinero D, Cao R, Hardcastle KI, Proust A, Kögerler P, Hill CL (2009) *J Am Chem Soc* 131:17360
96. Yin Q, Tan JM, Besson C, Geletii YV, Musaev DG, Kuznetsov AE, Luo Z, Hardcastle KI, Hill CL (2010) *Science* 328:342
97. Huang Z, Luo Z, Geletii YV, Vickers J, Yin Q, Wu D, Hou Y, Ding Y, Song J, Musaev DG, Hill CL, Lian T (2011) *J Am Chem Soc* 133:2068
98. Crabtree RH (2012) *Chem Rev* 112:1536
99. Schley ND, Blakemore JD, Subbaiyan NK, Incarvito CD, D'Souza F, Crabtree RH, Brudvig GW (2011) *J Am Chem Soc* 133:10473
100. Stracke JJ, Finke RG (2011) *J Am Chem Soc* 133:14872
101. Tanaka S, Annaka M, Sakai K (2012) *Chem Commun* 48:1653
102. Weinstock IA, Barbuzzi EMG, Wemple MW, Cowan JJ, Reiner RS, Sonnen DM, Heintz RA, Bond JS, Hill CL (2001) *Nature* 414:191
103. Surendranath Y, Kanan MW, Nocera DG (2010) *J Am Chem Soc* 132:16501
104. Duan L, Bozoglian F, Mandal S, Stewart B, Privalov T, Llobet A, Sun L (2012) *Nat Chem* Published online 25 March